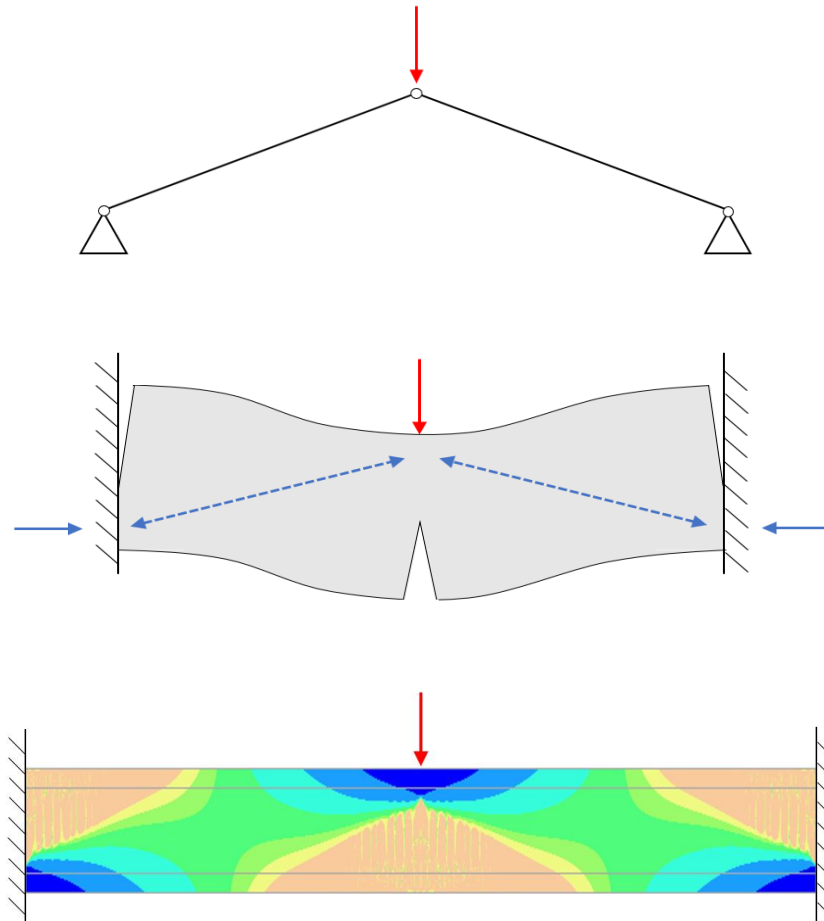# Modelling compressive membrane action and geometrical nonlinearity in one way concrete slabs

Douwe Haarsma

Modelling compressive membrane action and geometrical nonlinearity in one way concrete slabs

An analytical and numerical study on the ultimate capacity and second-order effects in restrained concrete slab strips

by

D.T. Haarsma

to obtain the degree of Master of Science
at the Delft University of Technology
to be defended publicly on Tuesday December 21, 2021 at 15:30 AM.

An electronic version of this thesis is available at: http://repository.tudelft.nl

TUDelft

Royal HaskoningDHV
Enhancing Society Together

Preface

This report presents my thesis "Modelling compressive membrane action and geometrical nonlinearity in one way concrete slabs" and is the result of research into the effect of geometrical nonlinearity on the capacity of restrained concrete slabs. It has been written as partial fulfilment of the requirements to obtain the master's degree in Structural Engineering with a specialisation in concrete structures at the Delft University of Technology. Royal HaskoningDHV offered the opportunity for the graduation research and for writing this thesis as an intern at their company from February to December 2021, for which I am grateful.

I would like to express my gratitude towards all the members of the thesis committee. I thank Jan Rots for his time, valuable feedback and judgement, proposing ideas for new directions in my research and for being the chair of my committee. I want to extend my gratitude to Kees Blom for introducing me to the topic, his helpful comments during the committee meetings, the one-on-one meetings in which he provided me with overview and direction in the entire research process and for kindly answering all my questions. I would like to thank Pierre Hoogenboom for his willingness to join the committee halfway through the graduation period, his critical view on the developed models and his valuable input during the committee meetings. My daily supervisor Marcel 't Hart deserves a particular note of thanks for introducing me to the topic, his endless support, his tips for modelling in DIANA, his constructive feedback and for always answering my questions during our weekly meetings. The guidance of the committee members throughout the entire period greatly contributed to the quality of this thesis and is very much appreciated.

Lastly, I want to thank my family and girlfriend for their unconditional support and advice in coping with the pressures of graduation.

I hope you enjoy your reading.

Douwe Haarsma
Houten, November 2021

Abstract

Increased traffic loads and ageing of concrete bridges and overpasses in the Netherlands make it necessary to reassess these existing structures. Consequently, the current condition and capacity of many concrete structures need to be evaluated. Residual capacity could be discovered during reassessments of concrete slabs due to a phenomenon called compressive membrane action (CMA). CMA is the formation of internal compressive arches caused by the lateral restraint. As a result, the load is not only transferred by bending action but also by arching action. Research has shown that the ultimate capacity can be significantly increased due to the occurrence of CMA. The goal of this study is to examine the influence of geometrical nonlinearity on this increase in capacity. Geometrical nonlinearity is the nonlinearity caused by considering the deformations of the structure in establishing the equilibrium. Also, accurate quantification of the capacity enhancement for a variety of concrete slab variants can be scientifically useful and increases the knowledge on CMA. The study is confined to one way reinforced and restrained concrete slabs, which are referred to as slab strips. The width dimension of the slab is not considered in this thesis.

The research method is a top-down approach, in which a literature study into nonlinearities and membrane action, as well as an analytical and numerical study into basic nonlinear models form the starting point for the more complex analytical and numerical approaches for analysing CMA. In this thesis, a new analytical method is presented to quantify the capacity enhancement due to CMA. More importantly, the geometrical nonlinear (GNL) effect on the capacity increase can be obtained by the analytical model. The analytical model assumes that the loaded and restrained concrete slab strip can be represented by two rigid bodies and two rigid supports separated by three discrete cracks. Calibration of the analytical model is performed with a finite element model in DIANA. Also, the finite element model validates the analytical results and is used to study the failure mode of a restrained concrete slab strip in detail. A qualitative comparison between the analytical model and experimental results from the literature has put the analytical results in perspective.

The enhancement factor – defined as the enhanced capacity divided by the conventional capacity – turned out to be varying between 1.35 and 4.7 for a large variety of examined restrained concrete slab strips with span-to-depth ratios above 10. The ultimate capacity of one way concrete slabs, which was obtained by the GNL calibrated analytical model and the GNL numerical model, is significantly increased due to CMA. The largest enhancement factor is found for slabs with a high degree of axial restraint (value according to the numerical model of 2.38), a low span-to-depth ratio (2.9), a high concrete compressive strength (3.4), a low positive reinforcement ratio (4.7) and a high negative reinforcement ratio (2.43). It appeared that the calibrated analytical model could predict the enhancement factor with sufficient accuracy with a mean and maximum deviation of respectively 1% and 19%.

The capacity enhancement due to CMA would have been even greater if geometrical nonlinearity was not accounted for. Geometrical nonlinearity reduces the increase in capacity because the formed compressive arches will tilt as a result of deflections, therefore leading to a decrease in both the internal lever arm of the introduced horizontal forces and the resisting arching moments. The reduction effect varies between 3% and 37% and is most severe for slabs with a high span-to-depth ratio (value according to the numerical model of 29%), a low positive reinforcement ratio (35%) or a high concrete compressive strength (28%). The calibrated analytical model sufficiently estimates the GNL reduction effect with a maximum deviation of about 12%.

An important finding was that the enhancement factor is larger for deep slabs than for slender slabs, while the reduction of the ultimate load due to geometrical nonlinearity is larger for slender slabs than for deep slabs. The larger enhancement factor, and the correlated stronger arching effect for deep slabs is due to the relatively large internal lever arm compared to the span length of the slab. On the other hand, deflections of slender slabs will cause a rapid percentage decrease in the internal lever arm and of the resisting arching moments. As a result,

the arching effect will fade out relatively quickly during a GNL analysis of a slender slab compared to a GNL analysis of a deep slab.

Furthermore, the numerical results showed that the restrained slab strips failed on the crushing of the concrete in the compression zone, which was also the assumed failure mode for the analytical model. Moreover, the degree of axial restraint of the slab is positively related to the ultimate capacity because the high compressive forces will lead to a stronger arching effect. The width of the compressive arch increases too, while the response gets less ductile when increasing the degree of axial restraint. Lastly, the enhancement factor is very sensitive to changes mainly in positive reinforcement ratio. The GNL effect is sensitive to changes mainly in positive reinforcement ratio and slenderness.

Experimental tests from the literature into the behaviour of one way and two way slabs confirm the qualitative outcomes of the analytical model, of which the most important were: CMA significantly increases the ultimate load, the restrained concrete slabs fail on crushing, and the enhancement factor is larger for slabs with lower conventional capacities. However, the absolute values for the ultimate capacity of the experimental and analytical slabs differ significantly due to a difference in boundary conditions, loading conditions and the assumption for purely one way load transfer for the analytical model.

Structural engineers should be aware that the capacity of restrained concrete slabs can increase significantly due to CMA, but geometrical nonlinearity reduces this increase in capacity. The enhanced capacity is therefore overestimated if geometrical nonlinearity is not accounted for. It should be borne in mind that the overestimation of the enhanced capacity is relatively most significant for slender slabs.

Contents

Abbreviations

LE   Linear elastic

GL   Geometrical linear

GNL   Geometrical nonlinear

MNL   Material nonlinear

MNL(EP)   Material nonlinear elastic-plastic

M(P)   Material plastic

FEM   Finite element method

FEA   Finite element analysis

FEAs   Finite element analyses

NLFEA   Nonlinear finite element analysis

CMA   Compressive membrane action

TMA   Tensile membrane action

EC   Eurocode

EC2   EN 1992-1-1 Eurocode 2

MF   Multiplication factor

UDL   Uniformly distributed load

Slab 1   First reference slab strip

Slab 2   Second reference slab strip

1

Introduction

1.1. Background

As many concrete bridges and overpasses in the Netherlands are built between 1950 and 1970, they are approaching the end of their design life [1]. In addition, the traffic load has increased substantially since their construction, and they are not designed for that. As a result, an enormous repair, reinforce and replace task for existing structures lies ahead of us in order to guarantee that the Dutch infrastructure complies with the required level of safety in the future.

An alternative for the replacement of existing structures is reassessment in order to check whether they may be used for a longer period. Since the linear calculation methods according to both the previous and current design codes provide safety margins and therefore lead to considerably robust designs, hidden capacities could be discovered when reassessing existing structures more realistically. A suitable tool for this is nonlinear finite element analysis (NLFEA). Recalculation with this sophisticated method could lead to the conclusion that an existing structure does not need to be replaced yet. This is an attractive alternative for replacement or applying reinforcements as it is more economical and prevents traffic disturbance. Also, it is more sustainable to exploit the full potential of the robust structures and possibly extend their service life if sufficient safety can be guaranteed. It is of importance to quantify the influence of the hidden capacities to be able to properly recalculate existing structures with sufficient understanding.

The hidden residual capacities can originate from enhanced material properties, such as the strength enhancement of concrete over time due to the ongoing hydration process, but they can also come from other sources. Another hidden capacity source in concrete structures is compressive membrane action (CMA). CMA is the formation of internal compressive arches caused by the lateral restraint [2]. As shown in Figure 1.1, a resultant compressive membrane force is present inside the arches that are created due to the lateral confinement of the bridge slab. The horizontal components of this membrane force will form a couple and the path between these forces is an extra load-bearing path.
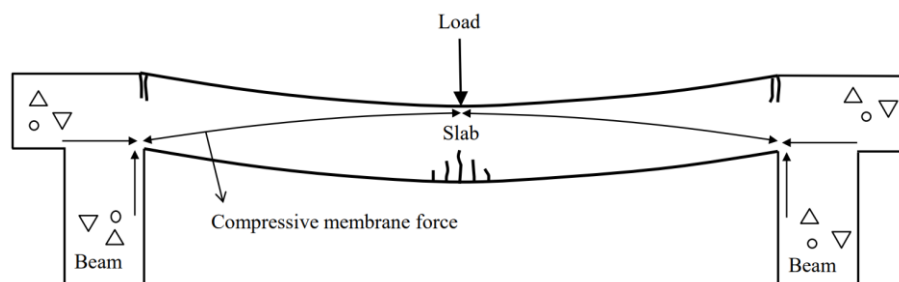

Figure 1.1: CMA in concrete bridge deck [3].

Research has shown that CMA, and consequently the presence of the load-bearing arch mechanism, can substantially enhance the bending as well as the punching shear capacity of laterally restrained concrete slabs [3][4][5]. Recalculation of such concrete slabs could reveal the hidden capacity effect of CMA, because it is not considered in the capacity calculations of the previous Dutch code and of the EN 1992-1-1 Eurocode 2 (EC2) [6].

The influence of CMA in laterally restrained concrete slabs was also investigated by Bakker during his graduation research [7]. Finite element modelling was used to estimate the enhancement factor – defined as the ultimate capacity according to the finite element model divided by the lowest value of the bending and punching shear capacity according to the previous Dutch code – for restrained concrete slabs. A sensitivity study presented in Bakker's thesis showed that the enhancement factor, and therefore the capacity enhancement due to CMA, was highest for high concrete strength, low positive reinforcement ratio, low slenderness, and a high degree of lateral restraint.

Load-induced deflections will change the geometry of structures. If this change is considered in the structural calculation, that is if the equilibrium equations are written based on the deformed geometry, the calculation can be considered geometrical nonlinear. Geometrical nonlinearity can influence the structural response if the deflections are non-negligible compared to the dimensions of the structure. This is of interest when recalculations are performed, and the structural engineer has to decide whether or not to include geometrical nonlinear (GNL) effects in the finite element analysis (FEA). According to the EC2, GNL effects may be neglected if their influence on the response is smaller than 10%. These effects should however be considered if it is likely that they have a significant influence on reaching the ultimate limit state in critical sections. The EC2 also states that geometrical nonlinearity should be considered for slender structures.

Another extensive finite element study on CMA is done by Ben-Gera in [8]. He developed a numerical model to quantify the contributions of several boundary conditions for the development of CMA in immersed tubes. In Ben-Gera's thesis, it was concluded that an increase in lateral stiffness of the roof slab of an immersed tube had a positive effect on the development of CMA and on the ultimate capacity of the roof slab. Another conclusion was that spalling during fire does not significantly limit the development of CMA, but the ultimate capacity does decrease by 7% over the course of a fire curve for immersed tubes developed by Arcadis. Reference is made to [8] for further information. Geometrical nonlinearity was neglected in the research due to its minor influence. However, geometrical nonlinearity could be of influence for the development of CMA if the deflections are non-negligible compared to the dimensions of the structure.

1.2. Objectives and scope

When reassessing laterally restrained structures by performing NLFEA, a higher ultimate capacity can be found because of the occurrence of CMA. Much research has been conducted on the beneficial effect of CMA in reinforced concrete slabs. However, research on the role that geometrical nonlinearity plays in the capacity enhancement of CMA is limited. Therefore, the conducted research covers:

> **The effect of geometrical nonlinearity on the capacity enhancement of compressive membrane action in one way concrete slabs**

The scope is confined to geometrical nonlinearity in combination with material nonlinearity. The main goal is to investigate to what extent geometrical nonlinearity affects the magnitude of CMA in one way concrete slabs and what causes the GNL effect. In this way, structural engineers could make a well-considered choice whether or not to include geometrical nonlinearity in reassessments or detailed structural calculations of restrained concrete structures which require a NLFEA. Another goal of this thesis is to quantify the capacity enhancement of laterally restrained reinforced concrete slabs with a new analytical as well as a numerical approach. In addition, this thesis contributes to the general knowledge about CMA.

The research focuses on the capacity of concrete slabs in the ultimate limit state. Hence, the serviceability limit state requirements, such as limitations of the crack width and deflections, or durability aspects, will not be

considered. Also, both loading and capacity values will not be corrected by safety factors since this research focuses on the fundamentals of structural behaviour. The same holds for the adopted material properties.

1.3. Research method

In order to achieve the goal of this research in a structured way, the process is divided into six steps which are shown in the stairway in Figure 1.2. The successive step is not started until the previous step has been completed. However, there will always be some overlap between the research steps. For example, literature will be relevant in each of the steps.
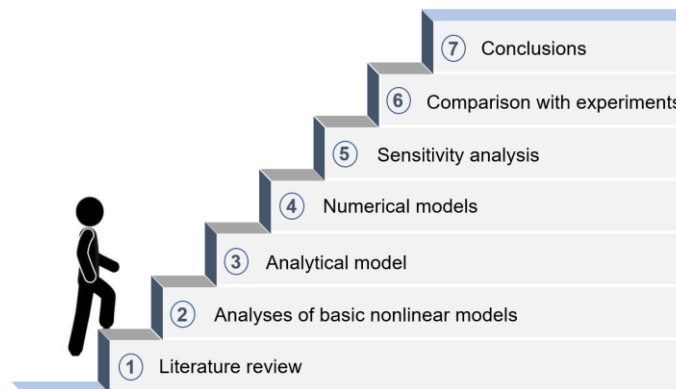

Figure 1.2: Step-wise research process.

① Literature review

The first step is to conduct a literature study on the concepts of structural behaviour, namely elasticity, plasticity, linearity, and nonlinearity. Then, the relevant sources of nonlinearity and the differences between linear and nonlinear structural analysis are discussed. The literature study is thereafter extended to CMA, tensile membrane action (TMA) and the relation between membrane action and nonlinearity.

② Analyses of basic nonlinear models

The second step is to introduce simple analytical models to study the influence of the structural concepts on the response of the models. The focus is on how nonlinearities and boundary conditions change the response. Also, special attention is paid to the GNL effects. Understanding the relevant concepts of mechanics is key in this part of the research process. NLFEA is performed when combinations of nonlinearities make it too complex to solve the basic models analytically. FEA program DIANA 10.4 is used for numerical modelling. A link is presented between the results of the conducted analyses and the outcomes of the literature study.

③ Analytical model

A new analytical model of a laterally restrained reinforced concrete slab is made during the third step of the research process. The analytical research in this step is limited to an internal strip of the concrete slab, which makes it possible to develop the model in 2D and reduce the complexity. The concrete slab is therefore a one way slab. Note that double plate bending and confinement of concrete are therefore not considered. Reasons for the development of an analytical model are to quantify the capacity enhancement due to CMA and to study the effect of geometrical nonlinearity on the response of the restrained concrete slab strip.

The starting point of the model is an analytical theory from the literature: McDowell et al. [9] developed a method to predict the structural behaviour of laterally restrained masonry walls. Their analytical model is modified to include steel reinforcement and the correct material properties. Two reference cases of reinforced concrete slap strips are used to visualize the response in load-deflection diagrams and to make the results comparable with each other and with numerical results. The results of the analytical model are obtained using Python programming language in Jupyter Notebook.

④ Numerical models

Validation of the analytical model is done with a finite element model which is referred to as the *numerical rigid body model* in the fourth research step. This model uses the same assumptions as in the analytical model, which makes the models nearly equivalent and comparable.

The analytical model uses many assumptions, which are sometimes rather arbitrary. Therefore, a realistic *numerical concrete slab model* is developed to predict the actual structural behaviour of laterally restrained concrete slabs more accurately. The nonlinear analyses of the models are performed in DIANA and based on the technical document of Rijkswaterstaat "Guidelines for Nonlinear Finite Element Analysis of Concrete Structures" [10]. It is worth mentioning that DIANA does not include GNL effects in NLFEA by default.

The numerical results of the two reference slabs are shown in load-deflection diagrams and thereafter compared with the analytical results. The goal of the *numerical rigid body model* is to check if the analytical model is constructed properly, and the goal of the *numerical concrete slab model* is to actually calibrate the analytical model and validate the analytical results. The numerical results will be explained in great detail, with a focus on the structural behaviour and the failure modes.

⑤ Sensitivity analysis

In this fifth step, a sensitivity analysis is performed to quantify the capacity enhancement and the magnitude of the GNL effect on the basis of many concrete slab strip variants. Thusly, the effect of variations in the analytical and numerical model parameters on these quantities is studied. Moreover, differences between the analytical and numerical results of the sensitivity analysis are discussed.

⑥ Comparison between analytical and experimental results

A comparison between the analytical results and available experimental results is made in this research step. It is a qualitative comparison, because equivalent experimental data is lacking. Validation of several qualitative findings in the previous research steps can be achieved.

⑦ Conclusions

The seventh step is drawing conclusions from the outcomes of the analytical models, the numerical models and the comparison with experimental data. Recommendations are made and further research options are proposed.

The research method can be regarded as a top-down approach wherein the general aspects – the ultimate goal of the research and the basic theoretical concepts – form the starting point for the detailed models. The results of the basic nonlinear models can be used to understand the outcomes of the more complex analytical and numerical models. In this way, the probability of achieving explainable and reproducible outcomes is increased.

1.4. Thesis outline

Chapter 2 presents a literature study into several concepts of structural behaviour. The basics of elasticity, plasticity, linearity and nonlinearity are described. Also, membrane action and its relation to nonlinearity are detailly discussed. In Chapter 3, the effect of nonlinearities on basic analytical models is studied. An analytical model for CMA in concrete slab strips is presented in Chapter 4. It focuses on the influence of geometrical nonlinearity on the response of the slab strip. Chapter 5 contains finite element analyses (FEAs) of laterally restrained concrete slab strips in order to calibrate and validate the analytical model. An extensive comparison between the analytical results and the numerical results is also included. In Chapter 6, a sensitivity study has been conducted to accurately quantify the capacity enhancement due to CMA and the GNL effect. Chapter 7 contains a comparison between analytical results and available experimental results from the literature. Finally, chapter 8 consists of the conclusions and recommendations of the research.

2

Literature review

2.1. Material behaviour

2.1.1. Stress-strain relation

The load on a structure introduces stresses into the material. Stress is the relationship between the applied load and the cross-sectional properties of the structure. For compression and tension, the stress is the force per area {2.1} and for bending, the stress is the bending moment over the section modulus {2.2}. As a result of stress, the material will deform. Strain is a measure for these deformations and can be defined as a change of shape. Moreover, strain can be expressed as the ratio between the elongation and the original length in the case uniaxial tension is present {2.3}. Hence, the strain has a negative value when compressive forces are introduced into the material according to the convention in structural mechanics.

$$\sigma = \frac{F}{A} \quad \text{\{2.1\}}$$

$$\sigma = \frac{M}{W} \quad \text{\{2.2\}}$$

$$\varepsilon = \frac{\Delta L}{L} \quad \text{\{2.3\}}$$

Hooke's law describes the directly proportional relationship between the stress and the strain of a material {2.4}. The ratio of stress to strain is the modulus of elasticity (i.e. E-modulus), which is a measure for the stiffness* of the material and has a constant value according to this law.

- *   **Stiffness** is a property of a structural part which is defined as the relationship between the applied load and the correlated structural response, for example the vertical displacement. The stiffness of a structure is not only depending on the material but also on the shape of the structure and the boundary conditions. For example, a simply supported I-shaped beam has a much larger stiffness than a cantilevered rectangular beam with the same cross-sectional area and length. The E-modulus is therefore not the same as structural stiffness, but it is one of the indicators for the stiffness of a structure. However, the quantity of the material stiffness is the E-modulus. It is therefore important to make a distinction between structural stiffness and material stiffness.

However, the law only applies up to a certain value of stress in the material for which the stress and strain are still linearly related. This value is called the proportionality limit and after this limit is reached, the material behaviour becomes nonlinear [11].

$$\sigma = E \cdot \varepsilon \quad \text{\{2.4\}}$$

In material science, linearity is therefore the linear stress-strain relationship of the material and can be described by Hooke's law (see Figure 2.1a). Nonlinearity, in this sense, is when the stiffness of the material is not constant and will change depending on the state of stress and strain. The result is a curve in the stress-strain diagram which is not straight (see Figure 2.1b). Most materials do at least have a minor nonlinear and/or curved region. Possible causes of this nonlinearity are inhomogeneity or non-isotropy of the materials and plasticity. Nevertheless, the material behaviour can often be approximated by a linear or bi-linear model, and the material itself can be assumed isotropic and homogeneous.
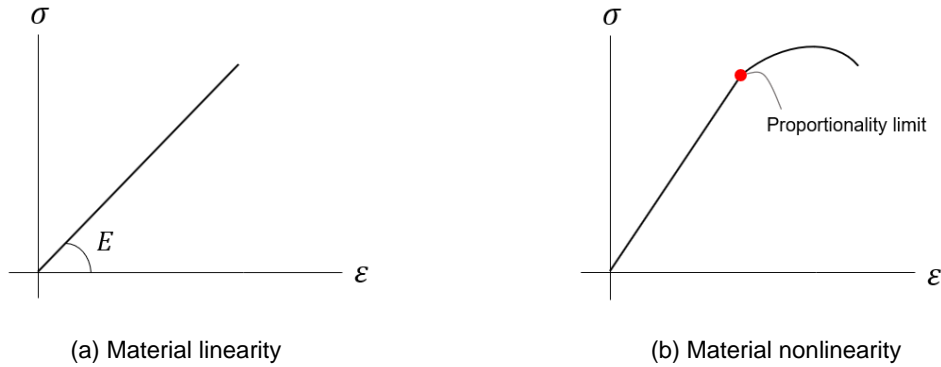

(a) Material linearity   (b) Material nonlinearity

Figure 2.1: Stress-strain diagrams of linear and nonlinear material behaviour.

2.1.2. Elasticity, plasticity and ductility

A material behaves elastically if it is able to completely return to its original shape after unloading [12]. The boundary for elastic material behaviour is called the elastic limit; if the stress is under this limit, the material behaves elastically. On the other hand, plastic material behaviour occurs when a permanent deformation will be present after the load has been removed. Thus, when the stress is exceeding the elastic limit, and the original shape is not restored after the stress has been removed, the material has shown plastic behaviour. Materials with both a so-called "elastic region" and a "plastic region" can be considered elastic-plastic materials (see Figure 2.2a). Full elasticity occurs when a material only has an elastic region (see Figure 2.2b) and full plasticity occurs when a material only has a plastic region (see Figure 2.2c).

Plasticity can thus be regarded as the ability of a material to undergo permanent deformation. Ductility is described by Zhu and Wu as tensile plasticity [13]. But, according to the mentioned researchers, the concepts of ductility and plasticity differ. A highly plastic material does not necessarily mean that the material is also very ductile. An example of such a material is a nanostructured metal. On the other hand, steel is highly plastic as well as highly ductile. Ductility is an important material property, because ductile materials warn before structural failure occurs. Unloading can then prevent failure of the structure, whereas reaching the peak load of brittle materials often means that failure of the material occurs shortly afterwards [14].

(a) Elastic-plasticity   (b) Elasticity   (c) Plasticity
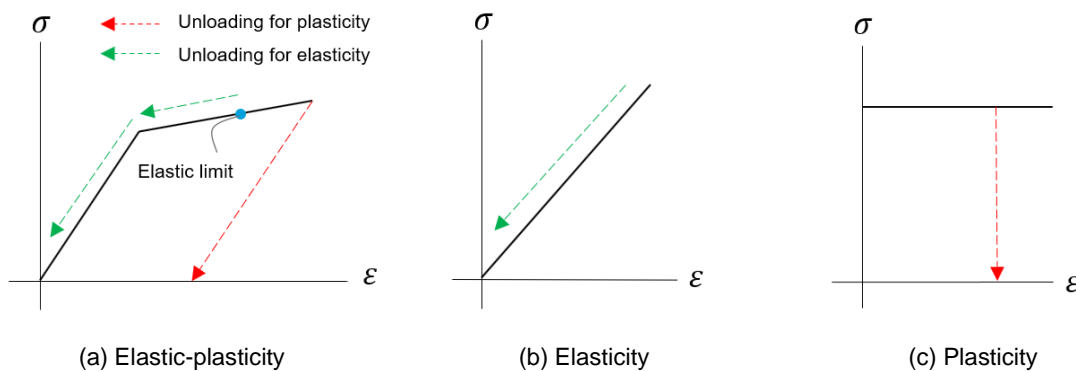
Figure 2.2: Stress-strain diagrams of elastic-plastic, elastic, and plastic materials.

Furthermore, a clear distinction must be made between elasticity and material linearity as well as between plasticity and material nonlinearity. Elasticity does not necessarily mean the material also behaves linearly (see Figure 2.2a). The proportionality limit and the elastic limit do not always coincide. The same goes for plasticity and nonlinearity and is shown in Figure 2.2c. Yet, in most cases linear behaviour goes hand in hand with elastic behaviour and that is the reason linear-elastic material behaviour is often referred to.

On a cross-sectional level, elastic-plastic materials can show both elastic and plastic behaviour simultaneously. This is illustrated with an example in which a simply supported beam is subjected to a point load at midspan (see Figure 2.3a). The material behaviour of the beam is represented by a bi-linear relationship with the stress f_y as proportionality limit (see Figure 2.3b) for both compression and tension. Point load F can be plotted against the vertical displacement w for the cross-section at midspan (see Figure 2.4a).

In region 1, the whole midspan cross-section shows linear-elastic behaviour. The behaviour becomes non-linear, and region 2 is entered, when f_y is reached in the outer fibres of the cross-section. In this region, the middle part of the cross-section still behaves linear-elastic while the outer parts show plastic material behaviour (elastic and plastic behaviour simultaneously). Note that in this region the linearity disappears, and the stiffness reduces. If the proportionality limit is reached in the entire cross-section, a plastic hinge is formed. At that moment, region 3 of the F-w graph is entered. The beam now behaves plastic because the midspan cross-section is fully plastic; the vertical displacement increases substantially without an increase in the load.

The formation of the plastic hinge at mid-span is shown in Figure 2.5. For statically determinate structures, failure occurs at the moment a plastic hinge is formed [15]. In contrast, statically indeterminate structures could allow for redistribution of forces and thereby for a further increase in the load after a plastic hinge has occurred.
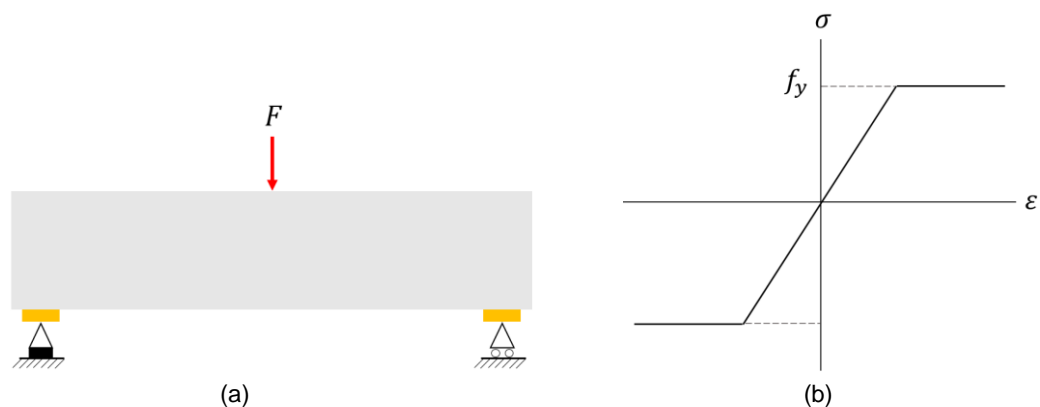

(a)   (b)

Figure 2.3: Simply supported beam subjected to a point load at midspan (a) and its material properties represented in a stress-strain diagram (b).

(a)   (b)
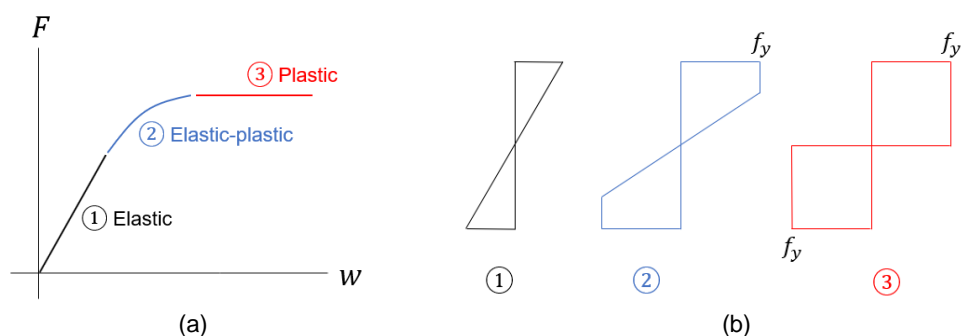
Figure 2.4: Force-displacement diagram (a) of a simply supported beam and the related cross-sectional stress diagrams (b).
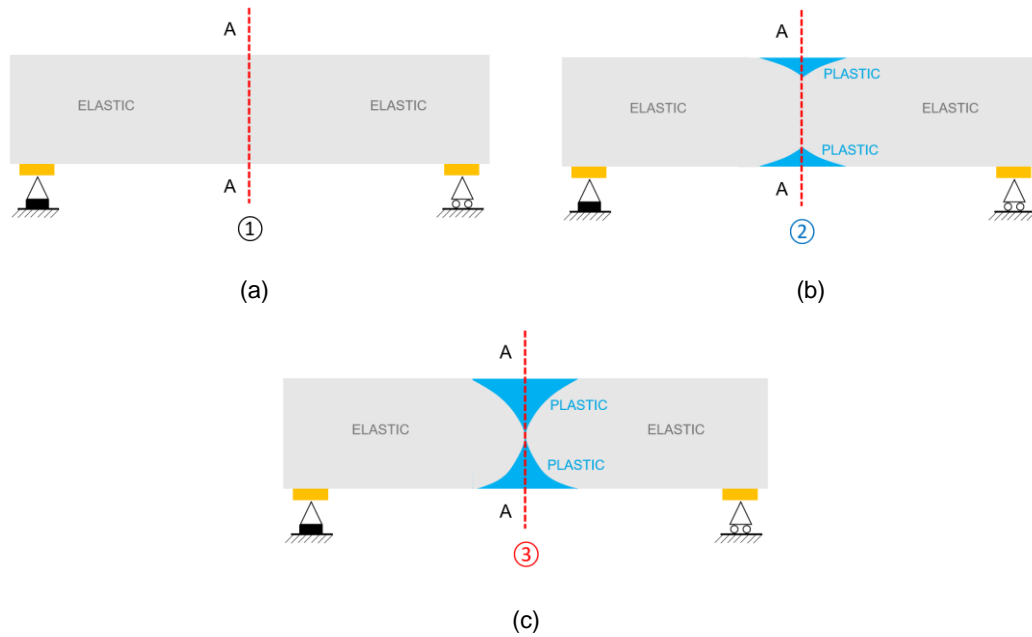
Figure 2.5: Plastic hinge formation in a simply supported beam.

2.1.3. Cracking of concrete

Concrete structures are reinforced with steel to accommodate large tensile stresses and to increase the maximum load resistance and ductility. The steel reinforcement is however not activated until cracking of the concrete is commenced. The formation of cracks in reinforced concrete structures can be divided into four stages according to the fib Model Code for Concrete Structures [16]. The four stages are first discussed based on a reinforced concrete tensile member loaded in pure tension (see Figure 2.6a). Figure 2.6b shows the idealised behaviour of the tensile member.
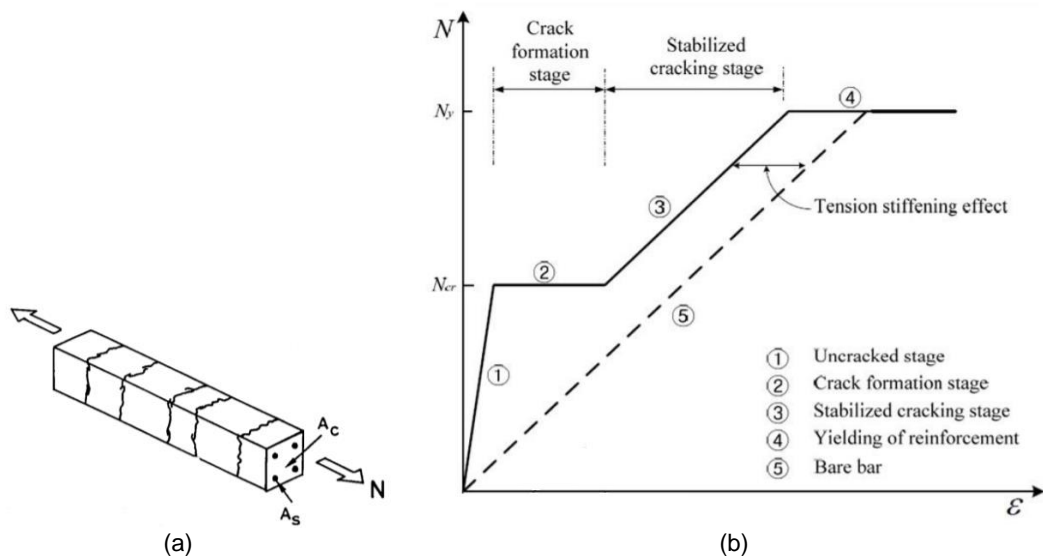

Figure 2.6: Reinforced concrete tensile member (a) and its idealised behaviour (b) [(b) adapted from [16]].

- In the **uncracked stage**, the deformations of the concrete and the steel reinforcement are equal. The stiffness is constant, and the behaviour of the tensile member can be assumed as linear-elastic.

- The concrete cracks if the tensile stress exceeds the tensile strength. The first crack will initiate the **crack formation stage**. At the first crack, the perfect bond between the concrete and the steel disappears and the redistribution of the stresses leads to an increase in the steel stress until all the

tensile forces are transmitted to the steel. Further from the crack, the bond stresses will be reintroduced at the interface between concrete and steel. Thus, the steel force is transferred to the concrete by bond stresses, which are caused by the slip between the concrete and the steel due to a difference in deformations after cracking. The concrete is then activated to carry the tensile force again. New cracks will occur until the crack pattern is fully developed. The crack formation stage is finished when the distance between the cracks is too small to reach the concrete tensile strength again.

- A fully developed crack pattern occurs at the start of the **stabilized cracking stage**, in which no new cracks are formed, and the crack width will increase due to elongation of the steel reinforcement only. This is because the bond stress, as well as the deformations of the concrete, remain constant. The load can increase in this range due to an increase in stress in the steel. Tension stiffening (see Figure 2.6) occurs due to the transmission of the stresses from the steel to the surrounding concrete between the cracks and leads to an increase in stiffness compared to a bare reinforcement bar.

- The end of the stabilised cracking stage, and thereby the beginning of the **yielding stage**, is initiated when the steel stress reaches the yield strength. At that moment, the load remains constant, and the maximum load resistance is reached.

The same four stages can be observed in an idealised moment-curvature (M-1/r) diagram of a reinforced concrete beam loaded in pure bending (see Figure 2.7).
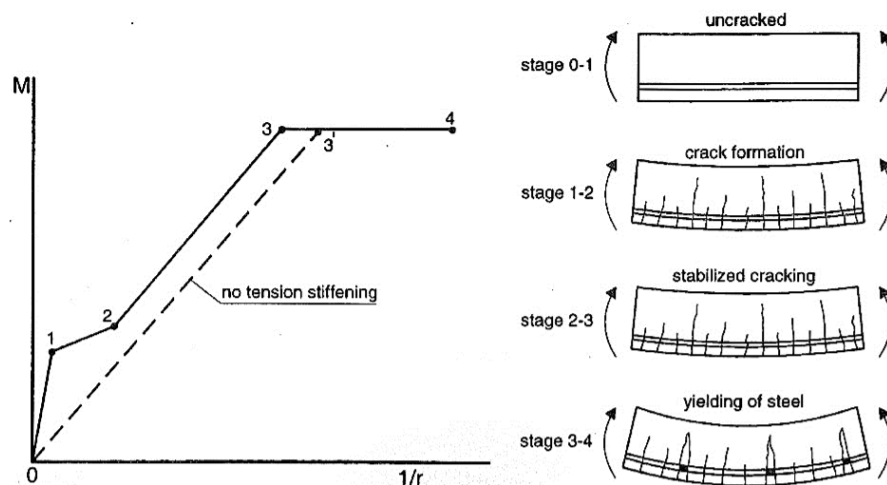

Figure 2.7: Idealised behaviour of reinforced concrete beam subjected to pure bending.

- In the **uncracked stage**, the stress diagrams in all sections of the beam can be considered linear. The strains of the concrete and the steel reinforcement are equal.

- In the **crack formation stage**, the stiffness is reduced due to cracking and the tensile stresses in the bottom zone of the beam are fully transferred to the steel reinforcement bar.

- In the **stabilized cracking stage**, the tensile stress in the steel and the compressive stress in the concrete increase. The steel forces are in a stable equilibrium with the compressive forces in the concrete.

- In the **yielding stage**, the steel stress has reached the yield strength. The strains of both the concrete and steel can still increase, while the steel stress can no longer increase. The reinforced concrete beam behaves fully plastic in this stage. It is assumed that failure of the beam occurs when the ultimate compressive strain of concrete is reached in the top fibre of the beam (see Figure 2.8). The calculation of the bending moment capacity M_u according to the EC2 is based on this assumption. The stresses are simplified by ignoring the tensile strength of concrete and assuming a linear or bi-linear stress distribution.
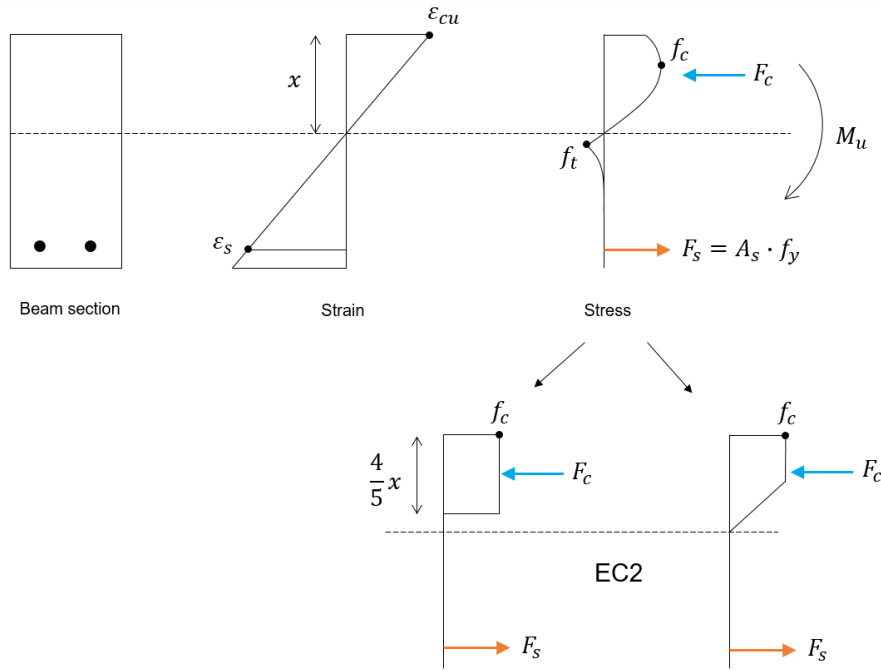
Figure 2.8: Strains and stresses in midspan cross-section of a reinforced concrete beam loaded in pure bending.

2.2. Structural analysis

When designing concrete structures, or structures of any other material, structural analysis is necessary to guarantee a design that meets the safety requirements. The analysis usually consists of a structural calculation that accounts for sufficient strength, stiffness, and stability. A structural analysis that includes nonlinearities can accurately predict actual structural behaviour. However, nonlinear analysis is complex, and the structural behaviour is therefore often described by simplified models. One of these models is linear structural analysis. Both linear analysis (2.2.1) and nonlinear analysis (2.2.2) will be discussed in detail. A comparison is made between linear and nonlinear analysis in section 2.2.3.

2.2.1. Linear analysis

In linear analysis, the relationship between the applied load and the resulting displacement is linear. A clear overview of linear structural systems is included in the book of Kim [17]. It states that a structural system is linear if all relationships – relations (1), (2) and (3) in Figure 2.9 – between the loads, stresses, strains and displacements are linear as well. Relation (1) is the equilibrium relation, relation (2) is the constitutive relation and relation (3) is the kinematic relation.
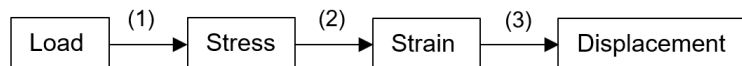

Figure 2.9: Related quantities in structural analysis (adapted from [17]).

These relationships can be explained by a simple example in which a rectangular block is subjected to uniaxial compression in the vertical direction (see Figure 2.10a). It is assumed that buckling will not occur, resulting in a stable structural system. The structural model is presented in 2D because it is only used to show the basic relations between the structural quantities.
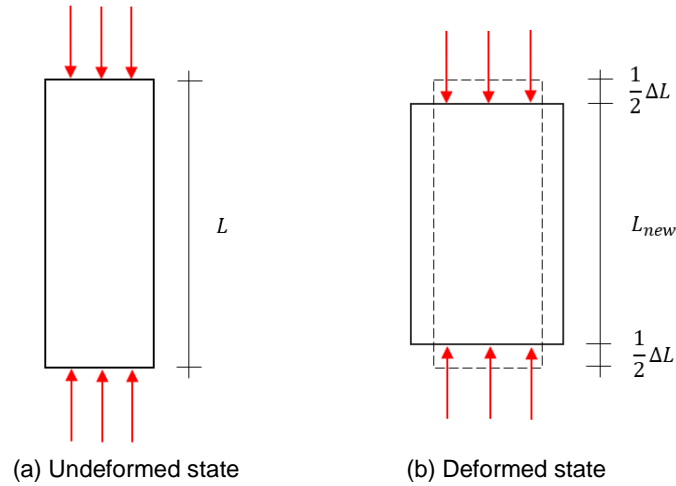
(a) Undeformed state   (b) Deformed state

Figure 2.10: Structural model of a rectangular block subjected to uniaxial compression.

(1) **Equilibrium relation:** The relationship between the load and the stress is depending on the magnitude of the load and is therefore nonlinear, because the cross-sectional area will increase due to Poisson's effect (see Figure 2.10b). However, if this increase is very small, the nonlinearity can be neglected.

(2) **Constitutive relation:** The relationship between the stress and the strain is again depending on the magnitude of the load. If a material is loaded with stress levels below the proportionality limit, the material behaves linearly. In this region, the slope of the stress-strain curve is the E-modulus. As soon as this limit is exceeded, the stiffness will change, and the material behaves nonlinear (i.e. material nonlinearity).

(3) **Kinematic relation:** The relationship between the strain and the displacement is in this example nonlinear as well. The strain is defined as the shortening divided by the length of the deformed bar {2.5}.

$$\varepsilon = \frac{\Delta L}{L_{new}} = \frac{\Delta L}{L - \Delta L} \quad \Bigg| \quad \{2.5\}$$

The new block length already includes the shortening, which makes the relationship nonlinear (i.e. geometrical nonlinearity, see 2.2.2). However, this nonlinear effect is neglectable when the new length is almost equal to the initial length.

In linear analysis, the above-described nonlinear effects are ignored. Therefore, relations (1), (2) and (3) are considered linear, resulting in a linear relationship between the applied load and the displacement. The results of linear structural analysis are approximations of actual structural behaviour, because structural systems are nonlinear by definition.

2.2.2. Nonlinear analysis

In nonlinear analysis, the relationship between the load and the response of the structure is not linear. Structural systems are nonlinear if one of the relations in Figure 2.9 is nonlinear. In fact, as is described in 2.2.1, structural systems are by definition nonlinear because all relations are affected by at least a small nonlinear effect. Several sources of nonlinearity can be distinguished. It is important to note that the below list is not complete. Only the sources of nonlinearity that are relevant for this thesis are listed.

- **Geometrical nonlinearity** is a source of nonlinearity that originates from the changes in geometry and is characterized by a nonlinear relationship between the displacement and the strain (relationship (3) in Figure 2.9). In *geometrical linear* (GL) analysis, the equilibrium equations are written based on the geometry of the undeformed structure and therefore deformations of the structure are not considered

in these equations. In real engineering practice, on the other hand, changes in geometry due to deformations will occur. Hence, one can no longer assume the strains can be determined based on the undeformed geometry. Therefore, if geometrical nonlinearity is considered, the equilibrium equations are written based on the geometry of the deformed structure.

If the deflections are small compared to the dimensions of the structure, geometrical nonlinearity has a small influence on the structural response. GNL behaviour is however of importance when large deflections occur, because then there is a large difference between the deformed geometry and the undeformed geometry. Relatively large deflections are more common in slender structures than in deep structures, because the deflections for slender structures are greater in relation to the height than for deep structures. It can thus be stated that – for comparable geometrical properties, material properties and boundary conditions – the more slender the structure, the more influence geometrical nonlinearity has on the structural behaviour. GNL effects are often referred to as second-order effects and they will be discussed in more detail in chapter 3.

- **Material nonlinearity** or physical nonlinearity is a source of nonlinearity that originates from the change in material properties (i.e. change in stiffness of the material) when the load is increased and is characterized by a nonlinear stress-strain relationship of the material (relationship (2) in Figure 2.9). Thus, there is a dependency of the material properties on the state of stress and strain, and in some cases also on the deformation history, the time, the temperature, and several other factors. Note that material nonlinearity was briefly discussed earlier in section 2.1.1. Typical examples of material nonlinearities are plasticity, cracking and creep; *plasticity* of materials occurs when the elastic limit is exceeded, which leads to a nonlinear stress-strain relation and permanent deformation after unloading; *cracking* will result in a decrease in stiffness of the material; *creep* is an increase in strain over time under constant stress. Nonlinear boundary conditions can also result in a physical nonlinear system, such as an edge support which can be represented by a spring with nonlinear properties.

- **Force nonlinearity** is a source of nonlinearity that originates from the dependency of the applied loads on the deformation. The magnitude or the direction of the load can change when the structure is deforming. Hence, force nonlinearity could be considered as a form of geometrical nonlinearity. An example of force nonlinearity is the follower forces, the direction of which remains perpendicular to the structure as it deforms [18] (see Figure 2.11).
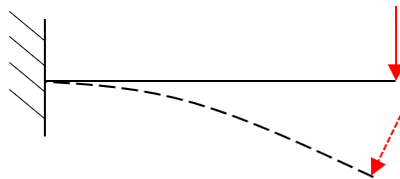

Figure 2.11: Follower force for a cantilever beam.

2.2.3. Comparison linear and nonlinear analysis

The stiffness matrix for the structural system defines the relation between the load and the displacements. The stiffness matrix stays constant during linear analysis, while this is not the case for nonlinear analysis. This is an important difference between linear and nonlinear analysis.

Actual structural behaviour does include all the nonlinear effects mentioned in section 2.2.2. However, when including these effects does not result in significantly different outcomes for structural systems (i.e. nonlinear effects are negligible), linear analysis can be used for describing the structural behaviour as well as for designing the structures as it gives a satisfactory approximation of the actual structural behaviour. The question rises why structural engineers should use this 'approximation' instead of considering nonlinear effects as well.

The first and most important reason is that solving linear systems required much less computational time and costs due to the simple form of the system of linear equations. Nonlinear systems are often too complex to solve, because the stiffness matrix is depending on the geometry and/or the nonlinear material properties. Linear systems are solved in just one calculation step, while the solution of nonlinear systems require multiple steps in an iterative process until balance is found. Furthermore, the linear system of equations does not have to be solved again if the load is changing, thus leading to the possibility of applying the principle of superposition [19]. This principle implies that the total response of the system can be determined by taking the sum of all individual responses.

Moreover, the safety margins that are created due to a linear approach will cover the uncertainties and thus substantially reduce the chance of structural failure. The result is that most concrete structures are over-dimensioned, and the structural robustness that goes along with this might become useful for future increasements of the traffic load or functionality changes of the structure. For example, if the owner of a bridge wants to add a traffic lane or increase the maximum allowable truck load, these residual capacities can be utilized for determining if the addition of a traffic line would be possible. If nonlinear analysis had been used to design this bridge, the residual capacities would presumably not have been large in magnitude as they would have been partially used already. It should however be noted that safety margins must always be used for designing structures since the chance of structural collapse must be extremely low. Therefore, residual capacities will be present in any structure, but if you exploit those capacities the chance of failure is likely to increase. This is something you want to avoid at all times.

On the other hand, nonlinear analysis can give insight into the actual behaviour of the structure. While the presence of residual hidden capacities in structures is common when a linear analysis is performed, these capacities reveal themselves in nonlinear analysis. This is of interest when reassessment of existing structures is carried out. By reassessing structures with a nonlinear approach, the resulting load-bearing capacity is sometimes higher than the one calculated when the structure was designed. Possible unnecessary replacement or reinforcement of the structures can be temporarily prevented. Especially in a structure in which CMA is an active load-bearing mechanism, the residual capacity will be significant, and the actual capacity will therefore be considerably higher than calculated with the design code.

2.3. Membrane action

2.3.1. Compressive membrane action

Compressive membrane action (CMA) is the phenomenon whereby internal forces form arching blocks that transfer the load by compression. It occurs due to deformations of the structure in combination with laterally restraining conditions. Load-induced deformations will cause the construction material to crack in the tensile zones of the structure. The cracks will lead to a relocation of the neutral axis, which goes along with the propensity of the material to expand. Horizontal forces, and subsequently CMA arise at the structure boundaries if this expansion is laterally restrained. Figure 2.12 shows the principle of CMA. Note that the slab is unusually thick to make the representation more clear.

Arching action is created by the horizontal forces which form the compressive arches. Thus, CMA is the arching action initiated by cracking of the construction material. The arching action provides an alternative load path and therefore an extra load-bearing mechanism in addition to flexural action of the structure. Another condition for the occurrence of CMA is that the compressive strength and the tensile strength of the construction material must be different [20]. Concrete fulfils this condition, because the compressive strength is much larger than the tensile strength. Hence, CMA will occur in cracking concrete structures that are partially or fully laterally restrained.
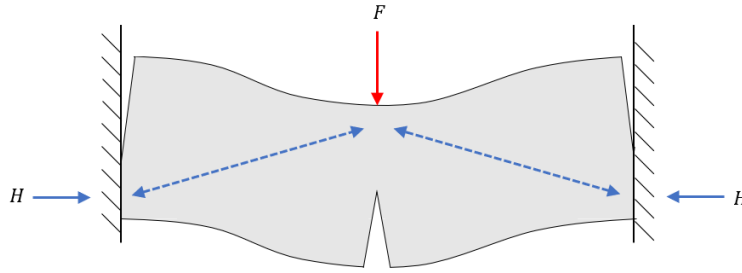
Figure 2.12: Simple representation of CMA in a deep concrete slab.

CMA can enhance the flexural as well as the punching shear capacity of concrete slabs [4]. This strength enhancement was first discovered by Westergaard and Slater in 1920 [21]. However, CMA was not recognized as the cause of the capacity increase until Ockleston examined a three story building in Johannesburg in 1958 [22]. In the decades that followed, many researchers tried to accurately predict the strength enhancement of CMA either with theoretical approaches ([23][24] among others) or with experiments ([25][26][5][3] among others). The experiments showed that, in addition to the expected strength enhancement, crushing of the concrete or punching shear failure was in most cases the governing failure mode in concrete slabs in which CMA was activated by the lateral restraint. Also, the crack width was found to be significantly smaller in restrained slabs than in unrestrained slabs according to the experimental research of Rankin et al. in [3].

The current Eurocodes do not consider the effects of CMA, because it is still difficult to quantify the gain in the capacity as well as predict the exact conditions under which it occurs, despite extensive research. The Eurocodes only consider the flexural action of concrete structures, even though arching action is activated by CMA. Therefore, if the conditions for the presence of CMA are met, the failure load calculated according to the Eurocode (EC) will be significantly lower than the actual failure load. Also, the calculated deflections of the structure will be overestimated. Thus, it can be concluded that laterally restrained concrete structures in Europe that are designed with the EC2 have an extra capacity, which can also be referred to as 'hidden capacity' because it was not considered in the calculations.

With the rise of FEA software programs with increasing computational capacity, the contribution of CMA can be better predicted. Even though FEAs have the propensity to overestimate the beneficial effect of CMA to a slight extent [20], it offers great potential in both predicting the capacity enhancement and investigating the affecting conditions under which it occurs.

2.3.2. Tensile membrane action

Tensile ties are formed under influence of significant deflection of laterally restrained structures (see Figure 2.13). This phenomenon is called tensile membrane action (TMA) and leads to an increase in stiffness and strength, which means the vertical displacements decrease and the load-bearing capacity increases. Thus, TMA and CMA both have the corresponding property of enhancing the capacity of structures.
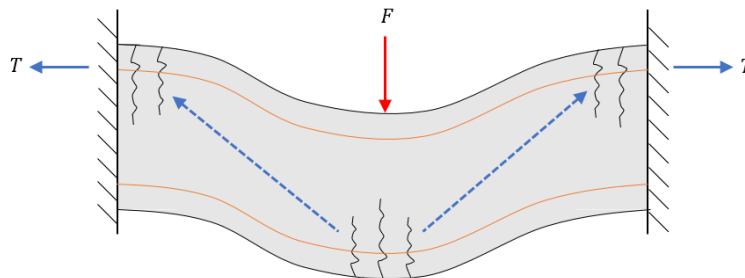

Figure 2.13: Simple representation of TMA in a deep concrete slab.

However, two side notes must be placed on the positive effects of TMA. Firstly, large deflections and deformations of the structure must be allowed before TMA will play a role. TMA therefore only develops after the initial failure of the slab due to the crushing of the concrete in the compression zones in combination with deep cracks in the tensile zones [27]. Consequently, TMA is not of interest for designing concrete slabs to avoid local failures. It only becomes important for progressive collapse analyses or in extreme conditions in which a middle support is removed from the structural system due to failure [28].

Secondly, structures must be able to accommodate the tensile forces in the ties to take advantage of the extra capacity provided by TMA. Since the concrete strength in tension is limited, it should be reinforced with steel bars to take up the tensile forces and allow the tensile ties to develop. TMA in reinforced concrete structures can thus be seen as a form of catenary action, in which the reinforcement – with concrete around it – is hanging between the supports. However, sincof ce this usually only happens when a middle support fails, it should be taken into consideration that the region that was designed for compression has become tensile.

2.3.3. Idealised response of restrained concrete slab

A fully laterally restrained and slender concrete slab is most likely to experience the positive effects of both CMA and TMA. In Figure 2.14, the typical load-deflection behaviour of such a restrained slab is compared to the behaviour of an unrestrained and simply supported slab. The only load-bearing mechanism for the unrestrained slab is bending action, while the loads on the restrained slab are transferred by bending action *and* membrane action (i.e. arching action).

For small deflections, CMA will enhance the capacity of the restrained slab compared to the unrestrained slab due to the built-up of horizontal forces and the subsequent arching action. The load-deflection curve thereafter decreases, and the stiffness becomes negative. For deep slabs, this is mainly due to the crushing of the concrete in the compression zone and for slender slabs mainly due to geometric instability of the structural system [28]. The latter reason is discussed in more detail later in section 2.3.4 and section 3.4. Eventually, after large deflections have occurred, the load will substantially increase again due to the occurrence of TMA. The slab is now almost completely in tension and failure is determined by the rupture of the reinforcement bars.
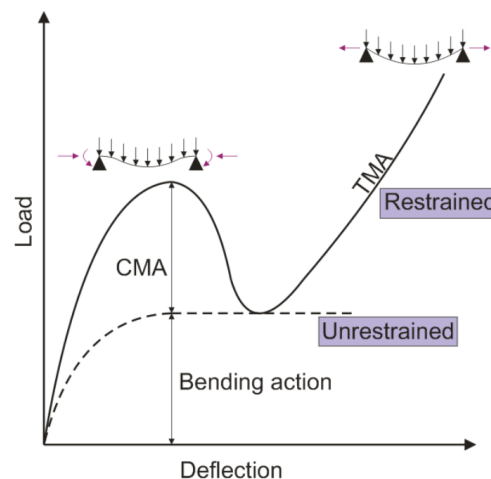

Figure 2.14: Idealised response of an unrestrained and fully restrained slab [28].

2.3.4. Membrane action and nonlinearity

TMA and nonlinearity

TMA can be seen as a GNL effect because it develops in the structure after large deflections have occurred and the structural configuration has largely changed. TMA can therefore not be discovered if a GL calculation is made. Yet, the concrete must crack under the influence of large deflections before TMA can develop, which means TMA cannot occur without considering material nonlinearity as well.

CMA and nonlinearity

Linear analysis of a laterally restrained concrete slab will not provide realistic results, because CMA is a nonlinear phenomenon. Since CMA is caused by the cracking of the concrete, it can be seen as a MNL effect. Yet, the change of geometry is also of influence as it affects the orientation of the arching blocks. As deflections are increasing, the imaginary resultant compressive arch (dashed blue line in Figure 2.15) will tilt. The magnitude of CMA is thus affected by geometrical nonlinearity.
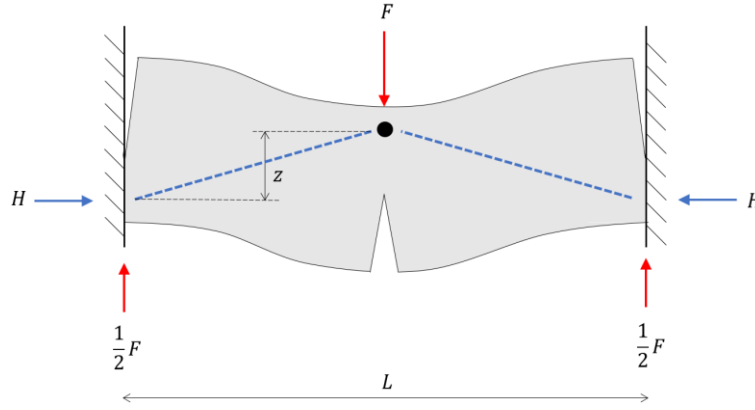
Figure 2.15: Support reactions and resultant compressive arch for a laterally restrained concrete slab strip.

Vecchio and Tang performed experimental tests of restrained and unrestrained large-scale reinforced concrete slabs under concentrated midspan loads [5]. One of the conclusions from the research was that geometrical nonlinearity significantly reduces the beneficial capacity effects of the restrained slab. Ignoring second-order effects would therefore lead to an overestimation of the failure load. The cause mentioned by the researchers was that large deflections of the slab, in combination with high axial compressive forces will lead to secondary moments that reduce the load-bearing capacity. However, the paper does not present a detailed explanation or quantification of this second-order effect. It is of great importance for this thesis to research this reduction effect based on simple structural mechanics principles.

The arching action in a laterally restrained concrete slab is further studied based on Figure 2.15. After significant deformations have occurred and the three plastic hinges at the supports and midspan are formed, the horizontal support reaction needs to make moment equilibrium with the vertical support reaction. Therefore, the rotational equilibrium in the black dot must be satisfied [29]. This entails that the positive bending moment generated by the vertical load F is equal to the resisting negative bending moment caused by the introduced horizontal compressive force H. The expression below is the result {2.6}.

$$H \cdot z = \frac{1}{2} F \cdot \frac{1}{2} L \quad \Big| \quad \{2.6\}$$

H is a function of F; the higher the vertical load, the larger the deformations and the higher the horizontal compressive forces. The force couple $H \cdot z$ indicates the magnitude of the negative bending moment and of therefore the magnitude of the arching action. It holds that the load-bearing capacity is directly and linearly related to the magnitude of the arching action. $H \cdot z$ is not only influenced by an increase in the vertical load, but also by a change of the position of the compressive arches. As a consequence of the position alteration of the resultant compressive arch, the lever arm z will be influenced. Two main causes lie at the basis of this change of position and thereby the change of the magnitude of $H \cdot z$.

(1) **Increase in the compression zone height** will cause a reduction of the internal lever arm z. As the acting load is increasing, the compressive stresses at the upper part of the midspan cross-section and the lower part of the slab strip end cross-section will rise. This is caused by both bending action and arching action. The ratio between the bending action and the arching action depends on the degree of lateral restraint; the higher the degree of lateral restraint, the more the vertical load will be transferred

by arching action in relation to bending action. In other words, the degree of lateral restraint is positively related to the magnitude of arching action. As a result of the rise of the compressive stresses, the height of the compression zones will increase and the centroid of the stress distribution will shift, which will cause a decrease in the internal lever arm as shown in Figure 2.16.

The effect of the increase in the compression zone is that the force couple $H \cdot z$, and consequently the magnitude of the arching action as well as the load-bearing capacity, decreases. Note that the net decrease in capacity is often not noticeable because in contrast to the internal lever arm, the load does increase. It could therefore be the case that the arching action increases despite a decrease in the internal lever arm.

(a)   (b)
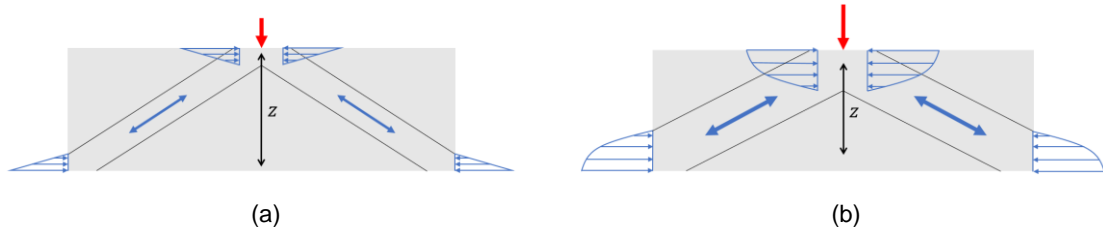
Figure 2.16: Small load and large internal lever arm of the arch (a); large load and small internal lever arm of the arch (b).

(2) **Increase in the midspan deflection** will cause a tilt of the compressive arch and thereby a reduction of the internal lever arm z. A visualization of this effect is given in Figure 2.17. The reduction is caused by a change of geometry and is therefore a GNL effect.

The effect of the increase in the midspan deflection is that the force couple $H \cdot z$, and therefore the load-bearing capacity, decreases. It is very important to note that this decrease in arching action will only be discovered in a structural analysis in which geometrical nonlinearity is accounted for.

(a)   (b)
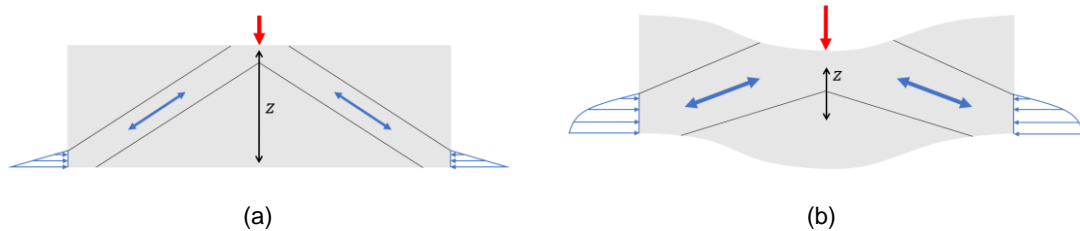
Figure 2.17: Small deflection and large internal lever arm of the arch (a); large deflection and small internal lever arm of the arch (b).

Equation {2.6} can also be influenced by a change of span length. However, the relative increase or decrease in the span length will in most cases be negligible, especially because the structure is partially or fully laterally restrained. It is for this reason that this thesis will assume a constant span length for all models of structures.

It can be concluded that the magnitude of CMA and the subsequent arching action is depending on the degree of lateral restraint and the deflections of the structure. The degree of lateral restraint is determined by the boundary conditions and is independent of geometrical changes of the structure. Therefore, the decrease in the internal lever arm due to the shift of the centroid of the compressive stresses will affect both a GL and a GNL model equally. In contrast, the influence of deflections on the internal lever arm is only apparent in GNL models.

As stated above under (2), geometrical nonlinearity could decrease the arching action and the load-bearing capacity. This finding is consistent with the research of Vecchio and Tang [5]. However, research on this effect and its magnitude is lacking. This effect could be of great importance for determining the actual behaviour of a restrained concrete slab, for instance during re-calculations with NLFEA. Hence, it is relevant to accurately quantify the effect of geometrical nonlinearity for a variety of concrete slab strip dimensions and boundary conditions in order to contribute to the knowledge on restrained concrete slabs. Analytical and numerical studies

are performed to quantify the capacity increase due to CMA and the second-order reduction effect. First, further knowledge about geometrical and material nonlinearity is gathered and presented on the basic nonlinear models from the literature in chapter 3.

3

Analyses of basic nonlinear models

3.1. Introduction

Geometrical nonlinearity affects the structural response because the geometry of a structure changes as a result of the loads. GNL effects will always have at least a small influence, because deflections of a structure will occur inevitably. These effects can have a significant impact if large deflections occur. Since the relation between the load and the displacement changes because of GNL effects, the response either gets stiffer or less stiff if these effects are included in the structural analysis. Moreover, the ductility can be altered under influence of these effects.

This chapter examines the influence of second-order effects on the response of basic nonlinear models. Also, the effect of combining geometrical nonlinearity with material nonlinearity is investigated. The main goal is to show and explain the effect of the nonlinearities on the response of the basic models in order to better understand the behaviour of more complex structures. First, the influence of geometrical nonlinearity, associated with the change of stiffness, is illustrated by an analytical example from the literature of a cantilever beam (3.2). Thereafter, the effect of material and geometrical nonlinearity is studied for two basic analytical models: section 3.3 discusses a rigid bar model and section 3.4 contains a detailed elaboration of a truss model. A finite element model of the truss is made to validate the analytical results (3.5). Also, finite element modelling is used to be able to combine material nonlinearity and geometrical nonlinearity.

3.2. Cantilever beam model

Geometrical nonlinearity affects the response of a cantilever beam loaded normal to the beam axis, as it does for all structures with a finite stiffness. The effect is however negligible if the shape of the structure hardly changes. It therefore holds that the magnitude of the GNL effect depends on the magnitude of the deflections and displacements compared to the dimensions of the structure; the effect will increase with larger deflections, because the deformed geometry will differ more and more from the undeformed geometry.

The mechanical model of the cantilever beam is shown in Figure 3.1. The vertical load is represented by a concentrated load at the free end, but it could also be a uniformly distributed load (UDL), which would be orientated normal to the beam axis as well.
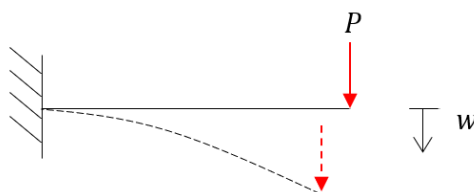
Figure 3.1: Mechanical model of a cantilever beam subjected to a point load.

Research has been conducted on the GNL behaviour of the cantilever beam compared to the behaviour predicted by the classical beam theory. Barten [30] first proposed a theoretical method for predicting the deflection of a cantilever beam loaded by a concentrated vertical load at the free end. Bisshopp and Drucker [31] also developed a method for concentrated loads, while Rohde [32] incorporated a UDL in her theory for cantilever beams.

Assumptions for these methods were that the length of the beam was constant and that deformations were elastic according to Euler-Bernoulli theory. It was also assumed that the load would remain vertically orientated, which means that it will not remain perpendicular to the beam axis. Thus, the principle of follower forces was not considered in their methods.

The results of the methods showed a nearly similar GNL effect and corresponding influence on the response, which can be outlined in a load-deflection diagrams (see Figure 3.2). It is important to note that the diagram in Figure 3.2a shows the deflection on the x-axis, while Figure 3.2b shows the deflection on the y-axis. Also, note that the deflection, as well as the load values, are shown as factors in which geometrical properties of the cantilever beam are included. However, the exact values are irrelevant since the focus is on the relative difference between the GL and GNL response.
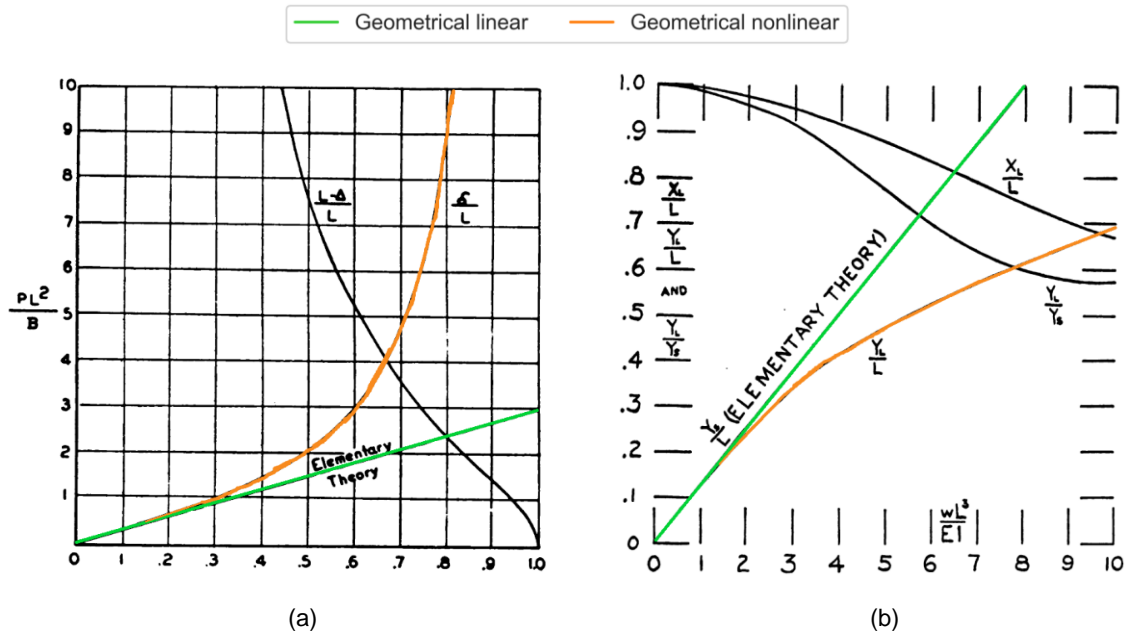
Figure 3.2: Load-deflection diagrams of a cantilever beam loaded by a concentrated load (a) and by a UDL (b) [(a) adapted from [31]; (b) adapted from [32]]

Their results show that the GNL effect, which is the difference between the graphs, increases for larger deflections. An important finding from the results is that the GNL model has a stiffer response than the GL model. This insinuates that the vertical deflection decreases, and the load-bearing capacity increases for the cantilever beam if geometrical nonlinearity is included. For small deflections, the linear model can very accurately predict the response of the cantilever. After significant deformations have occurred, the linear model will deviate too much from the nonlinear model to accurately predict the response.

3.3. Rigid bar model

3.3.1. Introduction

The rigid bar model in Figure 3.3 is proposed by Hartsuijker and Welleman in [33]. The bar with length l is simply supported at the bottom, which means the translations of the bar are restrained while it can freely rotate. At the top, the bar is subjected to a point load F and supported by a translational spring with spring stiffness k. w_o is the initial skew at the top and the horizontal displacement w is the considered degree of freedom.
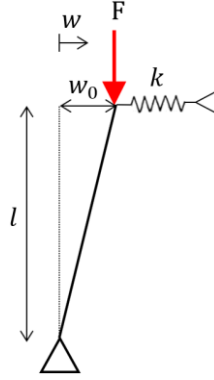
Figure 3.3: Rigid bar model.

It can be assumed that the moment arm of the spring force is equal to the length of the bar because this length is much greater than the displacement w. The point load F can be expressed as a function of the displacement w. This is done on the basis of a linear-elastic (LE), a geometrical nonlinear (GNL), an elastic-plastic material nonlinear (MNL(EP)) and a material plastic model (M(P)). The geometrical nonlinearity can also be combined with the elastic-plastic (GNL+MNL(EP)) and full plastic material models (GNL+M(P)). Note that the LE, the MNL(EP) and the M(P) model are GL models.

3.3.2. Equilibrium equations

The response can be obtained by deriving the moment equilibrium equation for all the models:

- **LE:** Equilibrium is reached when the moment resulting from the spring force is equal to the moment resulting from the point load F. Since linearity is assumed, the moment resulting from the point load F must be derived from the undeformed geometry. Therefore, its moment arm has a constant value w_0. Now, equation {3.1} holds, leading to an expression for the point load F {3.2}.

$$F \cdot w_0 = k \cdot l \cdot (w - w_0) \quad \text{\{3.1\}}$$

$$F = k \cdot l \cdot \frac{w - w_0}{w_0} \quad \text{\{3.2\}}$$

- **GNL:** When geometrical nonlinearity is considered, the moment resulting from the point load F must be derived from the deformed geometry. Therefore, its moment arm is equal to the horizontal displacement w. Now, equation {3.3} holds, leading to an expression for the point load F {3.4}.

$$F \cdot w = k \cdot l \cdot (w - w_0) \quad \text{\{3.3\}}$$

$$F = k \cdot l \cdot \frac{w - w_0}{w} \quad \text{\{3.4\}}$$

- **MNL(EP):** The spring is assumed to behave elastic-plastic; before the yielding force in the spring N_p is reached, it shows linear-elastic behaviour and thereafter it enters the non-linear plastic region (see Figure 3.4). After the proportionality limit is reached, the point load F remains constant. This results in two expressions (see {3.5}, {3.6}) for the point load F.

$$w < w_p \quad \rightarrow \quad F = k \cdot l \cdot \frac{w - w_0}{w_0} \quad \Big| \quad \{3.5\}$$

$$w \geq w_p \quad \rightarrow \quad F = k \cdot l \cdot \frac{w_p - w_0}{w_0} \quad \Big| \quad \{3.6\}$$
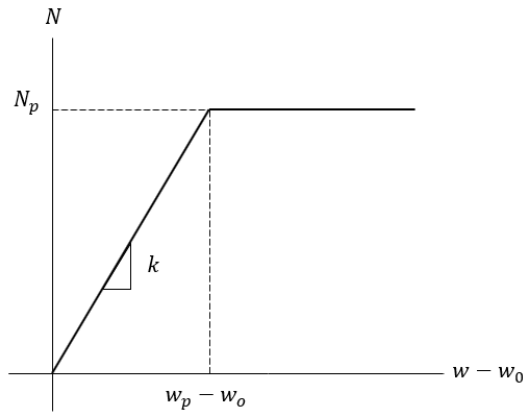
Figure 3.4: Elastic-plastic material behaviour of the spring.

- **M(P)**: The spring is assumed to show full plastic material behaviour. The spring force remains constant and is therefore independent of the displacement (see Figure 3.5). F will also be constant in the resulting static configuration, and its value is given in {3.7}.

$$F = \frac{N_p \cdot l}{w_0} \quad \Big| \quad \{3.7\}$$
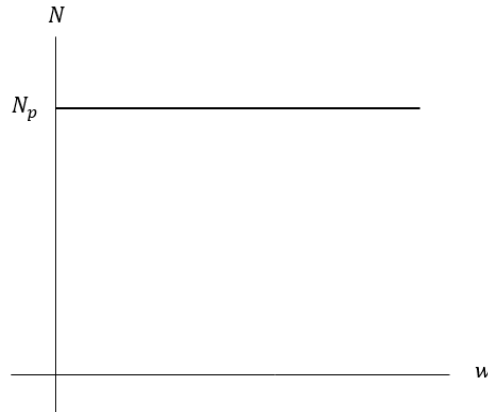
Figure 3.5: Full plastic material behaviour of the spring.

3.3.3. Results and discussion

The parameter values of the rigid bar model are defined in Table 3.1, and the results are presented in the load-displacement diagram in Figure 3.6. The displacement w is similar to the initial displacement w_0 and F equals zero if the graphs intersect with the x-axis.

Parameter	Value	Unit
l	1000	mm
w_0	1	mm
w_p	1.8	mm
N_p	800	kN
k	1000	N/mm
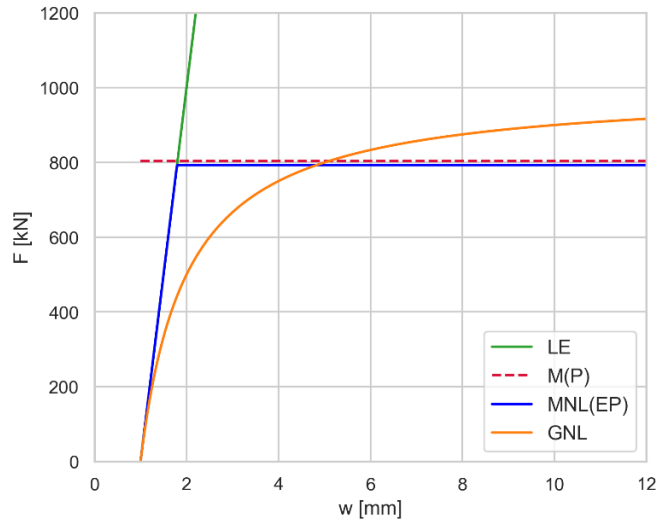
Table 3.1: Parameter values for the rigid bar model.

Figure 3.6: Load-displacement diagram of the rigid bar model for a LE, M(P), MNL(EP) and GNL model.

In the LE model, which does not consider any nonlinear effects, the point load F is directly proportional to the horizontal displacement w. This is because the equilibrium equations are written based on the undeformed geometry. In the GNL model, the graph representing the relationship between F and w has a nonlinear hyperbolic shape. The displacement is substantially increased when the point load is approaching the value $F = k \cdot l$. Thus, the response of the GNL model is much less stiff than that of the LE model.

In the MNL(EP) model, the structural system shows linear behaviour up until the spring force reaches the proportionality limit. Thereafter, the spring shows plastic behaviour and the horizontal displacement w is increasing while F remains constant. Full plasticity is assumed for the M(P) model, which results in a horizontal graph. This is because the spring force, which has a constant value from the start of the analysis, is linearly related to the vertical load F due to the neglect of geometrical nonlinearity.

Combination of nonlinearities

It is analysed what the response of the rigid bar model will be if geometrical nonlinearity is combined with elastic-plastic or with full plastic material behaviour.

- **GNL+M(P):** Full plasticity assumes the spring force is not depending on the displacement w and therefore has a constant value. Considering the second-order effects as well, the response becomes dependent on the displacement. The corresponding equilibrium equation is given below {3.15}. This results in an inversely proportional relationship between F and w, represented by the purple hyperbola in Figure 3.7. F must go down with increasing displacement in order to maintain the equilibrium.

$$F = \frac{N_p \cdot l}{w} \quad \bigg| \quad \{3.8\}$$

- **GNL+MNL(EP):** If elastic-plastic material behaviour is assumed, the material behaves physically linear before the yield force in the spring is reached. The response in this range can be described by equation {3.4} of the GNL model and is therefore equal to the orange hyperbola in Figure 3.6. Thereafter, the spring force, and therefore its resultant moment, remains constant. The response after $w = w_p$ can therefore be described by equation {3.8}. The intersection of the hyperbolas indicates the moment when the yield spring force is reached, and the stiffness of the structural system becomes negative (i.e. instability of the system).
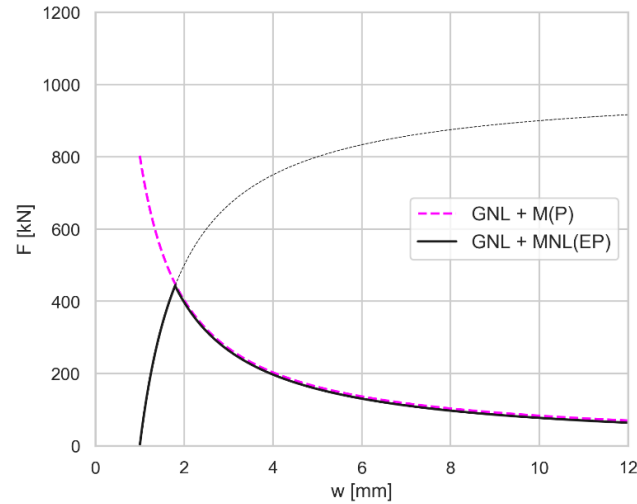
Figure 3.7: F-w diagram of the rigid bar model for a combination of GNL with MNL(EP) and M(P).

It can be concluded that nonlinearities have a significant impact on the response of the rigid bar model. Material nonlinearity induces a kink in the graphs when the yield spring force is reached. Therefore, the maximum load in the MNL(EP) models is lower than in the LE model after a certain displacement occurred. Geometrical nonlinearity results in a deflecting curve in the F-w diagram, leading to an increase in displacement for similar load values. Thus, a GL analysis leads to a stiffer response than a GNL analysis. It can therefore be concluded that the load-bearing capacity of the rigid bar is lower for the GNL calculation compared to the GL one.

3.4. Analytical truss model

3.4.1. Introduction

A study by Guice and Rhomberg showed that the structural response of laterally restrained concrete slabs could be approximated by an analytical truss model [27]. The formation of internal arches (CMA) and the development of catenary action after large deflections (TMA) of the slab are closely related to the behaviour of a truss model (see Figure 3.8). It is for this reason that their force-displacement curves showed great similarities. The simple truss model can thus be used as an analogy for the concrete slab in order to predict its complex behaviour. Moreover, Bathe showed in [34] that geometrical nonlinearity significantly affects the structural response of the simple truss model. For these reasons, it is relevant to analyse the truss model in great detail.

(a)

(b)
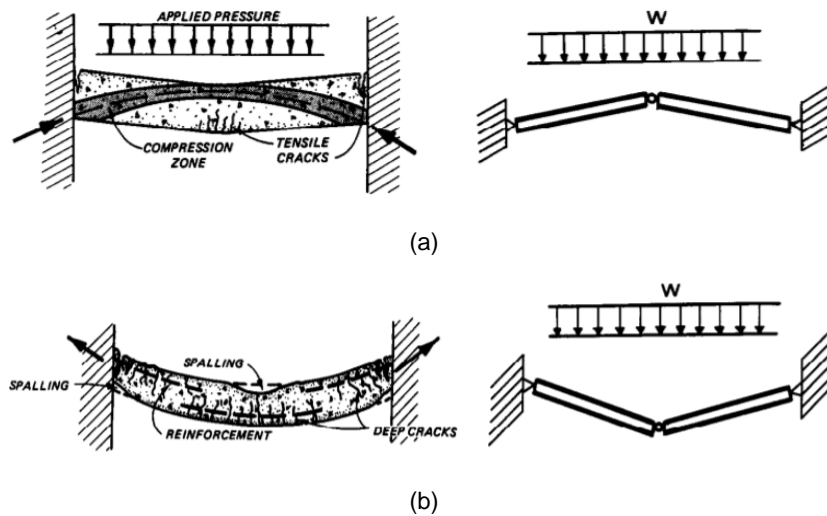
Figure 3.8: Truss analogy for CMA (a) and TMA (b) in a restrained concrete slab [27].

The truss consists of two identical truss elements simply supported as well as laterally restrained at both sides (see Figure 3.9). The model is often referred to as the 'three-hinged arch model' in literature, because the truss elements are hingedly connected to each other and the supports with a total of three hinges. The truss is loaded by a vertical point load in the middle and the axial stiffness of the elements is equal to EA. Poisson's ratio is assumed to be zero for the sake of simplicity. The dimensions of the model are given in Figure 3.9.
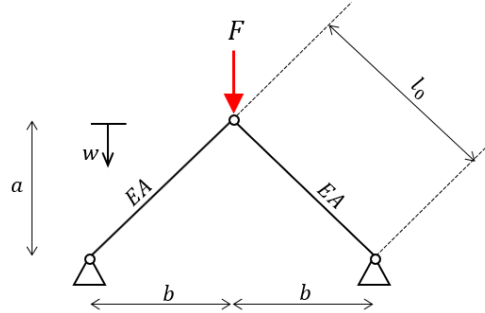
Figure 3.9: Truss model.

3.4.2. Equilibrium equations, results and discussion

The differences between a GL and a GNL analysis of the truss are investigated and explained. The material behaviour for both models is assumed to be linear (see Figure 3.10). The equations needed to obtain the load-displacement diagrams are given for the geometrical linear model (GL) and the geometrical nonlinear model (GNL).

- **GL / LE:** The kinematic equation {3.8} gives the relation between F and w based on the undeformed geometry. The constitutive equation {3.9} gives the relation between the strain and the internal normal force in the elements. The equilibrium equation {3.10} gives the relation between the normal force and the external load.
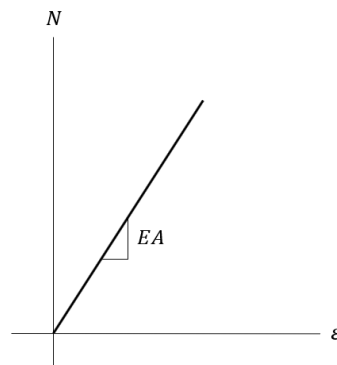
$$l_0 = \sqrt{a^2 + b^2} \qquad \{3.9\}$$

$$\varepsilon = -\frac{\frac{w}{l_0} \cdot a}{l_0} \qquad \{3.10\}$$

$$N = EA \cdot \varepsilon \qquad \{3.11\}$$

$$F = 2 \cdot N \cdot \frac{a}{l_0} \qquad \{3.12\}$$

Figure 3.10: Linear material behaviour of the truss model.

- **GNL:** The kinematic equation has now become nonlinear because the change of the length of the bar is taken into consideration when determining the strain (see {3.11} and {3.12}). The constitutive relation is similar to the one for the linear calculation (see {3.9}) because the axial stiffness is constant. The equilibrium equation {3.14} gives the nonlinear relation between the normal force and the external load.

$$l = \sqrt{(a - w)^2 + b^2} \qquad \{3.13\}$$

$$\varepsilon = -\frac{l_0 - l}{l} \qquad \{3.14\}$$

$$F = 2 \cdot N \cdot \frac{a - w}{l} \qquad \{3.15\}$$

The parameter values of the truss model are defined in Table 3.2, and the results are presented in the load-displacement diagram in Figure 3.11.

Parameter	Value	Unit
a	100	mm
b	1000	mm
l_0	1004.99	mm
E	30000	N/mm^2
A	100	mm^2
ε	0.00175	-
ν	0	-

Table 3.2: Parameter values for the truss model.
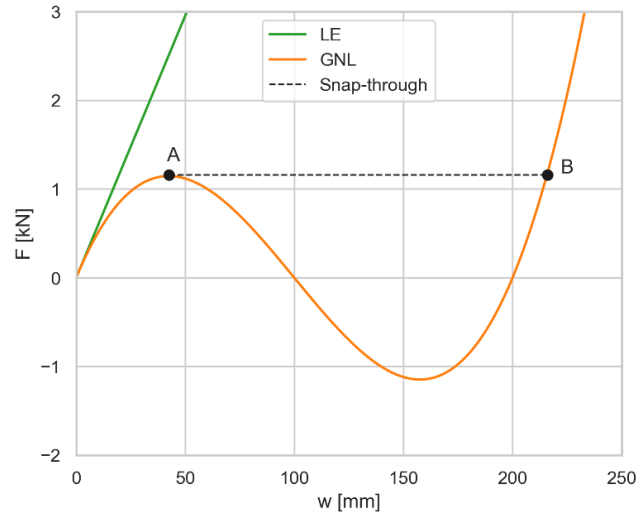
Figure 3.11: Load-displacement diagram of the truss model.

Geometrical linearity assumes the displacement w is directly proportional to the load F. The green curve in Figure 3.11 shows that, if the load is doubled, the displacement is also doubled when GNL effects are not considered. Due to deflections of the structure, however, the linearity of the structural system will disappear and the stiffness changes when the load is increased. The result is the orange curve in the force-displacement diagram of which every coordinate represents an equilibrium state of the structure.

Since the energy stored in the system is decreasing when the stiffness becomes negative, instability of the system occurs from point A onwards [35]. This curve also represents the equilibrium path that is followed when actual material behaviour is examined [34]. On the other hand, if such a truss structure is loaded by an incrementally increasing force during experimental research, or with forced-controlled analysis in finite element programs, the structure cannot cope with a decrease in the load just after point A and will therefore jump from point A to point C. This instability phenomenon is called snap-through [36].

It can be seen that the structural response is less stiff for the GNL analysis; the vertical load is lower for the same vertical displacement compared to the linear analysis. Also, it can be concluded that geometrical nonlinearity will affect the response only after a large vertical displacement has occurred. The values of the green and orange graphs are very close to each other for small vertical displacements (i.e. up to about 15 mm).

Explanation of GNL response

The GNL model leads to a constant change of stiffness with increasing displacements. This behaviour can be explained based on Figure 3.12. The normal force N in the elements is presented as a function of the displacement w, which results in a parabola with zeros at $w = 0$ and $w = 200$ (see Figure 3.12a). Although compressive forces are negative according to the convention in structural mechanics, to be able to properly explain the structural behaviour it is chosen to assume positive normal forces if the elements are compressed. Shortening of the truss elements will therefore be considered as a positive strain.

The maximum value of the strain, and therefore of the normal force N, is reached when the length of the truss elements is minimal. At that moment, the elements are completely horizontal. If the displacement is increased after that moment, the length of the elements will increase, resulting in a decrease in the strain and normal force. The normal force reaches zero again when the initial length of the elements is restored after 200 mm displacement. In the GNL calculation of the truss, the ratio between the vertical projection of the normal force and the normal force itself is decreasing with increasing displacements because the angle of the truss elements

becomes less steep. Since the vertical projection of the normal forces is equal to the vertical force F, the F/N-ratio will also decrease (see Figure 3.12b).

(a)   (b)
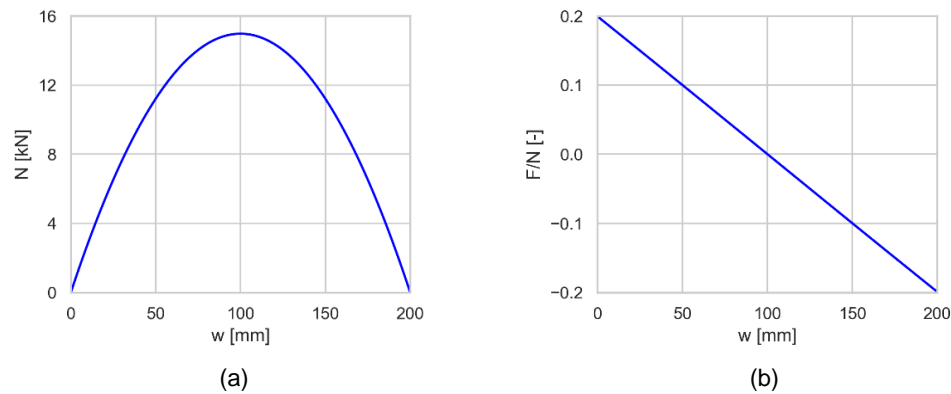
Figure 3.12: Normal force-displacement (N-w) diagram (a) and F/N-w diagram (b) of the truss model based on the GNL model.

The vertical force F must always make force equilibrium with the normal forces in the middle node. Both the normal force and its vertical projection are constantly changing with increasing displacements. This results in a sinusoidal-shaped graph in the F-w diagram. This information can now be used to extensively describe what happens in the five ranges and the two points of the GNL graph in Figure 3.13.

- **Range 1:** The normal force is substantially increasing, and the F/N-ratio is still large. Therefore, the vertical force F can increase in this range. It reaches a local maximum at the end of this range.

- **Range 2:** The normal force graph is concave down and increasing in this range. In order to meet the relatively low F/N-ratio, the vertical force F must go down because the increase in the normal force is not sufficient anymore.

- **Point A:** The vertical force has dropped to zero, because the elements are horizontal, and the normal force has no vertical projection anymore.

- **Range 3:** The vertical force gets a negative value, because the F/N-ratio drops below zero while the normal force is still positive and large. In order to make force equilibrium in the node at which the load is applied, the vertical force has to point upwards (i.e. F must become negative). Thus, the elements are still in compression when they already passed the horizontal. Therefore, the vertical force has to point upwards in order to fulfil the force equilibrium in the node.

- **Range 4:** Due to the substantial decrease in the normal force in this range, while the F/N-ratio decreases less substantially, the vertical force can become less negative again.

- **Point B:** The initial length of the truss elements is restored and all regarded quantities – strain, normal force and vertical force – are zero.

- **Range 5:** Tensile forces are introduced into the truss elements as they will be extended further and further. The negative normal forces allow the vertical force to become positive again because a positive F will make force equilibrium in the middle node. With increasing displacement, both the tensile force in the elements and the vertical force F will increase. The truss model is transformed from an arch mechanism into a catenary mechanism.
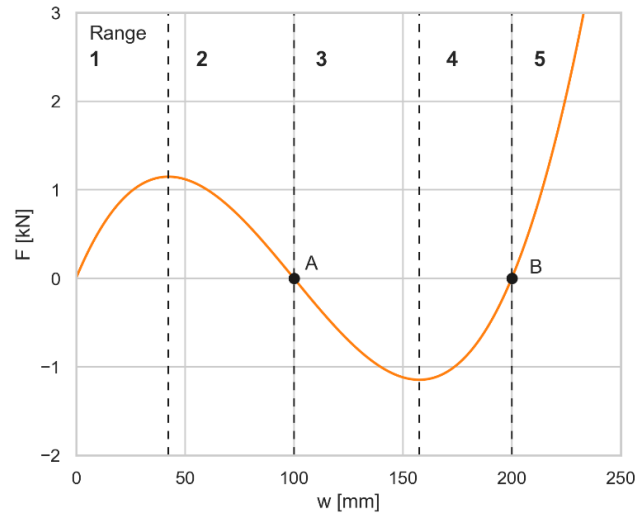
Figure 3.13: F-w diagram of the truss model for a GNL model divided into five ranges.

Lever arm principle

The LE and GNL model and their results can also be viewed in a different way. Instead of concentrating on the normal force in the truss elements, the focus can be laid on the support reactions and the requirement of equilibrium in the middle node, just as in section 2.3.4. The resulting support reactions need to make rotational equilibrium in the middle node of the truss model. The vertical support reaction ½ F creates a positive bending moment while the horizontal support reaction H creates a resisting negative bending moment. Hence, equation {3.15} must hold for any equilibrium state.

$$H \cdot z = \tfrac{1}{2} F \cdot b \quad\Big|\quad \{3.16\}$$

In the GNL model, the lever arm of H (referred to as z) reduces as the vertical load and deflection increase (see Figure 3.14). As a result, the resisting bending moment of $H \cdot z$ decreases with increasing displacement compared to the resisting moment in the LE model. This leads to increasingly divergent graphs of the GL and GNL model (see Figure 3.15). The stiffness and the maximum load in the plotted range are substantially reduced due to geometrical nonlinearity. The load is reduced by a factor of approximately 2.1 at a vertical displacement of 42 mm.
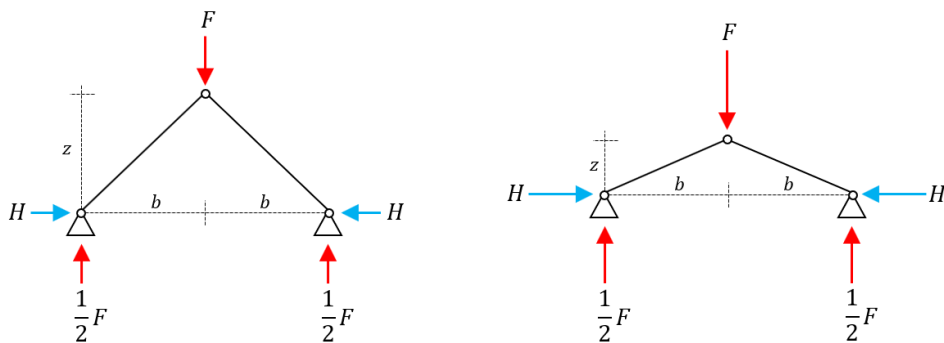
Figure 3.14: Decrease in lever arm z with increasing load and deflection.
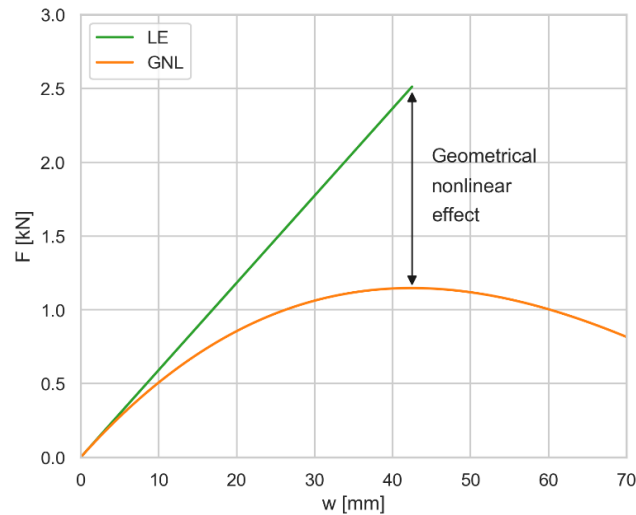
Figure 3.15: GNL effect on the response of the truss model with linear material properties.

Elastic-plastic and full plastic material behaviour

Geometrical nonlinearity is now combined with full plastic material behaviour. Also, geometrical linearity is combined with elastic-plastic and full plastic material behaviour. The results are presented in Figure 3.17.

- **MNL:** The kinematic and equilibrium equations are similar to the ones for the linear calculation (see equations {3.9} and {3.11}). Figure 3.16 shows the constitutive relation, which is a bilinear elastic-plastic relationship between the normal force and the strain. It should be noted that similar compressive and tensile material behaviour is assumed. The MNL model results in a bilinear relation between F and w. The structural response is linear up until the yield force is reached. After this limit, the normal force in the truss elements can no longer increase, resulting in a constant F. This behaviour is the same as for the rigid bar model (see section 3.3).
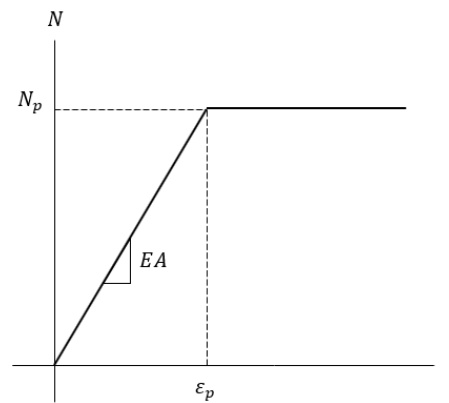
Figure 3.16: Constitutive relation of the MNL model for both compression and tension.

- **M(P):** The truss is assumed to show full plastic material behaviour. Therefore, the force is independent of the displacement and the plastic normal force will be present from the start.

- **GNL+M(P):** If geometrical nonlinearity is combined with full plastic material behaviour, the normal force is independent of the strain. Therefore, the graph of the GNL+M(P) model will follow the linearly decreasing pattern of the F/N-w diagram as long as the elements have not passed the horizontal yet. The normal force cannot decrease, so it will flip to tension the moment the horizontal is passed, which leads to a linearly increasing F.
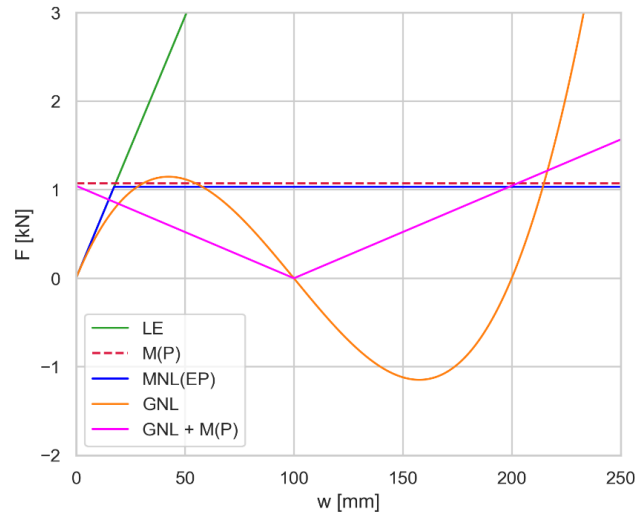
Figure 3.17: F-w diagram of the truss model for using a LE, M(P), MNL(EP), GNL and GNL+M(P) model.

Combination of nonlinearities

In order to solve the truss model with a combination of GNL and MNL(EP), an incrementally iterative solution procedure is required. Since such a solution procedure is complex to construct, and constructing it is irrelevant for this research, an analytical calculation with both nonlinearities included is omitted. The structural analysis program DIANA, which uses incremental iterative solution procedures for nonlinear analyses, is used instead. It is a powerful program to accurately predict structural behaviour by generating displacements based on the given geometry, loads and boundary conditions. The output consists among other things of cross-sectional stresses and strains, displacements, rotations, and reaction forces. The numerical method that is used to solve the differential equations is the finite element method (FEM).

3.5. Numerical truss model

3.5.1. Introduction

A 2D finite element model of the truss is made in order to combine geometrical and material nonlinearity. Also, the numerical results of the truss model can be compared with the analytical results. FEA is done with the FEM, which will be briefly introduced below.

The purpose of the FEM is to discretise continuum problems by reducing an infinite degree of freedom system to a finite degree of freedom system [37]. Because of this, problems that are too complex to solve analytically can still be solved. The continuum system is reduced to a discrete system by dividing it into a finite number of elements, which are connected to each other by nodes. The nodes in adjacent elements share the same displacement. Integration methods are used to determine the stress, strain and internal forces of each element based on the displacements.

FEA software can be used to accurately approximate the structural behaviour numerically. It can perform nonlinear analyses of complex models, which is essential for this research. However, FEA suffers from several drawbacks. First, the results are very much depending on the adopted mesh. If the element size is too small, the computational time will increase significantly. The analyses can then become rather costly. On the other hand, a relatively large element size could reduce the accuracy of the results. Furthermore, the results are largely influenced by the imposed boundary conditions. Therefore, the results of these analyses should always be treated with good care. Hence, analytical or experimental verification of the numerical results is often required. However, this could be difficult as analytical approaches are sometimes too complex or experimental research is lacking.

Geometrical linearity and nonlinearity in finite element analyses

In a MNL and GL analysis, the formulation of the equilibrium equations is based on the theory of small deformations, which entails that the geometrical properties of the elements are independent of any deformations and remain constant throughout the analysis. The theory assumes that the deformations are much smaller than the dimensions of the structure. In this case, the system of linear equations – represented by the stiffness matrix – is only depending on the variation of the material properties as a consequence of the change of deformations and displacements during the analysis. Thus, the calculation of the stiffness matrix for a particular load increment is not depending on the strains or rotations of the elements. Merely changing material properties will alter the stiffness matrix. In the case of linear material properties, the stiffness matrix will therefore be equal for each load increment because it is based on the initial geometry.

In a MNL and GNL analysis, the formulation of the equilibrium equations is based on the theory of large deformations, which means that the deformations can no longer be neglected compared to the dimensions of the structure. The equilibrium equations are now formulated by considering not only the changing material properties as a consequence of the deformations, but also the deformations themselves. In the case of linear material properties, the stiffness matrix will therefore be different for each load increment because it is based on the changing geometry.

3.5.2. Description of the model

The FEM-model of the truss consists of two lines that represent the truss elements. The translational supports restrain the displacement in x and y-direction. Furthermore, a vertical support must be added to the middle node in order to apply the vertical load as a downward displacement.
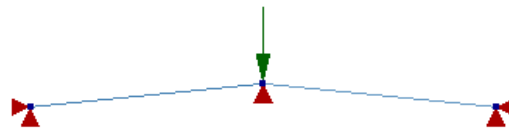
Figure 3.18: FEM-model of the truss.

Elements

Regular truss elements do not have the required degrees of freedom perpendicular to the element axis to perform a GNL analysis, which is why enhanced truss elements are used. Both regular and enhanced truss elements only have a stress component in their axial direction. They can be used to model bars that are hingedly connected on both sides and have a large length compared to their cross-sectional dimensions. It is assumed that the bending and shear deformations are zero. In contrast to regular truss elements, enhanced truss elements have an additional degree of freedom perpendicular to the element axis, which makes them suitable for a GNL analysis. In a two-dimensional DIANA model, the enhanced truss element is abbreviated as L4TRU element (see Figure 3.19). The element has two nodes and u_y is the additional degree of freedom perpendicular to the truss element axis.
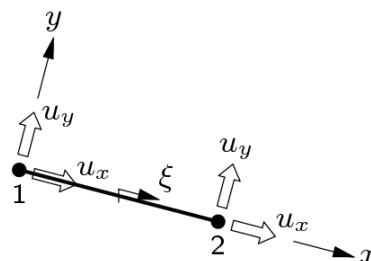
Figure 3.19: L4TRU element [38].

3.5.3. Analyses

The FEAs are displacement-controlled, which means that the load is introduced as a prescribed displacement. The final applied load is a vertical downward displacement of the middle node of 250 mm. It is incrementally applied with 100 load steps of 0.01, counting up to a load factor of 1.0. The mesh consists of two elements in total, because truss elements do not bend. The analyses which are performed are LE, M(P), MNL(EP), GNL, GNL+M(P) and GNL+MNL(EP). The numerical calculation is done with the Newton-Raphson method, which is the default calculation method in DIANA.

3.5.4. Results and discussion

The results of the analyses are shown in the load-displacement diagram in Figure 3.20. Also, the normal force is plotted against the displacement for the GNL analyses (see Figure 3.21).
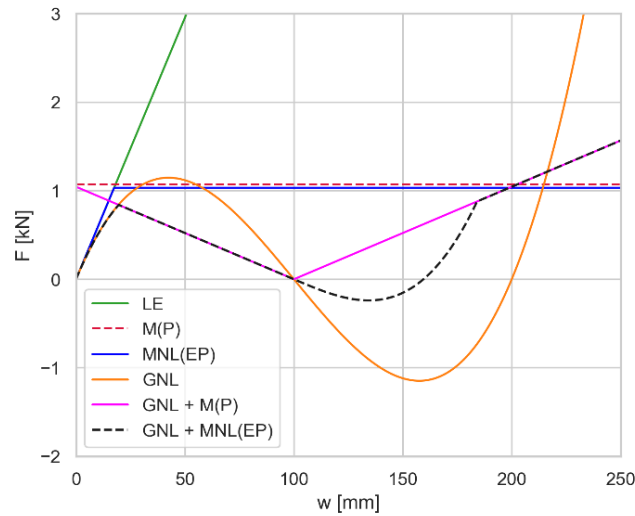
Figure 3.20: Load-displacement diagram of the numerical truss model for different analyses.
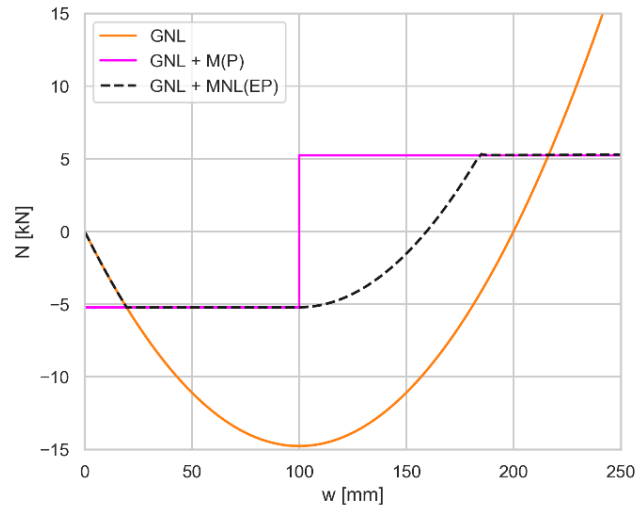
Figure 3.21: Normal force-displacement diagram for the GNL, GNL + M(P) and GNL + MNL(EP) analysis.

The first finding derived from Figure 3.20 is that the results of the numerical analyses correspond to the analytical results in section 3.4 (see Figure 3.17). This implies that the analytical equations of the truss model contain no errors.

The GNL+MNL(EP) model is equal to the GNL model when the material is still in the linear-elastic range. Entering the nonlinear-plastic range if the yielding force is reached will lead to instability of the system with a negative

slope in the F-w diagram. This is because the normal force N can no longer increase and the relation between the force and the displacement has become inversely proportional; with increasing displacement, the force must go down in order to maintain the equilibrium. The GNL+MNL(EP) model now follows the path of the GNL+M(P) model until the truss elements are horizontal. Then, the graph follows a likewise path as the GNL model, but the negative F will become positive earlier. The reason is that for the GNL+MNL(EP) model the normal force is limited by the yield value and therefore has a lower value at the moment when the truss elements are horizontal (see Figure 3.21). If the displacement is increased after the horizontal is passed, the normal force reaches zero much faster than in the GNL model. Thereafter, the tensile forces in the elements will be increased until the yield limit is reached again, resulting in a kink in the F-w diagram (see Figure 3.20). After the kink, the normal force is constant, and the enlargement of the vertical force will therefore only be due to the increase in the angle of the truss elements (i.e. changing of the 'force triangle'). The GNL+MNL(EP) model will follow the same path as the GNL+M(P) model in this range.

As can be seen in Figure 3.22, geometrical nonlinearity reduces the load-bearing capacity of the truss with nonlinear material properties by a factor of approximately 1.2. This reduction effect is present from 0 to 200 mm displacement. A similar effect was seen for the truss with linear material properties (see section 3.4). Again, this reduction is due to a decrease in the lever arm of the horizontal support reaction.
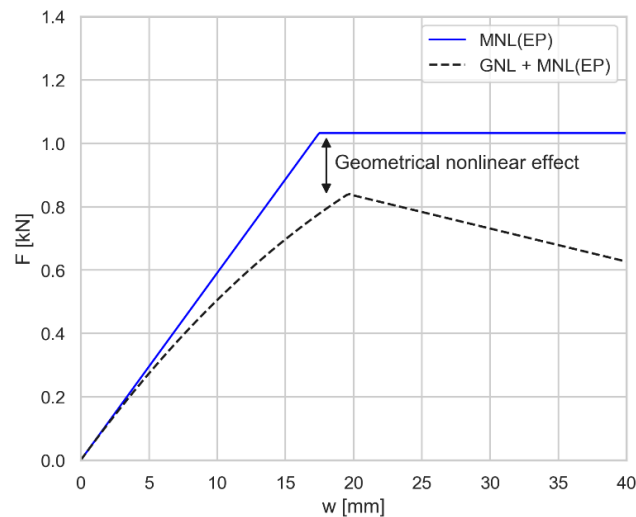
Figure 3.22: GNL effect on the response of the truss model with nonlinear material properties.

Comparison truss model and restrained concrete slab

The load-displacement curves of the truss model (see Figure 3.11) and the idealized laterally restrained concrete slab (see Figure 2.14) are very similar. The finding of Guice and Rhomberg in [27] is therefore analytically proven. Both curves can be split into three regions:

(1) **First increasing part:** The lateral restraint causes the built-up of horizontal forces that provide an extra load-bearing mechanism for the concrete slab. The load increases in this region due to both bending and arching action. For the truss model, the horizontal forces and the consequent resisting bending moments lead to the increase of the load-deflection curve. This can also be attributed to the lateral restraint.

(2) **Decreasing part:** The decreasing region of the truss curve is purely caused by geometrical nonlinearity, while the decreasing region of a concrete slab load-deflection curve is due to a combination of geometrical nonlinearity and crushing of the concrete in the compression zone. Yet, the lever arm principle can be applied to both the truss and the concrete slab. Reduction of the lever arm causes the resisting bending moment and the load-deflection curves to decrease. This is due to the second-order effect related to the deflection.

(3) **Second increasing part:** The load is increased again due to catenary action in the concrete slab. The increase of the load-displacement curve of the truss model is caused by the built-up of tensile forces in the truss elements.

Due to the similarities between the concrete slab and the truss, the resultant compressive arch and the resultant tensile tie in the concrete slab can be seen as internal truss elements which directly transfer the load to the support by arching action and catenary action. The arching action in the concrete slab shows great similarity with the load-bearing mechanism of the truss: both mechanisms transfer the load by compression. The tensile action of the concrete slab shows great similarity with the load-bearing mechanism of the truss after large deflection: both mechanisms transfer the load by tension. A large difference between the concrete slab and the truss model is that the reinforced concrete slab can also transfer the load by bending, resulting in two load-bearing mechanisms. Therefore, the graph representing the idealized response of the concrete slab has higher values than the load-displacement curve of the truss which intersects with the x-axis.

3.5.5. Model modifications

Additional vertical spring

An additional vertical translational spring is added to the middle node of the truss to model the additional load-bearing capacity due to bending. Consequently, the equilibrium equation of the GNL model (see equation {3.15}) changes to equation {3.18}.

$$F = 2 \cdot N \cdot \frac{a - w}{l} + k \cdot u \quad \Big| \quad \{3.18\}$$

The influence of varying the translational spring stiffness is examined for the GNL model only. The analytically obtained results are presented in a load-displacement diagram.
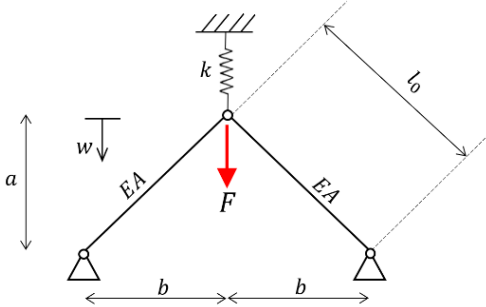
Figure 3.23: Truss model with additional vertical spring.
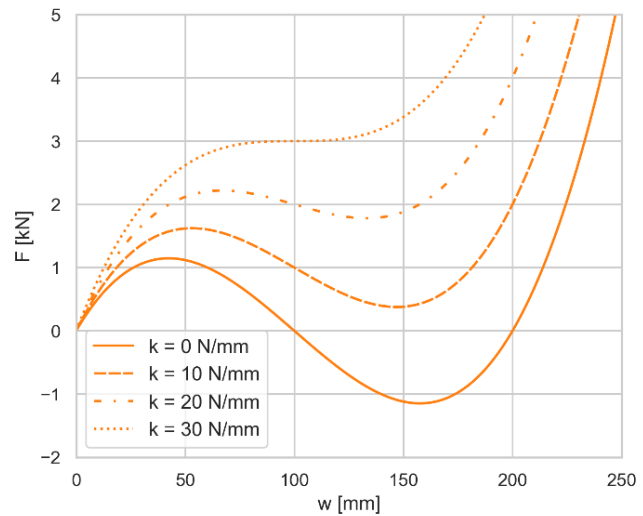
Figure 3.24: Effect of vertical spring stiffness on the response of the GNL model.

Figure 3.24 shows that the vertical spring influences the slope of the first increasing and decreasing parts. It holds that the greater the translational spring stiffness, the greater the structural stiffness of the truss. It can be concluded that the load-displacement behaviour of the truss model with an extra vertical spring shows great similarities with the idealised behaviour of a fully restrained concrete slab. Because the load values increase due to the vertical spring, the load-displacement diagram of the truss now resembles that of the concrete slab even more. The extra load-bearing capacity due to bending can be modelled reasonably well by the addition of the vertical spring.

Degree of lateral restraint

The basic truss model assumed that the supports are fully laterally restrained. However, full lateral restraint can often not be achieved in practice and if the truss model has zero lateral restraint, it cannot take up any load. Therefore, the actual degree of lateral restraint is between these two extremes. The influence of the degree of lateral restraint on the response can be studied by replacing the full lateral restraints with translational springs (see Figure 3.25). The spring stiffness k represents the degree of lateral restraint and can be varied to investigate its influence. A boundary spring connection in the x-direction is added to the support nodes to model the degree of lateral restraint. The SP1TR element in DIANA is used for this [38]. The two fully restraining supports are replaced by roller supports.
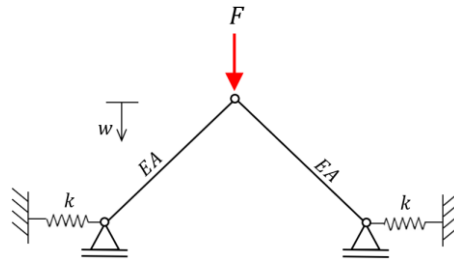
Figure 3.25: Truss model with translational springs in the lateral direction.

From the results in Figure 3.26 it can be concluded that the degree of lateral restraint affects the response; both the stiffness and the peak load in the first increasing part become larger with increasing lateral stiffness. Also, the tensile action is larger for higher spring stiffnesses. The degree of lateral restraint thus affects the degree of compressive and tensile action in the truss. Since the load-displacement behaviour of the truss is rather similar to that of a concrete slab, it is very likely that the magnitude of arching action will increase if the concrete slab is more laterally restrained. This is in line with the literature review, which stated that the arching action depends on the degree of lateral restraint and the relative share of arching action in relation to bending action increases for higher restraint values. The sensitivity analysis in chapter 6 will elaborate on this regarding concrete slabs.
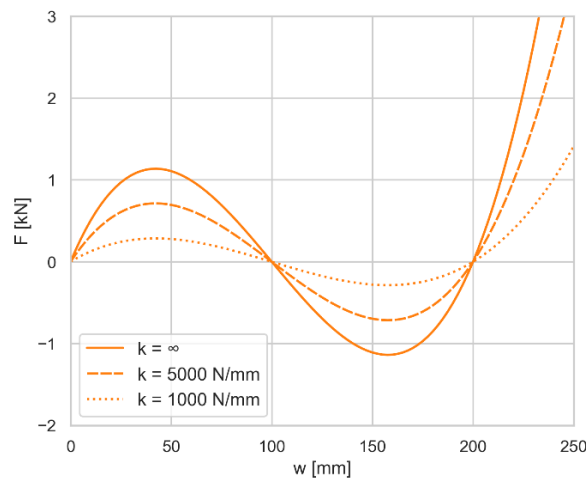
(a) Load-deflection GNL

(b) Load-deflection GNL+MNL(EP)
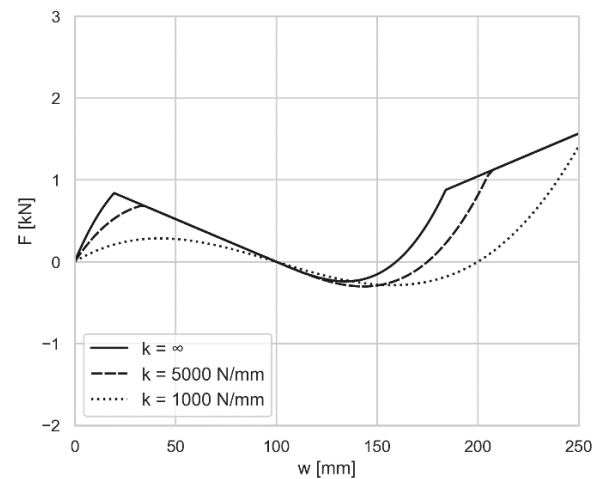
(c) Normal force-deflection GNL   (d) Normal force-deflection GNL+MNL(EP)
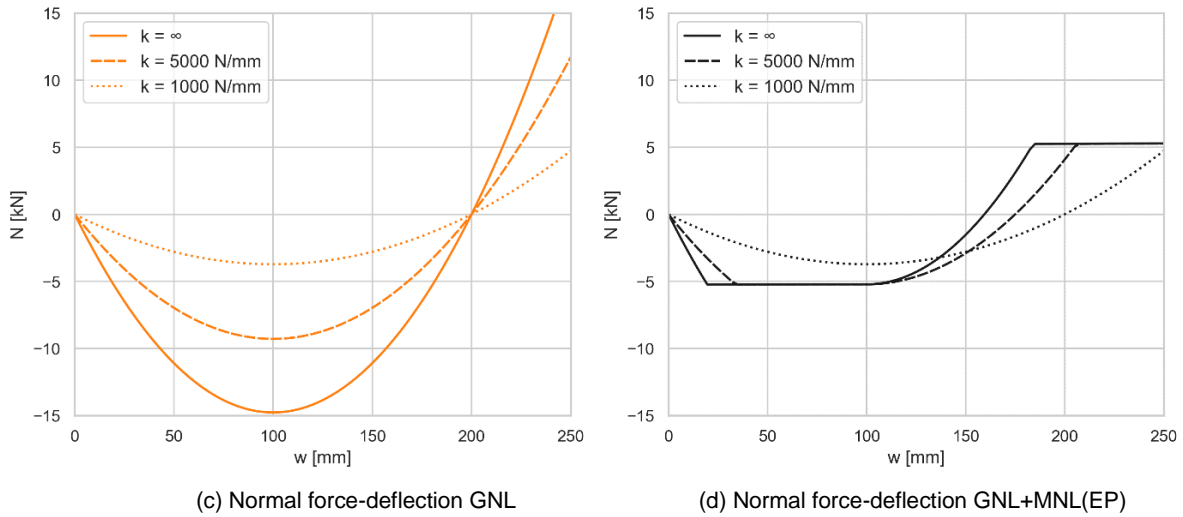
Figure 3.26: Results of the truss model for different degrees of lateral restraint.

3.6. Conclusion

Geometrical nonlinearity significantly affects the response of a cantilever beam, a rigid bar and a truss. The cantilever beam shows a stiffening effect, while the rigid bar and the truss shows a decrease in the resistance load due to geometrical nonlinearity. However, large deflections must be allowed for second-order effects to play a significant role in the load-displacement behaviour of the structures. This confirms the statements in the literature study that geometrical nonlinearity is of importance when there is a large difference between the deformed geometry and the undeformed geometry. Also, it holds that the larger the deflection, the larger the GNL effect. Elastic-plastic material behaviour ensures that the stiffness is changed at a certain moment in the analysis, resulting in a kink in the load-deflection diagram of the three examined models.

The response of a truss with an additional spring at the node where the truss elements meet shows great similarity with the load-deflection behaviour of a restrained concrete slab. The arching action in the concrete slab shows great similarity with the load-bearing mechanism of the truss: both mechanisms transfer the load by compression.

Geometrical nonlinearity reduces the stiffness and load resistance of the truss because the lever arm of horizontal forces at the supports decreases with increasing deflection. Consequently, the resisting bending moments at the supports are reduced. Thus, a GL model leads to a higher capacity of the truss than a GNL model. Higher degrees of lateral restraint lead to higher stiffness and peak load, because the degree of restraint determines the magnitude of the horizontal forces at the supports.

4
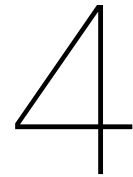
Analytical model

4.1. Introduction

In addition to bending, an alternative load path is introduced by CMA, which provides laterally restrained concrete slabs with two load-bearing mechanisms: 1) bending action; and 2) arching action. McDowell et al. [9] developed an analytical theory to estimate the arching action in masonry walls. Their model included geometrical nonlinearity, because real structural behaviour is also nonlinear.

The analytical approach for the masonry wall model is used to create a new modified model for laterally restrained concrete slab strips in order to predict its enhanced capacity. For simplicity reasons, only a single strip of a concrete slab is analysed. Therefore, tri-axial stress conditions and double bending are not accounted for in the model. Furthermore, the GNL model of the concrete slab strip could be converted into a GL model by neglecting the deflections of the structure when determining its response. Comparison between these two models could show the effect of geometrical nonlinearity on the enhanced ultimate capacity of laterally restrained concrete slab strips.

4.2. Description of the model

A new analytical model of a restrained reinforced concrete slab strip is made by utilizing the approach of McDowell et al. [9]. It is explicitly stated whenever assumptions, methods or formulas of the approach of in [9] are used. All steps for the set-up of the analytical model are discussed in detail. Several modifications have been made to the approach of McDowell et al. not only to change the material properties properly, but also to better predict the actual structural behaviour of the slab strip. The changes are named and described below:

- The slab strip is made of concrete instead of masonry, the material properties are adjusted accordingly.

- Steel reinforcement is included in the model, because modern concrete structures always have steel in them to take up the tensile forces and avoid brittle failure.

- Realistic unloading of concrete fibres is considered in the model.

- The contribution of the steel reinforcement in the compression zone is considered in the model.

The reinforced concrete slab strip is supported at two ends by its surrounding structures. Figure 4.1 shows an example of possible surrounding structures that provide the restraints of the slab strip. The basic analytical model assumes that the surrounding structures provide a full restraint, resulting in a perfectly clamped slab strip. Translational movement of the surrounding structures is not considered in the model, because it is assumed that the span length is constant.
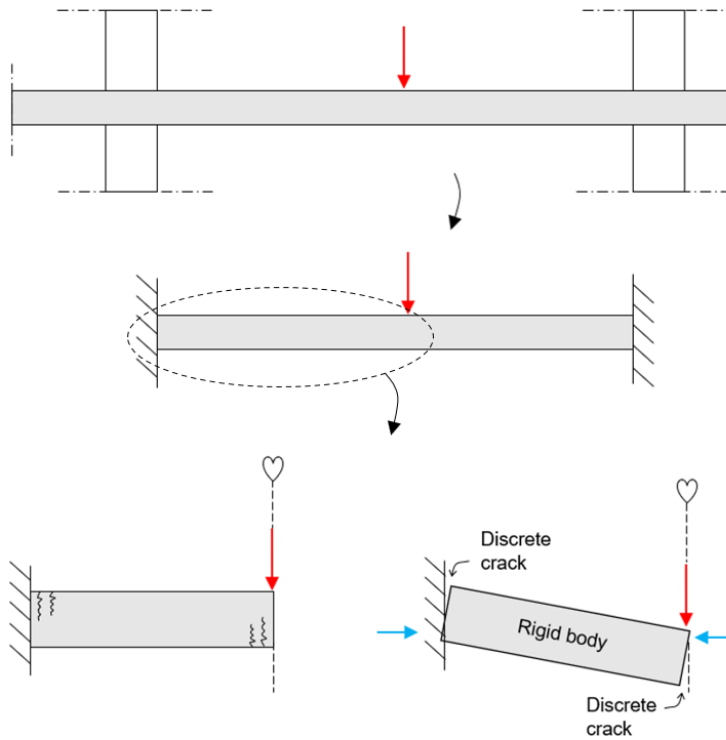
Figure 4.1: Origin of the analytical model of the rigid slab strip.

As a result of the applied vertical loading, the concrete slab strip will crack in the tensile zones. For a UDL, the flexural cracks start at the outer fibres of the cross-section at each slab strip end, and will thereafter also appear at the bottom of the middle section. For a point load at midspan, the flexural cracks will appear simultaneously in the tensile zones at the support and midspan (see Figure 4.1) because the structural system of the half slab strip is symmetrical. The bending moment and shear force are equal at the support and midspan through the entire loading phase (see Figure 4.2). A further increase in the load will lead to widening and lengthening of the cracks. As a consequence, plastic hinges will occur at these sections while the rest of the slab strip remains elastic. Because the clamped slab strip is statically indeterminate, redistribution of forces will prevent the strip from failing.
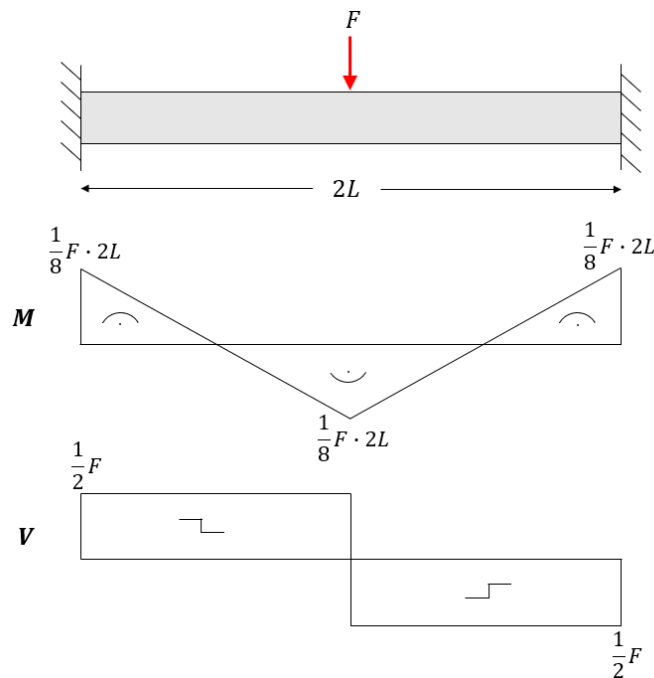
Figure 4.2: Bending moment and shear force diagram for a clamped concrete slab strip loaded with a point load.

As the vertical load is increased further, the cracked slab strip can be represented by two rigid bodies and three discrete cracks. The symmetry of the slab strip is used to simplify the model. The steel reinforcement is applied at the top and bottom of the slab strip. The value of the concrete cover (c) which is used for the model includes half of the rebar diameter. Thus, the assumed cover is the distance from the outside concrete fibre to the centreline of the steel reinforcement.

Other assumptions used for the model:

- Symmetrical crack patterns occur at the slab strip end and midspan.

- The compression zones at the slab strip end and midspan are equal, because the horizontal forces should be in equilibrium.

- Plane sections remain plane. Therefore, shear deformation is not accounted for in the model.

- The concrete slab strip is isotropic and homogeneous.

- The cross-section of the slab strip is solid and rectangular.

- Double bending is not considered.

- Concrete tensile strength is ignored because it has a very low value compared to the compressive strength.

- Loading is symmetrical and acts in a downwards vertical direction.

4.3. Material properties

Concrete properties

The parabolic stress-strain curve from the EC2 is used to describe the compressive behaviour of concrete for a single axis stress condition (see Figure 4.3). Equation 3.14 in the EC2 gives the exact formula of the stress-strain curve [6].
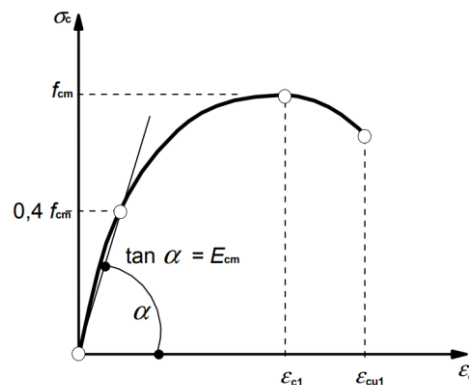
Figure 4.3: Parabolic compressive behaviour of concrete.

It is important to note that if the ultimate compressive strain ε_{cu1} is reached at some point in the analysis, and the compressive strain decreases again further into the analysis, the stress will remain zero. This is because it is assumed that if a concrete fibre has reached the ultimate strain value it is completely crushed and cannot take up any stress anymore. The corresponding unloading path goes via the x-axis to the origin of the diagram.

Steel reinforcement properties

The steel reinforcement is assumed to behave perfectly elastic-plastic, which can be described by a bi-linear stress-strain diagram (see Figure 4.4). Strain hardening of the steel is not considered. Note that the diagram

represents both the compressive and the tensile behaviour of the steel. The E-modulus of the steel reinforcement is 200000 MPa and the yield strength is 500 MPa.
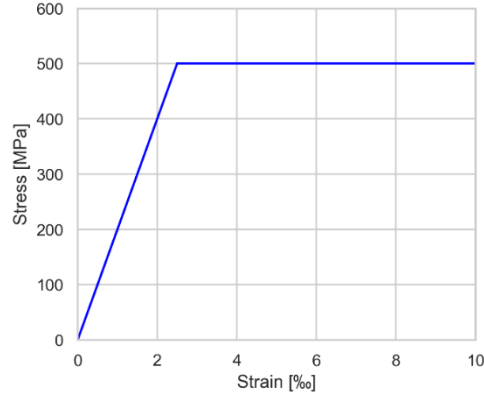
Figure 4.4: Stress-strain relation of the steel reinforcement.

4.4. Kinematic equations and internal forces

The response of the concrete slab strip can be obtained by imposing rigid body rotations and deriving the resultant moment of resistance introduced by the angular rotation (see Figure 4.5). Because the rotation is laterally restrained, the axial compressive forces in the concrete will form a pure moment that resists the motion of the rigid body. In addition, the tensile forces in the steel reinforcement will also counteract the imposed rotation. The resultant moment of resistance is determined by the introduced forces and by the lever arms between these forces.

Horizontal equilibrium requires that the forces acting at the slab strip end and midspan are equal. Since every cross-sectional fibre in contact with the slab strip end support represents a compressive stress, the contact areas at the slab strip end and midspan must be equal as well. As a consequence, McDowell et al. concluded that the contact depth must decrease with increasing rotation of the rigid body. It could also be concluded that the centre of rotation of the half slab strip is moving with increasing deflection, because the centre of rotation is always the first point in contact with the slab strip end support. First, McDowell et al. derived a relation between the rotation of the rigid body θ and the vertical deflection at midspan w from the geometry of the slab strip {4.1}. Note that the span length of the slab strip is $2L$. Thereafter, a relation between the decrease in the contact depth a and the vertical deflection at midspan w could also be derived {4.2}.

$$w = 2L \cdot \frac{1 - \cos\theta}{\sin\theta} \qquad \{4.1\}$$

$$a = \frac{w}{4} \qquad \{4.2\}$$
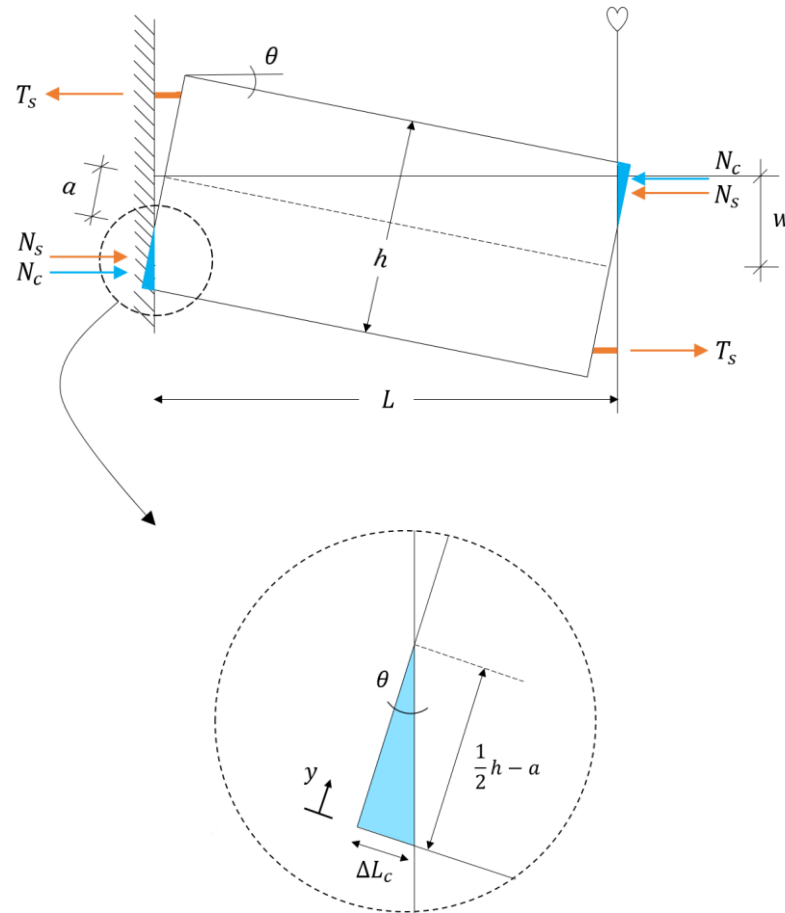
Figure 4.5: Deflected geometry of the fully restrained concrete slab strip.

Figure 4.5 shows that the displacement of the slab strip in the blue zone cannot occur because of the lateral restraint. Hence, as a result of the rotation, this restrained displacement introduces a compressive strain in the concrete slab strip. Considering the longitudinal direction of the slab strip, the maximum value of the compressive strain for each longitudinal concrete fibre is reached in the blue zone of Figure 4.5. McDowell et al. assumed that the minimum value of the compressive strain was located at the discrete crack and had a value of zero. Assuming a linear variation of the strain along each concrete fibre according to Euler-Bernoulli, the maximum compressive strain is twice the average strain. McDowell et al. noted that the multiplication factor (MF) – defined as the maximum strain divided by the average strain – of two was rather arbitrary, but the method was not considered completely illogical. The arbitrariness of this assumption makes it relevant to investigate the influence of the multiplication factor on the analytical results. Therefore, the factor is included as a variable in the analytical model.

The assumed multiplication factor MF affects the compressive strain distribution in the longitudinal direction of the concrete fibres that are shown in Figure 4.6a. The compressive strain distribution along a concrete fibre for two different multiplication factors is shown in Figure 4.6b. The areas under the three curves are similar, which requires that the MF=4 curve is an exponential function. The assumption of McDowell et al. for MF=2 holds for every longitudinal concrete fibre that is restrained at one side, which is in correspondence with the Euler-Bernoulli theory and the linear bending moment diagram presented in Figure 4.2. This implies that the multiplication factor and the strain distribution do not depend on the location on the vertical height axis of the slab. However, the strain distribution may be different for every longitudinal concrete fibre in compression because of nonlinearities. This will be discussed further in chapter 5. For now, it is assumed that the multiplication factor is unknown but has a constant value for every longitudinal concrete fibre in compression.
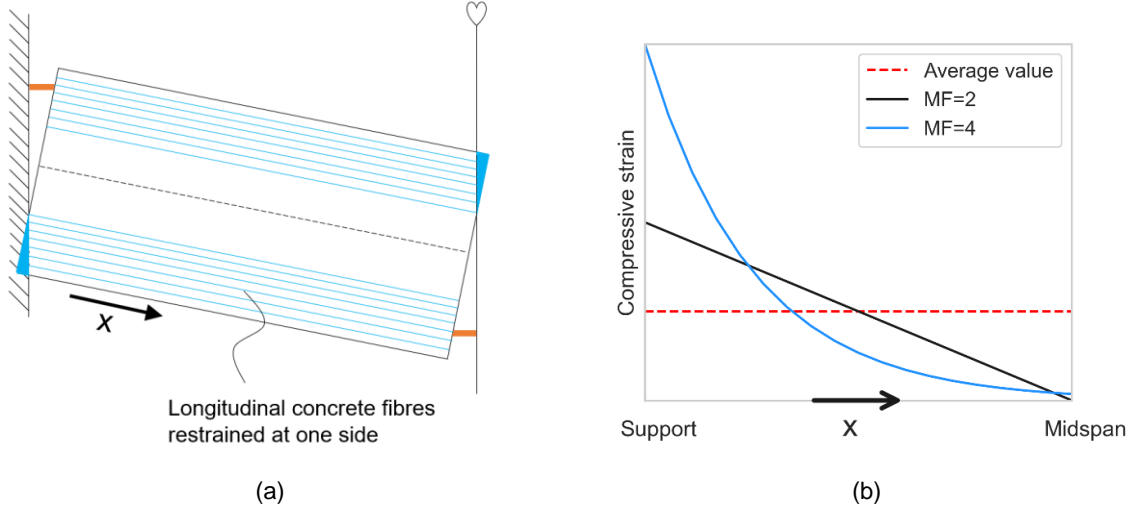
Figure 4.6: Restrained concrete fibres (a) and their assumed compressive strain distribution in the longitudinal direction for different values of the multiplication factor MF (b).

From the geometry illustrated in Figure 4.5 the maximum compressive strain in the outer concrete fibre (ε_{max}) can be determined. Subsequently, a relationship for the strain as a function of the height of the slab strip can be derived from this ($\varepsilon(y)$). Both ε_{max} and $\varepsilon(y)$ have negative values, because compressive strains have a negative sign. The maximum strain for the GNL model is calculated on the basis of the deformed slab strip. Therefore, the length of the slab strip is reduced by the difference in length. The GL model considers the original length of the bar in the calculation. It should be noted that the nonlinear effect will be minimal, because the length is much greater than the difference in length.

$$\varepsilon_{max,GL} = -MF \cdot \frac{\Delta L_c}{L} = -MF \cdot \frac{\tan\theta \left(\frac{1}{2}h - a\right)}{L} \quad \{4.3\}$$

$$\varepsilon_{max,GNL} = -MF \cdot \frac{\Delta L_c}{L} = -MF \cdot \frac{\tan\theta \left(\frac{1}{2}h - a\right)}{L - \tan\theta \left(\frac{1}{2}h - a\right)} \quad \{4.4\}$$

$$\varepsilon(y) = \frac{-\varepsilon_{max}}{\frac{1}{2}h - a} y + \varepsilon_{max} \quad \{4.5\}$$

Concrete contribution

The restrained strain introduces compressive stresses into the concrete slab strip. The adopted stress-strain relation of concrete is used to convert the strains into stresses. Integration of the stresses over the slab height will result in the axial compressive forces acting on the rigid body. The python script divides the slab strip height into 100 points in order to integrate using the trapezoidal rule.

$$N_c = \int \sigma dy \quad \{4.6\}$$

These resultant forces are the driving force behind the arching action, and the positions at which they act are determined by calculating the centroid of the stresses along the contact area.

$$\bar{y} = \frac{1}{N_c} \int (\sigma \cdot y) \, dy \quad \{4.7\}$$

Steel reinforcement contribution

The length of the tension reinforcement increases with increasing deflection of the slab strip. The positive strain of the tension reinforcement is determined by dividing the difference in length by the initial length of the deformed

part of the reinforcement bar. The difference in length can be derived from the geometry presented in Figure 4.7. The chosen value of the initial length is not very relevant, because yielding of the reinforcement will occur early in the analysis. The focus is on the ultimate load-bearing and deformation capacity of the slab strip, and not on the early structural behaviour of the slab strip. The initial length is therefore assumed to be half of the slab strip height.

$$\varepsilon_t = \frac{\Delta L_t}{L_{ini}} = \frac{\sin\theta \left(\frac{1}{2}h + a - c \right)}{\frac{1}{2}h} \qquad \{4.8\}$$

The length of the compression reinforcement decreases because, as with the concrete, the strain is restrained. The geometry of the slab strip end presented in Figure 4.7 is used to determine the length difference in the compression reinforcement. The assumption is again made that the initial length of the deformed reinforcement bar is half of the slab strip height.

$$\varepsilon_n = -\frac{\Delta L_n}{L_{ini}} = -\frac{\tan\theta \left(\frac{1}{2}h - a - c \right)}{\frac{1}{2}h} \qquad \{4.9\}$$

The strains are converted into stresses using the steel reinforcement properties presented in Figure 4.4. Subsequently, the stresses are converted to forces in the steel. The amount of steel reinforcement A_{eq} is the height of an equivalent rectangular strip of reinforcement of unit length.
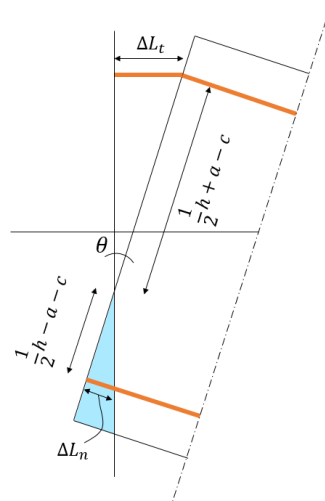
$$T_s = \sigma_T \cdot A_{eq} \qquad \{4.10\}$$

$$N_s = \sigma_N \cdot A_{eq} \qquad \{4.11\}$$

$$A_{eq} = \rho \cdot h \qquad \{4.12\}$$

Figure 4.7: Deflected geometry of concrete slab strip end.

4.5. Elaboration and results

The results of the analytical model can be obtained by equating the acting moment resulting from the loads with the resultant moment of resistance determined by the forces in the concrete and steel. First, the lever arms of the concrete and steel force couples for both the linear and the nonlinear model are determined (see Figure 4.8).
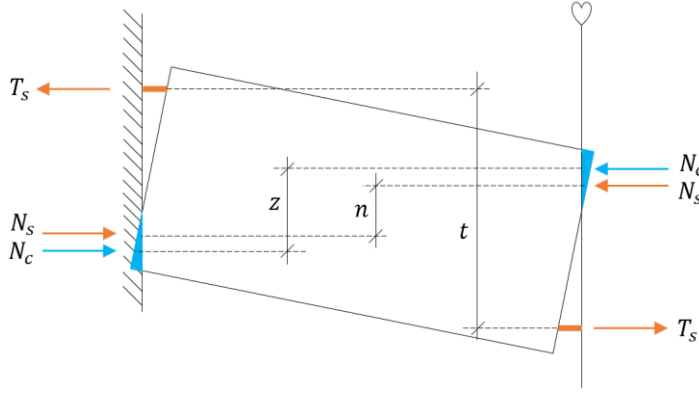
Figure 4.8: Lever arms of force couples for the GNL model.

Lever arm of the forces in the concrete

The lever arm of the forces in the concrete is determined by the vertical length between the positions of the resultant compressive forces N_c. The difference between the GNL response and the GL response is caused by a different value for the lever arm. The GL model excludes the vertical deflection at midspan for the determination of the lever arm. The arm for the linear model therefore only depends on the shift of the centroid of the concrete stress distribution.

$$z_{GL} = h - 2\bar{y} \quad \{4.13\}$$

$$z_{GNL} = h - 2\bar{y} - w \quad \{4.14\}$$

Lever arm of the forces in the steel reinforcement

The lever arms of the linear model are only determined by the concrete cover and are therefore similar for the compression and tension reinforcement. For the GNL model, lever arm t_{GNL} increases while lever arm n_{GNL} decreases with increasing deflection.

$$t_{GL} = n_{GL} = h - 2c \quad \{4.15\}$$

$$t_{GNL} = h - 2c + w \quad \{4.16\}$$

$$n_{GNL} = h - 2c - w \quad \{4.17\}$$

Total response

The resultant moment of resistance M_a can now be determined for both the GL and GNL model. Note that the axial forces N_c and N_s initially had negative values because they are compressive forces. In the equations below, it is assumed that all axial forces have positive values.

$$M_{a,GNL} = N_c \cdot z_{GNL} + N_s \cdot n_{GNL} + T \cdot t_{GNL} \quad \{4.13\}$$

$$M_{a,GL} = N_c \cdot z_{GL} + N_s \cdot n_{GL} + T \cdot t_{GL} \quad \{4.14\}$$

The acting moment resulting from the applied loading is in equilibrium with the resultant moment of resistance and it can therefore be created by any type of loading. It is chosen to load the slab strip with a point load at midspan and show its load-deflection behaviour accordingly. This is because it ensures that the structural system of the half slab strip is symmetrical, making the analytical results easier to compare with the results of numerical models. The corresponding moment equilibrium equation is presented below in {4.15}.

$$F = \frac{4M_a}{2L} \quad \{4.6\}$$

Reference slab strips

The reinforced concrete slab strip is loaded with a point load at midspan, which unit is chosen to be kN per mm width of the slab strip. The load is therefore actually a line load at midspan over the width of the slab. The structural behaviour of two reference slab strips – **Slab 1** and **Slab 2** – is presented in load-deflection diagrams. The slab strips have the same span length but differ in height and therefore in slenderness. Continuous reinforcements in the top and bottom of the reference slab strips are applied. The details of the slab strips are given in Table 4.1. Figure 4.9 represents the geometry of Slab 1 and Slab 2.

Two diagrams per slab strip are shown with different values for the multiplication factor (see Figure 4.10). Also, the ultimate bending capacity according to EC2 is plotted in the diagrams. The procedure for calculating the bending capacity and the corresponding failure load is given in Appendix A. The calculation of this *conventional capacity* does not include safety factors and can therefore sufficiently represent the actual capacity of a slab strip in which arching action will not contribute to carrying the load. The failure load for bending is determined based on plastic analysis of the statically indeterminate slab strips. The calculation assumes that the slab carries the load in only one direction. Therefore, the concrete slab must have two free and practically parallel edges or a length-to-width ratio higher than two when all four edges are supported according to the EC2. It is important to note that punching shear could be critical for concrete slabs loaded by point loads. However, punching shear will be disregarded in this thesis since the third dimension of the concrete slab is not considered.

Parameter	Unit	Slab 1	Slab 2
E_c	MPa	31000	33000
f_c	MPa	33	38
c	mm	19	31
h	mm	125	225
$2L$	mm	3600	3600
slenderness ($2L/h$)	-	28.8	16

(a)

Parameter	Unit	Slab 1	Slab 2
E_s	MPa	200000	200000
f_y	MPa	500	500
$\emptyset$	mm	8	12
spacing	mm	120	140
ρ_+	-	0.00335	0.00359
ρ_-	-	0.00335	0.00359

(b)

Table 4.1: Geometric and material properties of concrete (a) and steel reinforcement (b) of Slab 1 and Slab 2.
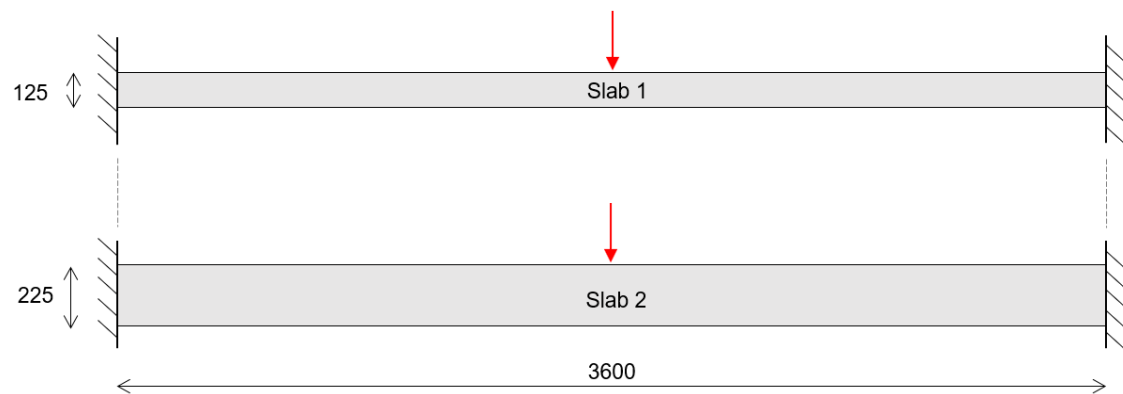
Figure 4.9: Geometric representation of Slab 1 and Slab 2.
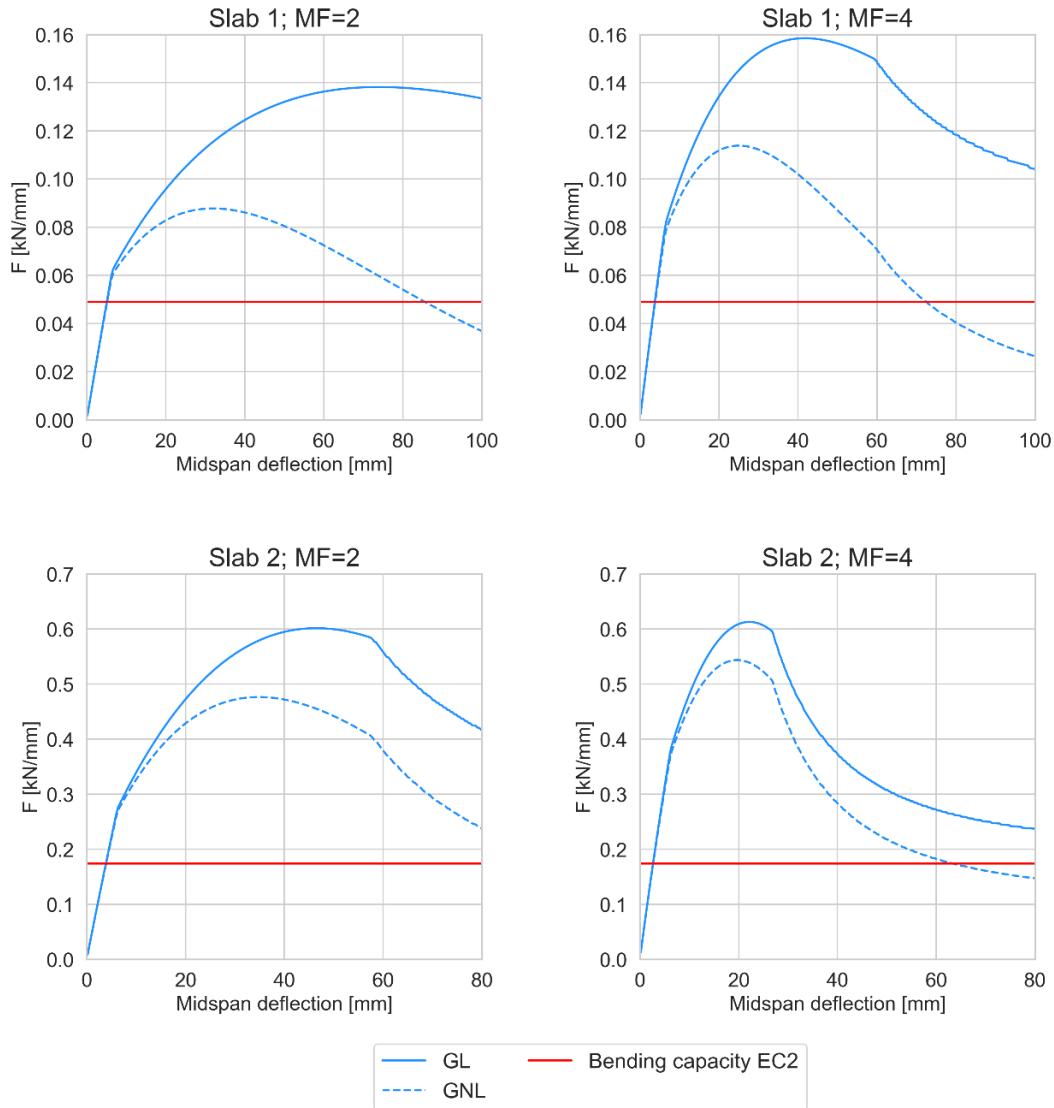
Figure 4.10: Analytically obtained load-deflection diagrams of Slab 1 and Slab 2.

Before any valid conclusions can be drawn from the results presented in Figure 4.10, an important aspect of the analytical model must be looked into. That aspect is the unloading of concrete fibres of the slab strip. Appendix A contains a study into the effect of unloading on the response of the slab strips. It turned out that even though unloading of the first concrete fibres takes place before the crushing of the first concrete fibres, the influence of unloading on the load-deflection behaviour is negligible. Unloading will therefore not be included in the analytical model.

4.6. Discussion and conclusions

In order to explain the load-deflection behaviour resulting from the analytical model, several points are indicated in the diagrams of Slab 1; MF=4 and Slab 2; MF=4. Thus, the meaning of points 1, 2, 3 and 4 is given for clarification of the analytical results, but also comparability with numerical results.

The behaviour of the slab strip is linear-elastic until yielding of the tensile reinforcement occurs at **point 1**. The tensile steel stress cannot increase anymore, resulting in reduced stiffness and a kink in the load-deflection curve. The compression reinforcement is yielding right after point 1. The curve is concave down (the stiffness is gradually decreasing) and increasing after point 1. Contributors to this increasement are the enlargement of the lever arm of the tensile reinforcement and the increase in the compressive stress in the concrete compression zones.

Point 2 indicates the moment when the compressive strain at maximum stress is reached in the outer fibres of the slab strip. The maximum load resistance is reached at **point 3**. It is due to second-order effects that point 3 lies before point 2 for Slab 1; MF=4. The reduction of the lever arm of the resultant compressive arch will cause a decrease in the load-deflection curve. At **point 4**, the ultimate concrete compressive strain value is reached, and the concrete stress drops to zero in the outer fibres. As a result, crushing of the concrete occurs and a second kink is introduced in the curve.
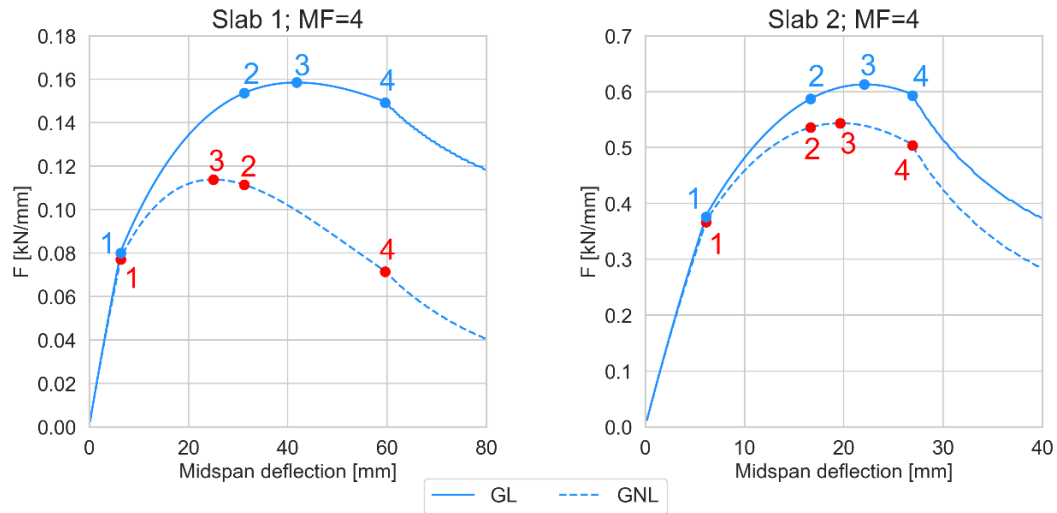
Figure 4.11: Analytically obtained load-deflection diagrams for MF=4.

Now, several conclusions can be drawn from the results of the reference slab strips presented in Figure 4.10. First, the actual ultimate capacity of the laterally restrained reinforced concrete slab strips is significantly higher than their conventional bending capacity. Note that the actual capacity is the capacity resulting from the realistic GNL model, and not the one resulting from the GL model. The enhancement factor, defined as the actual ultimate load divided by the conventional capacity, varies from about 1.8 to 3.1. CMA provides the additional load-bearing mechanism that causes this considerable increase in capacity.

The maximum load carried by arching action can be considered the ultimate load minus the bending capacity. The relative increase in capacity is larger for Slab 2 than for Slab 1, meaning that the arching effect is stronger for Slab 2. This is due to the relatively larger internal lever arm of the resultant compressive arch and the subsequent larger arching moment for the less slender Slab 2. This also indicates that arching action carries a relatively larger part of the load for Slab 2, while bending action carries a larger part of the load for Slab 1.

Secondly, second-order effects will cause a reduction of the ultimate load. The percentage decrease is between 11% and 57%. It can be concluded that the inclusion of GNL effects in the structural analysis results in a decrease in the magnitude of CMA (**GNL reduction effect**), because the internal lever arms of the resultant compressive forces in the concrete and the steel reinforcement are decreasing with increasing deflection of the slab strip. Therefore, the resultant moment of resistance of the GNL model will increasingly deviate from that of the GL model after yielding of the steel is initiated at the first kink in the graphs. The results of the analytical model show good agreement with the results of the truss model (see section 3.4) when it comes to the second-order reduction effect (GNL reduction effect). It can also be seen that the magnitude of the relative second-order effect is larger for larger slab slenderness. The reason is that the percentage decrease in the angle of the resultant compressive arch is higher for the slender Slab 1, and thus the internal lever arm and the secondary moment approach zero much faster. The relative difference between the ultimate capacities resulting from the GL and GNL model will therefore be larger for Slab 1.

Thirdly, the ductility of the slab strip is slightly decreased because of geometrical nonlinearity; the deflection at which the peak load is reached is smaller for the nonlinear model. Lastly, the assumed multiplication factor MF

has a large influence on the stiffness, ductility, peak load and magnitude of the GNL effect. Also, it affects the position of the first kink. Thus, the total response of the slab strip changed because of an alteration of the multiplication factor. The reason for this is that the multiplication factor determines the state of the compressive strain and therefore also of the compressive stress. A high multiplication factor will therefore lead to large stresses for relatively small midspan deflections, which will cause an increase in the initial stiffness. Also, the ultimate strain will be reached much faster, and as a result, the ductility is reduced.

4.6.1. Influence of multiplication factor MF

It is of interest to relatively quantify the effects of the multiplication factor MF on the stiffness, on the ductility, on the peak load and the GNL effect. This is done by comparing the results for different multiplication factors. The relative differences expressed in difference factors are shown in diagrams, in which the considered value is divided by the minimum value for all multiplication factors. Thus, the lowest value in the diagram is always 1.0. The GNL effect is shown on the basis of a difference factor which is defined as the GL peak load divided by the GNL peak load.
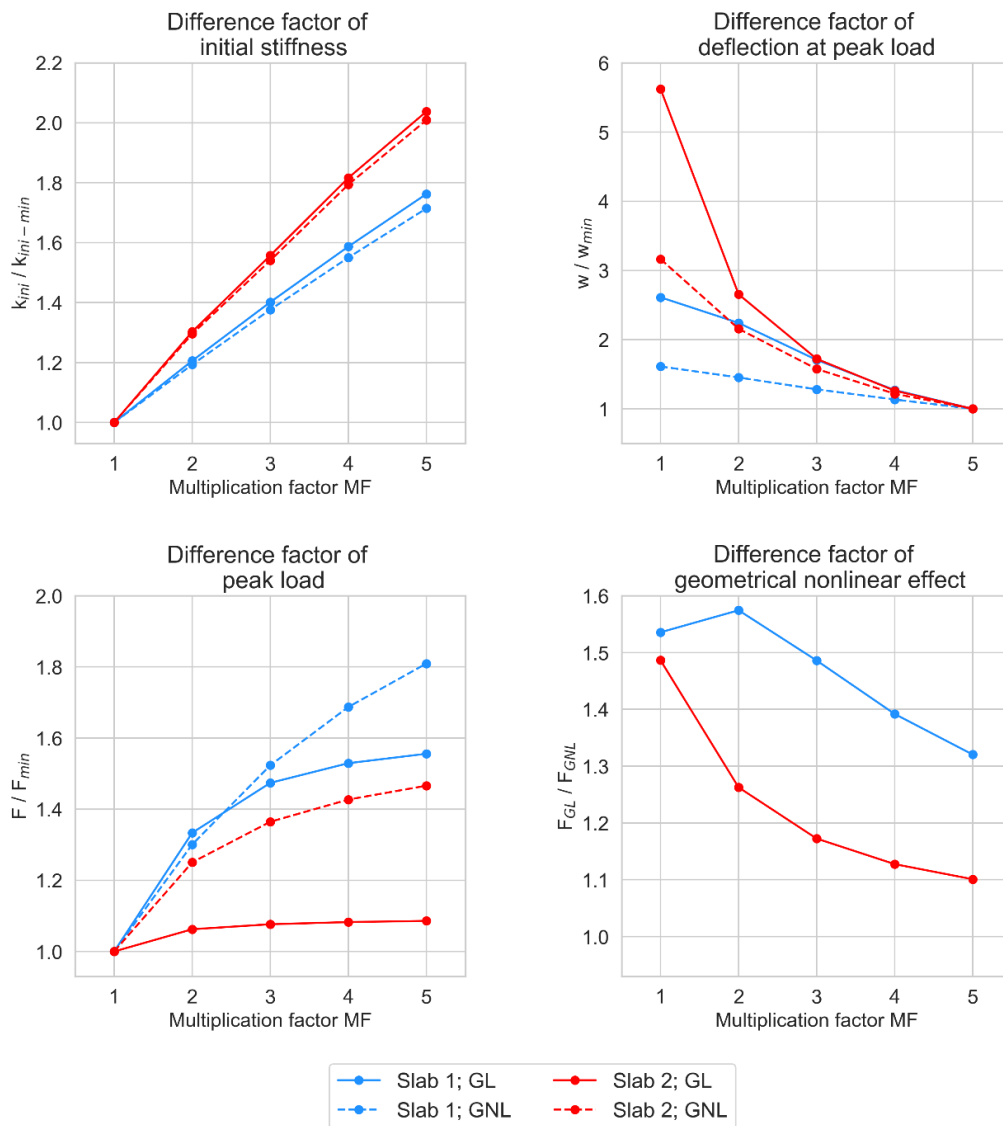
Figure 4.12: Influence of the multiplication factor on the response of Slab 1 and Slab 2.

Figure 4.12 shows that there is a strong relationship between the multiplication factor and all the regarded parameters that determine the total response of the slab strip. The initial stiffness of the slab strips is almost

linearly related to the multiplication factor. The three other diagrams show a relationship between MF and the difference factor that appears to be parabolic in most cases. Therefore, changes of MF for small values of MF greatly affect the response of the beam, while changes of MF for large values of MF do not have much influence on the response. The deflection at peak load is the parameter that is most affected by the multiplication factor.

An important finding is that multiplication factors between 2 and 5 lead to peak loads that do not differ significantly. The maximum deviation between the peak loads is about 38%. In addition, the geometrical nonlinear effect is not significantly changed when varying the multiplication factors between 2 and 5. The maximum deviation between the geometrical nonlinear effects is about 15%.

The question remains which value for the multiplication factor has to be chosen for the analytical model to represent reality as good as possible. Therefore, the value for the multiplication factor needs to be calibrated with a numerical model developed in DIANA (see chapter 5). The multiplication factor that results in the best fit between the response of the analytical and numerical model should be used. Even though the analytical model would then be calibrated, the developed numerical model can still be used to validate the analytical results because the calibration of the multiplication factor does not significantly affect the peak load and the geometrical nonlinear effect, as was stated in the paragraph above. However, it should be noted that the calibration will lead to a numerical validation that is less strong.

<div align="right">

5

</div>

Numerical models

5.1. Introduction

Finite element modelling in DIANA is used to calibrate the analytical model and validate the analytical results. Symmetry is again used to simplify the models and to reduce the calculation time. First, a numerical model is made which is nearly equivalent to the analytical model, meaning that the assumptions of the analytical model are modelled as good as possible. Thus, the nonlinearity in this model is concentrated at the supports of the half slab strip with a rigid body in between (see Figure 5.1a). The main goals of this *numerical rigid body model* is to check the correctness of the analytical model, detect possible errors and explain the differences in results of the equivalent models. The *numerical rigid body model* will be discussed in section 5.2.
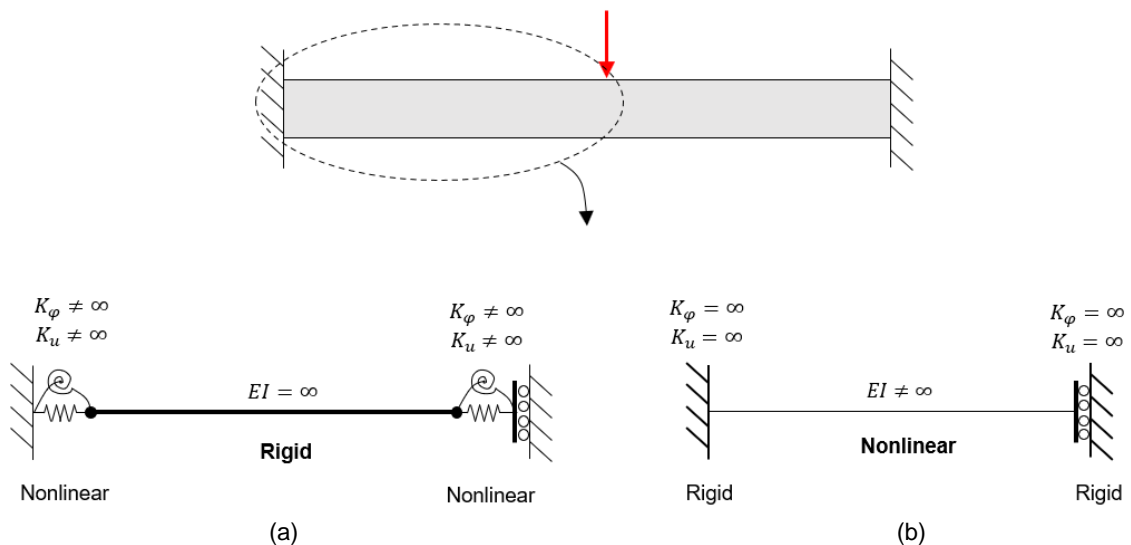
Figure 5.1: Simplified representation of the numerical rigid body model (a) and the numerical concrete slab model (b).

Second, a numerical model is made in which the nonlinearity is spread over the whole slab strip length, and the complete rigidity is moved from the body to the supports (see Figure 5.1b). Thus, the assumptions of the analytical model are not adopted for this *numerical concrete slab model*. In this model, local disturbances and shear forces can play a role in the structural behaviour of the slab strip. One could argue that this model, therefore, is more realistic than the *numerical rigid body model.* Therefore, the model is not only used to calibrate the analytical model, but also to check if the analytical model leads to realistic results. A comprehensive comparison is made between the analytical and numerical results, and differences are explained. The *numerical concrete slab model* will be discussed in section 5.3.

5.2. Numerical rigid body model

5.2.1. Introduction

Numerical validation of the analytical model is performed by constructing a FEM-model that adopts similar assumptions used for the analytical model. However, it is not possible to construct a numerical model which is completely equivalent to the analytical model due to the complexity of modelling the discrete cracks and the reduction of the contact depth such that it corresponds with the analytical model. Therefore, the material nonlinearity at the slab strip ends is dealt with differently in the numerical rigid body model than in the analytical model. Note that the rigid body is present in both models. A detailed description of the numerical rigid body model is given below in section 5.2.2.

5.2.2. Description of the model

The analytical model of the half slab strip basically consists of a rigid body with springs on both sides that represent the nonlinear material properties of the concrete and steel reinforcement (see Figure 5.2). A 'trick' is used to comply with the assumed bedding of nonlinear springs in the numerical rigid body model: two concrete strips are applied on either side of the rigid body to be able to develop nearly discrete cracks in the tensile zones and to generate equivalent horizontal forces in the compression zones. The concrete strips can therefore be regarded as a large number of springs over the height of the slab strip. In addition, steel rebars are applied through the concrete strips and the rigid body to represent the steel reinforcement springs. The rebars are connected to the supported edges.

The FEM-model is constructed in the two-dimensional environment of DIANA. The length of the rigid body is the same for both the analytical model and for the numerical model, which means that the concrete strips add some additional length to the FEM-model. The concrete strip at the slab strip end is horizontally and vertically supported, and the concrete strip at midspan is only horizontally supported to comply with the symmetry conditions. The rigid body is directly connected to the concrete strips without specific interface properties. The width of the slab strip is assumed to be 200 mm. It is important to note that this width value does not influence the results, since the load in the load-deflection diagrams is expressed as a line load in the third dimension of the model out of the plane of the modelled slab strip.
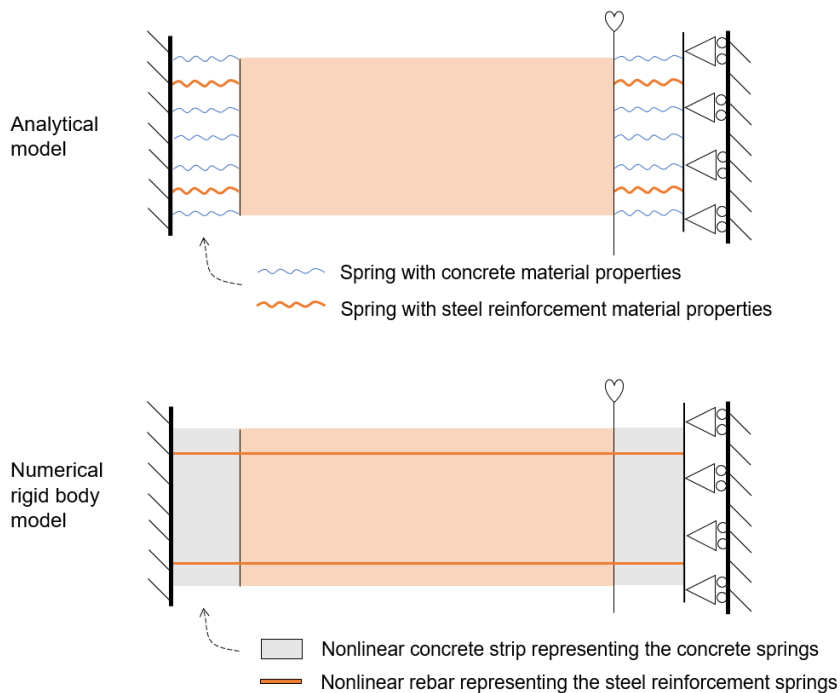
Figure 5.2: Comparison between the analytical model and the numerical rigid body model.

Concrete strip length

The length of the concrete strips is determined by two constraints:

- **Maximum length constraint**: the length of the strips should be small compared to the length of the rigid body, because the lever arms of the force couples from the internal forces in the concrete and the steel as well as the lever arm of the load will change too much compared to the analytical model if the strips become too long.

- **Minimum length constraint**: the length of the strips should not be too small, because the length difference of the strips can then become relatively large compared to the length of the strips itself as rigid body rotations are increasing, which will lead to overestimation of the compressive strains during the GNL analysis.

A balance between the two constraints has to be found in order to approach the analytical results as good as possible. In this way, proper validation of the analytical model can be achieved. A concrete strip length of 40 mm is chosen.

Tyings in the finite element model

Tyings are linear dependencies between nodal variables. They can for example be used to create symmetry in the model or to keep edges straight. A tying contains one or several degrees of freedom in a *master node* and one or several degrees of freedom in the *slave node*. The degrees of freedom of the slave node are derived from those of the master node. Therefore, the system of equations for the slave node is solved with its specified nodal variables as constraints [38].

Tyings can also be used to keep nodal displacements equal. These *equalities* come in handy for the numerical model of the laterally restrained slab strip. In order to prevent early instability of the concrete strips due to shear stresses, the vertical displacement of master node A is connected to the vertical displacement of slave node A'. The same holds for master node B and slave node B'. Note that the vertical displacement of slave node A' is zero, because master node A is vertically supported.
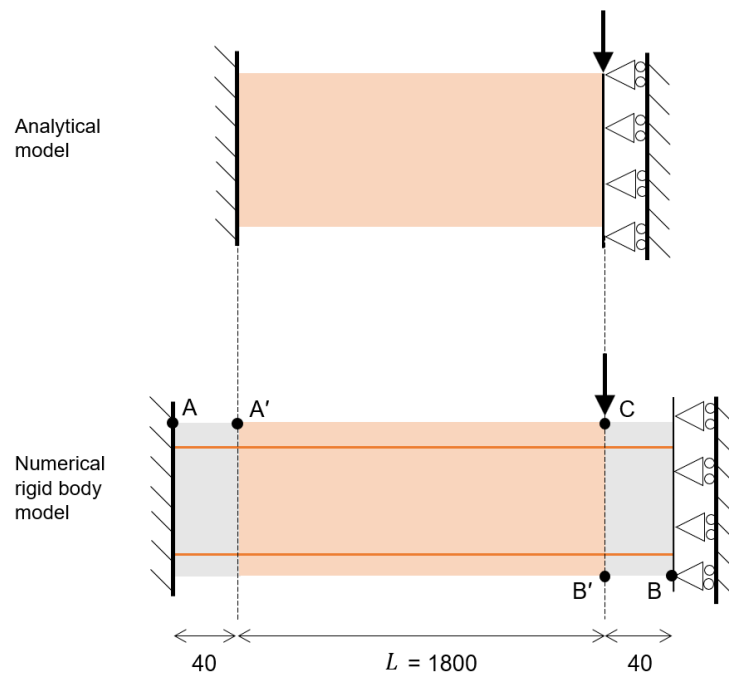
Figure 5.3: Tying locations and geometric properties of the numerical rigid body model.

The resulting numerical rigid body model of Slab 2 in DIANA is shown in Figure 5.4.
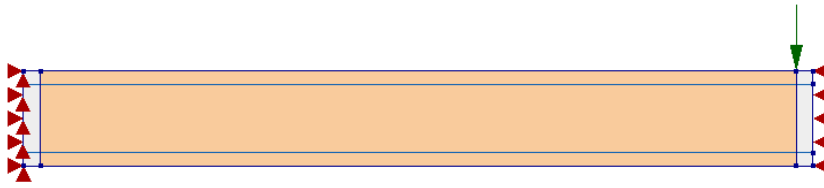
Figure 5.4: Numerical rigid body model of Slab 2 in DIANA.

Elements

The concrete strips and the rigid body are modelled with plane stress elements.

- **Plane stress elements:** These elements are suitable if the in-plane dimensions (x and y direction) of the model are large compared to its width (z-direction). It is therefore assumed that the stress components in the z-direction are zero. The elements, the loads and the boundary conditions must be defined in the xy-plane (see Figure 5.5).

  The used element type for the plane stress elements is CQ16M, which represent 8-noded quadrilateral elements with quadratic interpolation (see Figure 5.6). The elements are based on a 2 x 2 Gauss integration scheme.
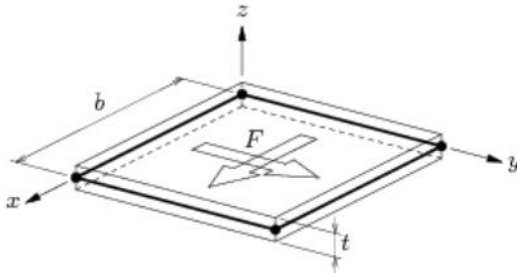
Figure 5.5: Plane stress element [38].
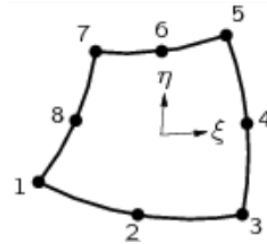
Figure 5.6: CQ16M element [38].

The steel reinforcement is modelled as an embedded bar inside the rigid body and the concrete strips.

- **Embedded reinforcements:** The embedded reinforcements add stiffness to the model without occupying space in the so-called mother elements, which are the plane stress elements in this case (see Figure 5.7). Also, the embedded reinforcements do not have degrees of freedom themselves nor do they affect the mass of the elements. The strains in the reinforcement are determined based on the displacement field of the mother elements. A perfect bond between the steel reinforcement and the material of the mother elements is assumed.
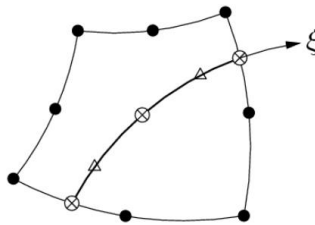
Figure 5.7: Embedded reinforcement bar inside plane stress element [38].

5.2.3. Material properties

Concrete properties

The stress-strain curve according to formula 3.14 of EC2 is used to describe the compression behaviour of the concrete in the DIANA model (see Figure 5.8). The values of the E-modulus and the compressive strains are modified according to the used assumptions for the concrete strain in the analytical model. This is done because the strain is numerically calculated on the basis of the length of the small strip instead of a larger part of the slab length. The E-modulus, the strain at maximum stress and the strain at ultimate stress are corrected according to the initial length difference. A difference factor DF is calculated as a function of multiplication factor MF, which is used to convert the values of E_{cm}, ε_{c1} and ε_{cu1} to their modified equivalents in the numerical rigid body model ($E_{cm,mod}$, $\varepsilon_{c1,mod}$, $\varepsilon_{cu1,mod}$).

$$DF = MF \cdot \frac{L_{strip}}{L} = MF \cdot \frac{40}{1800} \qquad \{5.1\}$$

$$E_{cm,mod} = E_{cm} \cdot DF \qquad \{5.2\}$$

$$\varepsilon_{c1,mod} = \frac{\varepsilon_{c1}}{DF} \qquad \{5.3\}$$

$$\varepsilon_{cu1,mod} = \frac{\varepsilon_{cu1}}{DF} \qquad \{5.4\}$$

The tensile behaviour of the concrete is assumed to be brittle with a very low value for the tensile strength (see Figure 5.9). This allows the two cracks to develop almost immediately, just as in the analytical model.
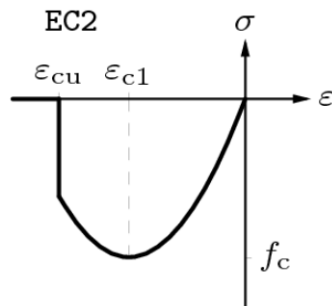
Figure 5.8: EC2 compression behaviour of concrete in DIANA [38].
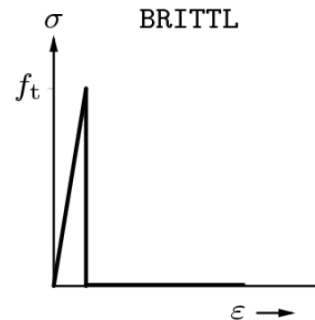
Figure 5.9: Brittle tensile behaviour of concrete in DIANA [38].

Steel reinforcement properties

The material properties of the steel reinforcement are equal to those used for the analytical model (see Figure 4.4 in section 4.3). The steel reinforcement has a yield strength of 500 MPa, an E-modulus of 200000 MPa and is modelled with a plasticity range according to Von Mises. A very small positive slope is added to the plastic plateau in order to avoid numerical problems.

Rigid material properties

The rigid body is assumed to have an infinite stiffness in the analytical model. A good approximation of this is a very stiff and nearly completely rigid material with an E-modulus of 1e12 N/mm^2. The rigid material is assumed to be linear elastic and isotropic.

5.2.4. Analyses

Mesh

In the analytical model, the height of the slab strip is divided into 100 concrete fibres for which the strains and stresses are calculated. Therefore, the mesh of the equivalent numerical model also consists of 100 elements over the height of the slab strip (see Figure 5.10). The rigid body is divided into 50 elements in the longitudinal direction, and its elements thus have a width of 36 mm. Furthermore, the width of the concrete strip elements is equal to the width of the concrete strips themselves.
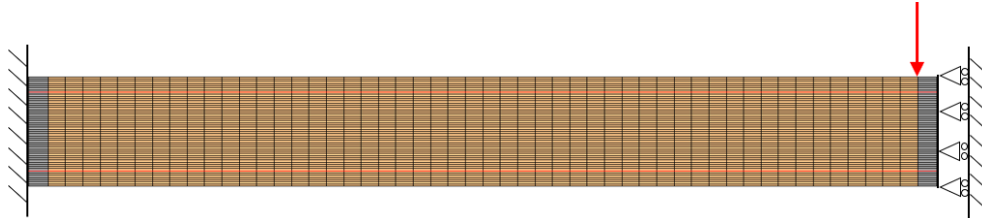
Figure 5.10: Mesh of numerical rigid body model of Slab 2.

Load introduction

The FEAs are displacement-controlled. A final vertical downward displacement of node C of 100 mm is incrementally applied in 200 load steps (see Figure 5.3).

Nonlinearities and solving method

The nonlinear material properties of the concrete strips and the embedded steel reinforcements require that all numerical models include material nonlinearity. Both a GL and a GNL analysis are performed for both Slab 1 and Slab 2. The Newton-Raphson method is used for the numerical calculations. Also, an energy convergence norm is used with a tolerance of 0.001.

5.2.5. Results

The results of the analyses are shown in the load-deflection diagrams in Figure 5.11. For comparison, the analytical results are also included in the diagrams.
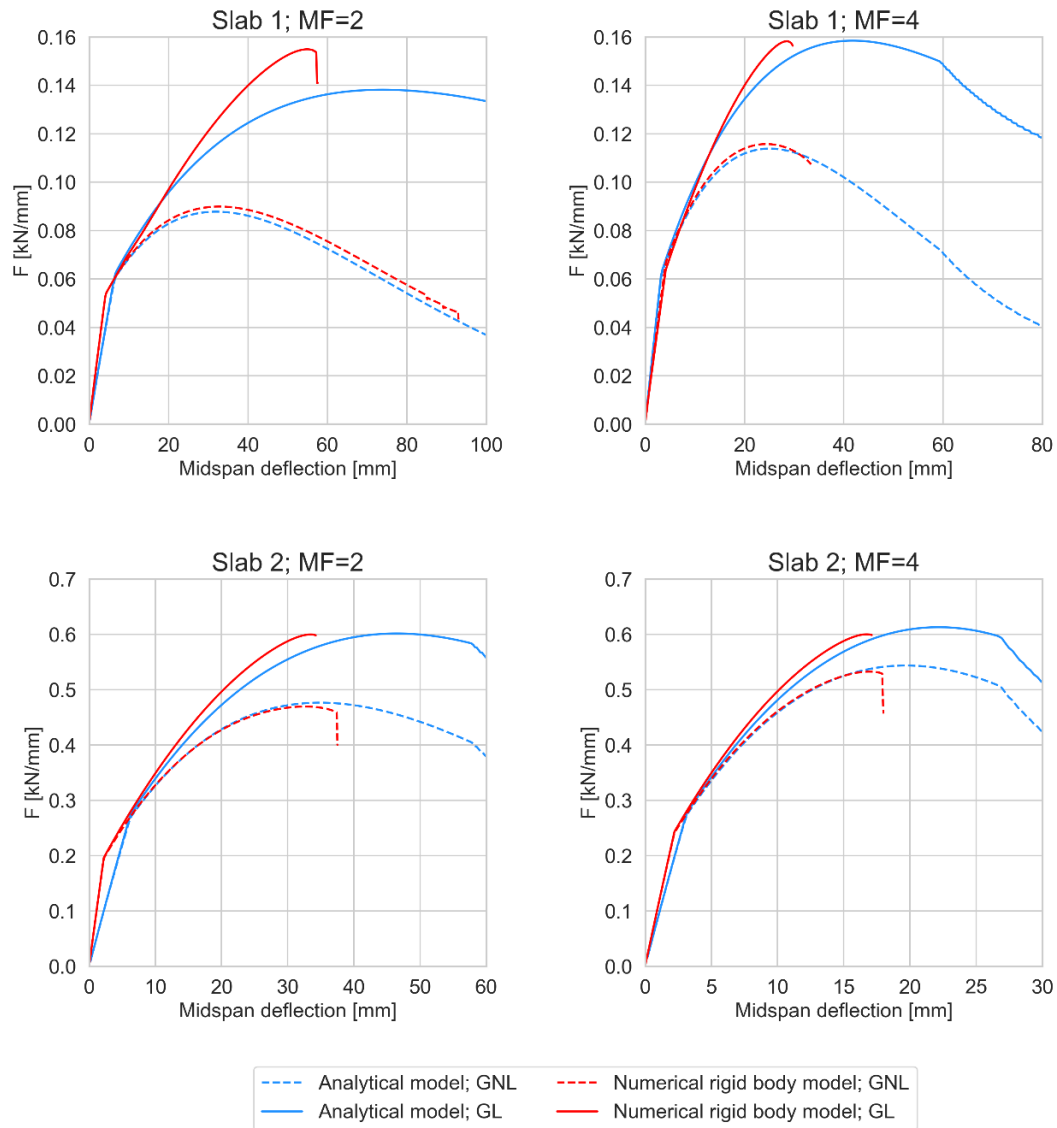
Figure 5.11: Results of the analytical model and the numerical rigid body model presented in load-deflection diagrams.

5.2.6. Discussion and conclusions

As can be seen in Figure 5.11, the load-deflection behaviour of Slab 1 and Slab 2 shows good agreement with the predicted behaviour according to the analytical model. Even though small differences can be observed, the peak loads according to the analytical and numerical model are almost similar except for the Slab 1; MF=2 result. The majority of the small differences listed below can be explained on the basis of the design of the numerical rigid body model:

- **Initial stiffness and position of the first kink**: The position of the kink depends on the assumed length of the concrete strips. An increase in the concrete strip length would lead to a shift of the kink in the numerical model curve. Also, the strain calculation of the steel reinforcement in the analytical model was rather arbitrary (see section 4.4 for the explanation) and based on an initial length of half of the slab strip height. A decrease in the initial length would immediately lead to a higher initial stiffness and a change of the position of the kink. In sum, the small differences in stiffness and first kink position are caused by the assumptions of both models. It should be noted that these differences are not relevant for this research, because the maximum load and the ductility are much more important quantities in this case.

- **Stiffness after the first kink**: The stiffnesses after the first kink of the GNL models are very similar and the differences are negligible. The small difference can be explained: because the strip length is much smaller than half the length of the slab strip assumed for strain calculation of the analytical model, the strain calculated according to the theory of large deformations will have different values in the numerical and analytical models for similar midspan deflection values.

  The stiffness after the first kink of the GL numerical models is larger than that of the GL linear analytical models. This is partly due to the choice for the length of the concrete strips, which is a balance between the two constraints explained in 5.2.2. A very small part of the difference in stiffness is caused by the tying in the top-left node of the rigid body: the top-left node of the rigid body in the numerical model does not move in the vertical downward direction while this node moves downwards with (½h+a)(1-cosθ) in the analytical model. Moreover, the chosen mesh could be of influence on the results. However, division of the concrete strips into more elements in the longitudinal direction of the slab strip does not lead to realistic results.

It can be concluded that the analytical model is constructed properly and contains no major errors. No further conclusions can be drawn based on the results of the numerical rigid body model. The more realistic numerical concrete slab model discussed in section 5.3 can give insight into whether the analytical model gives valid results.

5.3. Numerical concrete slab model

5.3.1. Introduction

The actual behaviour of restrained concrete structures could be approximated with FEA if proper material properties, boundary conditions, mesh and calculation procedures are chosen. The technical document of Rijkswaterstaat "Guidelines for Nonlinear Finite Element Analysis of Concrete Structures" includes guidelines to enhance the robustness of the analyses and to reduce the intrinsic model factors that affect the results [10]. In this way, actual structural behaviour can be accurately predicted because of guidelines that are based on scientific research. Yet, it cannot simply be assumed that the results of the finite element models will represent the exact behaviour of the concrete structure outside: it will always remain an approximation. Nevertheless, the numerical concrete slab model is used for calibration and validation of the analytical model.

5.3.2. Description of the model

The 2D FEM-model consists of a slab strip made of concrete with steel rebars at the top and bottom. Again, half of the slab strip is modelled with symmetry conditions. Thus, the slab strip is fully clamped at one end and horizontally restrained at the other. In order to achieve nearly symmetrical crack patterns at both sides of the half slab strip, the load is applied as a point load at midspan. In this way, the shear force will be constant over the full length of the slab strip. In addition, the bending moments at the side support and midspan are equal. This would not be the case if a UDL would have been applied. A study into the differences between the application of a point load or UDL is included in Appendix B. Also, equal loading conditions for the analytical and numerical model will provide comparable results. The finite element model of Slab 2 is shown in Figure 5.12.
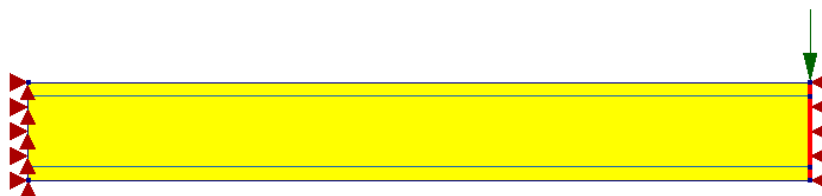
Figure 5.12: Numerical concrete slab model of Slab 2 in DIANA.

A tying is used to prevent stress concentration at the top-right corner of the slab strip. The top-right master node is connected to the slave edge at the right side of the concrete slab strip (see the red edge in Figure 5.12) such that the vertical displacements are equal. The width of the slab strip is again assumed to be 200 mm.

Elements

The concrete slab strip is modelled with plane stress elements and the steel rebars are modelled with embedded reinforcements. An extensive explanation of plane stress elements and embedded reinforcements can be found in section 5.2.2.

5.3.3. Material properties

Concrete properties

The concrete is modelled according to the "Guidelines for Nonlinear Finite Element Analysis of Concrete Structures" [10]. Cracking, tensile behaviour and compressive behaviour are specified as follows.

- **Cracking:** The concrete is modelled with a total strain-based crack model wherein the cracks are smeared over the element area (see Figure 5.13). The advantage of this smeared cracking model compared to a discrete cracking model is that the cracks can occur at any location and in any direction in the mesh. Thus, if you do not know in advance where the cracks will be in the mesh, a smeared cracking model is recommended. This is usually the case for a reinforced concrete slab.
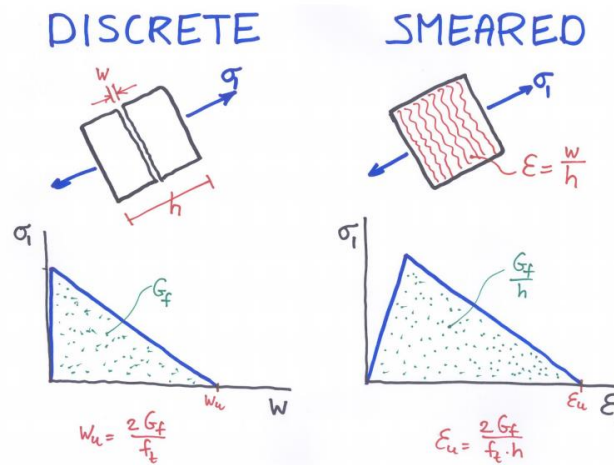
Figure 5.13: Discrete and smeared cracking model.

The cracks will occur perpendicular to the principal tensile stresses. The principal tensile stresses can rotate due to non-proportional loading or redistribution of forces [39]. As a result, the cracks are loaded in shear. There are two models available in DIANA to deal with this consequence:

(1) **Fixed crack model:** the position of the crack is fixed, even if the principal tensile stresses rotate. The friction between the two crack surfaces is accounted for in a shear retention model.

(2) **Rotating crack model:** the crack will rotate and stay perpendicular to the principal tensile stresses.

A smeared cracking model can lead to stress-locking; the stresses are locked-in while they should actually decrease at some locations. The result is that the response of a smeared cracking model is stiffer than that of a discrete cracking model, which can lead to an overestimation of the failure load [40]. Stress-locking is more severe for fixed cracking models. Therefore, a rotating cracking model is used for modelling the concrete.

- **Tensile behaviour:** The Hordijk relation is used to describe the tensile behaviour of the concrete (see Figure 5.14). Tensile softening is implemented in this stress-strain relation. The area under the curve is the fracture energy G_f divided by the equivalent height of the element. Fracture energy is defined as the amount of energy needed to open a crack. The maximum stress is the tensile strength of the concrete (f_{ct}). Both parameters, together with the E-modulus, the ultimate tensile strain and the Poisson's ratio, are given in Table 5.1.

Parameter	Unit	Slab 1	Slab 2
E_c	MPa	31000	33000
v	-	0.2	0.2
f_{ct}	MPa	1.80	2.03
G_F	N/mm	0.096	0.098
ε_{ult}	-	0.044	0.022

Table 5.1: Concrete material properties (1).
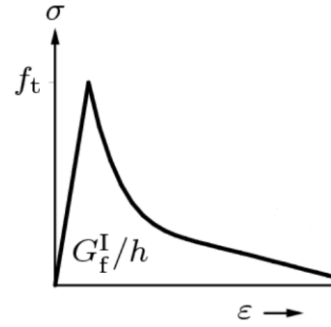
Figure 5.14: Hordijk tensile behaviour of concrete [38].

- **Compressive behaviour:** A parabolic stress-strain relation is adopted for representing the compressive behaviour of concrete wherein a softening branch is included (see Figure 5.15). The reduction model of Vecchio and Collins [41] is used to account for tension-compression interaction and lateral cracking. Parameter β_σ^{min} is the lower bound value of the reduction curve (see Figure 5.16). The relevant parameters of the compressive behaviour are given in Table 5.2.
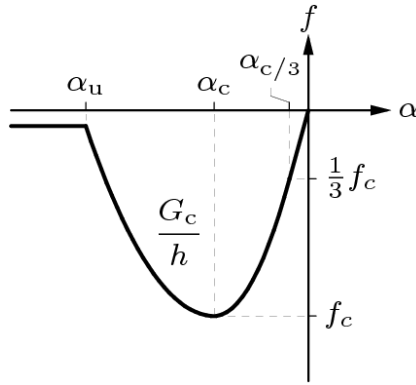
Figure 5.15: Parabolic compression behaviour of concrete in DIANA [38].
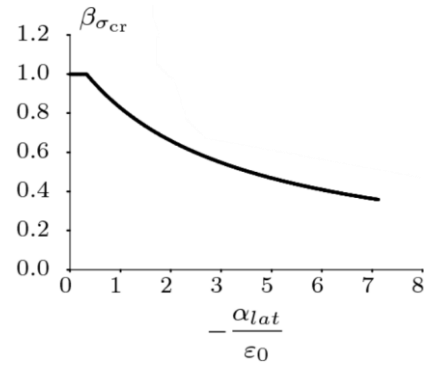
Figure 5.16: Reduction factor due to lateral cracking according to Vecchio and Collins [41][38].

Parameter	Unit	Slab 1	Slab 2
f_c	MPa	33	38
G_C	N/mm	25.94	27.73
α_c	-	-0.0018	-0.0019
α_u	-	-0.190	-0.099
β_σ^{min}	-	0.4	0.4

Table 5.2: Concrete material properties (2).

Steel reinforcement properties

The material properties of the steel reinforcement are equal to those used for the analytical model (see Figure 4.4 in section 4.3). The steel reinforcement has a yield strength of 500 MPa and is modelled with a plasticity range according to Von Mises. A small positive slope is added to the plastic plateau.

5.3.4. Analyses

Mesh

The mesh consists of 20 square elements over the height of the slab strip. Note that Slab 1 and Slab 2, therefore, have different element sizes: 6.25x6.25 mm for Slab 1 and 11.25x11.25 mm for Slab 2. The element size is

chosen to avoid inaccurate results as well as a disproportionate computational time. Appendix B contains a small study into the variation of the mesh size of Slab 1. The mesh of Slab 2 is shown in Figure 5.17.
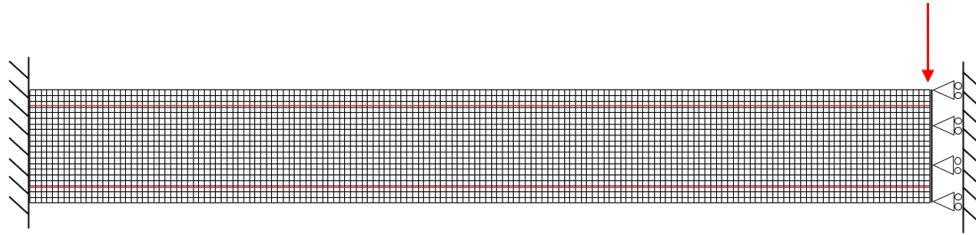
Figure 5.17: Mesh of the numerical concrete slab model of Slab 2.

Load introduction

The analyses are displacement-controlled. For the analyses of Slab 1, the load is applied as a vertical downward displacement at the top-right node of 50 mm. It is incrementally applied with 250 load steps. For the analyses of Slab 2, the load is applied as a vertical downward displacement at the top-right node of 25 mm. It is again incrementally applied with 250 load steps.

Nonlinearities and solving method

The analyses that are performed are a GL as well as a GNL analysis for each reference slab strip. Both the analyses also consider material nonlinearity. The solving method to generate the numerical results is again the Regular Newton-Raphson method in combination with an energy-based convergence norm with a tolerance of 0.001. Appendix B contains a small study into the stability of and the differences between several numerical calculation methods used for the analyses. The line-search algorithm is used to achieve convergence faster. The analyses are stopped if no convergence is reached within 80 iterations. Note that non-convergence does not necessarily mean that the concrete slab strip has failed.

5.3.5. Results and discussion

Calibration of the analytical model

The multiplication factor of the analytical model is calibrated with the results of the numerical concrete slab model. The first step for calibration is to verify with the numerical model whether the compressive strain distribution, and therefore the multiplication factor, is dependent on the location in the vertical height axis of the slab. This is done by studying the compression strains of Slab 1. It turned out that according to the numerical concrete slab model the strain distribution depends on the vertical position of the horizontal concrete fibre. The exponential progression of the compressive strain curve assumed for the analytical model was confirmed by the analytical model when considering the bottom fibre only. On the other hand, the distribution of the strain seems to be more linear at 34.4 mm from the bottom fibre. For three concrete fibres (bottom fibre, 21.9 mm from the bottom and 34.4 mm from bottom) in compression, the strain values resulting from the numerical concrete slab model were underestimated by the analytical model. The Euler-Bernoulli theory can describe the behaviour of the bottom fibre, which is affected largely by nonlinearities, less accurate than the two other fibres closer to the neutral axis of Slab 1. Appendix B.4 contains a further elaboration of the findings mentioned in this paragraph.

It can be concluded that the multiplication factor differs for each concrete fibre. The multiplication factor decreases with decreasing distance to the neutral axis of the slab. However, the exact multiplication factor for each concrete fibre is difficult to determine. Hence, only one value for the multiplication factor MF is chosen to approach the actual structural behaviour as good as possible. This value of MF could therefore be considered an average value of the multiplication factor for all longitudinal concrete fibres in compression.

The best fit of the numerical and analytical results occurs with a multiplication factor of MF=4. Appendix B.1 contains an elaboration on this calibration. It is likely that the multiplication factor does not depend on the geometric and material properties of the slab strips, because the multiplication factor 4 results in the best fit for

both Slab 1 and Slab 2. Yet, it is important to put the calibration in the right perspective: MF=4 provides the best fit between the analytical and 2D numerical results of the slab strips, but does say little about the relation between the analytical model that adopts a multiplication factor of 4 and the actual behaviour of slabs or slab strips. This is because double curvature plate bending, supporting conditions and restraining conditions can affect the response of actual slabs. It may be that a multiplication factor that deviates slightly from 4 is in better agreement with experimental tests of restrained slab or beams.

It is important to note again that calibration of the analytical model with the numerical concrete slab model makes the numerical validation of the analytical model less strong. The results of the analytical model and the numerical concrete slab model are presented in load-deflection diagrams. In addition, several contour plots are used to show the evolution of tensile strains, compressive strains and compressive stresses of the numerical models.

Load-deflection diagram and contour plots of Slab 1

The load-deflection diagram of Slab 1 is presented in Figure 5.18. Several indicative points (points A-F) on the curves are highlighted. Their meaning is explained later in this section.
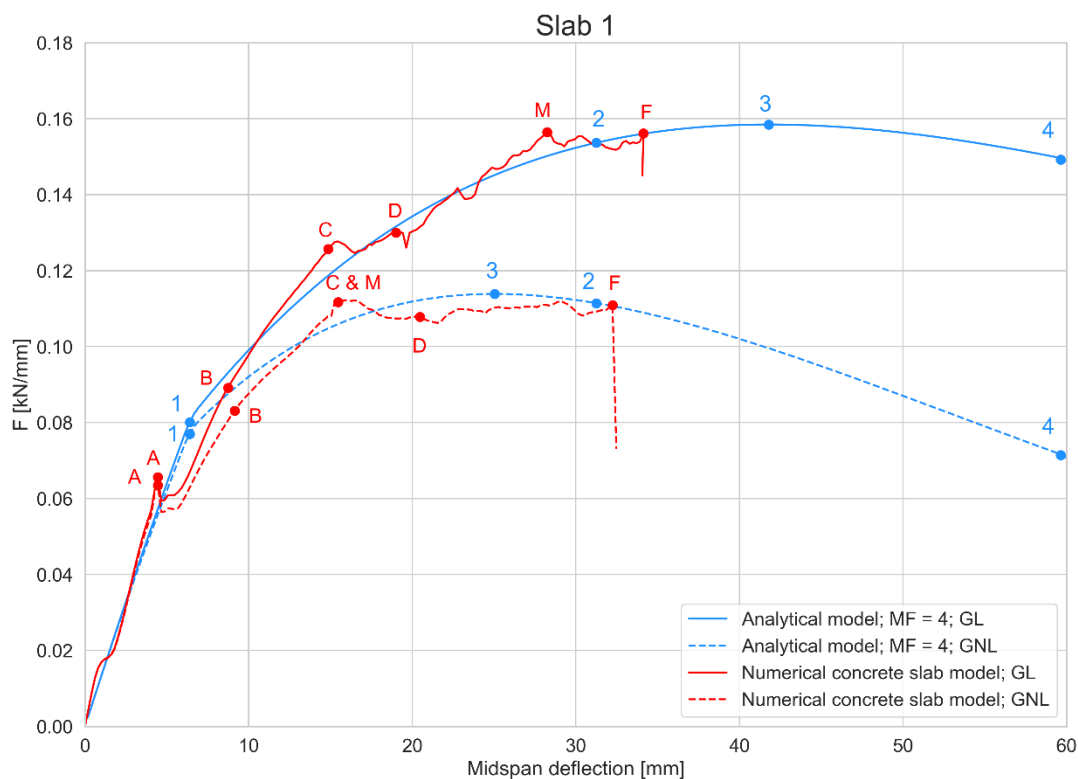
Figure 5.18: Load-deflection diagram of Slab 1.

Contour plots of the principal tensile strains, the principal compressive strains and the principal compressive stresses are presented in this paragraph in order to show the behaviour of Slab 1 throughout the numerical analysis (see Figure 5.20, Figure 5.21 and Figure 5.22). The legends for the principal tensile strains and the principal compressive strains are based on the adopted stress-strain curves. In this way, it is clearly visible where a certain concrete fibre is located on the stress-strain curve. The legends are presented in Figure 5.19. The idea for the legends is taken from the MSc thesis of Hoogen [42], who showed the crack pattern in a similar way. The contour plots are results of the GNL analysis of Slab 1, because this analysis represents the actual behaviour of the slab strip. Also, the crack patterns and compressive strains and stresses for the GL and GNL analysis are so similar that the difference is barely noticeable in contour plots. The contour plots are shown for some of the indicative points used in the load-deflection diagram in Figure 5.18. A height scale factor of 2 is used to make the contour plots of the principal compressive stresses in Figure 5.22 more clear.

(a)   (b)
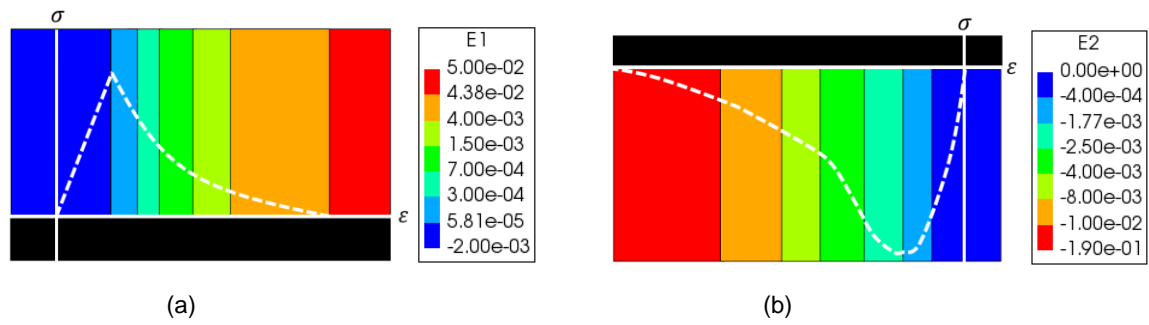
Figure 5.19: Legends for contour plots of the principal tensile strains (a) and the principal compressive strains (b) for Slab 1.
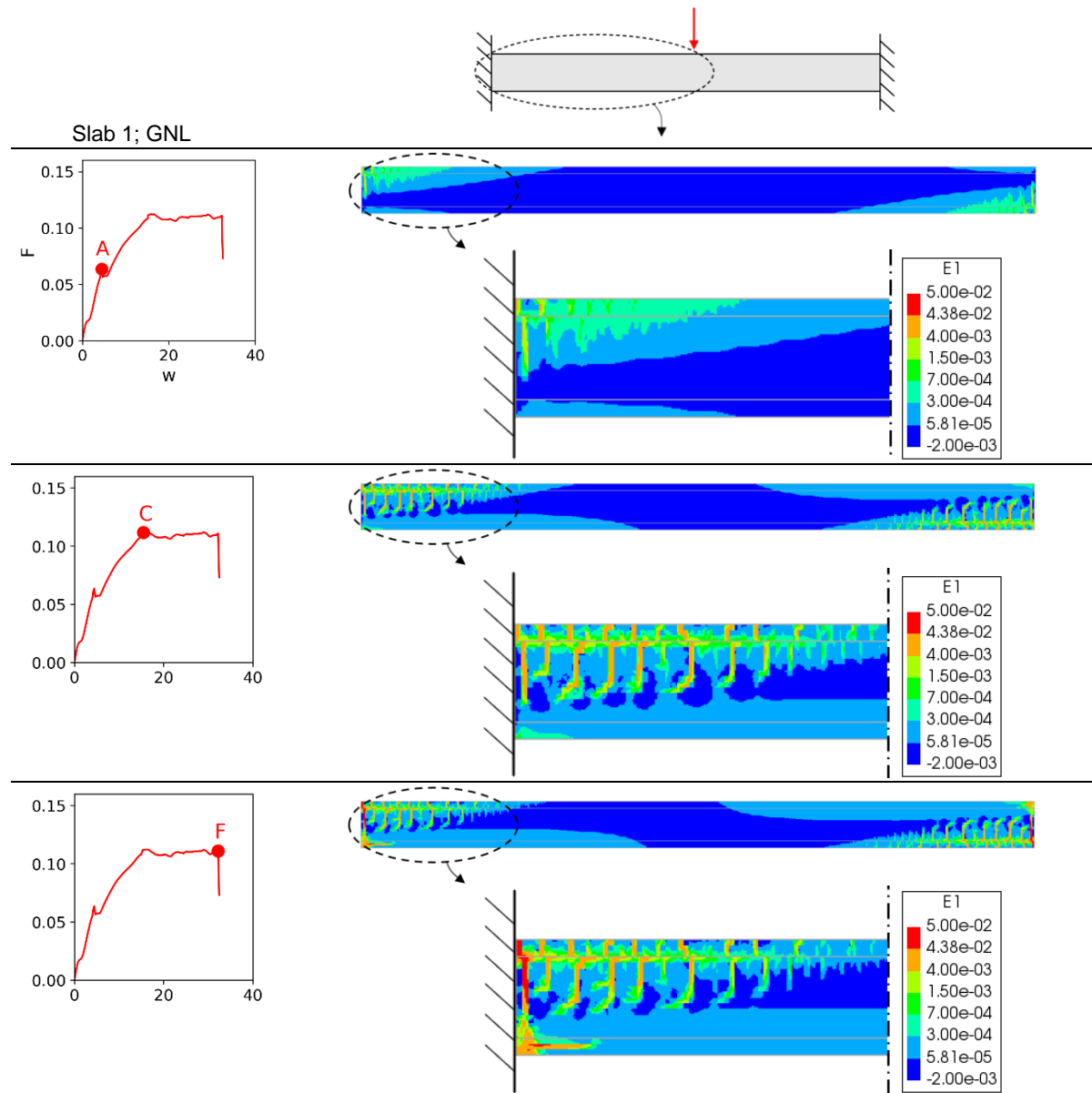
Figure 5.20: Principal tensile strains for the GNL analysis of Slab 1.
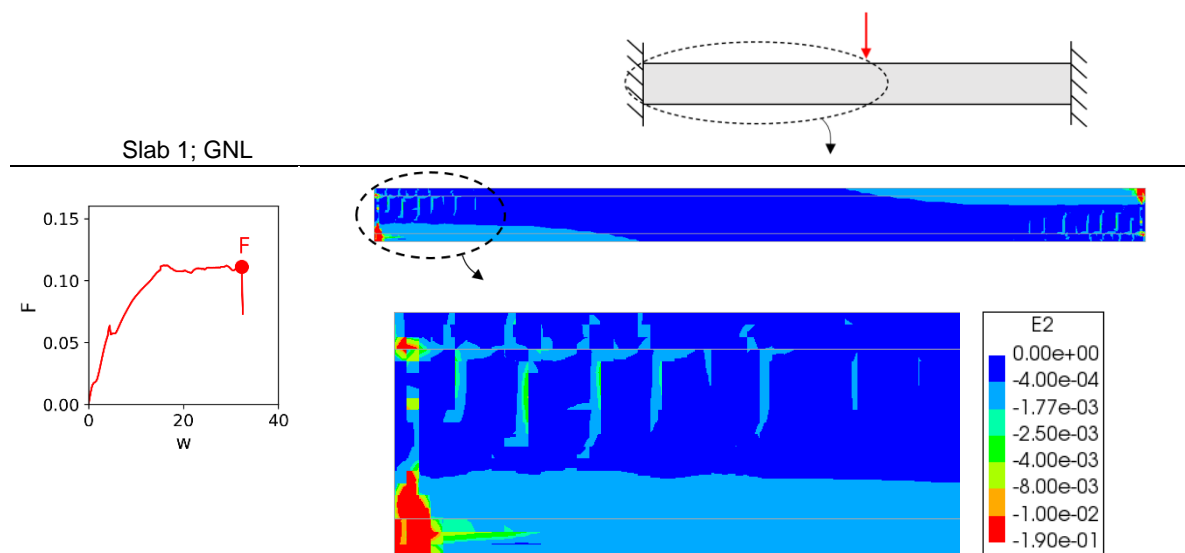
Figure 5.21: Principal compressive strains at failure for the GNL analysis of Slab 1.
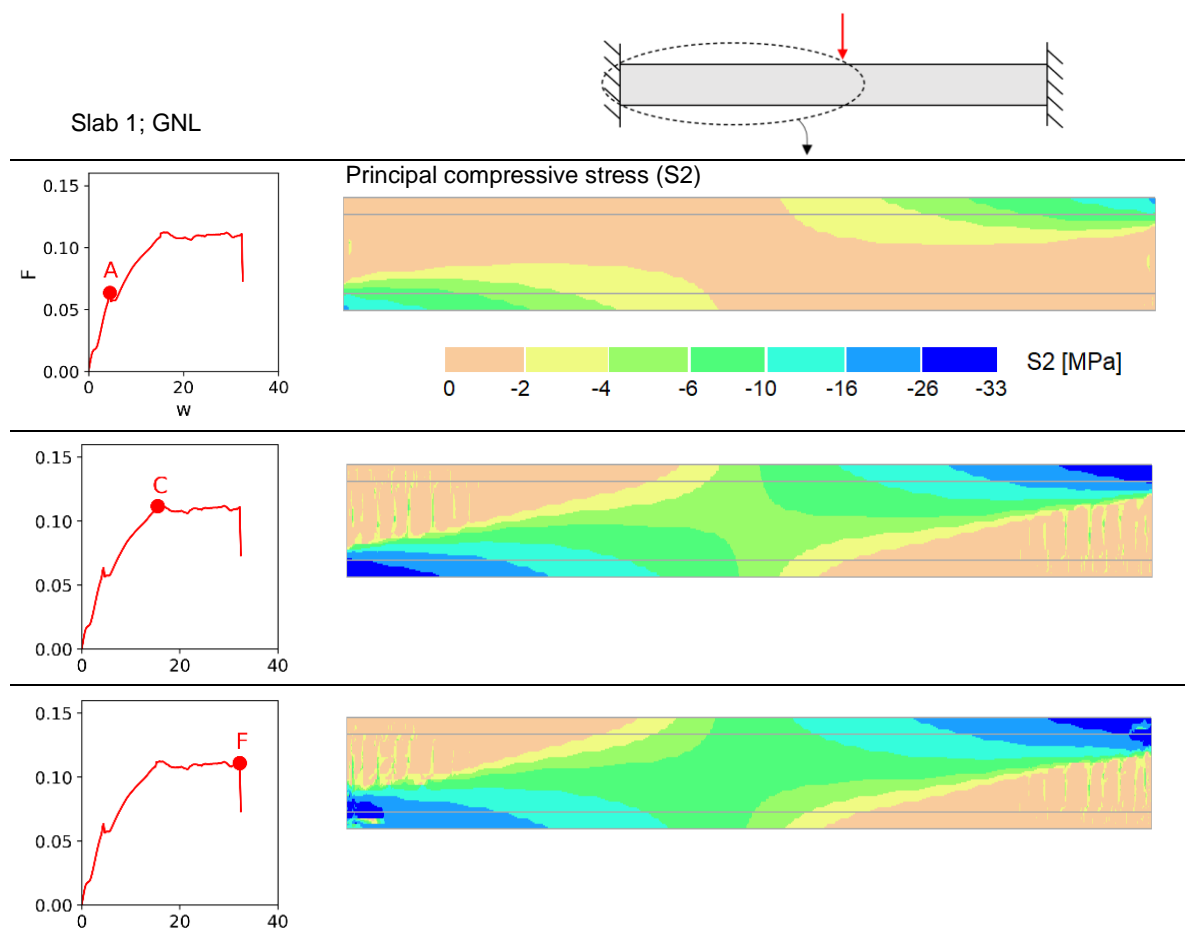
Figure 5.22: Compressive arch development for the GNL analysis of Slab 1 (height scale factor of 2).

The in-plane principal stresses (i.e. stress trajectories) for a specific indicative point in the GNL analysis are shown in Figure 5.23.
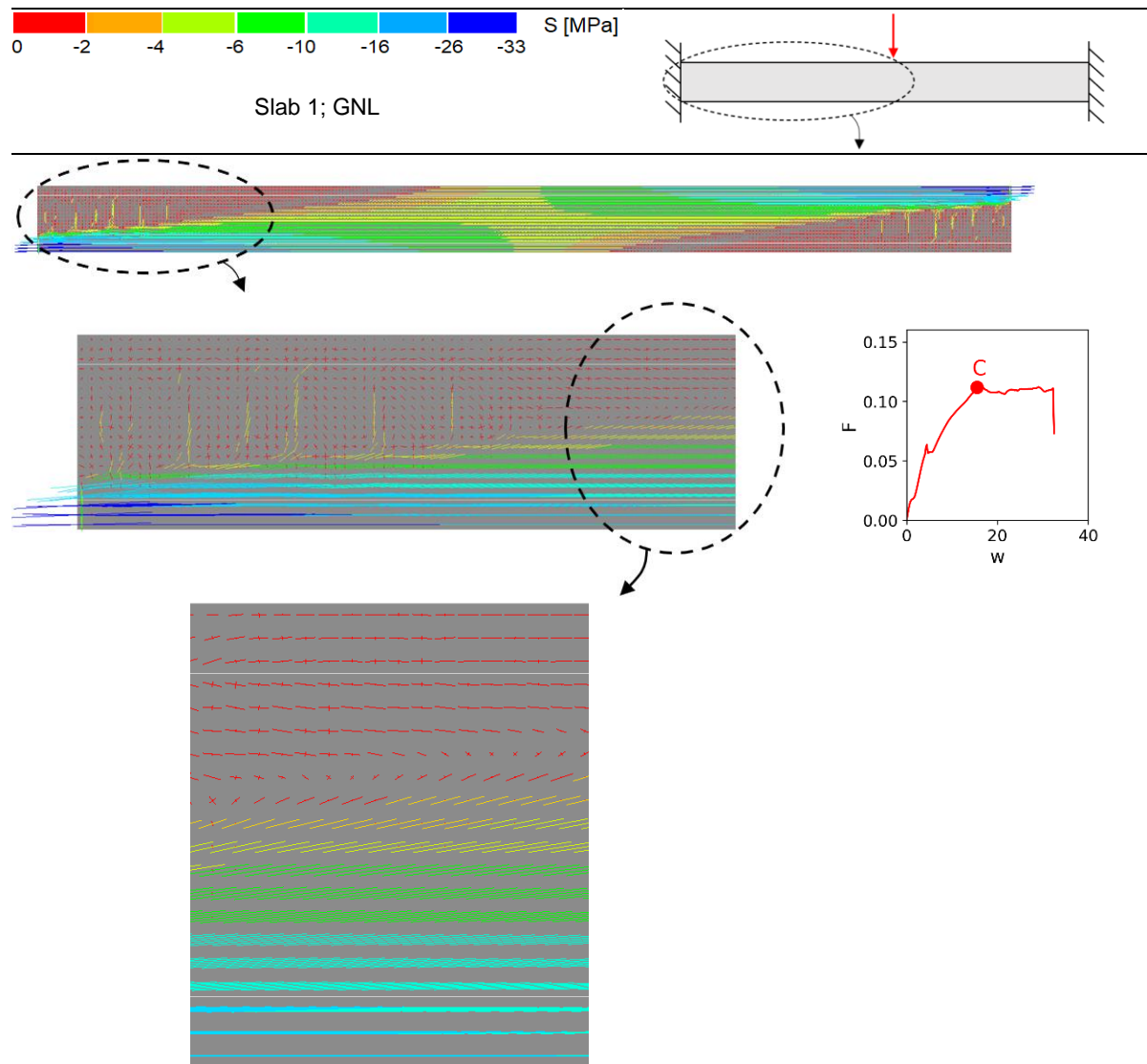
Figure 5.23: In-plane principal stresses for point C in the GNL analysis of Slab 1.

Only relevant plots are shown in this paragraph. More contour plots and plots of the stress trajectories throughout the entire analysis of Slab 1 can be found in Appendix B. These plots will show the structural behaviour for several indicative points in the analysis.

Discussion of load-deflection diagram and contour plots of Slab 1

GL load-deflection curve

The red curve in the load-deflection diagram of Figure 5.18, representing the result of the GL numerical model of Slab 1, is discussed in detail. The maximum load resistance has a value of 0.157 kN/mm, which is significantly higher than the bending capacity of 0.049 kN/mm calculated with EC2 (see Appendix A). The capacity is increased with a factor of approximately 3.2.

The concrete slab strip behaves linear-elastic up to point A. In this linear-elastic stage, the cross-sectional stress diagram is still linear, and the deformations of the concrete and the steel reinforcement are equal. **Point A** indicates the moment when the first two cracks occur simultaneously in the tensile zones at the end support and at midspan of the concrete slab strip because the tensile stress will exceed the concrete tensile strength (see Figure 5.20).

The crack formation stage begins from point A onwards. New cracks will occur until the crack pattern is fully developed. For unrestrained reinforced concrete slabs, the crack formation stage is often characterised by an increase in deformations with a rather constant load. Due to arching action, however, the load is increased between point A and point B after a very small decreasing and horizontal parts of the load-deflection curve. Thus, the stiffness reduction after cracking is commenced is not significant because of the arching action.

Point B indicates the point at which the maximum compressive strain in the outer concrete fibres reaches the value for which the compressive stress is equal to the compressive strength. That is when the compressive stress has reached its maximum value. The compressive stress – compressive strain curve will be decreasing from this point onwards. Between point A and point B, crack formation is still ongoing and the compressive force in the arch is substantially increasing. It is important to note that the compressive strain value at point B is an extrapolated value from the integration point to the lower-left node. Extrapolated values are often less accurate than values at the integration points. The compressive strain at maximum stress in the lower-left integration point is reached right after point B at about 9.5 mm midspan deflection.

Just after point B, a fully developed crack pattern is achieved, and the stabilised cracking stage is commenced. The steel forces are in a stable equilibrium with the compressive forces in the concrete. The stiffness between point B and point C is therefore almost constant and the increase in the load is caused by both bending and arching action.

Point C denotes the moment when the stress in the tensile reinforcement has reached its maximum value. Thus, the tensile reinforcement is yielding, leading to a significant decrease in stiffness. From this moment onwards, bending action will not contribute to a further increase in the load. The maximum load resistance is reached at **point M**. At that moment, a mechanism is formed because of the formation of plastic hinges at the support and midspan. Arching action increases the load from point C to point M. In between, the compression reinforcement is yielding at **point D**. The load remains rather constant after point M. Failure of the concrete slab strip occurs at **point F**. The corresponding failure mode is crushing of the concrete in the compression zones. It should be noted that there is a possibility that the load could increase again after very large deflections have occurred in either the GNL model or in an actual displacement-controlled experiment. TMA would then be the cause of this increase in capacity.

Comparison GL and GNL load-deflection curve

The GNL numerical strip shows similar load-deflection behaviour as the GL numerical strip, because the same stages can be distinguished (see Figure 5.18). However, the GNL red dashed curve is increasingly deviating from the GL red solid curve from point A onwards. Thus, second-order effects will result in a decrease in the load resistance because the internal lever arm, the resultant horizontal force couple and consequently the arching action are reduced due to the deflection of the slab strip. The second-order effect reduces the ultimate capacity by approximately 39% (**GNL reduction effect**).

Yet, the capacity of the GNL slab strip is still much higher than the conventional bending capacity. The enhancement factor is approximately 2.3. Because the GNL model describes the actual structural behaviour, it is numerically validated that the capacity of the concrete slab strip is substantially enhanced due to the development of CMA.

After the tensile reinforcement is yielding at point C, the load will not increase anymore. This is in contrast with the result of the GL model, in which arching action could still enlarge the resistance. In the GNL model, the magnitude of the compressive force couple has already reached its maximum at point C. The ductility decreases only slightly due to the second-order effect.

Comparison GL analytical and numerical load-deflection curve

The meaning of points 1 to 4 is described in section 4.6. The differences between the numerical and analytical results are described and explained. Point B and point 2 essentially have the same meaning, but are far apart. The parabolic compression behaviour assumed for the numerical model in DIANA has a far larger softening branch in the compressive stress-compressive strain diagram than the parabolic curve from EC2 assumed for the analytical model. In addition, the ultimate compressive strain value for the concrete in DIANA (α_c, see Table 5.2) has a considerably higher absolute value than the assumed value of 0.0035 for the analytical model. This explains why point 2 and point 3 are much closer to each other than point B and point M.

The maximum load resistance according to the analytical model shows good agreement with the maximum load resistance following from the numerical model (point 3 and point M). The ductility of the slab strip, however, is overestimated by the analytical model. Moreover, the initial stiffnesses of both models are almost equal. It should be emphasized again that the initial stiffness according to the analytical model is strongly influenced by fairly arbitrary assumptions for the strain in the reinforcing steel. Furthermore, the analytical blue curve gives a good estimation of the overall load-deflection behaviour of the concrete slab strip in DIANA since it goes through the red points as some sort of trend line. This makes sense since the multiplication factor of the analytical model is calibrated to provide the best agreement with the numerical results.

Comparison GNL analytical and numerical load-deflection curve

The GNL analytical model shows good agreement with the numerical results. Analytical estimation of the numerical peak load can be considered accurate. As for the GL model, the blue dashed curve estimates the response of the numerical slab strip quite well. Moreover, because of equal peak loads for the analytical and numerical models, the capacity enhancement factor and the magnitude of the second-order effect are well estimated by the analytical model. The ductility according to the numerical model agrees reasonably well with that of the analytical model. This also leads to the observation that the ductility difference between the linear and nonlinear model is overestimated by the analytical model.

Contour plots

The principal tensile strain contour plot in Figure 5.20 shows that the crack pattern at both supports – the side support and the midspan support – are nearly identical. This is because of the symmetry of the structural system of the half slab strip. Flexural cracks will develop in the concrete slab strip from point A onwards. It can be seen that the cracks are mainly vertically orientated and are located near the side support and near midspan. The cause of the small slant of the flexural cracks is shear stress. Only the red crack is completely open since the value of the principal tensile strain is higher here than the ultimate tensile strain value. The steel reinforcement in this tensile zone has prevented uncontrollable crack width in an earlier stage in the analysis. The two opened cracks occur exactly at the locations assumed for the analytical model.

The lower-left red zone in the principal compressive strain plot in Figure 5.21 shows that a significant part of the fibres in the compression zones at the support and midspan is in the softening branch of the compression curve. This is an indication of failure due to the crushing of the concrete.

Compressive arches will develop inside the concrete slab strip due to the lateral restraint. The development of one of the compressive arches is shown in Figure 5.22. It can be seen that the compressive stresses in the arch are increasing with increasing midspan deflection. Thus, the arching effect will be stronger as the deflection increases.

The plot of the in-plane principal stresses in Figure 5.23 shows the principal stress directions in the concrete slab strip. Shear stresses are zero in the principal coordinate system. The principal stresses are directed from the bottom left to the top right of the half slab strip. The stresses are orientated at a slight angle, which changes in the GNL analysis. Considerably high compressive stresses can be observed at the bottom left and the top right of the half slab strip.

A more detailed study into the principal compressive strains and stresses in the compression zone at the side support of Slab 1 is done in the paragraphs below to gain more insight into the behaviour of the concrete in this region and the failure mode of the slab strip. Also, a comparison with the analytical results can be made. The principal compressive strains and stresses are equal for the side support and midspan cross-section because of symmetrical crack patterns. It is for this reason that the principal strains and stresses are studied near the side support only.

Principal compressive strains and stresses of Slab 1

Principal compressive strains at the support section

The principal compressive strains at the side support cross-section (see Figure 5.24) are plotted over half of the height of the slab strip. It is of interest to study the state of strain in the compression zone in which crushing will occur. The strains according to both the analytical and numerical model are given. Four numerical graphs are shown in each diagram in which the location of the result and the nonlinearity differs. INT means that the strain value is obtained from the location of the integration point. NODE means that the strain value is obtained from the location of the node. The NODE results are extrapolated values, while the INT results present the actual results of the FEAs.
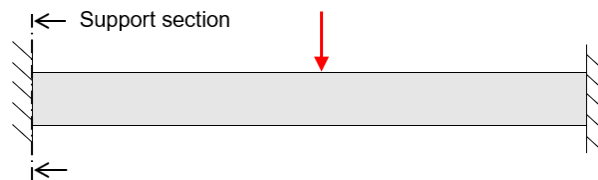
Figure 5.24: Support section of Slab 1 (not to scale).

The principal compressive strain is plotted for five specific midspan deflections. Points B, C and D of the GNL model in Figure 5.18 are used because they are equally distributed over the load-deflection curve. Also, a point for a very small midspan deflection of 1 mm is chosen, and it is referred to as point 0. The failure point F is the last point that is used for the plots. Note that the deflection of point F_{GNL} and point F_{GL} differs. The plots belonging to this last point can therefore not be used to compare the GL and GNL strains. It is still chosen because it is of interest to see the strains and stresses at failure for both models.

Point	Midspan deflection
0	1 mm
B_{GNL}	9.1 mm
C_{GNL}	15.4 mm
D_{GNL}	20.5 mm
F_{GL} / F_{GNL}	32.2 / 34.1 mm

Table 5.3: Points used for strain and stress plots of Slab 1.

The strains at maximum stress according to the analytical and the numerical model are plotted with vertical dashed lines. The red dot indicates the position of the concrete fibre in which the strain at maximum stress is just reached according to the GL numerical model. The white dot and blue dot have a similar meaning as the red dot, but respectively for the GNL numerical model and the analytical model.
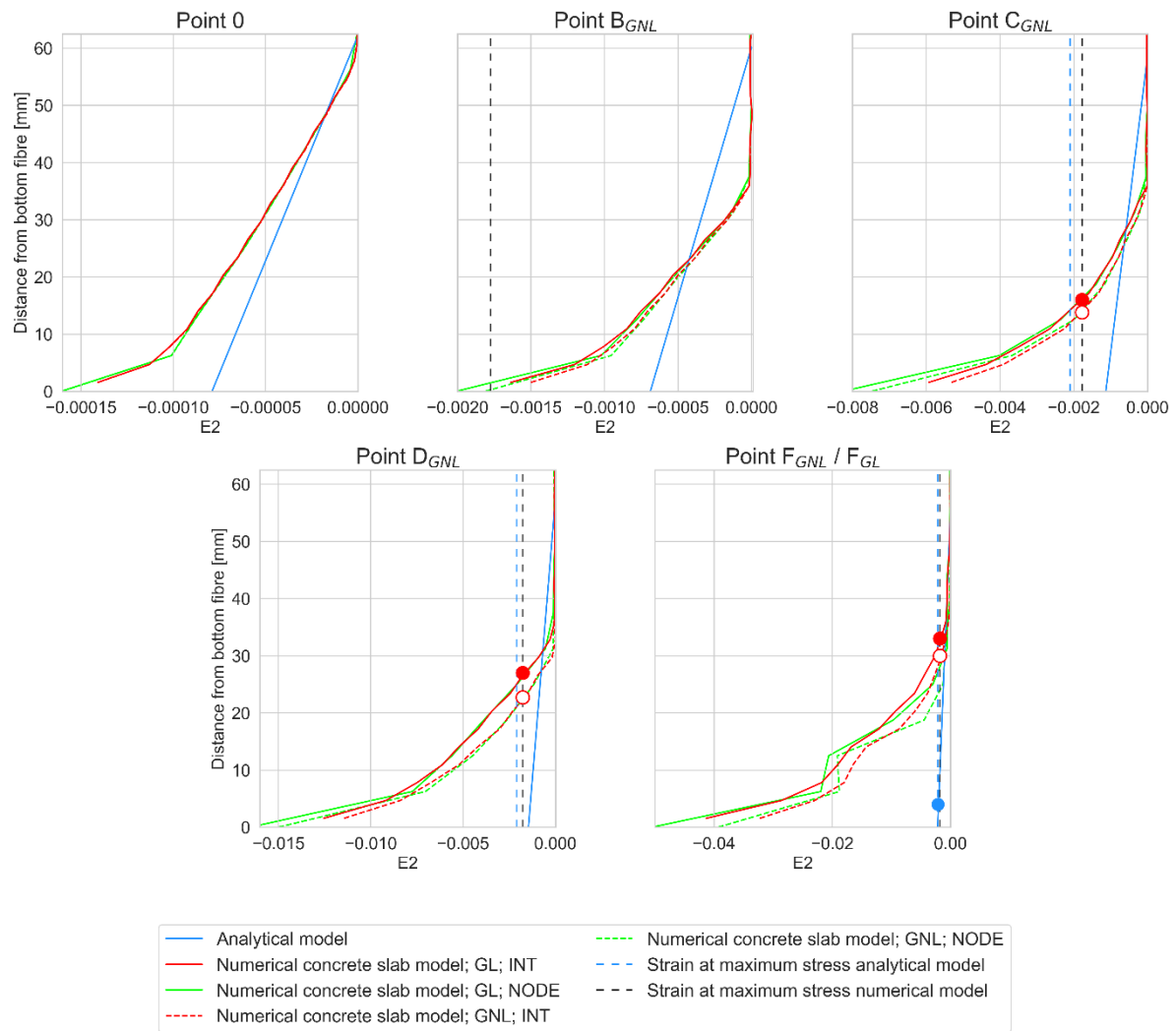
Figure 5.25: Principal compressive strains at the support section of Slab 1.

Numerical results: The results at the integrations points and the nodes agree reasonably well, meaning that extrapolation of the results does in this case not lead to inaccurate results. However, note that the principal strain at the nodes for points B-F slightly overestimates the strain values at the integration points in the zone close to bottom fibre.

The compressive strains at the support have an exponential or parabolic distribution over half the height of the slab strip. For each point, the maximum principal compressive strain occurs in the bottom fibre. The point of zero principal strain seems to be shifting downwards as deflections are increasing. For example, at point 0 zero strain is achieved at about 60 mm from the bottom fibre, while at point D it is achieved at about 35 mm from the bottom fibre. This shift is largest between point 0 and point B and very minimal between point B and point D. Yet, the principal compression strain seems to increase between point D and point F at a distance of 35-40 mm from the bottom fibre. Therefore, the compression zone decreases from point 0 to point D, and thereafter increases again.

The principal compressive strain in the outer fibre reaches the strain value at maximum stress at point B. As mentioned before, this strain value is the value at the lower-left node. Right after point B, the principal compressive strain at the integration point also reaches the strain value at maximum stress, which is a turning point value in the compressive stress-compressive strain diagram. Any compressive strains greater than this turning point value will no longer lead to an increase in compressive stress. Theoretically, the stress should even decrease for strains greater than this value. As can be seen in Figure 5.25, the red and white dot move further and further up in the

diagram with increasing midspan deflection. This means that in more and more concrete fibres in this section the concrete compressive capacity is reached.

The difference between the numerical results of the GL and GNL model is very small. Yet, the difference seems to become larger with increasing midspan deflection. This makes sense since the deformed geometry differs more from the undeformed geometry for larger deflections, leading to an increase in the second-order effect. The GNL model leads to slightly lower strains, because the change in length is considered in the calculation of the strain.

Analytical results and comparison with numerical results: First, the difference between the principal compressive strains resulting from the analytical GL and GNL model is so small that the results of both models can be presented by one and the same blue graph. This is in contrast with the numerical results. Second, the analytical model assumed a linear strain distribution over the height of the slab strip, which is not in line with the numerical result. As can be seen in Figure 5.25, the analytical model underestimates the principal compressive strains at the support. This underestimation is greatest in the extreme fibres and at large midspan deflections. It holds that the greater the deflection, the greater the relative difference between the compressive strains of the analytical and numerical model in the outer concrete fibre.

Thirdly, the decrease in the contact depth assumed for the analytical model does not match with the decrease in the compression zone of the numerical result. The numerical model shows that the decrease in the compression zone is larger than analytically predicted. Also, the abrupt increase in contact depth between point D and point F is against the expectation of the analytical model. Lastly, the compressive strain in the outer fibre reaches the strain value at maximum stress between point D and point F, which is much later than for the numerical model.

Principal compressive stresses at the support section

In Figure 5.26, the principal compressive stresses are presented in the same way as the principal compressive strains in Figure 5.25. The positions of the red, white and blue dot correspond to the positions in the principal strain diagrams in Figure 5.25.
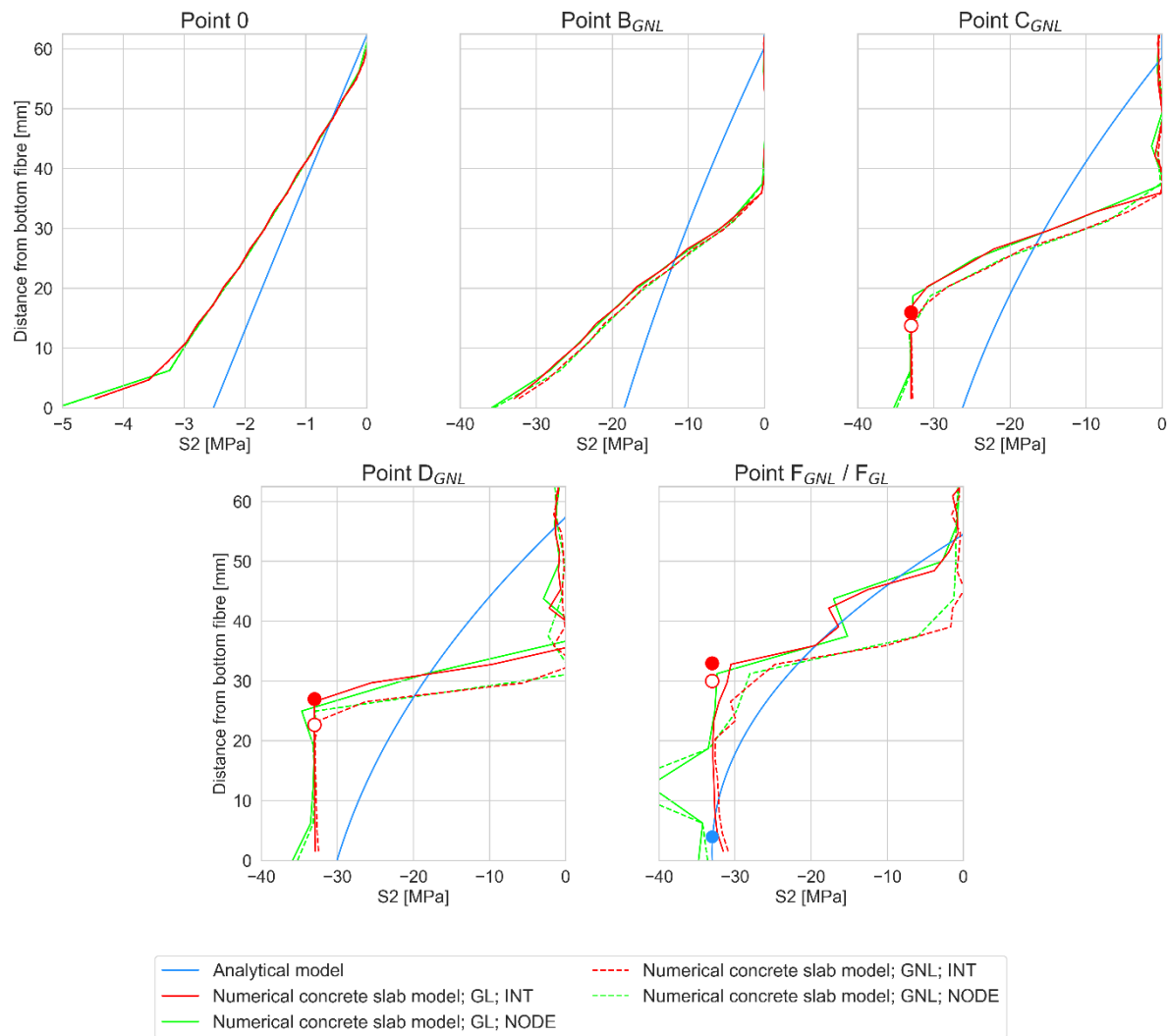
Figure 5.26: Principal compressive stresses at the support section of Slab 1.

Numerical results: The first observation is that the stresses at the integration points are very similar to the stresses at the nodes. However, the stresses exceed the concrete compressive strength close to bottom fibre level at points C, D and F. Here, extrapolation of the stress values leads to inaccurate results. Secondly, the stress diagrams of the numerical model are in reasonable agreement with the strain diagrams considering the assumed stress-strain relation of concrete in compression. One exception is the small deviation of the red and white dot in the stress diagram of point F, in which the stresses in the integration points are lower than the compression strength.

As with the strains, the stresses of the GNL are slightly lower than the stresses of the GL model. However, the significant difference between the GL and GNL load-deflection curve is only for a very small part caused by the difference in compressive stresses. The difference between the curves is mainly caused by the difference in the internal lever arm of the resisting bending moments.

Moreover, the stress diagrams clearly show that the compression zone increases between point D and point F, which is in correspondence with the principal strain diagrams. Also, it holds that the slope of the softening curve of the concrete compression behaviour is very small because of the small element size and the subsequent large compressive fracture energy and ultimate compressive strain. Therefore, the decrease in compressive stress in the outer fibre is relatively small, even though the strain value is many times greater than the strain value at maximum stress.

The area under the stress curve is related to the compressive fracture energy. Varying the compressive fracture energy may largely influences the response of the restrained slab strip. A study of this variation is included in Appendix B.

No clear sign of complete crushing of the concrete can be seen in the principal stress diagrams at this support section: the stress barely decreases and the principal strain value at failure is not close to the ultimate strain value assumed for the concrete. It could be that crushing of the concrete is more severe at a certain horizontal distance from the side support. Therefore, the principles strains and stresses are plotted for a vertical cross-section at a horizontal distance of 6.25 mm from the side support (section A-A). This is done in the paragraph below (see "Principal compressive strains and stresses at section A-A"), but first the analytical results of the principal compressive stresses in Figure 5.26 will be discussed, and a comparison is made between the analytical and numerical results.

Analytical results and comparison with numerical results: The analytical compressive stress plots are almost linear for point 0 and point B. From point C onwards, the non-linearity of the plot increases. Meanwhile, the compression zone decreases marginally because this is required to maintain the horizontal equilibrium of the rigid body. It is only between point D and point F that the principal compressive stress reaches the maximum capacity.clar

The compressive stress in the outer concrete fibres is considerably lower for the analytical model than for the numerical model. On the other hand, the stress at a distance between 35 and 60 mm from the bottom fibre is overestimated by the analytical model. Yet, the areas under the stress diagrams of the analytical and numerical models are nearly equal. Thus, the underestimation of the compression zone by the analytical model seems to be compensated by the underestimation of the compressive strain. It is likely that the equal areas under the stress diagrams lead to similar load-deflection behaviour and similar maximum load resistances. Another clear difference is that the maximum strength is reached much earlier in the numerical analyses than predicted by the analytical model. This difference was observed before in the principal strain diagram in Figure 5.25.

<u>Principal compressive strains and stresses at section A-A</u>

The principal compressive strains and stresses of section A-A (see Figure 5.27) are studied to gain more insight into the crushing of the concrete in the zone near the side support. Due to the similarities of the GL and GNL principal strains and stresses for the support section, the principal strains and stresses are now only plotted for the GNL model. After all, the GNL model represents the actual structural behaviour.
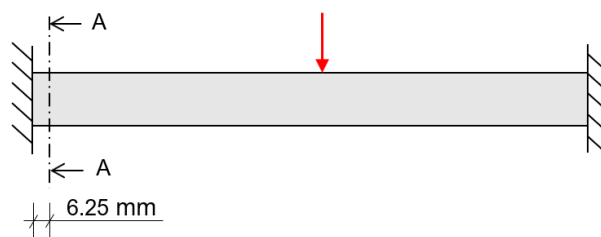
Figure 5.27: Section A-A of Slab 1 (not to scale).
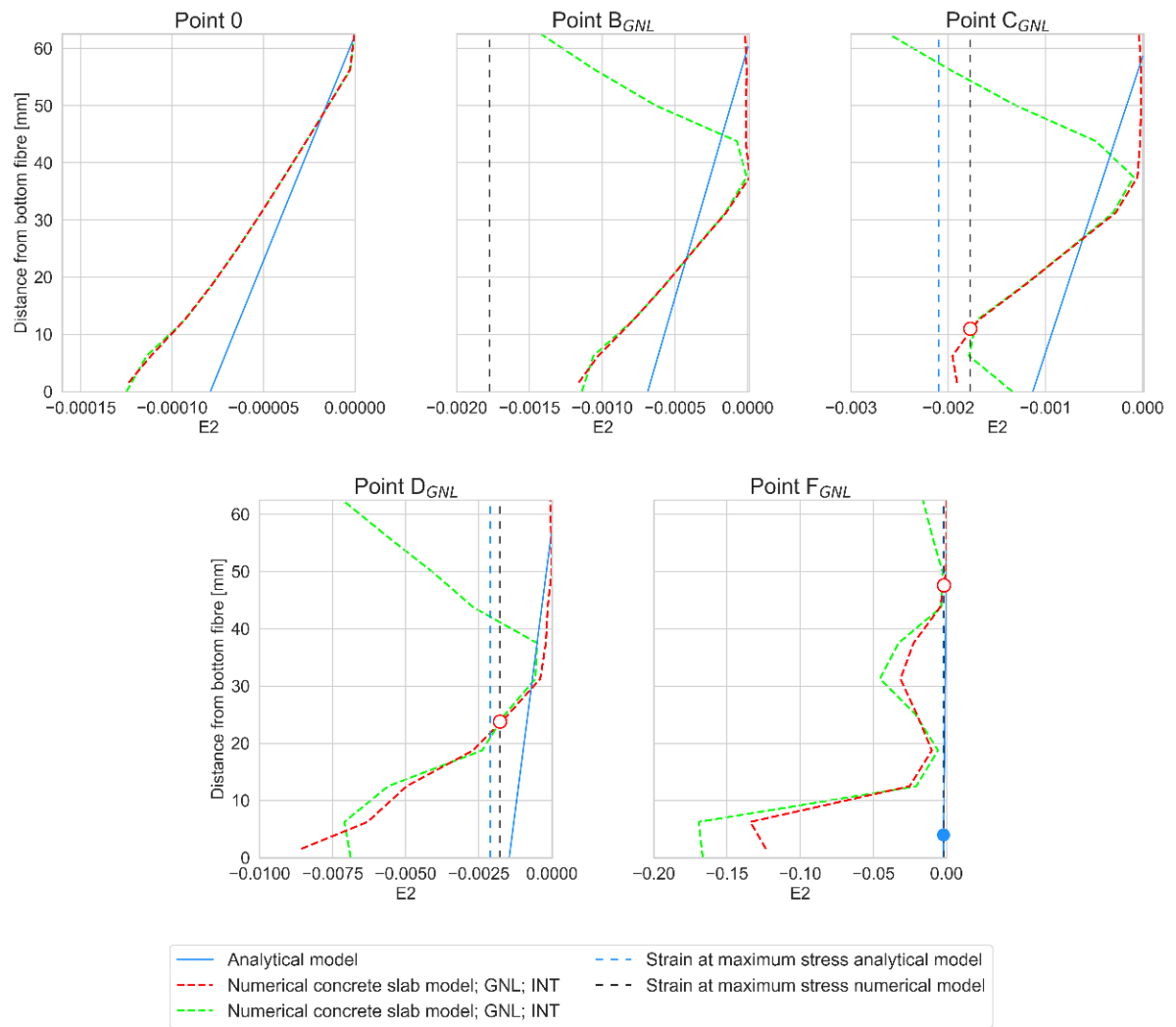
Figure 5.28: Principal compressive strains at section A-A of Slab 1.
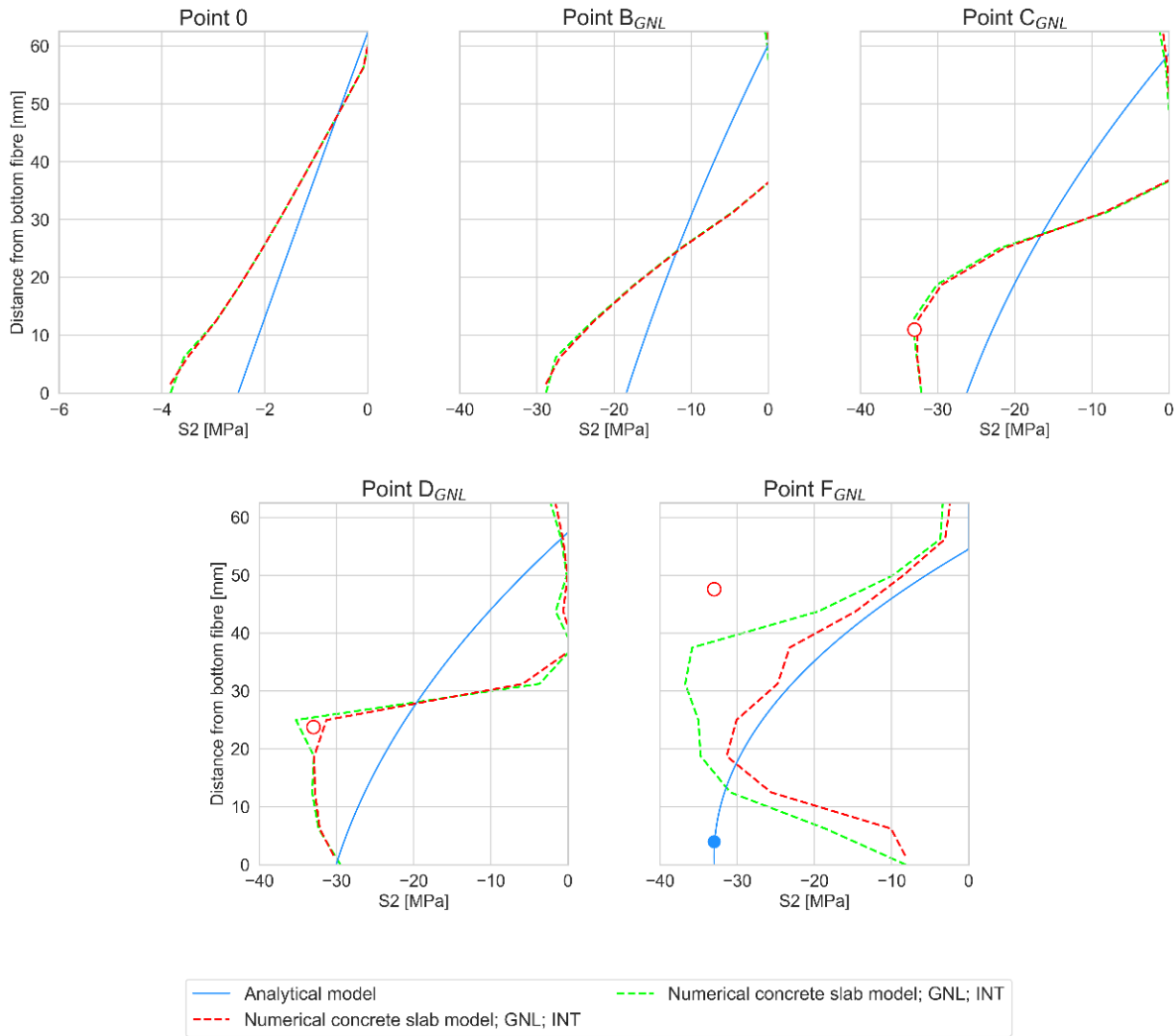
Figure 5.29: Principal compressive stresses at section A-A of Slab 1.

The principal strain plots of section A-A represent similar results as those of the support section: the compressive strain increases with increasing deflection; the compressive zone depth decreases considerably between point 0 and point B and in most cases, the strain in the bottom fibre is the largest. An important difference between the principal strain plots of section A-A and the support section is the maximum strain value at failure. This value is considerably larger for section A-A than for the support section. The value is close to the ultimate compressive strain value for which the concrete is completely softened. Figure 5.29 shows that the principal compressive stress at the outer fibre of this cross-section has dropped considerably at failure. These observations provide strong evidence that crushing of the concrete leads to final failure of Slab 1.

Load-deflection behaviour and contour plots of Slab 2

The load-deflection diagram of Slab 2 is presented in Figure 5.30. Points A, B, C, D, M and F are also used for the load-deflection diagram of Slab 2. The descriptions given in the paragraph "Discussion of load-deflection diagram and contour plots of Slab 1" will also hold for these diagrams, meaning that each point has the same meaning in the Slab 1 and Slab 2 diagram. For example, point M will always indicate the maximum resistance load.
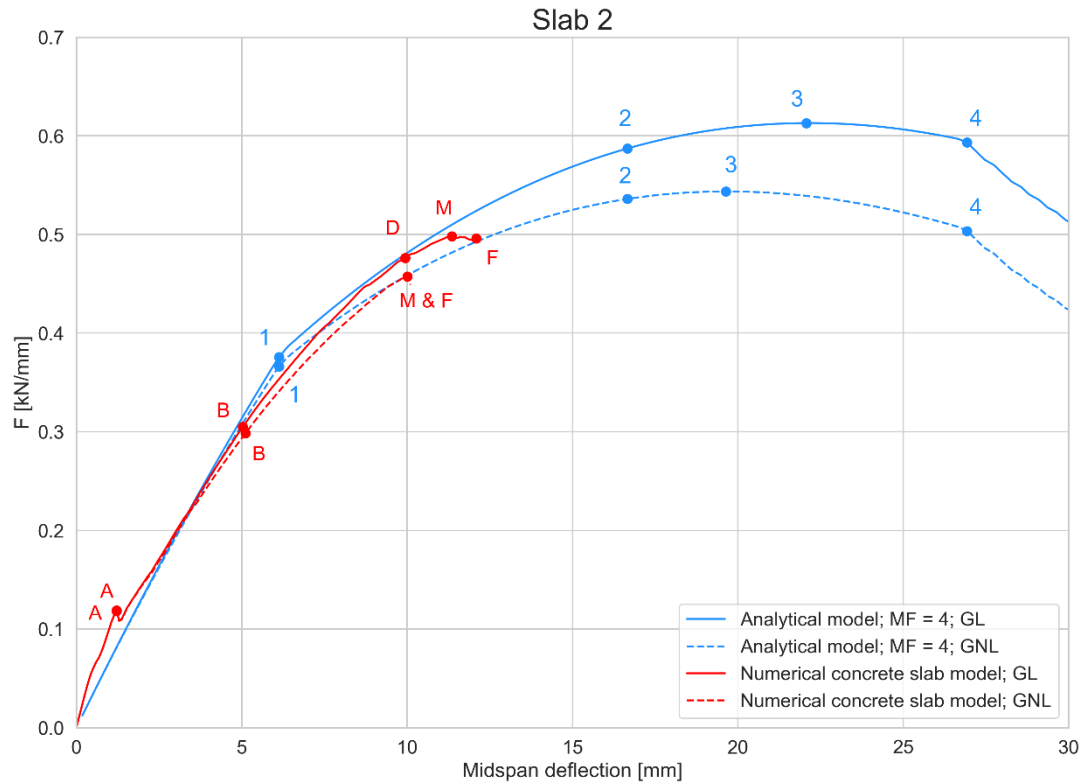
Figure 5.30: Load-deflection diagram of Slab 2.

Contour plots of the principal tensile strains, the principal compressive strains and the principal compressive stresses are presented in this paragraph in order to show the behaviour of Slab 2 throughout the numerical analysis (see Figure 5.32, Figure 5.33 and Figure 5.34). The legends used for the plots are presented in Figure 5.31.
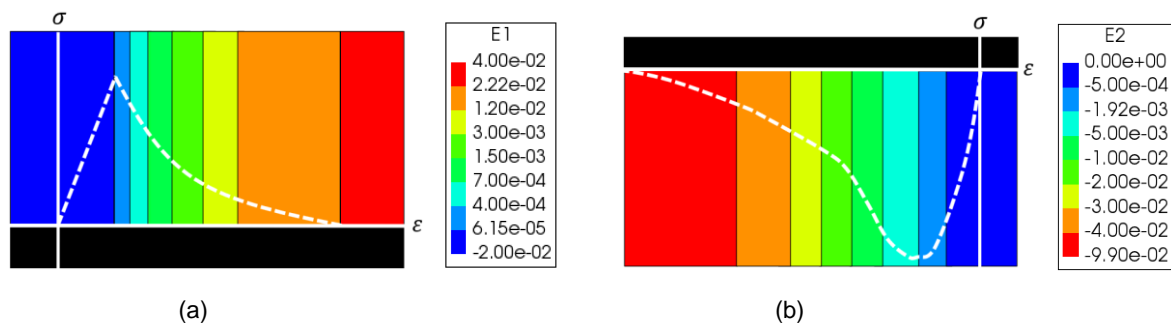
Figure 5.31: Legends for contour plots of the principal tensile strains (a) and the principal compressive strains (b) for Slab 2.
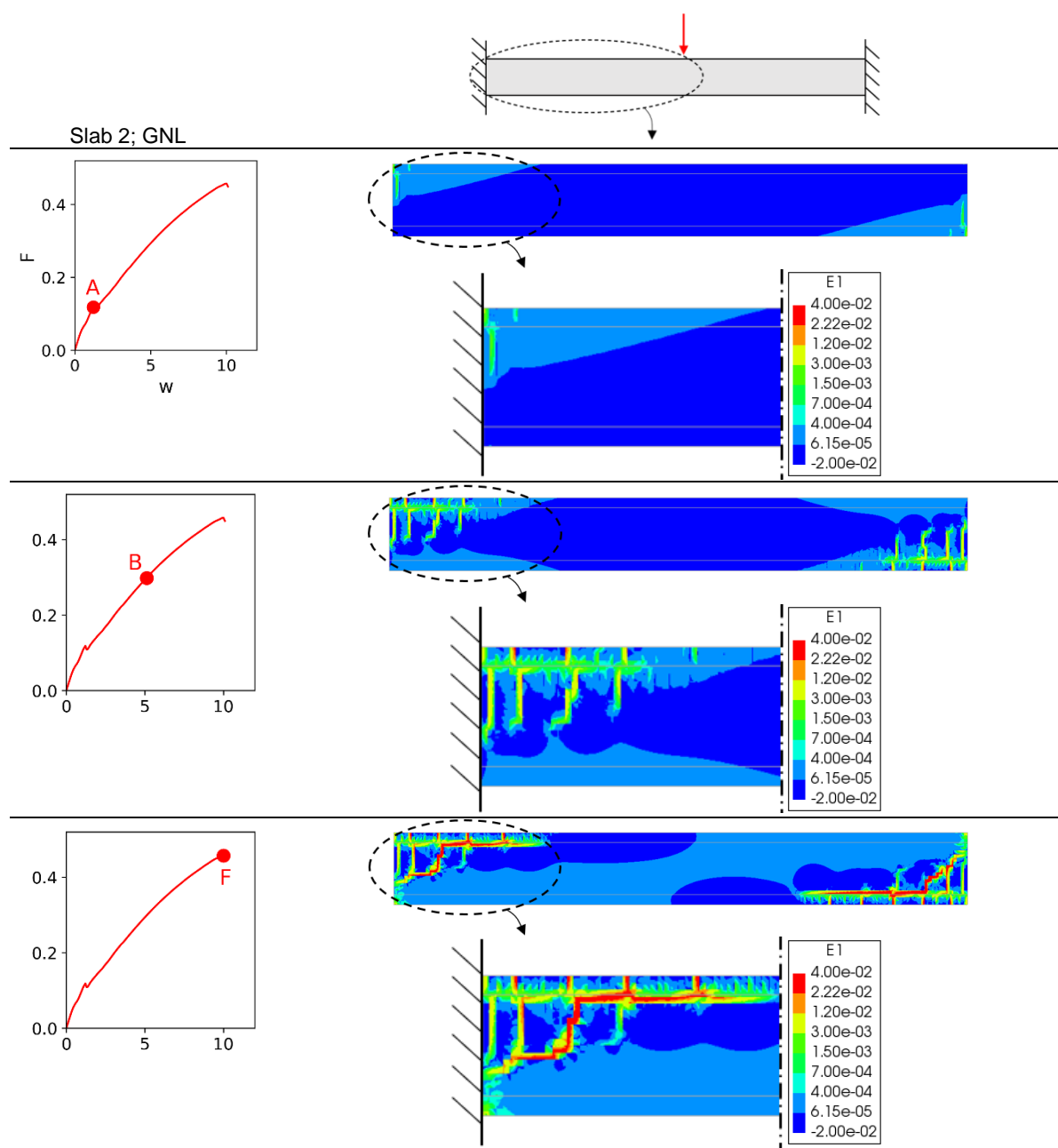
Figure 5.32: Principal tensile strains for the GNL analysis of Slab 2.
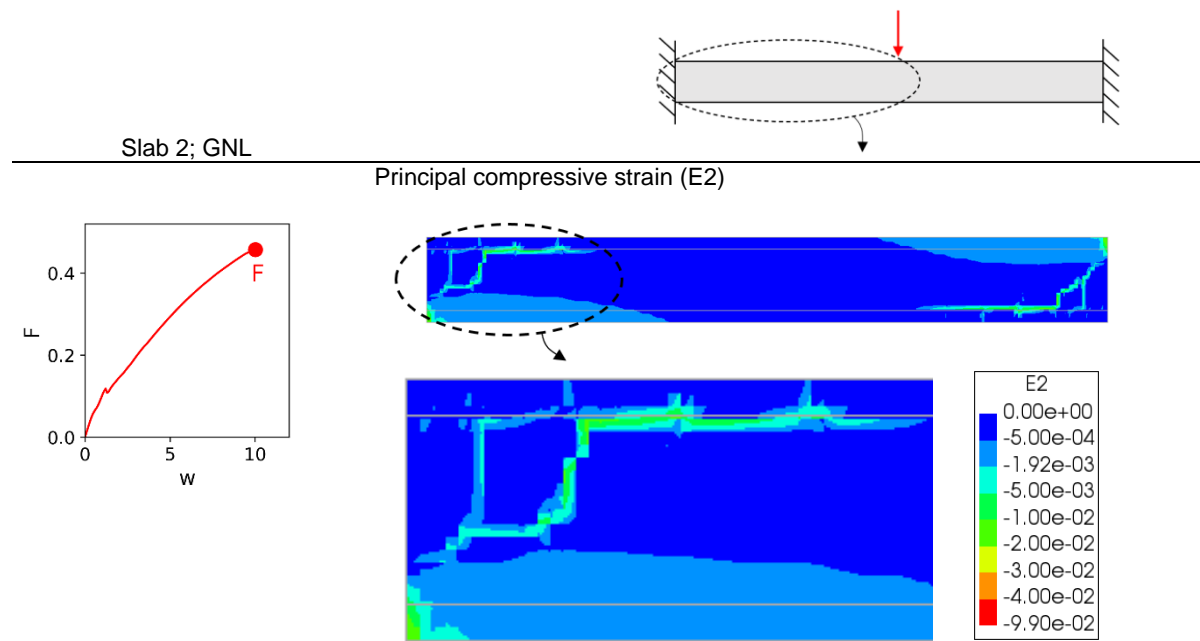
Figure 5.33: Principal compressive strains at failure for the GNL analysis of Slab 2.
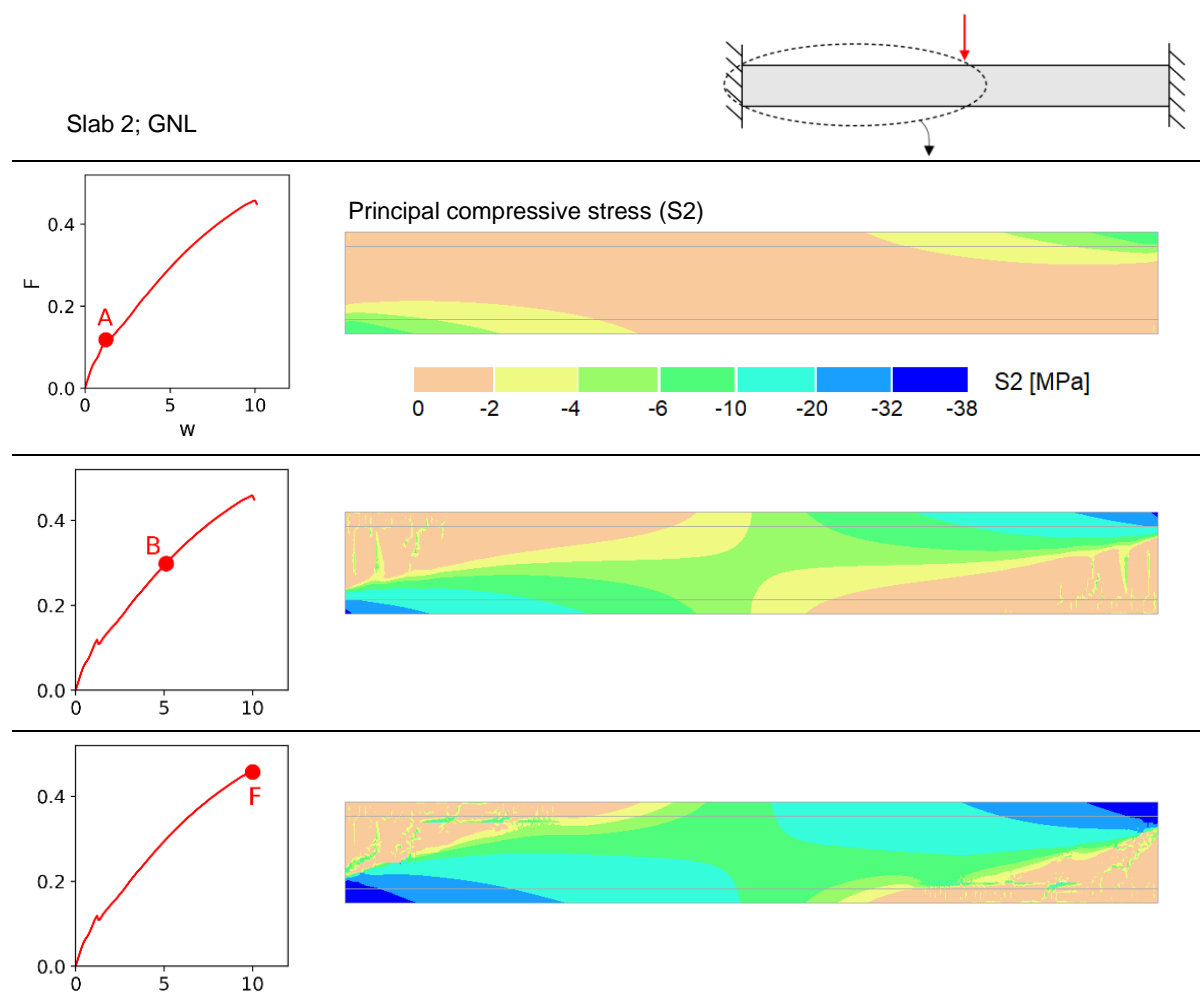
Figure 5.34: Compressive arch development for the GNL analysis of Slab 2.

The in-plane principal stresses (i.e. stress trajectories) are shown in Figure 5.35.
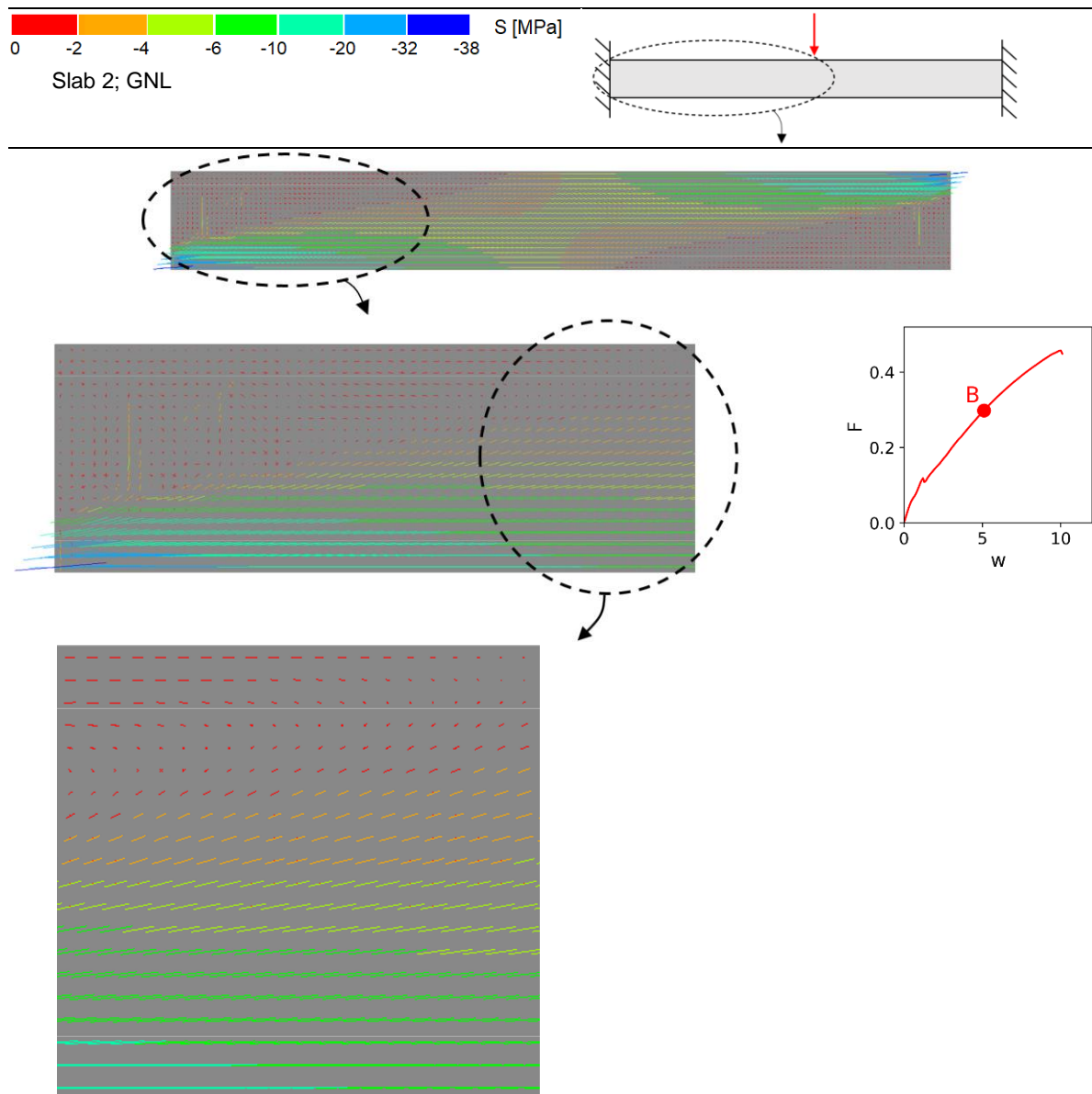
Figure 5.35: In-plane principal stresses for point B in the GNL analysis of Slab 2.

Discussion of load-deflection behaviour and contour plots of Slab 2

From the load-deflection diagram of Slab 2 in Figure 5.30 it can be seen that the development of arching ensures that the stiffness is hardly reduced after the formation of tensile cracks. Remarkably, the tensile reinforcement does not yield during the analyses. This likely is because an insignificant part of the load on the non-slender Slab 2 is carried by bending action. On the other hand, the compression reinforcement is yielding at point D, meaning that the maximum compressive strains in the compression reinforcement are larger than the maximum tensile strains in the tensile reinforcement. It can thus be concluded that arching action is the predominant load-bearing mechanism for Slab 2.

The analytical model gives an accurate approximation of the numerical results of Slab 2 until sudden numerical failure of the concrete slab strip occurs. Thus, the analytical model overestimates the maximum load resistance of the concrete slab strip. With a bending capacity of about 0.17 kN/mm according to the EC2, the enhancement factor is 2.6 according to the numerical model and 3.1 according to the analytical model. Moreover, geometrical nonlinearity will result in less ductility and a lower capacity of the slab strip. The second-order reduction effect is however limited, with a percentage of less than 10%. In contrast, this effect is more than 10% according to the analytical model.

Numerical instability of Slab 2 occurs prior to failure of the analytical strip possibly because of an unforeseen local mechanism caused by a combination of bending and shear stresses. Shear stresses are ignored in the analytical model, while they clearly play a role in the structural behaviour of Slab 2. At the end of the numerical analysis, two large diagonal tensile cracks have appeared at the locations where the shear forces are maximum (see Figure 5.32). The vertical flexural cracks have propagated perpendicular to the principal tensile stresses, which are diagonally oriented. At the last load step of both analyses, convergence could not be found within the maximum of 80 iterations. Therefore, the analyses are stopped, but this does not necessarily mean that the concrete slab has failed. Figure 5.33 supports this statement since the fibres in the compression zone are not far in the compressive softening branch. Two methods are used to find out what the actual failure load of Slab 2 is and whether the load and/or ductility could be increased:

(1) **Method 1:** Application of shear reinforcement to mitigate the diagonal tension cracks.

(2) **Method 2:** Changing the vertical supporting conditions and allowing for non-converged load steps within the analyses.

Method 1: Additional shear reinforcement

Propagation of the diagonal cracks can be mitigated by applying shear reinforcement in the concrete slab strip. The reinforced concrete slab strip would then most probably fail on bending and consequent crushing of the concrete. It might be that the capacity of the slab strip is then closer to the analytically predicted capacity.

It is studied whether the above statements are true by applying shear reinforcement in Slab 2. The shear reinforcement is applied at either side of the half slab strip, because the bending stresses are maximum here. The shear reinforcement is modelled with embedded grid reinforcements with dimensions 225x250 mm. This is done to allow for an immediate vertical transfer of tensile forces right next to the support. This cannot be achieved with ordinary vertical stirrups. In addition, ordinary stirrups can lead to kinks in the load-deflection curve, while the grid provides continuous additional vertical stiffness. Note that it is required that the geometry of the horizontal rebars of the grid reinforcements is set to zero to prevent additional stiffness in the longitudinal direction of the slab strip.
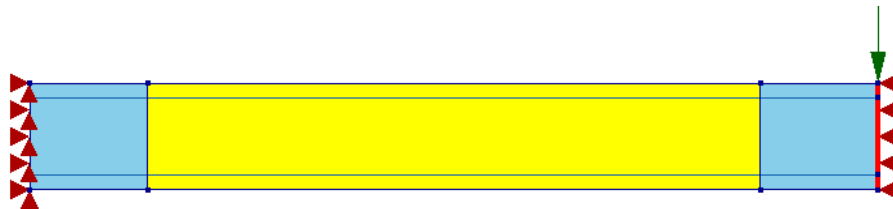
Figure 5.36: Numerical concrete slab model of Slab 2 with shear reinforcement in DIANA.

Load-deflection diagram and contour plots of Slab 2 with shear reinforcement

The load-deflection diagram of Slab 2 with shear reinforcement is given in Figure 5.37. Figure 5.38 and Figure 5.39 show respectively the principal tensile strains and the principal compressive strains and stresses at failure (point F) of the GNL model.
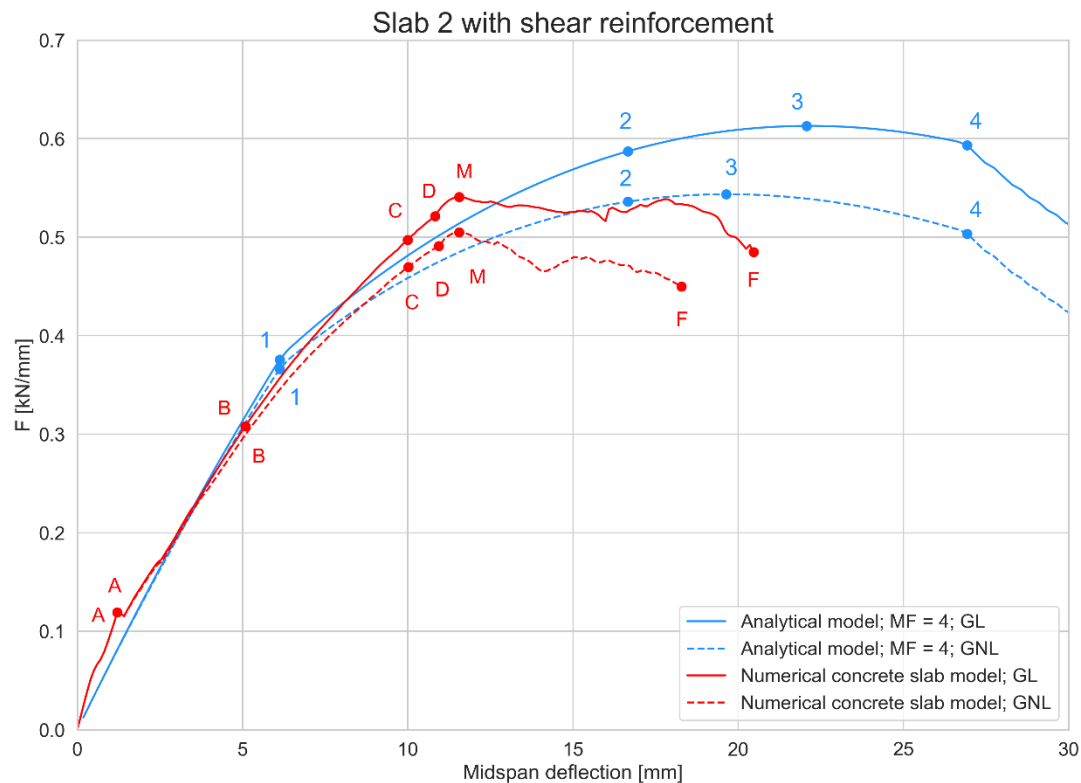
Figure 5.37: Load-deflection diagram of Slab 2 with shear reinforcement.
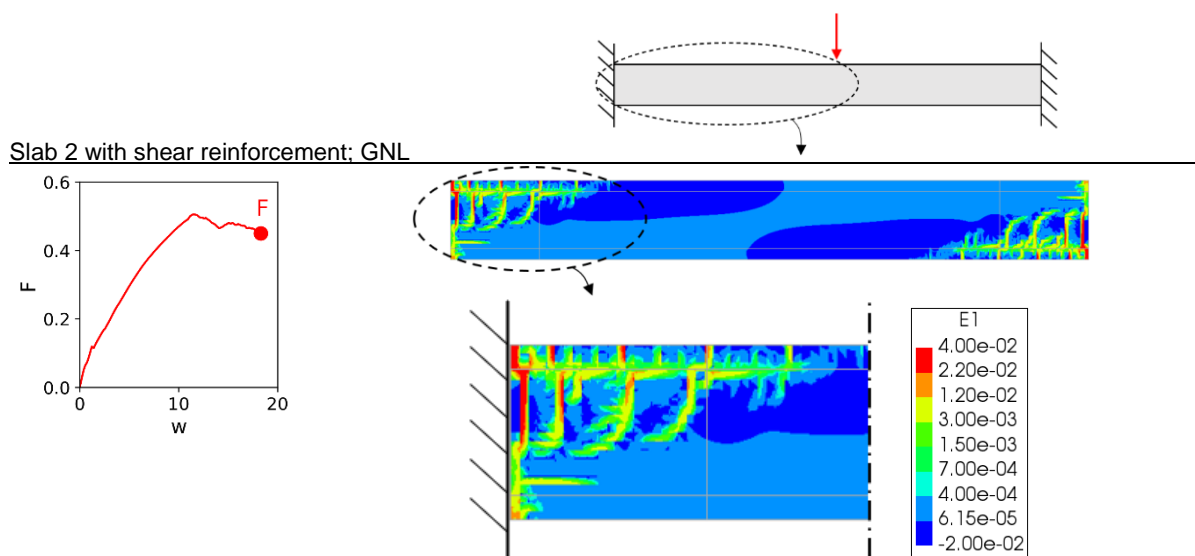
Figure 5.38: Principal tensile strains at failure for the GNL analysis of Slab 2 with shear reinforcement.
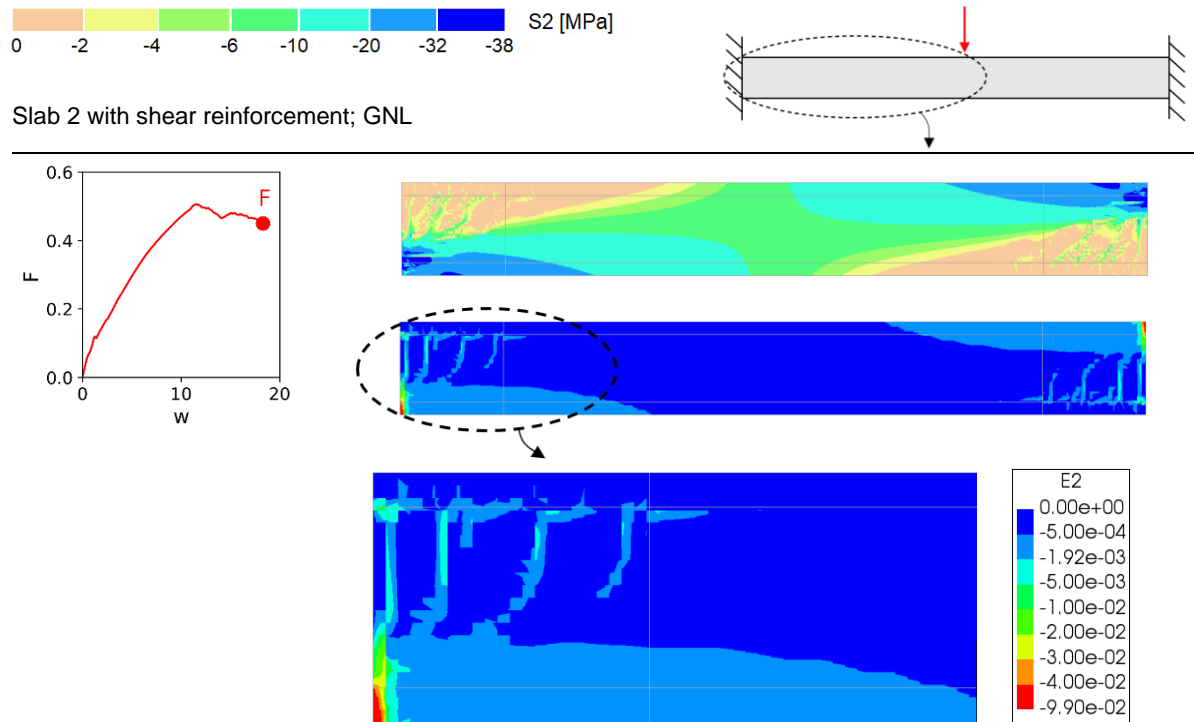
Figure 5.39: Principal compressive strains and stresses at failure for the GNL analysis of Slab 2 with shear reinforcement.

Discussion

When comparing the load-deflection diagrams of Slab 2 without (see Figure 5.30) and with shear reinforcement (see Figure 5.37), it can be seen that the application of additional shear reinforcement has significantly increased the ductility of Slab 2. The deflection at failure is now much closer to the deflection at maximum capacity of the analytical model. It is likely that early numerical instability is prevented because of the mitigation of the diagonal tension cracks. This can be seen in the principal tensile strain plot in Figure 5.38, in which the only opened crack is a vertical crack near the support. Furthermore, the red zone in Figure 5.39 indicates that Slab 2 now fails on the crushing of the concrete in the compression zones. Therefore, the ultimate capacity is about 10% higher than without shear reinforcement. Yet, the numerical ultimate capacity is still below the analytical ultimate capacity, with a difference of about 7%. Furthermore, the second-order reduction effect of the ultimate capacity is barely changed; the difference in the capacity of the GL and GNL model is nearly similar for the slab strip without shear reinforcement.

Principal compressive strains and stresses

In Figure 5.40, the principal compressive strains and stresses are plotted over half the height of Slab 2 for the support section at the moment of failure. Plots of the stress and strain for more indicative points on the load-deflection diagram can be found in Appendix B. The strain (E2) diagram shows that the ultimate compressive strain value α_u of -0.1 is reached at the lower-left node of the model at the moment of failure. This means that the concrete in the lower-left corner is completely crushed. Contradictorily, the principal compressive stress at the lower-left node is not zero but about 17 MPa. Yet, this value is significantly lower than the compressive strength of the used concrete and indicates crushing of the concrete. Failure of the modified Slab 2 according to method 1 is therefore due to the crushing of the concrete in the compression zones at midspan and near the support.
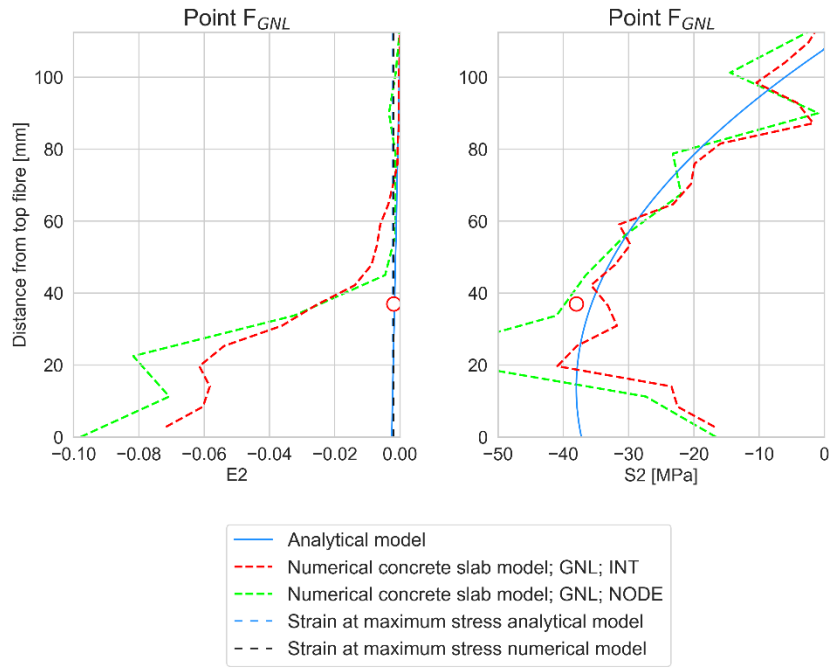
Figure 5.40: Principal compressive strains and stresses at failure at the support section of Slab 2 with shear reinforcement.

Method 2: Change of vertical support and allowing for non-convergence

The discrete vertical support over the entire height of the slab could be the cause of the non-converged last load step of the analyses of Slab 2. Such a vertical edge support is unrealistic as it could never be achieved in practice. Supporting the slab vertically at one location under the slab is much more realistic. Therefore, a small linear-elastic steel plate (E = 210000 MPa, v = 0.3) is applied for the vertical support of the slab. The modified numerical concrete slab model and the corresponding used mesh are shown in Figure 5.41. In addition to the change of the vertical support, the numerical tolerances are being extended by allowing non-converged load steps in the analyses. Therefore, the analyses will not be stopped if convergence is not found within 80 iterations. In the results of the numerical analyses, the modified concrete slab is referred to as "Slab 2 including non-convergence".
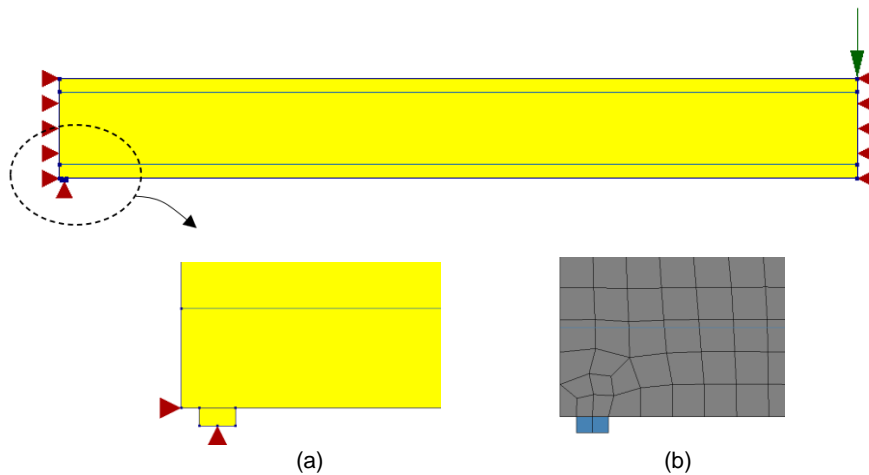
Figure 5.41: Modified numerical concrete slab model of Slab 2 (a) and its mesh (b).

Load-deflection diagram and contour plots of Slab 2 including non-convergence

The load-deflection diagram of Slab 2 with shear reinforcement is given in Figure 5.42. Figure 5.43 and Figure 5.44 show respectively the principal tensile strains and the principal compressive strains and stresses at failure (point F) of the GNL model.
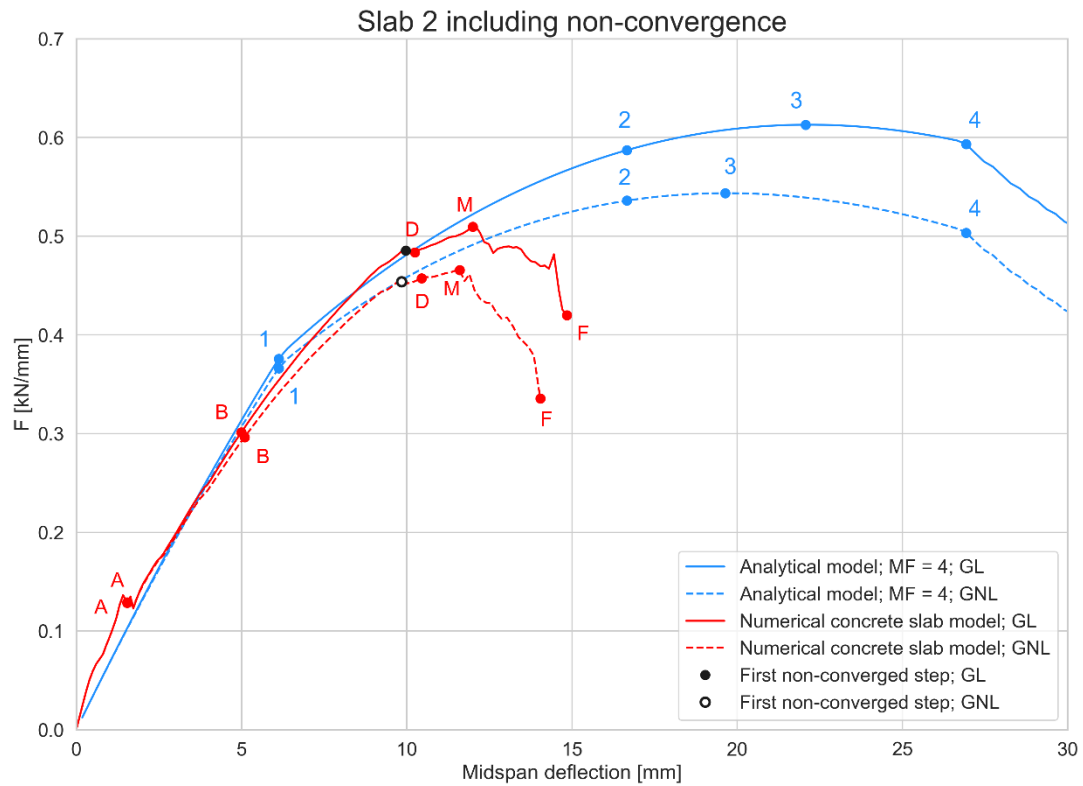
Figure 5.42: Load-deflection diagram of Slab 2 including non-convergence.
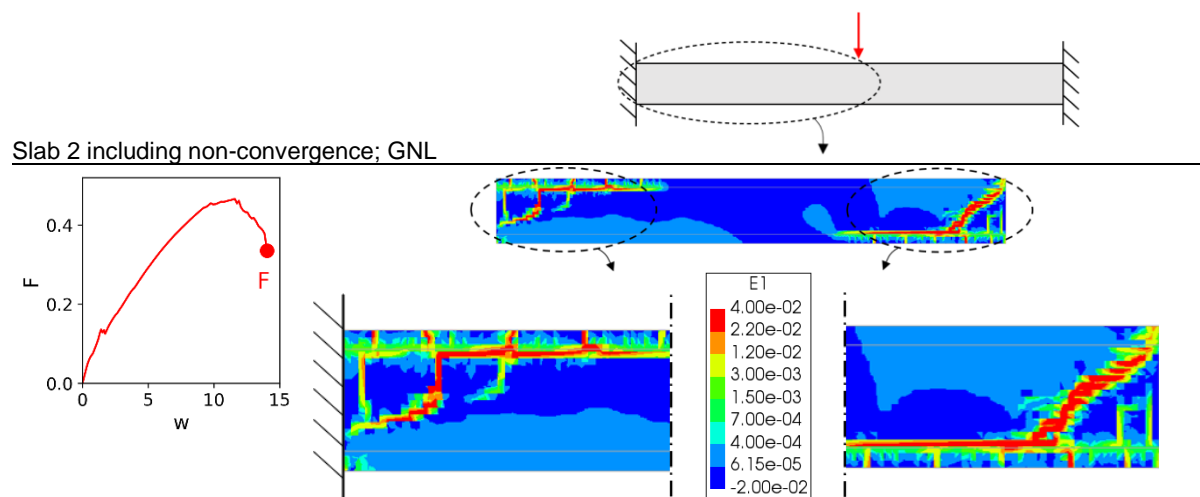
Figure 5.43: Principal tensile strains at failure for GNL analysis of Slab 2 including non-convergence.
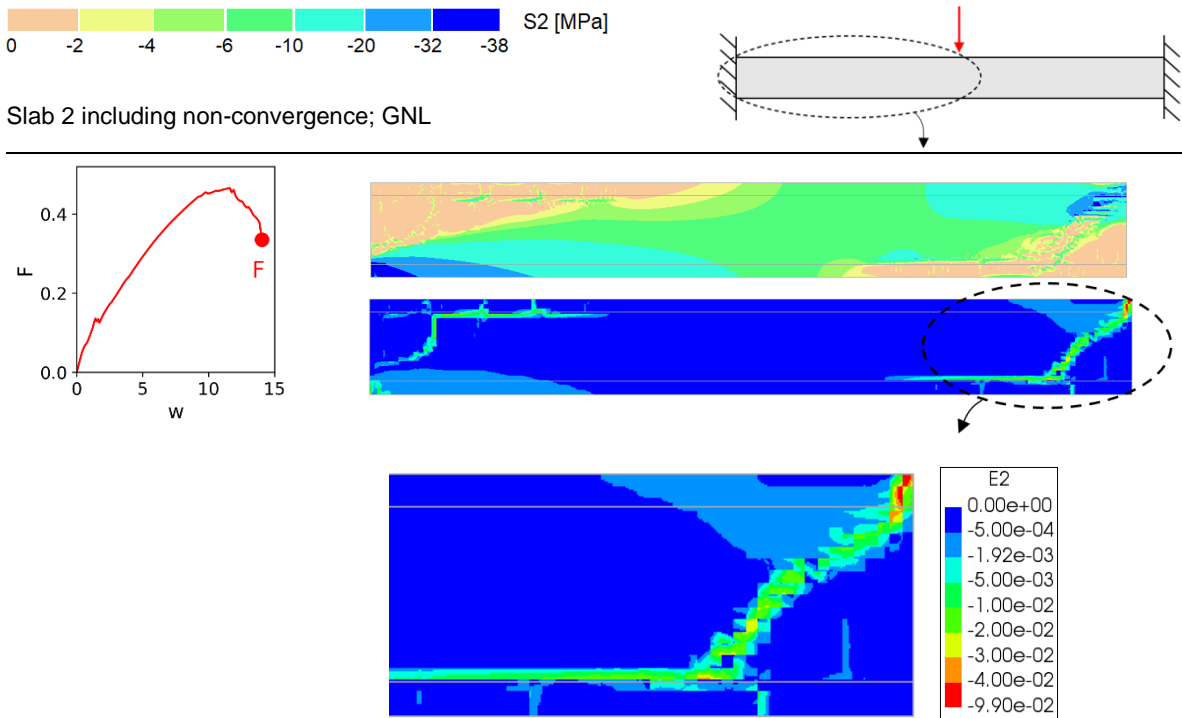
Figure 5.44: Principal compressive strains and stresses at failure for the GNL analysis of Slab 2 including non-convergence.

Discussion

When comparing the load-deflection diagrams of the unmodified Slab 2 (see Figure 5.30) with Slab 2 including non-convergence and a modified vertical support (see Figure 5.42), it can be seen that the change of the vertical supporting conditions and allowing for non-converged load steps has barely changed the ultimate capacity and ductility of Slab 2. It can therefore be concluded that the numerical instability of the unmodified Slab 2 gave an accurate estimate of the actual moment of failure. It should be noted that the limited number of non-converged load steps is still within acceptable limits with a maximum relative energy variation of about 0.1. Figure 5.43 shows that the crack patterns are not symmetrical anymore, because of the change of supporting conditions at the side support. A large diagonal crack near midspan has occurred at failure. The concrete in the top region near midspan is crushed, which can also be seen in the red zone in Figure 5.44. The principal compressive stress plots in the next paragraph will reveal the degree of crushing.

Principal compressive strains and stresses

In Figure 5.46, the principal compressive strains and stresses are plotted over half the height of Slab 2 for the midspan cross-section (see Figure 5.45) at the moment of failure. Plots of the stress and strain for more indicative points on the load-deflection diagram can be found in Appendix B. Note that the compression zone is located at the top of this section. Hence, the label on the y-axis is the distance from the top fibre. A clear sign of crushing of the concrete can be seen in the stress (S2) diagram; the compressive stress has dropped significantly near the top fibre at midspan. Failure of the modified Slab 2 according to method 2 is therefore due to the crushing of the concrete in the compression zone at midspan.
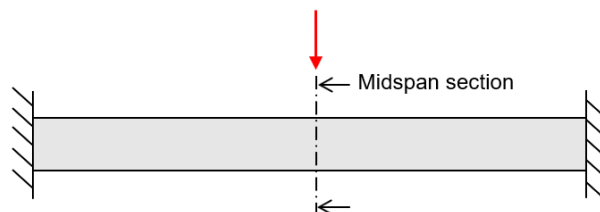
Figure 5.45: Midspan section of Slab 2 (not to scale).
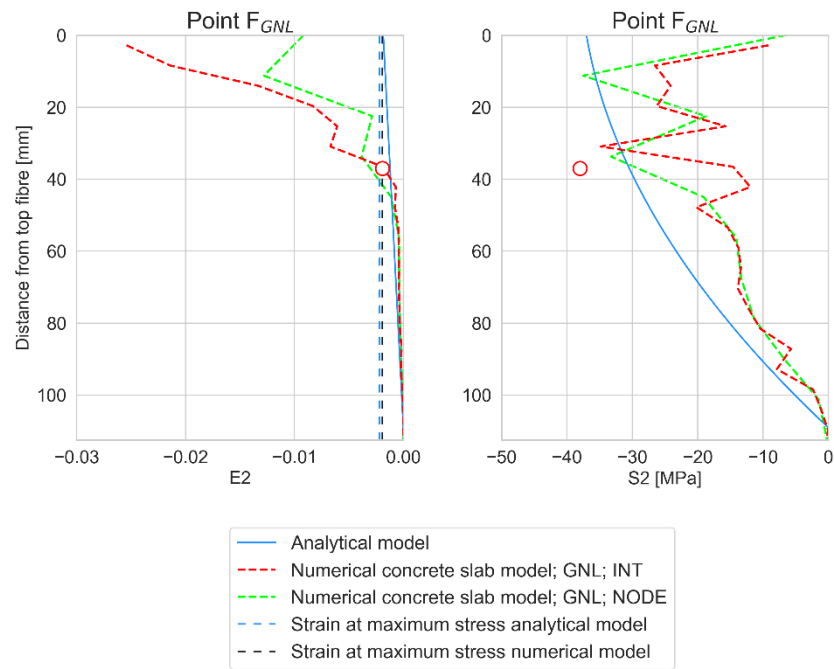
Figure 5.46: Principal compressive strains and stresses at failure at the support section of Slab 2 including non-convergence.

Comparison results of Slab 1 and Slab 2

Several agreements and differences between the results of Slab 1 and Slab 2 are listed below:

- Slab 1 and Slab 2 both fail on bending and the consequent crushing of the concrete in the compression zones. The compressive stress in the compression zones was substantially dropped because of the large deformations (compressive strains) in these zones. The built-up of the compressive strains and stresses was due to the lateral restraint.

- The stiffness reduction after cracking is lower for Slab 2 than for Slab 1. This is because the arching effect is relatively stronger for the deep Slab 2 than for the slender Slab 1. This is in line with the conclusions of the analytical results in 4.6. For both restrained slabs, it holds that the arching will reduce the stiffness decrease after cracking is commenced.

- Shear stresses play a more significant role in the structural behaviour of Slab 2 than of Slab 1. Large diagonal tension cracks have developed in Slab 2, while the cracks in Slab 1 are mainly vertically oriented.

- The second-order reduction effect of the ultimate capacity and the ultimate capacity itself of Slab 1 are accurately predicted by the analytical model. In contrast, the reduction effect and the ultimate capacity are overestimated by the analytical model for Slab 2. This could be an indication that the analytical model provides better estimates for slender slabs than for deep slabs. A sensitivity study can provide a definitive answer to this statement.

$$6$$

Sensitivity analysis

6.1. Introduction

It has been analytically and numerically proven that CMA will enhance the ultimate capacity of laterally restrained concrete one way slabs. However, the proof only consists of the results of the two reference concrete slab strips (Slab 1 and Slab 2). The study of more slab strip variants will strengthen the statement and it is therefore chosen to perform a sensitivity study. Other important reasons are to accurately quantify the capacity enhancement and the GNL reduction effect, to study the effect of fluctuations in the model parameters on the results of the analytical model and to identify the critical parameters with significant influence on the results. Another reason is to determine the accuracy of the analytical estimations.

6.1.1. Model parameters

Slab 1 is used for the sensitivity analysis. The sensitivity of five model parameters is researched. The principle of the sensitivity analysis is that one of the model parameters below is varied, while the other parameter values are kept constant according to Table 4.1 in section 4.5.

- Degree of axial restraint

- Slenderness

- Concrete compressive strength

- Positive reinforcement ratio

- Negative reinforcement ratio

6.1.2. Presentation of results

The results of the sensitivity analysis are presented with two diagrams for each model parameter. Both analytical and numerical results are presented in each diagram. Additional results are shown if relevant. It is important to note that for each model parameter 10 numerical models are constructed with values spread over the considered range of the parameter. This number is considered sufficient to detect a trend. On the other hand, the analytical plots are based on 100 points in the considered range. The numerical analyses use the same mesh size, calculation method and load steps as the analyses of Slab 1 in chapter 5.

The first diagram shows the enhanced capacity of the slab strip, in which the enhanced ultimate load (P_e) is normalised by the conventional ultimate load according to the bending moment resistance calculation of the EC2 excluding safety factors (P_{EC2}). Figure 6.1 contains an illustration of the values to be compared in a load-deflection diagram. Note that the analytical and numerical enhanced ultimate loads are the ones resulting from the GNL models, because actual structural behaviour is also nonlinear. Two graphs are plotted in the first diagram: 1) the bending load enhancement factor according to the analytical model; 2) the bending load enhancement factor

according to the numerical model. It holds that factors higher than 1.0 imply that the failure load is increased due to the development of CMA. In addition, a factor of 1.0 means that CMA has not developed and bending action is the only load-bearing mechanism. However, this may be false in some cases since the capacity values calculated with the EC2 may differ slightly from the actual capacity.

The second diagram shows the decrease in the ultimate capacity P_e due to geometrical nonlinearity expressed in percentages (see Figure 6.1). The percentage indicates the magnitude of the GNL reduction effect.
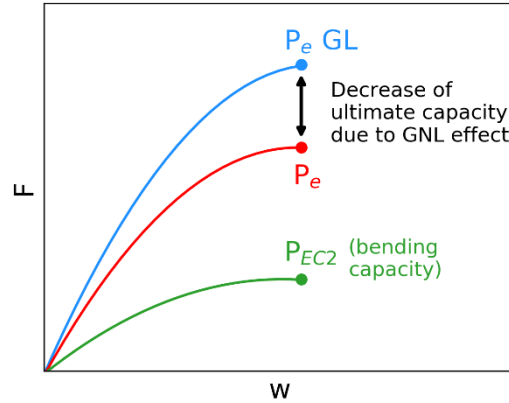
Figure 6.1: Illustration of enhanced capacities ($P_e\ GL$ and P_e) and conventional bending capacity (P_{EC2}).

6.2. Sensitivity analysis

This section presents the results and the discussion of the sensitivity analysis per model parameter.

6.2.1. Degree of axial restraint

The presented basic analytical model assumes completely rigid supports, but concrete slabs can never be perfectly clamped in practice because surrounding structures cannot provide complete rigidity. In fact, the surrounding structures will support the concrete slab with a certain degree of axial restraint and a certain degree of rotational restraint. The degrees of restraint can be modelled with linear elastic translational and linear elastic rotational springs. The assumed mechanical scheme is shown in Figure 6.2, in which the three red dots are the formed plastic hinges. In this section, the degree of axial restraint will be varied to study its influence on the response of the slab strip. The degree of rotational restraint is not regarded[1]. Thus, the degree of rotational restraint is assumed to be infinite. As with the basic analytical model, the calculation is based on full plasticity of the structural system.
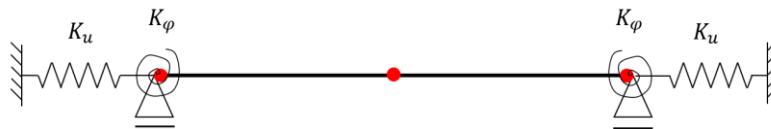
Figure 6.2: Simplified model of the concrete slab strip with three plastic hinges.

The degree of axial restraint will affect the force transfer by arching action. It is expected that high degrees of axial restraints will result in very small movements of the support as well as a built-up of high horizontal forces. Both the analytical and the numerical model must be modified to be able to vary the degree of axial restraint. The descriptions of the modified models are given in the paragraphs below.

---

[1] The reason is that equilibrium was not found in the modified analytical model with a rotational spring.

Description of the modified analytical model

The concrete slab strip is connected to a rigid bar with a bedding of horizontal translational springs which represent the material behaviour of concrete and steel. The basic analytical model in chapter 4 assumes that the rigid bar is rigidly connected to the earth[2] and cannot translate or rotate. To be able to vary the degree of axial restraint, the basic model is modified by connecting the rigid bar to a translational spring. Instead of a direct connection to the earth, the rigid bar is now horizontally connected to the earth by this spring. It should be noted that the rigid bar cannot rotate or translate in the vertical direction.
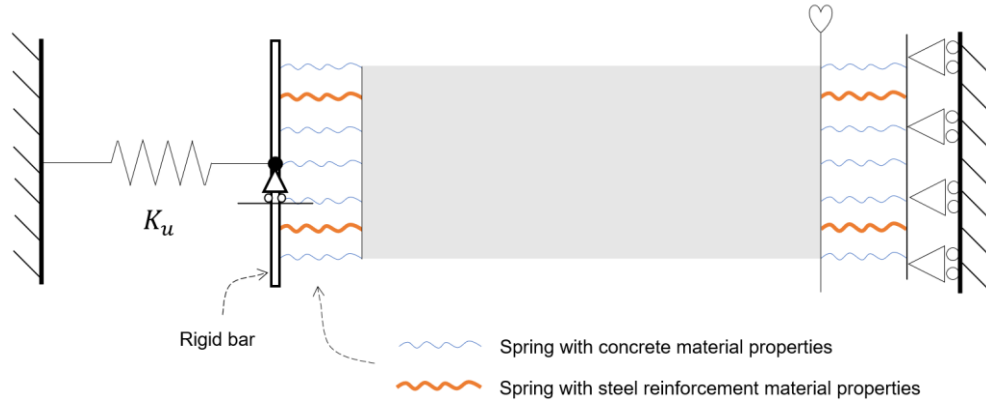
Figure 6.3: Model of the restrained half concrete slab strip.

Force and moment balance are the principles used to solve the structural system and obtain the response of the slab strip for different degrees of axial restraint. An iterative procedure is considered most appropriate to find the horizontal and moment equilibrium of the system for each rotation of the slab strip. The first step is to impose a small rotation θ_i and assume a value for a, which is the distance to the centre of rotation as described in section 4.4. Note that negative values for a imply that the contact depth is larger than half the height of the slab strip. The spring forces at the midspan cross-section (N_{cR}, N_{sR} and T_{sR}) can be derived from the geometry, from the current rotation and position of the slab strip. Subsequently, the fixed end moment M_R and axial force F_R can be determined based on the spring forces (see Figure 6.4).

Equilibrium of the system requires that the bending moment and axial force at the slab strip end (M_L and F_L) are equal to the bending moment and the axial force at midspan (M_R and F_R) and that they act in the opposite direction. Followingly, the horizontal translation of the rigid bar u can be calculated with the known degree of axial restraint K_u (see {6.1}). As a result, the length of the bedding springs at the slab strip end will change. The forces in the springs (N_{cLL}, N_{sLL} and T_{sLL}) and consequently the resultant axial force and the bending moment (M_{LL} and F_{LL}) can be determined based on the current extensions and compressions of the springs. It is now needed to check if the horizontal and moment equilibrium of the structural system are satisfied. If this is not the case, another value for a needs to be assumed until equilibrium is reached.

$$u = \frac{F}{K_u} \qquad \{6.1\}$$

Based on the spring forces in both beddings, the resultant moment of resistance M_a for imposed rotation θ_i can be determined. The change of span length is so small compared to the span length that it is ignored for the calculation of M_a. The subsequent point of equilibrium is determined by imposing a new rotation of the slab strip θ_{i+1}. The step-wise calculation procedure and the Python script for obtaining a load-deflection diagram for known degrees of axial restraint is given in Appendix C.

---

[2] Earth in this example means a fixed point in space.
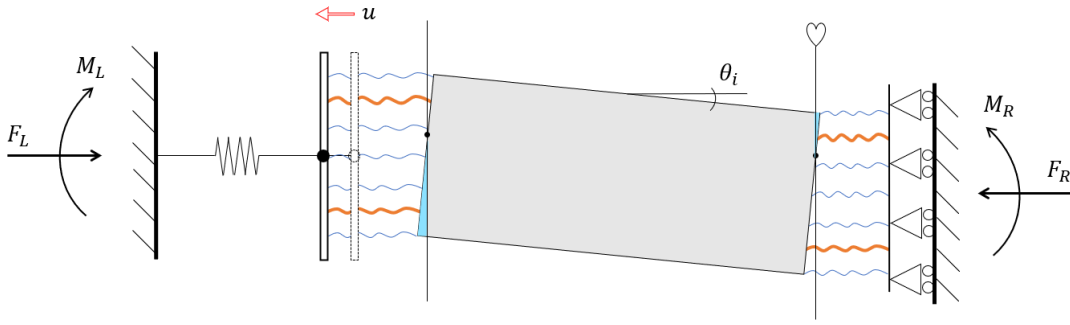
Figure 6.4: A deflected model of the restrained half concrete slab strip.

Validation of the modified analytical model

The modified analytical model has to be compared to the basic analytical model to guarantee valid results for this section. This is done by inputting an extremely high value for the axial stiffness in the modified analytical model, which makes the concrete slab strips in both models fully restrained and therefore comparable. Two indicators are used to compare the models: the load-deflection curve and the decrease in the contact depth. Both indicators are obtained for the basic as well as the modified analytical model, and they should be equal if the modified analytical model is constructed properly. The results are shown in Figure 6.5.

(a)   (b)
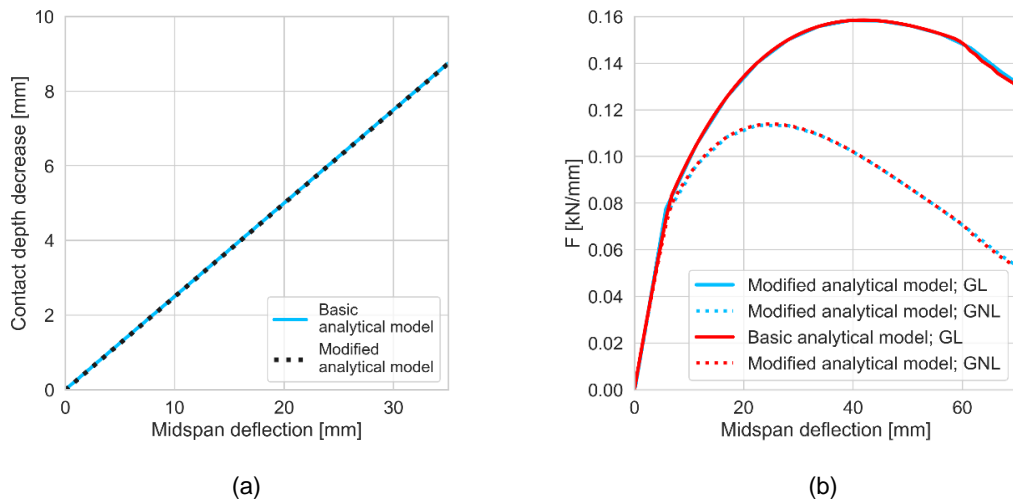
Figure 6.5: Comparison between the basic analytical model and the modified analytical model with the contact depth decrease (a) and the load (b) plotted against the midspan deflection.

From the results in Figure 6.5, it can be concluded that both models give similar results. The decrease in the contact depth is equal for both models and the load-deflection behaviour is also similar. Thus, the modified analytical model is considered to give valid results based on the similarities of the indicators.

Description of the modified numerical model

The boundary conditions of the numerical concrete slab model must be modified to be able to vary the degree of axial restraint. The previously fully clamped edge must now be unrestrained in the longitudinal axis (x-direction) of the slab strip. Also, rotation and upward or downward movement (z-direction) of the edge needs to be prevented. Therefore, a small and rigid strip is applied directly against the concrete edge (see Figure 6.6). The embedded reinforcements pass through the interface.

The small strip is vertically supported at the middle left node (Node A) with a roller, to restrain the movement in the z-direction and to allow the translational movement in the x-direction. A boundary spring connection is applied at the same node to model the translational spring. The rotation of the rigid strip is restrained with the use of a

tying: the movement in the x-direction of the complete left edge of the rigid strip (Edge A) is set equal to that of the middle left node (Node A).

The value of the axial stiffness K_u according to the analytical mode must be multiplied with the assumed with of 200 mm to get comparable results.
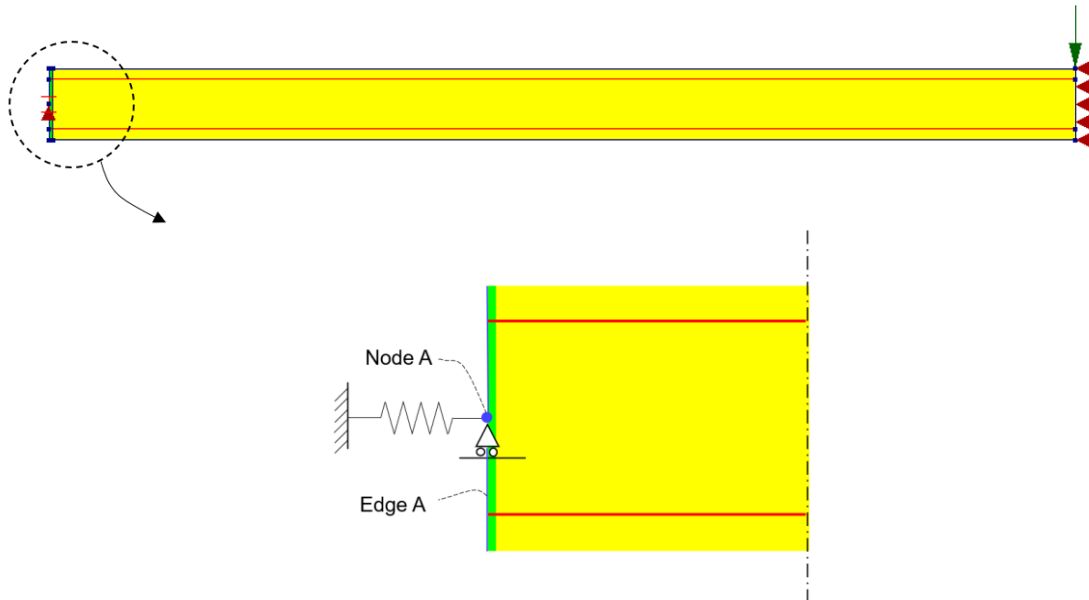
Figure 6.6: Modified numerical concrete slab model.

Load-deflection behaviour

Figure 6.7 presents the load-deflection diagram of Slab 1 for two different degrees of axial restraint. It can be seen that the stiffness before the first crack is independent of the degree of axial restraint according to the numerical model. On the other hand, the post-cracking stiffness is significantly higher for the higher degree of axial restraint, because of the development of larger horizontal forces which provide the membrane action. Therefore, the ultimate capacity increases with increasing axial restraint. Further, it is seen that the response of the slab strip is more ductile for a lower degree of axial restraint. The analytical model appears to overestimate the ductility increase for the GL model, but predicts it quite accurately for the GNL model.

Remarkably, the load-deflection curve of the modified numerical model with an axial stiffness of K_u = 40000 N/mm/mm is different than that of the basic numerical model developed in chapter 5 (see Figure 5.18). The most noticeable difference is the higher GNL peak lead, and consequently the lower second-order effect for the modified numerical model. This may be caused by the design of the support region in the modified numerical model. The small and rigid strip that is added could influence the results of the analyses. Yet, the results are still considered valid because the difference is not significant.
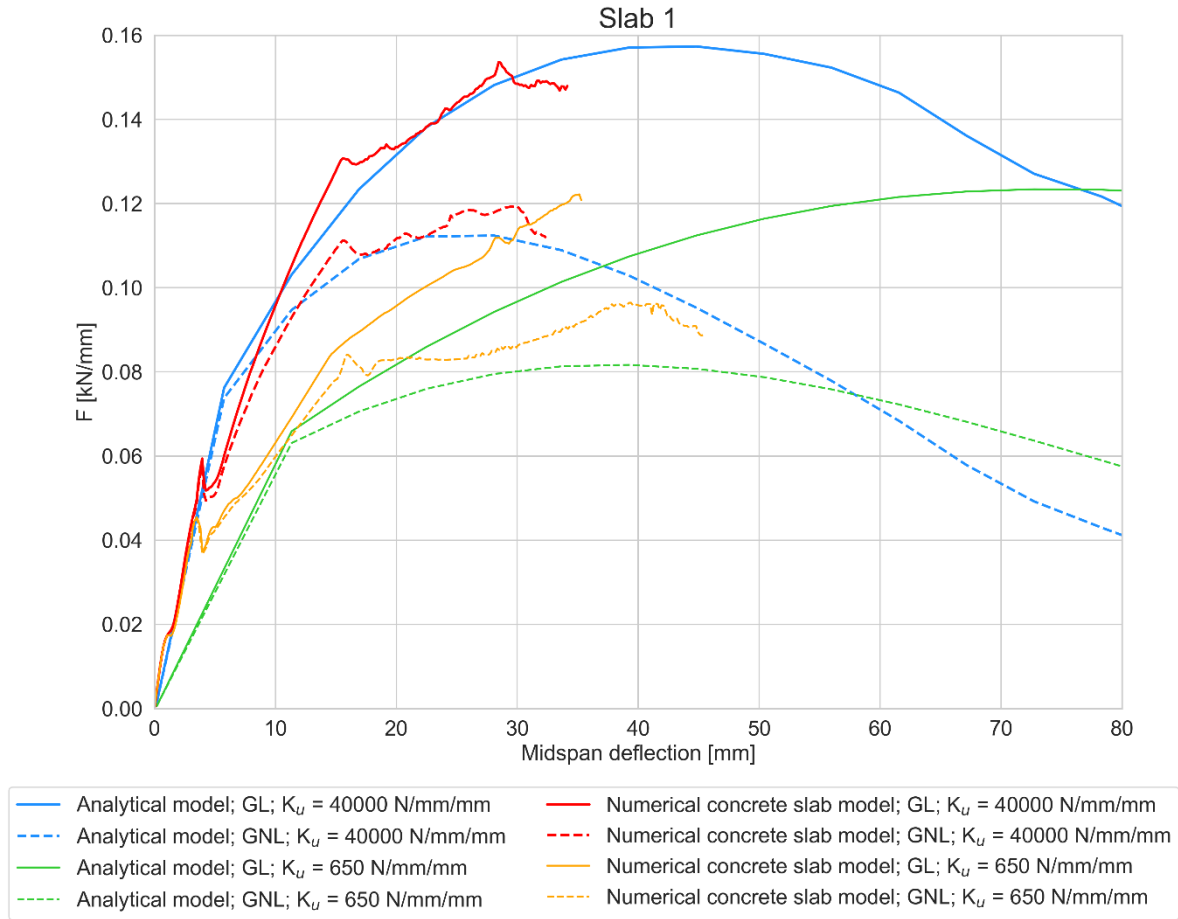
Figure 6.7: Load-deflection diagram of Slab 1 for different degrees of axial restraint.

Compressive arch development

The axial restraint will allow for a redistribution of forces into compressive arches. Figure 6.8 shows the formation of the compressive arches for the two values of axial restraint by plotting the principal compressive stresses. An absolute scale factor for the height of the slab strip of 2 is used in order to present the compressive arch more clear.

For similar deflection values, the compressive stresses in the compressive arch are higher for the larger value of axial restraint. Thus, the arching effect will be stronger for higher degrees of axial restraint. This finding is also in line with the literature study (see section 2.3.4). Furthermore, the width of the total compressive arch seems to be larger for the larger value of axial restraint. The results in Figure 6.8 also correspond with the results of the laterally restrained truss for which higher values of the normal force in the elements were found for higher degrees of restraint (see section 3.5.5).
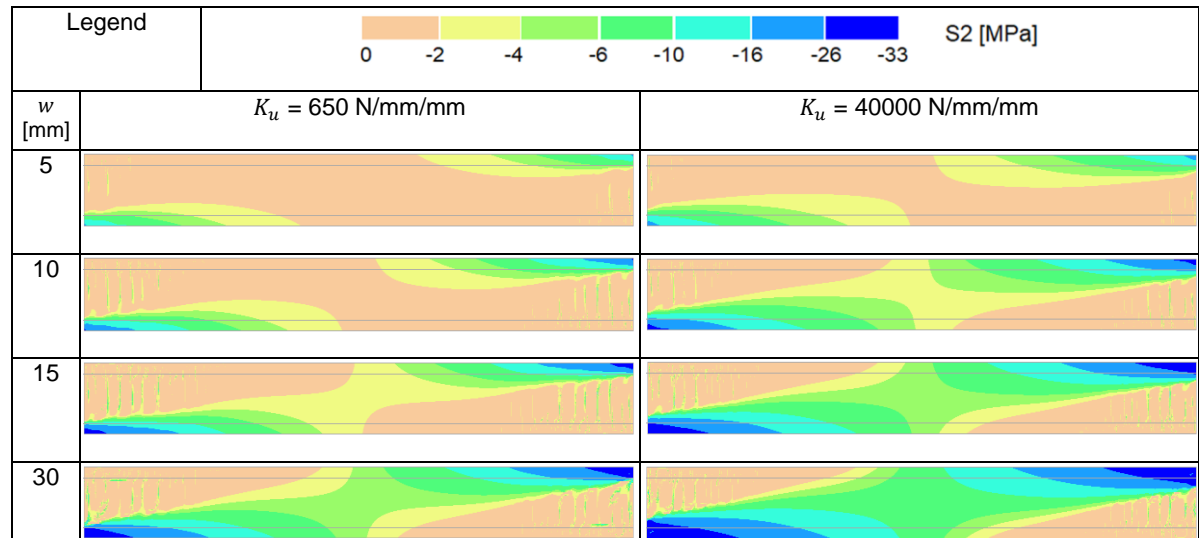
Figure 6.8: Compressive arch development for different degrees of axial restraint.

Results sensitivity analysis

The results of the sensitivity analysis of the degree of axial restraint are shown in Figure 6.9. Note that the enhanced capacity diagram plots the x-coordinates on a logarithmic scale because the graphs are then easier to view. The modified analytical model could not reach equilibrium for values below K_u = 250 N/mm/mm, which explains why the analytical graphs stop there. The conventional ultimate load calculation for low axial degrees of restraint is still based on the formation of three plastic hinges. As for the modified numerical model, it is assumed in the calculation that the span length remains constant. Consequently, the conventional ultimate load also has a constant value in this section.
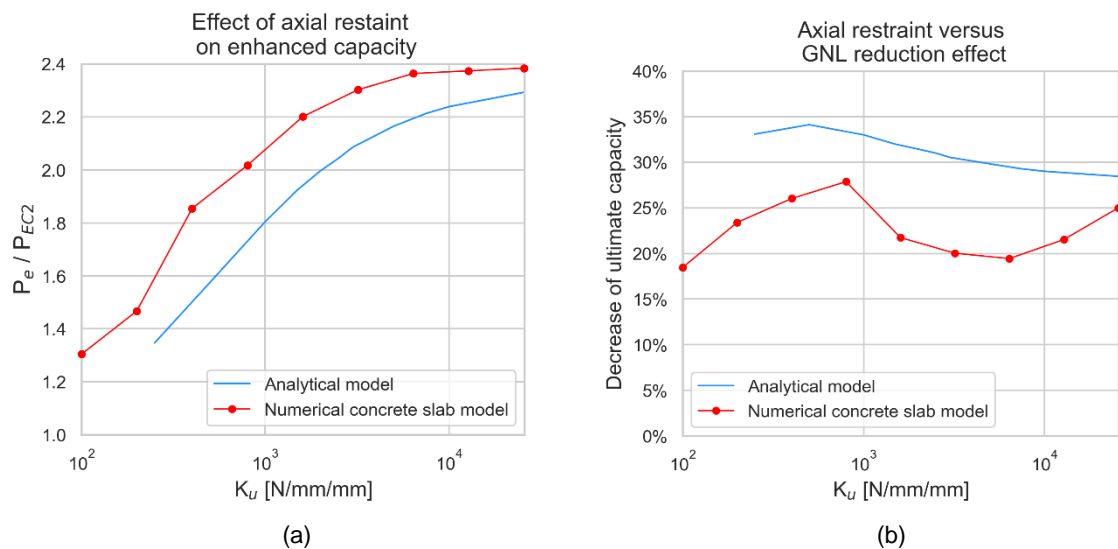
Figure 6.9: Degree of axial restraint sensitivity analysis.

Enhanced capacity

Both the analytical and numerical results show that the degree of axial restraint has a large influence on the capacity enhancement of the reinforced concrete slab strip (see Figure 6.9). The built-up of horizontal compressive forces is strongly influenced by the axial restraint. It holds that the higher the degree of axial restraint, the more arching action can develop. It can be seen that for weak axial restraints, an increase in restraint will have a large effect on the capacity enhancement factor. On the other hand, for strong axial restraint, it holds that an increase in restraint will have a small effect on the enhanced capacity. Thus, increasing the axial stiffness of

the support to enhance the capacity is very effective for small restraints and much less effective for large restraints.

The numerical model results in enhancement factors between 1.6 and 2.38 for degrees of axial restraint between 250 N/mm/mm and 25600 N/mm/mm. The analytical model results in enhancement factors between 1.35 and 2.29 for the same range of degrees of axial restraint. The analytical graphs have lower values than the numerical graphs for the entire range. Thus, the analytical model underestimates the capacity enhancement due to CMA. However, similar trends for both models can be observed. The estimation accuracy of the analytical model can be expressed in the mean deviation and maximum deviation from the numerical result. In this case, the mean and maximum deviation from the numerical enhancement factor are respectively 9.7% and 18.9%, which is rather inaccurate.

<u>GNL reduction effect</u>

The numerical result of Figure 6.9b shows that there is no clear relationship between the degree of axial restraint and the magnitude of the second-order effect. The percentage decrease fluctuates between 19% and 28%, and reaches its maximum at K_u = 800 N/mm/mm. The analytical result shows a decrease of the second-order effect for higher degrees of axial restraint. Yet, the GNL reduction effect increases between 250 N/mm/mm and 500 N/mm/mm. It is very clear that the analytical model overestimates the second-order effect for nearly fully as well as partially restrained concrete slab strips. The mean and maximum deviation between the analytical and numerical GNL reduction effect are respectively 7.4% and 10%.

6.2.2. Slenderness

In order to study the effect of the slenderness of the concrete slab strip on the structural response in both the GL and the GNL model, the height of the slab is varied while the span length is kept constant. This means that the amount of steel in the concrete slab increases because the reinforcement ratios have to be constant. The finite element models always consist of 20 square elements over the height of the slab strip, meaning that the element size is different for each model. Note that the cover-to-height ratio is decreasing with decreasing slenderness because the cover has a constant value. The slenderness is varied between 5 and 30. It should be noted that a slenderness between 5 and 10 are not practical or economical for concrete slabs. The slenderness of bridge decks or concrete slabs is usually between 15 and 25. The zone of interest is therefore – with some additional expansion of the range – between span-to-depth ratios of 10 and 30.

The results of the sensitivity analysis of the slenderness are shown in the figures on the next page. Figure 6.10 shows the effect of the slenderness on the enhanced capacity and the influence of geometrical nonlinearity on the peak load. Figure 6.11 contains a diagram in which the enhanced capacity divided by the minimal value of the enhanced capacity for all examined slab strips is plotted against the slenderness. The zone of interest regarding the slenderness is shown in all three diagrams.
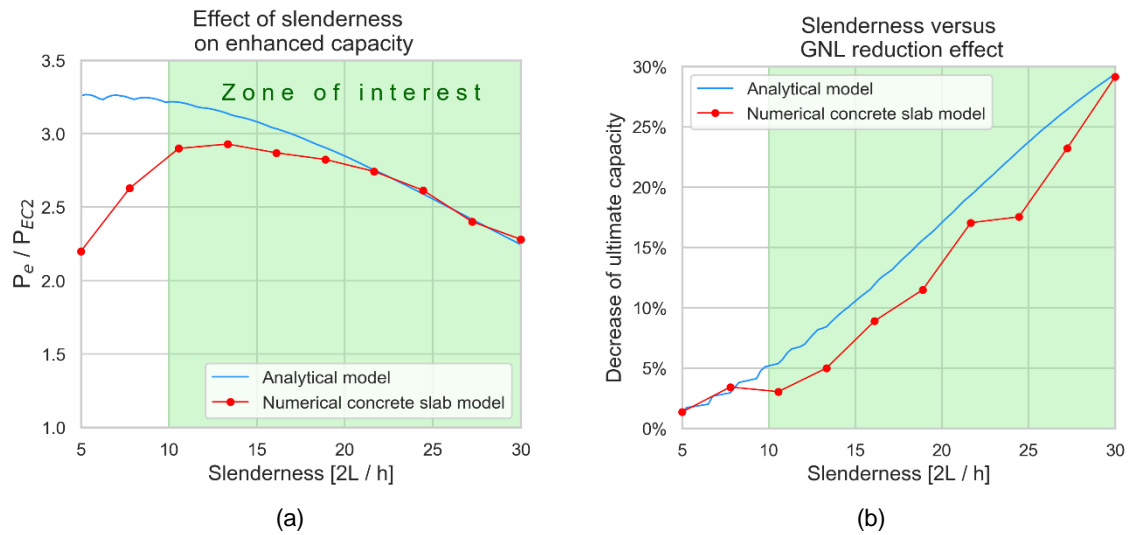
Figure 6.10: Slenderness sensitivity analysis.
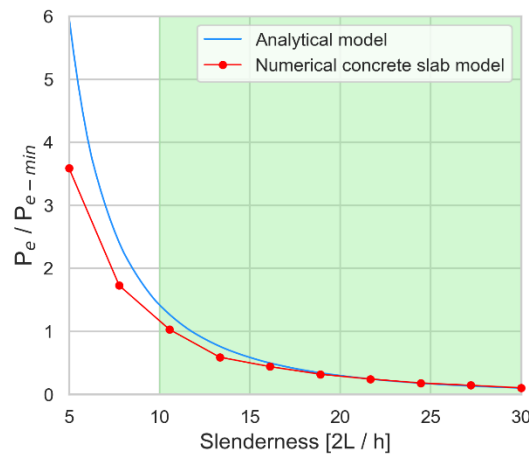
Figure 6.11: Enhanced capacity plotted against slenderness.

Enhanced capacity

In Figure 6.11, it can be seen that lowering the span-to-depth ratio of the slab has a positive effect on the absolute value of the ultimate capacity. In addition, Figure 6.10a shows that the slenderness has a large impact on the enhanced capacity compared to the conventional bending capacity: the enhancement factor is decreasing with increasing slenderness. This trend is observable for realistic span-to-depth ratios between 10 and 30. Thus, it can be concluded that the arching effect is stronger for deep slabs. This is because the angle of the fictitious compressive arch inside the concrete slab strip is larger for deep slabs. This means that for comparable deflections, the percentage decrease in the angle is smaller for deep slabs. Consequently, the internal lever arm and the arching moment formed by the compressive forces in the concrete and the steel reinforcement are larger for deep slab strips than for slender slab strips. The internal lever arm approaches zero much later for deep slab strips. It can also be concluded that arching action is the predominant load-bearing mechanism for deep slab strips, while it is the bending action that supports most of the load for highly slender slab strips. A calculation according to the EC2 of a restrained slab or beam with a span-to-depth ratio between 10 and 20 will highly underestimate the ultimate capacity.

The enhancement factor for span-to-depth ratios between 10 and 30 varies from about 2.3 to 2.9 for the numerical model and from 2.3 to 3.2 for the analytical model. The mean and maximum deviation between the enhancement factors according to the two models is respectively 3.4% and 10%. The analytical and numerical results are very similar for span-to-depth ratios above 20. Although the analytical graph still shows the same trend as the

numerical graph for a span-to-depth ratio between 10 and 20, the increase in capacity is overestimated by the analytical model in this range. This was also seen in chapter 5, in which the capacity of the Slab 2 (slenderness of 16) was analytically overestimated while the capacity of Slab 1 (slenderness of 28.8) was in good agreement with the analytical result. Even after the application of shear reinforcement, changing the vertical supporting conditions and allowing for non-converged load steps, Slab 2 still had a lower capacity than estimated by the analytical model. It can therefore be concluded that the analytical model provides better estimates for slender slabs than for less slender or deep slabs.

GNL reduction effect

The analytical and the numerical model show the same trend: the GNL effect increases as the span-to-depth ratio of the slab strip becomes larger. It is therefore important to consider geometrical nonlinearity for restrained slender concrete slabs and beams. The cause of this was explained earlier in section 4.6: the percentage decrease in the angle of the resultant compressive arch is higher for the slender slab strips, and thus the internal lever arm and the secondary moment approaches zero much faster. This observation is consistent with the literature review, which stated that the more slender the structure, the more influence geometrical nonlinearity has on the structural behaviour. The second-order effect is overestimated by the analytical model for span-to-depth ratios between 8 and 30. The overestimation is the largest for a span-to-depth ratio of 24.4. Geometrical nonlinearity has a negligible (lower than 10%) influence for span-to-depth ratios of concrete slabs below 14.6 and 17.2 according to respectively the analytical and numerical model. The mean deviation between the analytical result and the numerical result is 2.3%, and the maximum deviation is 5.5%. The analytical estimations are therefore quite accurate in this case.

An important finding is that Figure 6.10a and Figure 6.10b show opposite trends. GNL effects of restrained high slender slabs are of large influence on its response, while the increase in capacity of these slabs is limited. On the other hand, load-bearing arching action is of larger influence for the capacity of deep slabs, while the GNL effect is very low with a percentage of less than 10%.

6.2.3. Concrete compressive strength

The concrete compressive strength is varied between 20 MPa and 63 MPa. Figure 6.12 shows how sensitive the enhancement factor and the second-order effect are for fluctuations in the concrete strength.
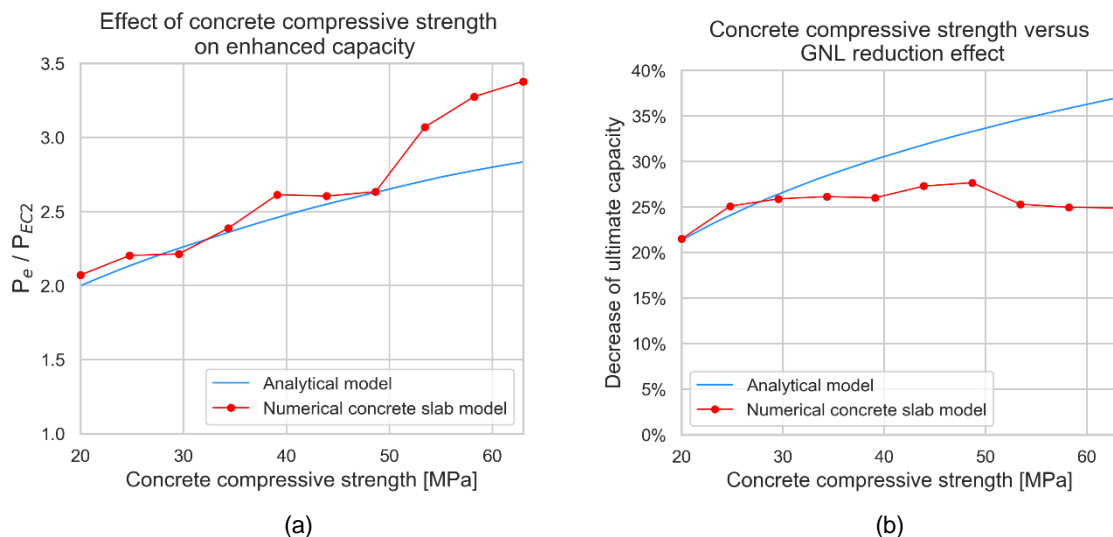
Figure 6.12: Concrete compressive strength sensitivity analysis.

Enhanced capacity

From Figure 6.12a it can be concluded that the concrete compressive strength has a positive effect on the increase in capacity due to CMA. This applies to both the analytical and numerical result. The enhancement factor varies between 2 and 2.8 for the analytical model and between 2 and 3.4 for the numerical model in the range of concrete compressive strengths between 20 MPa and 63 MPa. The horizontal stresses in the compression zone of the slab strip are higher for a larger concrete compressive strength, resulting in a larger resisting arching moment. However, the ultimate load according to the EC2 also increases with a larger concrete compressive strength. Thus, the graph is rising because the magnitude of CMA increases faster than the ultimate load according to the EC2. Mind that a design calculation according to the EC2 will highly underestimate the failure load of restrained high-strength concrete slabs or beams.

The analytical results show good agreement with the numerical result: similar curve trends can be observed, and the enhancement values are close to each other up to a strength of 50 MPa. At higher strengths, the values differ more from each other and the analytical model underestimates the ultimate capacity. The mean and maximum deviation between the enhancement factors of the analytical and numerical model are in this case respectively 5.8% and 16%.

GNL reduction effect

While the analytical model shows a linear and significant increase of the GNL reduction effect, the numerical model shows completely different results: the GNL reduction effect is slightly increasing up to a strength of 48 MPa and thereafter decreases (see Figure 6.12b). The percentage decrease varies from 22% to 37% for the analytical model and from 22% to 28% for the numerical model. A conclusion that can be drawn from the results is that the analytical model overestimates the second-order effect more for higher compressive strength values than for lower compressive strength values. The analytical model does not provide very accurate estimations with a mean and maximum deviation from the GNL reduction effect according to the numerical model of respectively 4.8% and 12.1%.

6.2.4. Positive reinforcement ratio

Until now, the positive and negative reinforcement ratios were equal. The FEM-models therefore used continuous reinforcement at the top and bottom of the slab strips. Now, the rebars are split in the middle of the half slab strip in order to be able to vary the positive as well as the negative reinforcement ratio. As can be seen in Figure 6.13, the ends of the rebars now share the same node in the middle of the model. The positive reinforcement ratio is varied between 0.001 and 0.007. The results of the positive reinforcement ratio sensitivity analysis are presented in Figure 6.14.
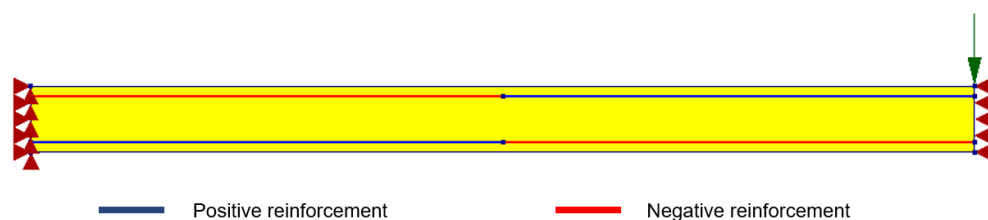
Figure 6.13: Modified FEM-model of Slab 1 to vary the positive and negative reinforcement ratio.
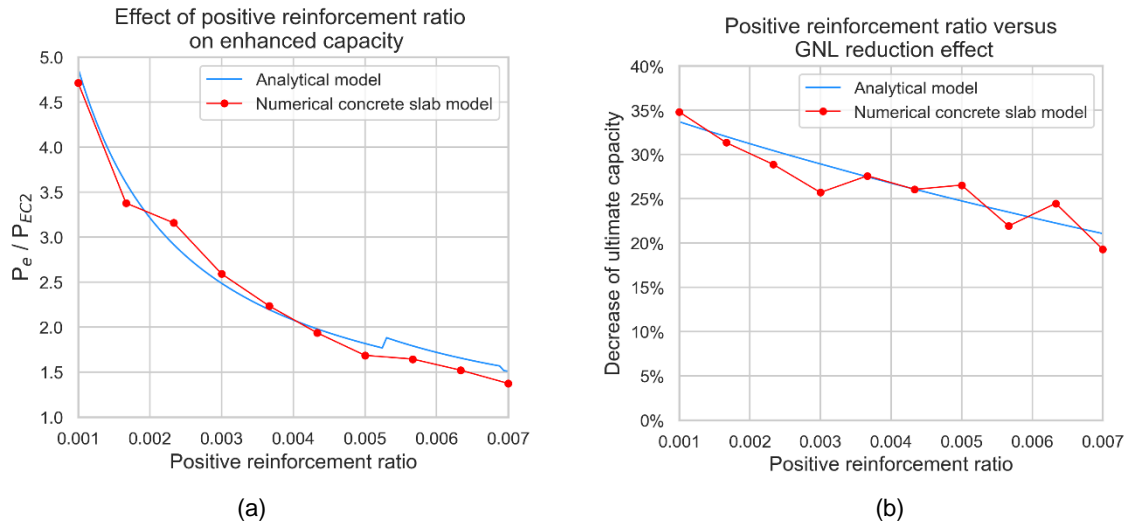
Figure 6.14: Positive reinforcement ratio sensitivity analysis.

Enhanced capacity

Figure 6.14a shows that the positive reinforcement ratio is exponentially related to the enhancement factor; applying low positive reinforcement ratios in laterally restrained concrete slab strips leads to a larger difference between the enhanced capacity and the conventional bending capacity. The reason is that the bending capacity decreases significantly with decreasing reinforcement ratios while the resting arching moment and the enhanced capacity of the restrained slab strip decrease only slightly. This is because a major part of the moment of resistance is determined by the horizontal forces in the concrete and not by the tensile steel reinforcement. For a low positive reinforcement ratio, the arching effect is still very high in magnitude.

The analytical result is nearly similar to the numerical result and can therefore be used to estimate the influence of the positive reinforcement ratio on the enhanced capacity. The enhancement factors for both models vary between about 1.5 and 4.7. Yet, deviations between the models of 9.9% are observable. The mean deviation is 3.4%.

GNL reduction effect

Both graphs in Figure 6.14b show roughly the same trend: the high amount of tensile reinforcement reduces the GNL effect on the ultimate capacity of the slab strip. The cause is that the moment of resistance resulting from the tensile forces in the steel reinforcement will increase with increasing deflection due to an increase in the lever arm. The load resistance will therefore increase less rapidly with each increase in deflection than with a low reinforcement ratio. The difference factor for both models is between approximately 1.25 and 1.52.

Figure 6.14b clearly shows that the numerical plot is very discontinuous, while the analytical plot is almost a straight line. Nevertheless, the values do not differ significantly from each other and the trends are nearly equal. The GNL reduction effect is estimated very accurately by the analytical model in this case because the mean and maximum deviation are respectively only 0.4% and 3.2%.

6.2.5. Negative reinforcement ratio

The negative reinforcement ratio is varied between 0.001 and 0.007. The results of sensitivity analysis are presented in Figure 6.15.
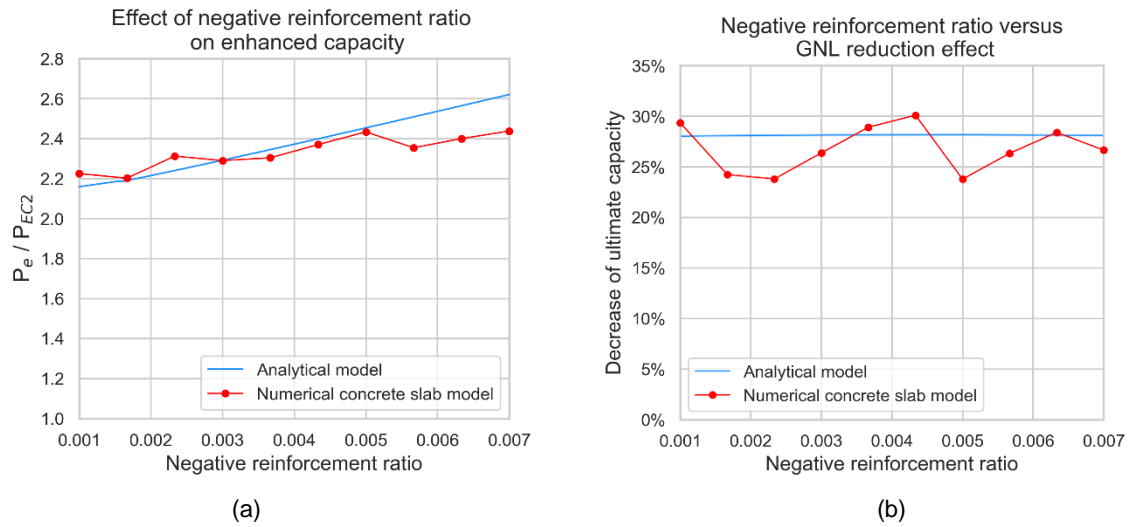
Figure 6.15: Negative reinforcement ratio sensitivity analysis.

Enhanced capacity

According to the analytical and numerical model, the negative reinforcement ratio is almost linearly related to the enhancement factor. The enhancement factor varies between about 2.2 and 2.62. Figure 6.15a shows that the more negative reinforcement is applied, the more arching action will be developed. This finding is underlined by the numerical graph, whose values fluctuate around the analytical graph. The finding makes sense since the forces in the compression reinforcement, and subsequently the arching moment will increase if more steel is applied in the compression zones. In addition, the conventional bending capacity will only be slightly influenced by the negative reinforcement ratio. Figure 6.15a also shows that the analytical overestimation of the ultimate capacity of the restrained slap strip is highest for large negative reinforcement ratios. In contrast, the analytical model tends to marginally underestimate the enhancement factor for low negative reinforcement ratios. However, it can be argued that the analytical model can predict the numerical results quite accurately due to the great similarities of the graphs. The mean and maximum deviation between the analytical and numerical result are respectively 1.8% and 7.5%.

GNL reduction effect

Figure 6.15b shows that the negative reinforcement ratio has a negligible influence on the difference between the GL and GNL peak load according to the analytical model. The effect of geometrical nonlinearity on the ultimate capacity remains approximately 28%. On the other hand, the numerical result shows that the negative reinforcement ratio has a considerable influence on the second-order effect. However, no clear relationship can be observed between the positive reinforcement ratio and the increase in capacity. The percentage of the GNL effect varies between 24% and 30%. In most cases, the analyses of the numerical model result in lower capacities than the analytical model. The mean and maximum deviation between the GNL reduction effects according to both models are respectively 1.3% and 4.4%.

6.3. Summary and conclusions

The findings of the sensitivity analysis are summarised in tables and boxplots. Table 6.1 and Table 6.2 contain the maximum and minimum values for respectively the enhancement factor and the GNL reduction effect for all examined slab strips in this chapter according to the analytical and numerical model. The corresponding values for the model parameter are also included in these tables.

Enhancement factor	**Analytical**		**Numerical**	
Degree of axial restraint	250 N/mm/mm →	1.35	100 N/mm/mm →	1.3
	25000 N/mm/mm →	2.29	25000 N/mm/mm →	2.38
Slenderness	30 →	2.3	30 →	2.3
	10 →	3.2	13 →	2.9
Concrete compressive strength	20 MPa →	2	20 MPa →	2
	63 MPa →	2.8	63 MPa →	3.4
Positive reinforcement ratio	0.001 →	4.7	0.001 →	4.7
	0.007 →	1.5	0.007 →	1.4
Negative reinforcement ratio	0.001 →	2.17	0.00167 →	2.2
	0.007 →	2.62	0.007 →	2.43

Table 6.1: Maximum and minimum values of the enhancement factor with their corresponding model parameter value.

GNL reduction effect	**Analytical**		**Numerical**	
Degree of axial restraint	500 N/mm/mm →	34%	800 N/mm/mm →	28%
	25000 N/mm/mm →	29%	100 N/mm/mm →	19%
Slenderness	10 →	5%	10 →	3%
	30 →	29%	30 →	29%
Concrete compressive strength	20 MPa →	22%	20 MPa →	22%
	63 MPa →	37%	48 MPa →	28%
Positive reinforcement ratio	0.001 →	34%	0.001 →	35%
	0.007 →	21%	0.007 →	19%
Negative reinforcement ratio	*all* →	28%	0.0023 →	24%
	all →	28%	0.0043 →	30%

Table 6.2: Maximum and minimum percentages of the GNL reduction effect with their corresponding model parameter value.

The accuracy of the analytical model for estimating the GNL reduction effect and the enhancement factor is presented in boxplots. The percentage deviation of the analytical result from the numerical result is shown per model parameter in Figure 6.16 and for all examined cases in Figure 6.17. Each boxplot also contains a white dot representing the mean deviation.
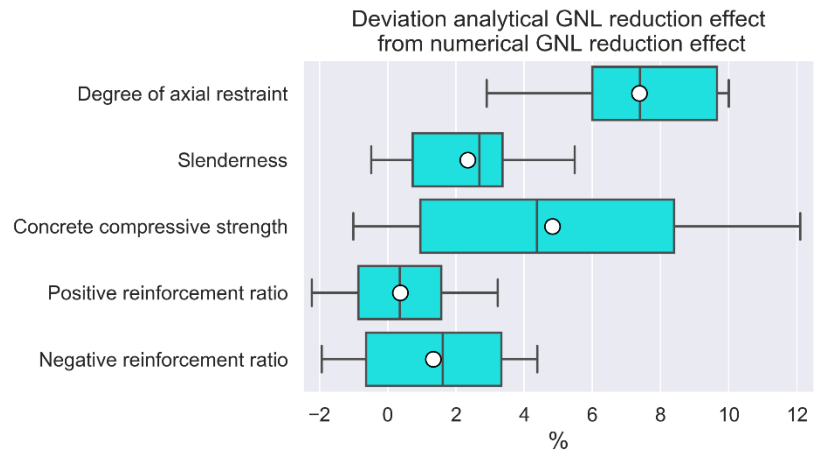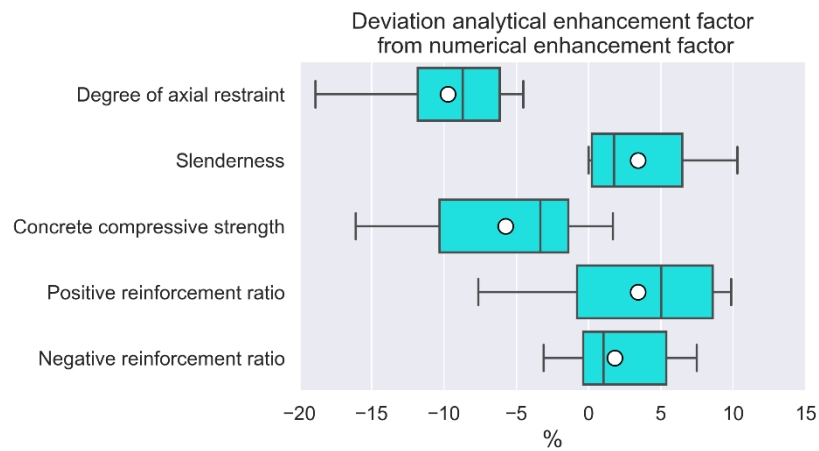
Figure 6.16: Boxplots of GNL reduction effect sensitivity analysis (a) and enhancement factor sensitivity analysis (b) per model parameter.
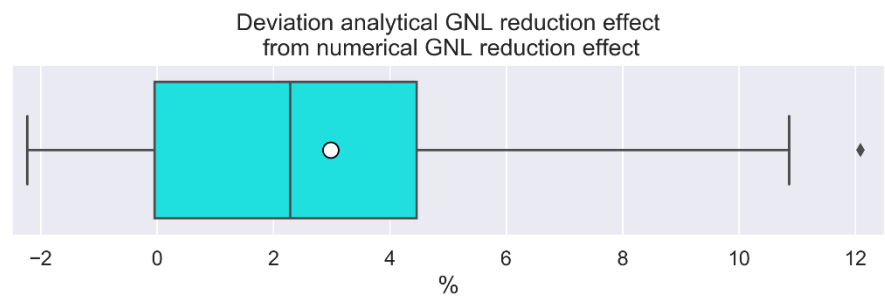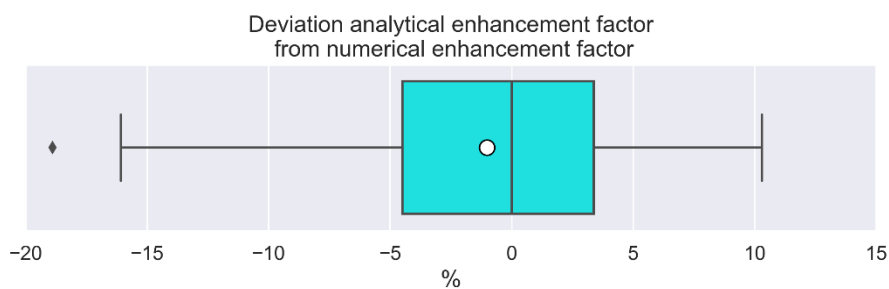
Figure 6.17: Boxplots of GNL reduction effect sensitivity analysis (a) and enhancement factor sensitivity analysis (b) for all examined cases.

The sensitivity analysis showed that the enhancement factor varies between 1.3 and 4.7 for a variety of partially and fully restrained slab strips with a slenderness above 10. The effect of geometrical nonlinearity on the ultimate capacity (GNL reduction effect) varies between 3% and 37% for the same slap strips. The most critical parameters that greatly affect the enhancement factor are the positive reinforcement ratio, the degree of axial restraint and the concrete compressive strength. Besides, the GNL reduction effect is sensitive to changes in slenderness and positive reinforcement ratio.

The analytical model could estimate the GNL reduction effect sufficiently accurate because the mean and maximum deviation between the analytical result and the numerical result are respectively 3% and 12.1% for all examined cases. In addition, more than 75% of all values are within a range of only 5% deviation. Figure 6.17b shows that the GNL reduction effect is overestimated by the analytical model in most cases. The analytical model could also estimate the enhancement factor sufficiently accurate because the mean and maximum deviation between the analytical result and the numerical result are respectively 1% and 18.9% for all examined cases (see Figure 6.17a). In addition, half of all the deviation values are between -4% and +3%.

Also, the sensitivity analysis showed that the estimations of the analytical model exhibit similar trends as the numerical model. Especially enhancement factors for variations in the positive reinforcement ratio, negative reinforcement ratio, concrete compressive strength up to 50 MPa and slenderness above 20 can be described accurately by the analytical model. Besides, the analytical model leads to inaccurate estimations of the GNL effect when varying the concrete compressive strength and the degree of axial restraint. In contrast, the influence of the positive reinforcement ratio and the slenderness on the GNL effect could be estimated properly by the analytical model. The overestimation of the enhancement factor by the analytical model was most severe for deep concrete slabs and low degrees of axial restraint.

The findings of Bakker (MSc thesis, [7]) discussed in section 1.1 were confirmed by both the presented analytical and numerical model: the enhancement factor is highest for high concrete compressive strength, low positive reinforcement ratio, low slenderness, and a high degree of axial restraint. It should be noted that the punching shear was not considered in this thesis, while Bakker did consider this phenomenon when determining the enhancement factor of the concrete slabs. In addition, the calculation of the conventional capacity is in this thesis is based on the EC2, while Bakker used the previous Dutch design code in his research.

7

Comparison between analytical and experimental results

7.1. Introduction

In this chapter, a comparison is made between the results of the analytical model and test results from experimental research. An attempt is made at the experimental validation of the analytical model. First, the essential differences between the analytical model and experimental tests are described in section 7.2. The qualitative comparison between the analytical model and two experiments from the literature with one way and two way slabs is made in section 7.3. Section 7.4 presents the conclusions from the comparison.

A comparison between the test results from experiments and results from equivalent developable numerical models could be relevant for the validation of the experimental results. However, the development and post-processing of these numerical models would take a lot of time, which was not available. In addition, numerical validation was not considered essential for this thesis, as the stated goals could be achieved without this validation.

7.2. Differences between analytical model and experiments

The presented analytical model in chapter 4 is two dimensional, which implies that the third dimension out of the plane of the slab strip (i.e. width) is not considered in these models. It is assumed that there is no difference in deflections or stresses over the width of the slab; every fibre in the third dimension of the models acts similarly. The slab strip will transfer the load in only one direction. Figure 7.1a represents the top view of the slab used for the analytical model, which is now referred to as slab (a). The deflection of the centre of the slab is equal to the deflection at the sides of the slab at midspan.

On the other hand, actual concrete slabs tested during experimental research are by definition three-dimensional. Double curvature will therefore lead to a deviation of deflections at the midspan cross-section; the centre (red point) will deflect more than the sides (blue points) (see Figure 7.1b). Yet, most of the load is still transferred in one direction due to the high length-to-width ratio. Also, only the short edges are clamped. Slab (b) can therefore be considered a one way slab. Hence, it is likely that the effects of the double curvature are very limited and that the analytical slab strip model can be used to predict the behaviour of slab (b). Increase in the width of slab (b) will increase the double plate bending and increase the differences between the longitudinal centre cross-section and the side cross-sections. In addition, confinement of the concrete in the middle of the slab could play a more significant role in a wider slab (b). Therefore, a model of slab (a) could give less accurate estimations of the load-deflection behaviour of a wider slab (b).

Tested slabs can also be clamped at all four edges. Figure 7.1c presents a pure two way slab (slab (c)), in which the load is equally transferred in both directions due to a length-to-width ratio of 1.0. In this four-side supported

slab, each support carries an equal share of the load. The curvature in both directions is also equal, resulting in a perfect double curvature of the slab. Each point on the blue line has the same deflection value, and the maximum deflection occurs in the middle of the slab. A model of slab (a) or slab (b) cannot simply be used to predict the load-deflection behaviour of slab (c) because of three reasons: 1) confinement of concrete is more significant in slab (c), which could result in a higher concrete compressive strength and a larger softening branch of concrete in compression; 2) different supporting conditions: two-side supported versus four-side supported; 3) different length-to-width ratio. These three aspects have a considerable effect on the structural stiffness, the load transfer and the crack pattern of the slab. Therefore, slab (c) can actually not be compared to slab (a) or slab (b). The only two ways to compare could be to use empirical formulas based on experimental data or to develop a theoretical method. However, relevant experimental data to develop empirical formulas is lacking and the development of such a comparison theory is very complex and time-consuming.
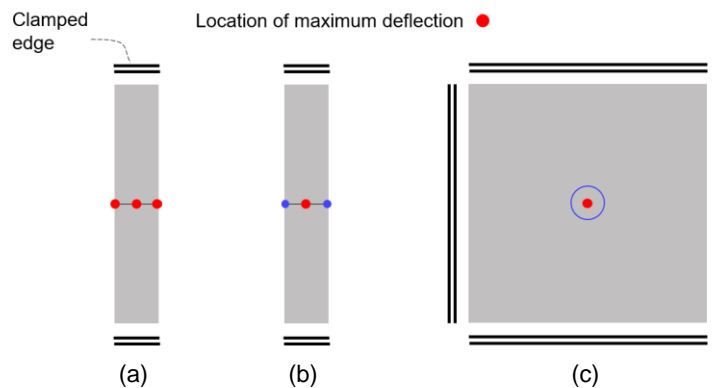
Figure 7.1: Three different kinds of concrete slabs.

Besides, the support conditions used in the analytical model are different from those of experimentally tested slabs. The basic analytical model assumes complete rigid supports; the supported edges of the slab cannot rotate or translate. This is practically impossible during experimental testing. Thus, tested slabs will always have a finite degree of restraint. The modified analytical model could be used to estimate the response for tested slabs with finite degrees of axial restraint if the value of this degree was known. However, this value is usually unknown.

Experimental research on the capacity enhancement due to CMA is mainly done on two way slabs. One way slabs are examined less often. In addition, the examined slabs are not perfectly clamped, because infinite rigidity cannot be achieved. Therefore, an actual quantitative comparison between the analytical and experimental results from the literature is rather useless. Hence, experimental validation of the quantitative analytical results presented in this thesis is not yet possible. On the other hand, a qualitative comparison can put the analytical results in perspective.

7.3. Qualitative comparison

Two experimental programs are compared with results obtained with the developed analytical method. The differences between the experimental and analytical results are explained. The first experimental program consists of testing of nearly rigidly restrained two way slabs loaded with a UDL. The second experimental program consists of testing of partially laterally restrained one way slabs loaded with a line load at midspan. Thus, in the first program some support conditions match with the analytical model, and in the second program the loading and the one way load transfer match with the analytical model. Thereby, the differences with the analytical model, which assumes two rigid supports, one way load transfer and line loading at midspan, are also apparent.

7.3.1. Two way slab

Rankin et al. researched the strength enhancement due to CMA by testing laterally restrained and unrestrained slabs [3]. The span length and span width of the slabs are both 950 mm. The thickness of the slabs is 50 mm, resulting in a slenderness of 19. The slabs have some additional length and width to clamp all four edges with the use of a steel supporting frame. The unrestrained slabs are rotationally restrained but laterally unrestrained at their edges. The restrained slabs are both rotationally and laterally restrained at their edges. A UDL is incrementally applied on top of the slabs. The yield strength of the steel reinforcement is 510 N/mm^2 for all slabs. The ultimate load of five examined slabs is determined with the analytical method presented in this thesis (see chapter 4). Geometric and material properties of the steel and concrete are presented for each slab in Table 7.1.
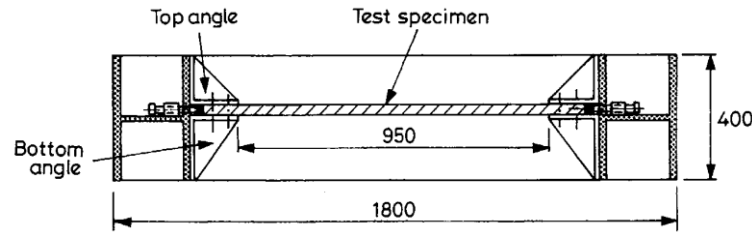
Figure 7.2: Test set-up two way slab [3].

Parameter	Unit	S1R	S2R	S4R	S6R	S7R
f_c	MPa	42.3	37	30.4	38.8	34.5
d	mm	-	38	38	38	38
ρ	-	-	0.00258	0.00516	0.00258	0.00516
$\bar{\rho}$	-	-	0.00258	0.00516	0.00516	-

Table 7.1: Properties of the two way slabs.

Figure 7.3a shows the results of the experimental program of Rankin et al. The ultimate load of the tested restrained and unrestrained slabs is plotted against the conventional yieldline capacity according to Wood [43]. Also, the diagram includes a graph for the theoretical ultimate load for a rigidly restrained slab [43]. For the experimental results, the enhancement factor is defined as the ultimate capacity of the restrained slab divided by the ultimate capacity of the unrestrained slab. It was found that the ultimate load of the restrained slab had an average value of approximately 440 kN/m2, which is significantly higher than the ultimate capacity of the equivalent unrestrained slabs. The corresponding enhancement factor is between 1.7 and 5.9.
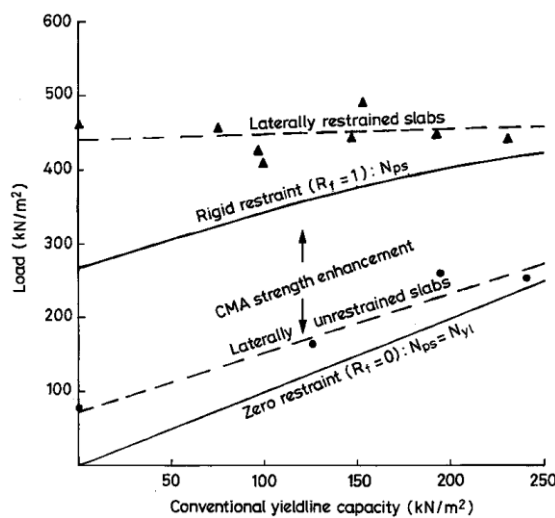
(a)
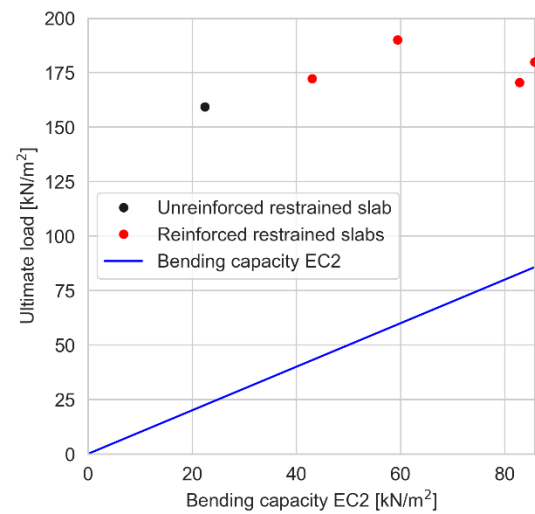
(b)

Figure 7.3: Enhanced ultimate capacity plotted against the conventional capacity according to the experiments (a) and to the analytical model (b).

The analytical results show that the average ultimate load of about 175 kN/m^2 with a difference factor of 2.5 is significantly lower than the ultimate load according to the tests. This is because the test slabs can transfer the load in two directions to all four supporting edges, while the analytical model assumes one way load transfer. In addition, the tested concrete is confined, which possibly results in higher strength. Therefore, this is a logical outcome of the comparison. Further, the enhancement factor according to the analytical model is between 2 and 4 for the reinforced slabs and approximately 7 for the unreinforced slab. It should be noted that the ultimate load for the unreinforced slab is determined by the tensile strength of concrete. The bending moment capacity is doubled because plastic analysis allows for an increase in the load.

Thus, two important similarities between the experimental and analytical results are that 1) the unreinforced slab leads to the largest enhancement factor and 2) the enhancement factor for the reinforced slabs is in the same order of magnitude. The first similarity (1) is because the conventional capacity, either the yieldline capacity of the slab or the bending capacity of the slab strip, is very low for the unreinforced slab. As a result, there is a large difference between the conventional capacity and the actual enhanced capacity. It can even be concluded that there is a relation between the conventional capacity and the enhancement factor for both the analytical and experimental results: the higher the conventional capacity, the lower the enhancement factor. Furthermore, no valuable conclusions can be drawn from the second similarity (2), because the analytical model and the tested slabs can actually not be compared based on quantitative results. Other relevant similarities between the experimental and analytical results are: the failure mode is crushing of the concrete, the steel had yielded before the crushing of the concrete occurred, the stiffness of the restrained slab is significantly higher, and the response of the restrained slab is less ductile.

Crushing of the tested concrete slabs occurs along the diagonals at the top of the slab as seen in Figure 7.4. This crushing pattern is completely different than assumed for the analytical model, where crushing on top only occurs near midspan.
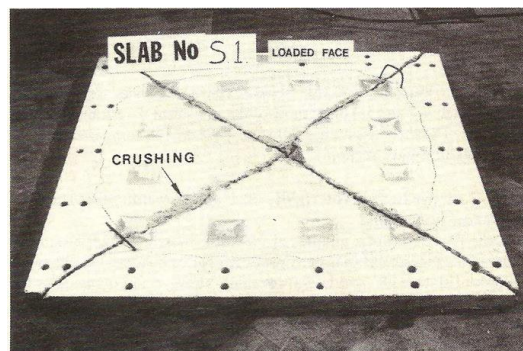
Figure 7.4: Crushing pattern of restrained two way slab [3].

7.3.2. One way slab

Vecchio and Tang tested a laterally restrained as well as an unrestrained one way slab [5]. The loading is applied as a line load at midspan. The slabs are vertically supported by two columns and at the two short edges of the slab (see Figure 7.5a). The horizontal movement of the restrained slab is restrained at these edges. The mechanical schemes of the tested slabs are presented in Figure 7.5b. The structural system can be schematised by a slab strip with translational and rotational springs at the column supports (see Figure 7.5c). The span of the analytical model is assumed to be 3076 mm, which is the heart-to-heart distance of the columns. The steel reinforcement has a yield strength of 454 N/mm^2 and an ultimate strength of 649 N/mm^2. The analytical model adopts the steel properties accordingly.
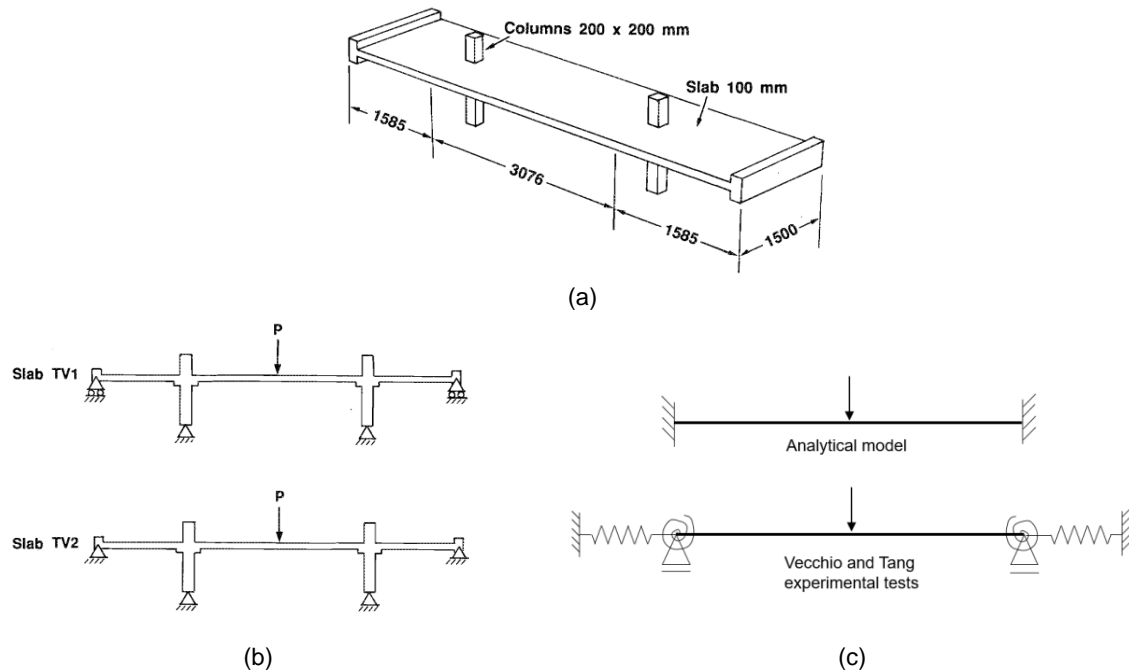
Figure 7.5: Test set-up one way slab (a), comparisons between the restrained and unrestrained slabs (b) and between the experimental and analytical mechanical models (c).

Parameter	Unit	TV1	TV2
f_c	MPa	29.7	30.2
E_c	MPa	30500	32200
d	mm	84	84
$\rho_{support}$	-	0.0066	0.0066
$\rho_{midspan}$	-	0.0033	0.0033

Table 7.2: Properties of the one way slabs.

As can be seen in Table 7.3, the capacity of the restrained slab resulting from the analytical model is about 35% higher than the capacity resulting from the experiment. The infinite degree of restraint for the analytical model leads to a higher capacity than the finite degree of restraint of the tested slab, because the compressive forces and consequently the arching action will be higher in magnitude due to the lateral restraint. Further, the enhancement factor resulting from the tests is 1.4, and the enhancement factor resulting from the analytical model is 1.7. No further conclusions can be drawn from this outcome.

Ultimate load	**Analytical**	**Experimental**
Unrestrained	64.8 kN	63 kN
Restrained	122 kN	89 kN

Table 7.3: Ultimate loads of the one way slabs.

The crack pattern of the restrained slab is presented in Figure 7.6. The cracks in the slab occur at the expected locations near the columns at the top and near midspan at the bottom. The cracks at the columns are oriented in both the width and in the longitudinal direction, while the cracks at midspan are mostly oriented in the width direction. The experimental result regarding the crack pattern thus differs from the analytical result, which assumes cracks at midspan and at the supports in only the width direction over the entire width of the slab. However, the crack pattern of the restrained one way slabs is much more similar to the crack pattern assumed for the analytical model than that of the two way slab.
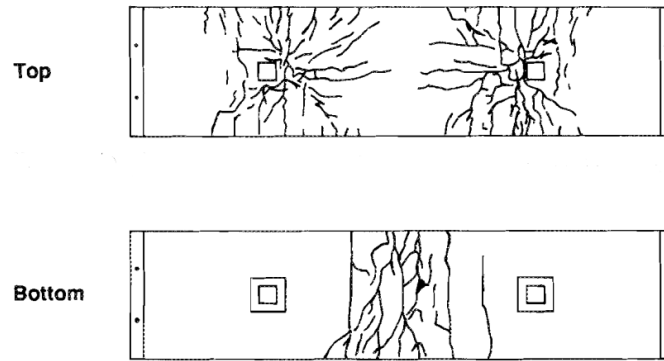
Figure 7.6: Crack pattern of restrained one way slab [5].

7.4. Conclusion

The analytical model can predict the capacity of the considered one way slab (factor 1.35) better than the capacity of a two way slab (factor 2.5). Supporting conditions, length-to-width ratio and degree of restraint influence the prediction accuracy of the analytical model and thereby the difference factor. In the qualitative comparison, several similarities were found between the analytical and experimental results, the most important of which were: the slabs fail on the crushing of the concrete, the enhancement factor is larger for slabs with lower conventional capacities, and a significant increase in the ultimate load was found due to CMA. On the other hand, the crack pattern assumed for the analytical model does not match with the crack pattern of the tested slabs due to a difference in boundary conditions and due to the double curvature of the slabs.

It can be concluded that the qualitative analytical outcomes are in reasonable agreement with the qualitative experimental outcomes. The quantitative difference between the ultimate loads is however still large. It should however be noted that quantitative comparison is in this case not very useful, because of the essential differences between the set-up of the analytical model and the experiments. Further experimental research is necessary to quantitively validate the analytical results presented in this thesis. Suitable experimental tests for validation would be a fully clamped beam or one way slab loaded with a point or line load at midspan.

8
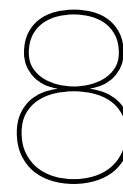
Conclusions and Recommendations

8.1. Conclusions

The main goal of this research was to investigate to what extent geometrical nonlinearity affects the magnitude of compressive membrane action (CMA) and what causes the geometrical nonlinear (GNL) effect. Another goal was to quantify the capacity enhancement due to CMA. Therefore, a new analytical model is developed to predict the load-deflection behaviour and the enhanced capacity of laterally restrained and reinforced concrete slab strips. Because the analytical model can be adjusted for both a geometrical linear (GL) and GNL approach of the structural analysis, it is possible to derive the magnitude of the GNL effect from this. The used method for the analytical model was obtained from a developed theory from the literature by McDowell et al. for predicting the arching action in masonry walls [9].

A literature study showed that CMA is a material nonlinear effect because it is initiated by the cracking of the concrete. Furthermore, it was found that geometrical nonlinearity reduces the capacity increase of CMA due to a tilt of the compressive arches as a result of deflections. Thus, the resisting arching moments resulting from the lateral restraint will decrease with increasing deflection because of a reduction of the internal lever arm of the introduced horizontal compressive forces. The result is a lower ultimate capacity for restrained concrete slabs when geometrical nonlinearity is accounted for. Because actual structural behaviour is GNL, the capacity will be overestimated in a GL structural analysis of restrained concrete slabs. This finding was strengthened with a detailed study into the behaviour of a laterally restrained truss. The statement of Guice and Rhomberg in [27] that the behaviour of a restrained concrete slab shows great similarity with that of a restrained truss was proven. Geometrical nonlinearity contributed to the reduction of the resisting bending moments and the ultimate capacity of the truss.

The developed analytical model confirmed the capacity enhancement due to CMA. It was found that the analytically obtained ultimate capacity of restrained slab strips was significantly higher than the conventional bending capacity according to the Eurocode 2 excluding design factors. It should be noted that geometrical nonlinearity was included in the calculation of the ultimate capacity because actual structural behaviour is nonlinear. A numerical model developed in DIANA was used to calibrate the analytical model and validate its results.

From a sensitivity analysis of the calibrated analytical model and the numerical model, it was found that the enhancement factor – defined as the increased capacity divided by the conventional capacity – is highest for restrained slabs with a high degree of axial restraint, low span-to-depth ratio (but higher than 10), high concrete compressive strength, low positive reinforcement ratio or high negative reinforcement ratio. Figure 8.1 shows the ranges of the enhancement factor for five varied model parameters. The figure also includes the parameter values corresponding to the maximum and minimum values of the enhancement factor. The enhancement factor is

sensitive to changes mainly in positive reinforcement ratio, and to a lesser extent in degree of axial restraint and concrete compressive strength.

The increase in capacity due to CMA was found to be even greater if geometrical nonlinearity was not included in the models. Thus, geometrical nonlinearity reduces the increased ultimate capacity of restrained slabs. The cause of this GNL reduction effect is explained two paragraphs above. The GNL reduction effect is most severe for slabs with a high span-to-depth ratio, a low positive reinforcement ratio or a high concrete compressive strength. Furthermore, the GNL effect is sensitive to changes mainly in slenderness and positive reinforcement ratio (see Figure 8.2).
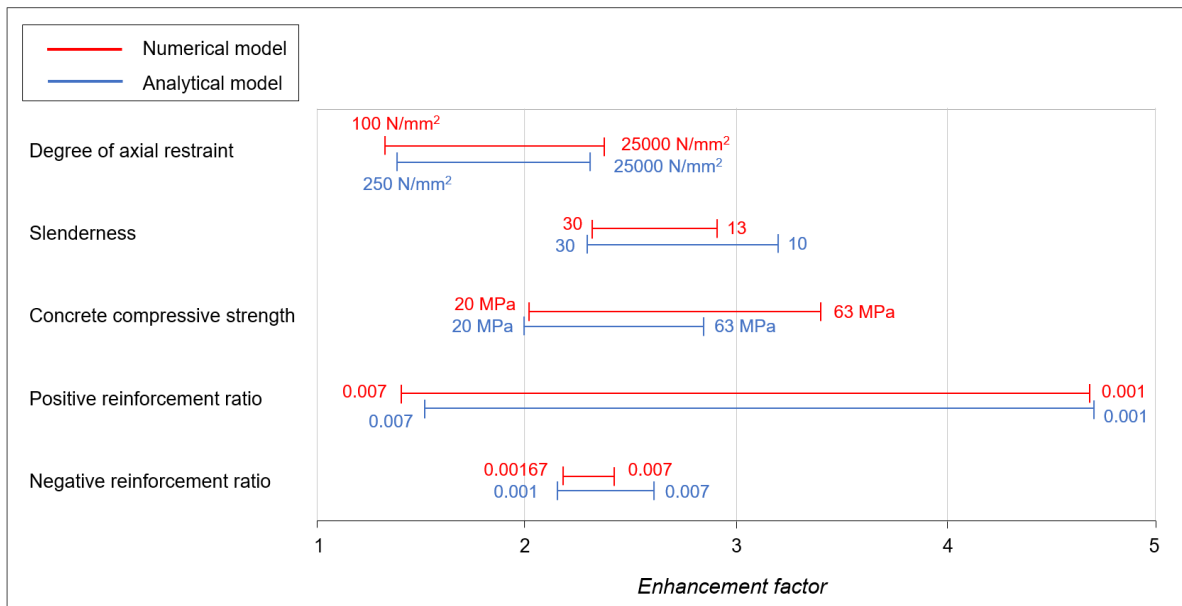
Figure 8.1: Enhancement factor sensitivity analysis.
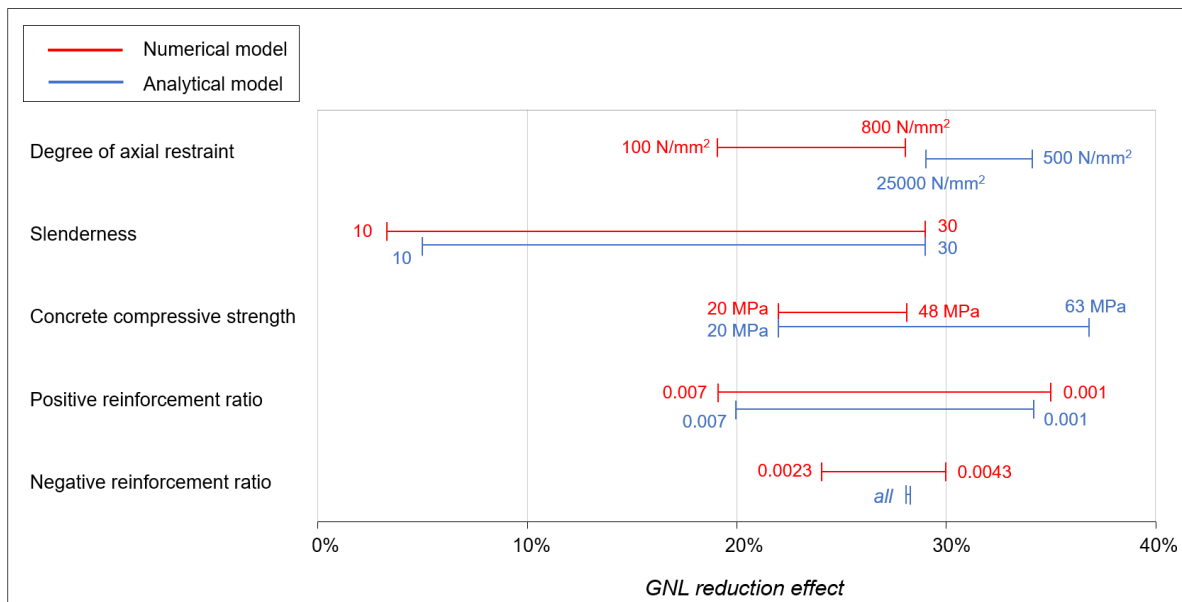
Figure 8.2: GNL reduction effect sensitivity analysis.

An important conclusion from the sensitivity analysis is that the GNL reduction effect was much more severe for slender slab strips, while the capacity enhancement and thereby the relative magnitude of CMA were larger for deep slab strips. The capacity enhancement is larger for deep slab strips because the internal lever arm is relatively large compared to the span length, resulting in a stronger arching effect. The GNL reduction effect is larger for slender slabs because the percentage decrease in the angle of the compressive arches with the horizontal is higher for comparable deflections, and therefore the internal lever arm, as well as the resisting arching moments, approach zero much faster for slender slabs. This finding is summarised in Table 8.1, in which the relative magnitude of CMA and the GNL reduction effect are shown for slender and deep slabs.

Magnitude of $\rightarrow$	CMA	GNL effect
Deep slab	Large ⬆	Small ⬇
Slender slab	Small ⬇	Large ⬆

Table 8.1: Relative magnitude of CMA and the GNL effect for deep and slender slabs.

Other conclusions from the results of the analytical model, the numerical model, the sensitivity analysis and the comparison between the analytical results and experiments from the literature:

- The calibrated analytical model could predict the enhancement factor with a mean deviation of 1% and a maximum deviation of 18.9% for slabs with span-to-depth ratios above 10. Numerically obtained enhancement factors for variations in the positive reinforcement ratio, negative reinforcement ratio, concrete compressive strength up to 50 MPa and slenderness above 20 are estimated accurately by the analytical model. Also, the GNL reduction effect was estimated sufficiently accurate by the analytical model with a mean and maximum deviation of respectively 3% and 12.1%. Mainly variations in the positive reinforcement ratio and the slenderness could be estimated accurately. It can therefore be concluded that the numerical model successfully validates the ultimate capacity and the GNL effect obtained by the analytical model.

- Strong evidence was found that failure of the slab strip was due to the crushing of concrete fibres in the compression zones near the support and near midspan. The compressive strains were so high, mainly due to significant arching action, that the compressive stress approached zero in these zones.

- The response of the slab strip is more ductile for a lower degree of axial restraint. In contrast, the width of the compressive arches and the ultimate capacity are larger for higher degrees of axial restraint. Moreover, the type of loading affects the orientation of the resultant compressive arches: a point load at midspan leads to straight compressive arches, while a uniformly distributed load results in curved compressive arches.

- From a qualitative comparison between the analytical results and experimental data on two way slabs (Rankin et al. in [3]) and one way slabs (Vecchio and Tang in [5]), it can be concluded that the analytical method leads to qualitative results that are sufficiently consistent with reality. Several qualitative outcomes of the analytical model agreed with the experimental results: a significant increase in the ultimate load was found due to CMA, crushing was the failure mode of the slabs, and the enhancement factor was larger for slabs with lower conventional capacities. The quantitative outcomes did not match: the absolute values for the ultimate capacities differed significantly due to a difference in boundary conditions, loading conditions and the assumption for purely one way load transfer for the analytical model.

8.2. Recommendations

The study shows that the ultimate capacity of restrained concrete slabs is considerably higher than the conventionally calculated capacity because of the development of CMA. Analytical, numerical and experimental results showed that the capacity enhancement is larger for slabs that have a low conventional capacity. Also, the enhancement due to CMA is large for deep slabs and small for slender slabs. This increase in capacity is however overestimated in a GL calculation. Therefore, structural engineers should be aware that geometrical nonlinearity partially nullifies the positive effects of CMA on the capacity of restrained slabs. This is most important when the overestimation of the ultimate capacity in a GL calculation is more than 10%, which is the case for slabs with span-to-depth ratios higher than 14.6 and 17.2 according to respectively the analytical and numerical model (f_c = 33 MPa, ρ = 0.34%)

It is therefore of importance to consider geometrical nonlinearity in restrained slender slabs even though the increase in capacity due to CMA is limited. On the other hand, it is of importance to consider CMA in deep slabs, while geometrical nonlinear effects can be ignored. It is recommended to realize as a structural engineer that only if geometrical nonlinearity is included in a structural analysis of slender concrete slabs which are laterally restrained, the outcomes will sufficiently represent the actual structural behaviour.

It is advisable to experimentally validate the analytical model in a follow-up study to strengthen the quantitative findings presented in this thesis. Validation can be done with experiments of fully clamped beams or slabs with a large length-to-width ratio subjected to a line load at midspan. The test results could then be compared with the quantitative outcomes of the analytical model. Besides, the development and post-processing of numerical models of these experiments can be relevant in addition to this follow-up research. Also, further work can focus on the influence of shear stresses – which were not considered in the analytical model – in a restrained concrete slab or on implementing the degree of rotational restraint in the analytical method.

The developed analytical model uses assumptions for the compressive strain distribution in the concrete slabs that are not verified in detail. It is recommended to conduct new research on the assumptions that describe the compressive strain distribution in the longitudinal direction of a concrete slab with the so-called multiplication factor MF (see section 4.6 and section 5.3). Moreover, further research can be conducted to investigate the potential of using the developed analytical method to describe the structural behaviour due to tensile membrane action in slender concrete slabs.

Furthermore, it could be that three-dimensional compressive arches will increase the capacity of concrete slabs even more. The width dimension of the slab can therefore also be considered in a follow-up study, with a focus on double plate bending, confinement of the concrete and the cracking and crushing patterns. Finite element models can be developed in the three-dimensional environment in DIANA in order to examine the influence of both compressive membrane action and geometrical nonlinearity on the response of solid concrete slabs with various supporting conditions. Then, the conventional punching shear capacity can be also be compared with the enhanced ultimate capacity.

Bibliography

[1]   L. Walta, "Langer zullen ze leven: werkelijke conditie kunstwerken verandert onderhoudsplan," *Ing.*, vol. 1, pp. 42–46, 2015.

[2]   N. Vessali, "Compressive Membrane Action in Reinforced Concrete Beams," 2015.

[3]   G. I. B. Rankin, R. A. Niblock, A. S. Skates, and A. E. Long, "Compressive membrane action strength enhancement in uniformly loaded, laterally restrained slabs," *Struct. Eng. London*, vol. 69, no. 16, pp. 287–295, 1991.

[4]   S. Amir, "PhD Thesis: Compressive Membrane Action in Prestressed Concrete Deck Slabs," Delft University of Technology, 2014.

[5]   F. L. Vecchio and K. Tang, "Membrane action in reinforced concrete slabs," *Can. J. Civ. Eng.*, vol. 17, no. 5, pp. 686–697, 1990.

[6]   *EN 1992-1-1. Eurocode 2: design of concrete structures – part 1-1: general rules and rules for buildings*. 2004.

[7]   G. J. Bakker, "MSc thesis: A finite element model for the deck of plate-girder bridges including compressive membrane action, which predicts the ultimate collapse load," Delft University of Technology, 2008.

[8]   T. Ben-Gera, "MSc Thesis: Compressive Membrane Action in Immersed Tubes," Delft University of Technology, 2019.

[9]   E. L. McDowell, K. E. McKee, and E. Sevin, "Arching Action Theory of Masonry Walls," *By Am. Soc. Civ. Eng. J. Struct. Div.*, vol. 82, no. 2, pp. 915-1-915–18, 1956.

[10]   M. A. N. Hendriks and M. Roosen, "Guidelines for nonlinear finite element analysis of concrete structures," *Rijkswaterstaat Tech. Doc. (RTD), Rijkswaterstaat Cent. Infrastructure, RTD, 1016-12020*, 2020.

[11]   M. W. Verver and A. L. Fraaij, *Materiaalkunde*, 4th ed. Noordhoff Uitgevers, 2015.

[12]   D. François, A. Pineau, and A. Zaoui, *Mechanical Behaviour of Materials: Volume I: Elasticity and Plasticity*. Dordrecht: Springer, 1998.

[13]   Y. T. Zhu and X. L. Wu, "Ductility and plasticity of nanostructured metals: differences and issues," *Mater. Today Nano*, vol. 2, pp. 15–20, 2018, doi: 10.1016/j.mtnano.2018.09.004.

[14]   A. P. Mouritz, *Introduction to Aerospace Materials*. Cambrdge: Woodhead Publishing Limited, 2012.

[15]   T. H. G. Megson, *Structural and Stress Analysis*. 2019.

[16]   2010 International Federation for Structural Concrete, *fib Model Code for Concrete Structures*. Lausanne, 2013.

[17]   N. Kim, *Introduction Analysis Finite Element to Nonlinear*. 2018.

[18]   M. Peksen, *Multiphysics Modelling Materials, Components, and Systems*. 2018.

[19]   R. K. Livesley, *Matrix Methods of Structural Analysis*. Michigan: Pergamon Press, 1975.

[20]   D. Collings and J. Sagaseta, "A review of arching and compressive membrane action in concrete bridges," *Proc. Inst. Civ. Eng. Bridg. Eng.*, vol. 169, no. 4, pp. 271–284, 2016, doi: 10.1680/bren.14.00039.

[21]   H. M. Westergaard and W. A. Slater, "Moments and stresses in slabs," *Proc. Am. Concr. Inst.*, pp. 415–538, 1921.

[22]   A. J. Ockleston, "Arching action in reinforced concrete slabs," *Struct. Eng.*, vol. 36, no. 6, pp. 197–201, 1958.

[23]   K. P. Christiansen, "The effect of membrane stresses on the ultimate strength of an interior panel in a

reinforced concrete slab," *Struct. Eng.*, vol. 41, no. 8, pp. 261–265, 1963.

[24]   R. Park and W. Gamble, *Reinforced Concrete Slabs*. New York: Wiley, 1980.

[25]   B. Batchelor, B. E. Hewitt, P. Csagoly, and M. Holowka, "Investigation of the ultimate strength of deck slabs of composite steel/concrete bridges," *Transp. Res. Rec. Proc. Bridg. Eng. Conf.*, vol. 1, no. 664, pp. 162–170, 1978.

[26]   P. Csagoly, M. Holowka, and R. Dorton, "The true behaviour of thin concrete bridge slabs," *Transp. Res. Rec.*, vol. 1, no. 664, pp. 171–179, 1978.

[27]   L. K. Guice and E. J. Rhomberg, "An analogous model for slabs using a truss element," *Computers and Structures*, vol. 31, no. 5. pp. 767–774, 1989, doi: 10.1016/0045-7949(89)90211-3.

[28]   W. Botte, R. Caspeele, D. Gouverneur, and L. Taerwe, "Influence of membrane action on robustness indicators and a global resistance factor design," *Bridg. Maintenance, Safety, Manag. Life Ext. - Proc. 7th Int. Conf. Bridg. Maintenance, Saf. Manag. IABMAS 2014*, no. July, pp. 2038–2046, 2014, doi: 10.1201/b17063-315.

[29]   D. R. W. Martens and A. T. Vermeltfoort, "Arching effect in laterally loaded urm walls," *Proc. 13th Can. Mason. Symp.*, no. 2017, pp. 1–12, 2017.

[30]   H. J. Barten, "On the deflection of a cantilever beam," *Q. Appl. Math.*, vol. 2, no. 2, pp. 168–171, 1944, doi: 10.1090/qam/10879.

[31]   K. E. Bisshopp and D. C. Drucker, "Large deflection of cantilever beams," *Q. Appl. Math.*, vol. 3, no. 3, pp. 272–275, 1945, doi: 10.1090/qam/13360.

[32]   F. V. Rohde, "Large deflections of a cantilever beam with uniformly distributed load," *Q. Appl. Math.*, vol. 11, no. 3, pp. 337–338, 1953, doi: 10.1090/qam/56438.

[33]   C. Hartsuijker and J. W. Welleman, "Constructiemechanica 3, TU Delft," no. December, pp. 21–22, 2007.

[34]   K. J. Bathe, *Finite Element Procedures*. Prentice Hall, 2014.

[35]   Y.-C. Wang, "Stability of Discrete Mechanical Systems Containing Negative Stiffness Components," 2011.

[36]   S. Krenk, "Non-linear modeling and analysis of solids and structures - chapter intro non-linear problem," no. 1989, p. 1991.

[37]   O. C. Zienkiewicz, R. L. Taylor, and J. Z. Zhu, *The Finite Element Method: its Basis and Fundamentals*. Oxford: Elsevier Butterworth-Heinemann, 2005.

[38]   D. Ferreira, Ed., *DIANA User's Manual.* Delft: DIANA FEA BV, 2020.

[39]   S. Chattopadhyay, "Investigation of proportional and non-proportional loadings using Mohr's circle," *ASEE Annu. Conf. Expo. Conf. Proc.*, 2012, doi: 10.18260/1-2--21616.

[40]   J. G. Rots, "PhD Thesis: Computational modeling of concrete fracture," Delft University of Technology, 1988.

[41]   F. J. Vecchio and M. P. Collins, "Compression response of cracked reinforced concrete," *J. Struct. Eng.*, vol. 119, no. 12, pp. 3590–3610, 1993, doi: 10.1360/csb1994-39-15-1380.

[42]   M. G. M. van den Hoogen, "MSc Thesis: Beam or Truss Mechanism for shear in concrete," Delft University of Technology, 2013.

[43]   R. H.- Wood, *Plastic and elastic design of slabs and plates*, 1st ed. London: Thames & Hudson, 1961.

List of Figures

List of Tables

A

Appendix – Chapter 4:
Analytical model

A.1. Failure load determination

First, the bending moment resistance M_u is calculated according to EN 1992-1-1 Eurocode 2. The calculation procedure is given in Figure A.1. Note that the values for the concrete and steel strength are not corrected by design factors. Followingly, plastic analysis is used to determine the final failure load for the statically indeterminate concrete slab strip.
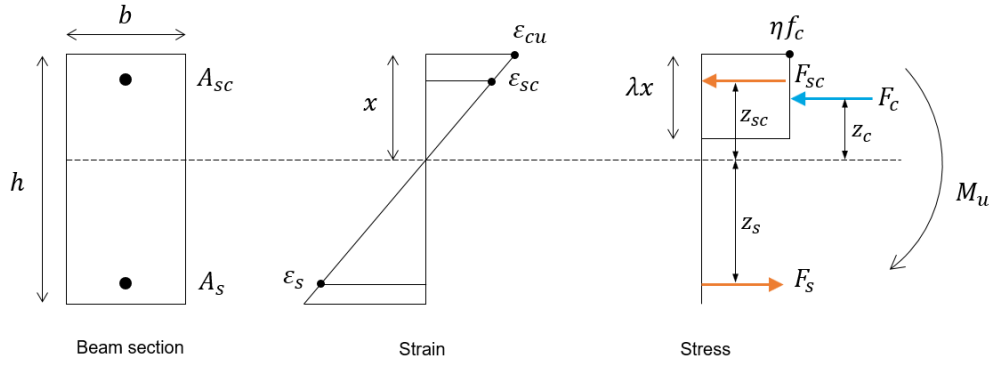
Assume a value for the compression zone depth	x
Calculate the reinforcement strains	$\varepsilon_{sc} = \varepsilon_{cu} \cdot \dfrac{x - c_{sc}}{x}$ $\varepsilon_s = \varepsilon_{cu} \cdot \dfrac{h - c_s - x}{x}$
Calculate the reinforcement stresses	$f_{sc} = \begin{cases} \varepsilon_s E_s & \varepsilon_s < \epsilon_y \\ \varepsilon_y E_s & \varepsilon_s \geq \epsilon_y \end{cases}$
Calculate the forces in the concrete and steel	$F_c = \eta f_c \cdot \lambda x$ $F_{sc} = f_{sc} \cdot A_{sc}$ $F_s = f_s \cdot A_s$
Check the horizontal equilibrium	$F_c + F_{cs} - F_s > 0.001$ $F_c + F_{cs} - F_s < 0.001$
Calculate the lever arms of the forces	$z_c = x - \dfrac{1}{2}\lambda x$ $z_{sc} = x - c_{sc}$ $z_s = h - c_s - x$
Calculate the bending moment resistance	$M_u = F_c \cdot z_c + F_{sc} \cdot z_{sc} + F_s \cdot z_s$

Figure A.1: Bending moment resistance calculation according to the EC2.

For statically determined slab strips, it holds that the formation of one plastic hinge will lead to failure. Thus, a further increase in the load will result in the total collapse of the slab strip. In contrast, more than one plastic hinge has to be formed to cause the collapse of statically indeterminate slab strips. Therefore, a further increase in the load after one plastic hinge is formed will not lead to collapse, but to redistribution of forces. Failure of the slab strip will now only occur when the plastic hinges can form a collapse mechanism. The result is an increase in the failure load for statically indeterminate structures compared to statically determinate structures.

Plastic analysis of the considered concrete slab strip will be done with the virtual work method in order to determine the failure load. The principle of this method is that the external work is equal to the internal work, which means that the work done by the external loads during the virtual displacement is equal to the internal work at the hinges. Furthermore, it is assumed that the angles remain small, so that the angle θ is equal to $tan\theta$ and $sin\theta$.
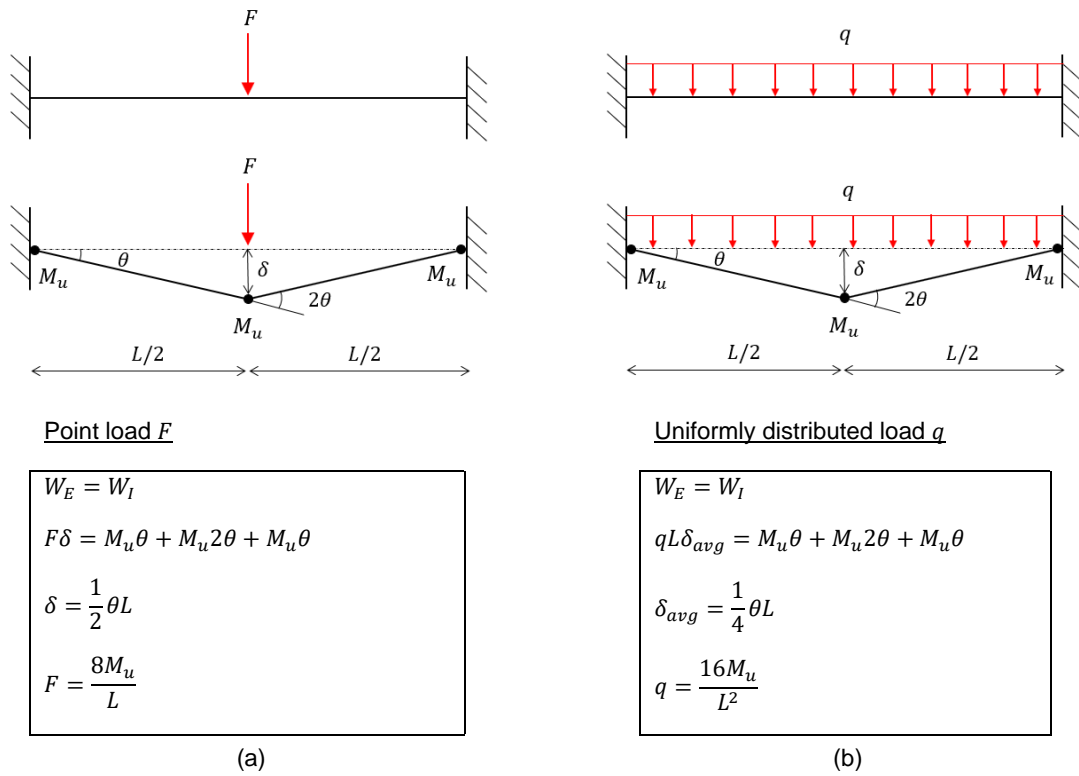
Figure A.2: Failure load determination for a point load (a) and a UDL (b) with virtual work method.

Figure A.2 contains the elaboration of the failure load determination with the virtual work method. For the statically indeterminate slab strip, the failure load is two times larger than the failure load of a statically determined slab strip. Figure A.3 shows the Excel sheet used for the determination of the bending resistance and the failure load of both Slab 1 and Slab 2.

Slab 1				Slab 2		
Parameter	Value	Unit		Parameter	Value	Unit
Ø	8	mm		Ø	12	mm
spacing	120	mm		spacing	140	mm
c	15	mm		c	25	mm
h	125	mm		h	225	mm
L	3600	mm		L	3600	mm
b	200	mm		b	200	mm
d	106	mm		d	194	mm
c_s	19	mm		c_s	31	mm
c_cs	19	mm		c_cs	31	mm
ρ	0,00335	-		ρ	0,00359	-
As	83,776	mm^2		As	161,568	mm^2
fyk	500	MPa		fyk	500	MPa
fck	25	MPa		fck	30	MPa
Es	200000	MPa		Es	200000	MPa
e_cu	0,0035	-		e_cu	0,0035	-
ey	0,0025	-		ey	0,0025	-
λ	0,8	-		λ	0,8	-
η	1	-		η	1	-
x	14,727	mm		x	23,869	mm
Fc	58,91	N		Fc	114,57	N
es_above	-0,0010	-		es_above	-0,0010	-
es_below	0,0217	-		es_below	0,0249	-
fs_above	-203,13	MPa		fs_above	-209,13	MPa
fs_below	500	MPa		fs_below	500	MPa
Fcs	-17,02	N		Fcs	-33,79	N
Fs	41,89	N		Fs	80,78	N
41,888	41,888	N		80,784	80,784	N
If diff < 0.001 -->				If diff < 0.001 -->		
z_c	8,84	mm		z_c	14,32	mm
z_cs	-4,27	mm		z_cs	-7,13	mm
z_s	91,27	mm		z_s	170,13	mm
Mu	4,416	kNm		Mu	15,626	kNm
Fu	9,814	kN		Fu	34,724	kN
Bending capacity =	0,0491	kN/mm		Bending capacity =	0,1736	kN/mm

Figure A.3: Excel sheet for calculation of the bending resistance of Slab 1 and Slab 2.

A.2. Unloading of concrete fibres

This section cannot be understood without prior knowledge from chapter 4.

Due to the reduction of the contact depth with increasing rotation of the rigid body, the restrained strain of some concrete fibres will decrease. As a result, unloading of these fibres is initiated. Unloading in this sense means the reduction of the restrained strain, which leads to a change of the stress in the concrete.

The developed analytical model in chapter 4 uses the optimistic unloading path of Figure A.4. This unloading path follows the same predetermined stress-strain relation as for loading. It is named optimistic because for this unloading path the stress may increase again if the concrete fibre is unloaded by a decrease in the compressive strain. It is important to note that the results of Slab 1 and Slab 2 (see chapter 4) are based on the optimistic unloading path.

Three other unloading paths have been chosen to study the influence of unloading on the structural response of the laterally restrained concrete slab strip. The secant unloading path is represented by a straight line to the origin. The stress decreases linearly for the elastic unloading path with the E-modulus as slope. If the stress reaches zero, the stress will remain zero while returning to the origin. The instant unloading path assumes that the stress drops directly to zero at the moment when the compressive strain decreases. The results are presented in load-deflection diagrams (see Figure A.5).
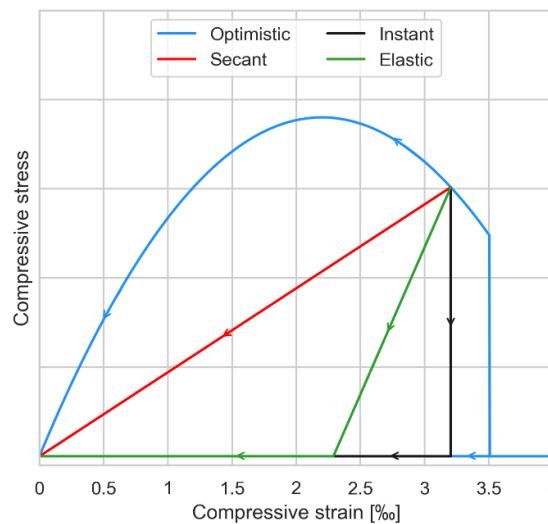
Figure A.4: Four unloading paths for concrete in compression.
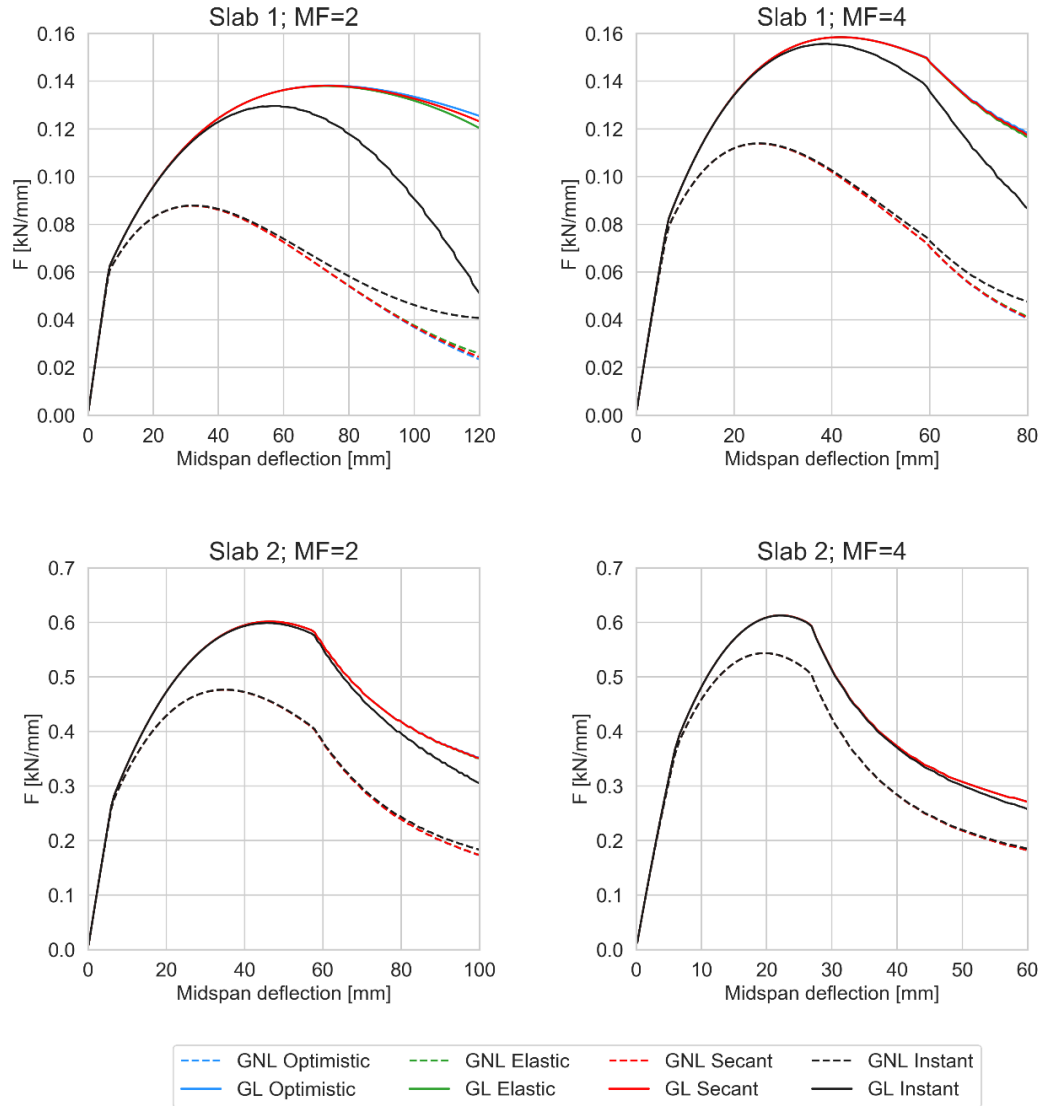
Figure A.5: Analytically obtained load-deflection diagrams for different unloading paths.

In Figure A.5, minimal differences can be seen between the load-deflection diagrams for the different unloading paths. The differences are so small for Slab 2 that they are negligible. Furthermore, the instant path of Slab 1 results in a lower peak load and shows different post-peak behaviour, especially for the linear model. This effect is more severe for MF=2. The same differences can be spotted for Slab 2, but they are much smaller in magnitude. It seems that the larger the span-to-depth ratio of the concrete slab strip, the more influence the unloading paths have on the behaviour of the slab strip.

Based on the instant unloading path, it can be concluded that the unloading of the first concrete fibres takes place before the crushing of the first concrete fibres. Yet, the instant path is disregarded as it is rather unrealistic. The optimistic, elastic and secant unloading paths still lead to similar peak loads. The small differences caused by the type of unloading can therefore be neglected. Since the differences between the graphs are insignificant, it has been chosen to continue with the optimistic unloading path, which gives almost the same results as the secant and elastic unloading path.

Unloading of the steel compression reinforcement will not occur, because the failure of the slab strip occurs long before the reduction of the contact depth is large enough to unload the compression reinforcement. In other words, the distance between the compression reinforcement and half the height of the concrete slab is so large that the compressive stresses in the compression reinforcement will never decrease with increasing deflection.

<div style="text-align: right; font-size: 4em;">B</div>

Appendix – Chapter 5: Numerical models

B.1. Calibration of the multiplication factor MF

Calibration of the multiplication factor of the analytical model with the numerical results is performed. This is done based on the results of the two reference slabs strips Slab 1 and Slab 2. Attention is paid to the agreement of the analytical and numerical peak loads, stiffness, ductility and the overall deflection behaviour. Figure B.1 presents load-deflection diagrams of Slab 1 and Slab 2 with the analytical results for different multiplication factors as well as the numerical result. It can be seen that the multiplication factor should be between 3 and 5. From the factors 3-5 (0.2 between each examined value), the value of 4 provides the best agreement between the analytical and numerical results, especially for Slab 1. This value is therefore chosen to be used for the numerical models of the slab strips in chapters 5 and chapter 6.
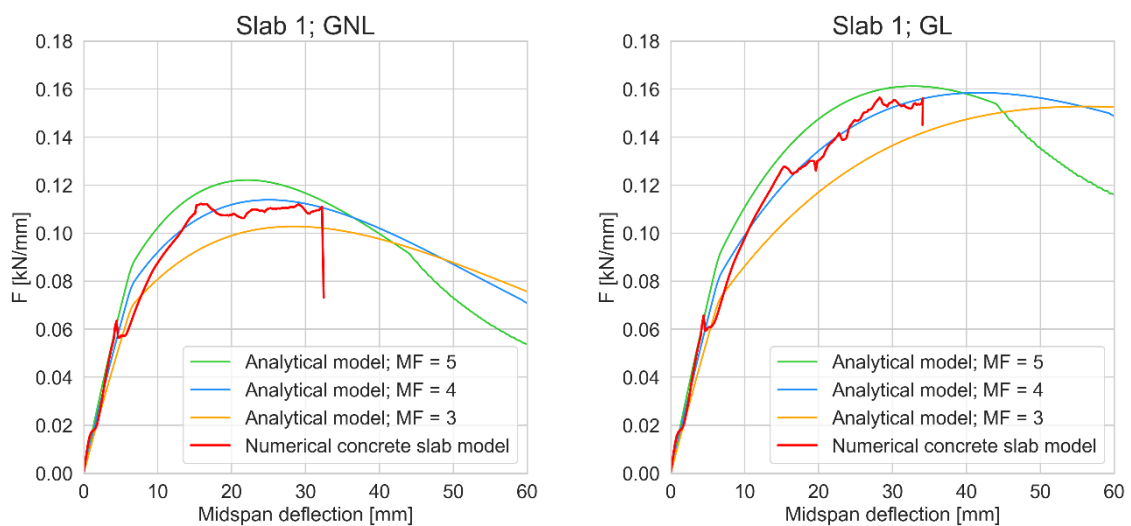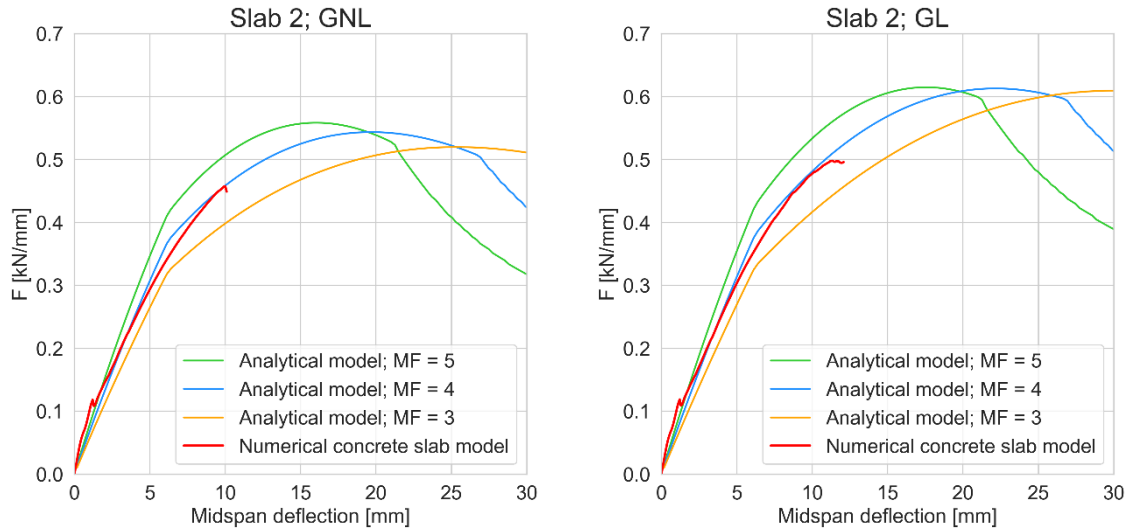
Figure B.1: Load-deflection diagrams of Slab 1 and Slab 2 for different multiplication factors.

B.2. Variations in numerical modelling

The results of the finite element analyses can be largely affected by the mesh size and the used numerical calculation method. Therefore, the element size and the used calculation method are varied for Slab 1 in order to study their influence on the load-deflection behaviour.

Element size

A proper mesh of the numerical model has to be chosen to avoid a disproportional calculation time. In addition, the results of the FEAs have to be as accurate as possible to approach actual structural behaviour. It often holds that the smaller the mesh, the more accurate the results but the longer the calculation time. Two different element sizes are chosen to study their influence on the results of the numerical analyses of Slab 1. Mind that all the elements are squares.
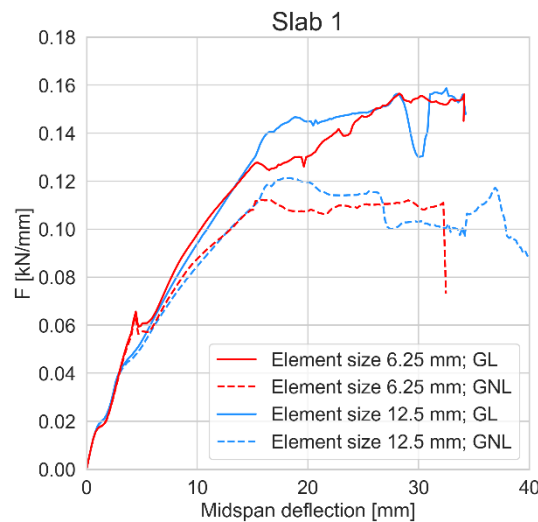
Figure B.2: Load-deflection diagram of Slab 1 for different element sizes.

In Figure B.2, the GL and GNL nonlinear load-deflection curves are given for the two different element sizes. It can be seen that the results are strongly affected by the mesh. The load-deflection curves differ on – among others – the following things: the length of the linear-elastic range, the moment of the first crack, the GNL peak load and the GNL ductility. Note that the difference between the GL and GNL peak load is smaller for the larger

element size. Since the larger element size causes some instant jumps of the graphs, these results can be considered less stable. Therefore, the element size of 6.25x6.25 mm is used for the numerical analyses in chapters 5 and 6. An even smaller element size than 6.25x6.25 mm results in a calculation time that is too long. Slab 1 is thus divided into 20 elements over the height. This is also done for Slab 2.

Calculation method

Several numerical calculation methods can be used for the FEAs in DIANA. Three different calculation methods – Regular Newton-Raphson (RNR), Modified Newton-Raphson and Secant Quasi-Newton BFGS (SQN) – are compared on the basis of the load-deflection diagrams they 'produce'. The load-deflection curves of Slab 1 for the different calculation methods are shown in Figure B.3. Note that the curves produced by the Modified Newton-Raphson and the Secant Quasi-Newton BFGS method show so many similarities that their results are presented by one and the same graph.

It is seen that the Modified Newton-Raphson as well as the Secant Quasi-Newton BFGS method lead to deviating results between 13.5 and 20 mm deflection. The load-deflection behaviour in this range does not seem to be accurate because of the sudden high peaks. The Regular Newton-Raphson appears to result in stable load-deflection behaviour, without sudden high or low peaks.

It can also be seen that the ultimate loads of the GL models are very similar if the high peaks are not considered. Further, the GNL peak load is higher for the Modified Newton-Raphson and the Secant Quasi-Newton BFGS methods. As a result, the second-order reduction effect is smaller for these methods if the high peaks are not considered. The stability of the results need to be guaranteed as much as possible, thus the Regular Newton-Raphson method is chosen as the numerical calculation method for the FEAs in chapters 5 and 6.
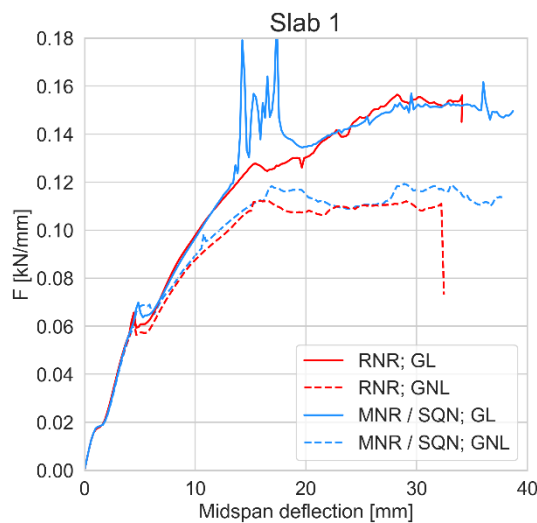
Figure B.3: Load-deflection diagram of Slab 1 for different numerical calculation methods.

B.3. Variations in compressive fracture energy and type of loading

Compressive fracture energy

The compressive fracture energy G_c is defined as the energy needed to create a compressive fracture. The compressive fracture energy is equal to the area under the compressive stress – compressive strain curve divided by the crushing-band width. It is of interest to study the influence of G_c on the load-deflection behaviour of the slab strip because the failure mode of Slab 1 is the crushing of the concrete.
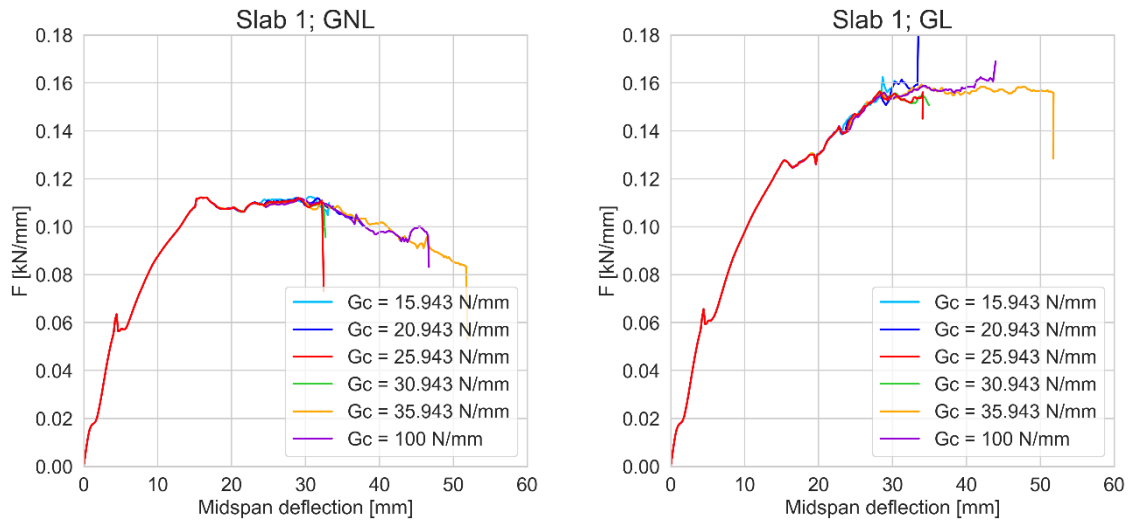
Figure B.4: Load-deflection diagrams for different values of the compressive fracture energy.

The results presented in Figure B.4 show that the compressive fracture energy greatly affects the ductility of the slab strip. This is because the value of G_c is directly related to the size of the softening branch as well as the ultimate compressive strain value. Higher values for G_c will delay the moment the ultimate strain value is reached (or nearly reached) in one or more concrete fibres. At that moment, the compressive stress is dropped to zero and the fibre is completely crushed. Crushing will therefore occur at a larger midspan deflection for higher values of the compressive fracture energy. Remarkably, there is a certain limit to this effect, as a G_c value of 100 N/mm results in less ductility than a G_c value of 35.943 N/mm.

Furthermore, G_c does not appear to influence the peak load and the load-deflection behaviour up to 24 mm. This makes sense since the compressive strength is limited to a value of 33 MPa for every analysis presented in the load-deflection diagrams. Yet, marginal differences between the peak loads of the GL model can be seen. Since the focus of this thesis is mainly on the ultimate capacity of the slab strips, the recommended value of 25.943 N/mm according to the "Guidelines of Nonlinear Finite Element Analysis" [10] is used for the numerical analyses. Values between 20.943 and 30.943 can still be reasonable but lead to nearly similar results as seen in Figure B.4.

Uniformly distributed load

Since the presented analytical model in chapter 4 is based on the moment equilibrium of the rigid body, any type of loading can be applied on the slab strip. A uniformly distributed load (UDL) is applied over the whole length of Slab 1. Both analytical and numerical results are obtained for this model. Comparisons are made between the analytical and numerical results, and between the two different types of loadings on the slab strip: the point load used in chapters 4, 5 and 6 and the UDL. The load-deflection diagram for the UDL is presented in Figure B.5.
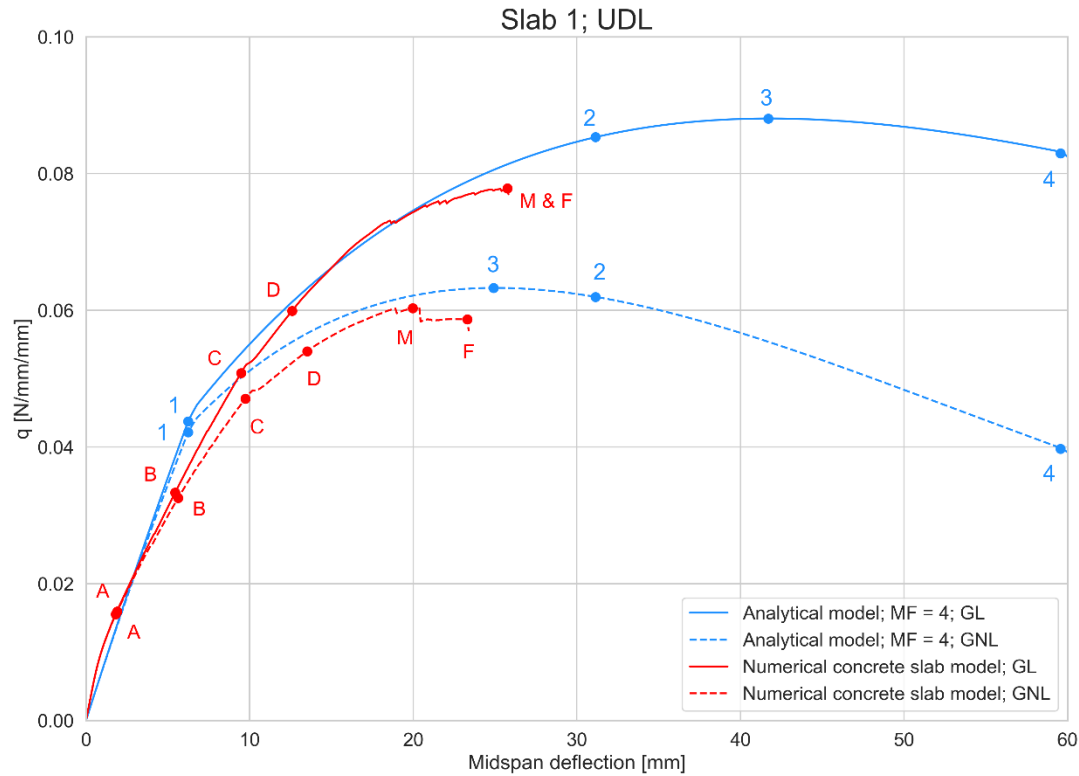
Figure B.5: Load-deflection diagram of Slab 1 loaded with a UDL.

Numerical results

The ultimate capacity of 0.06 N/mm/mm is substantially higher than the conventional bending capacity of 0.027 N/mm/mm, with an enhancement factor of approximately 2.2. The load resistance is reduced due to geometrical nonlinearity. Further, it can be seen that the stiffness reduction after cracking is rather low due to significant arching action. Points C and D indicate respectively the moments that the tensile and compression reinforcement will yield. However, yielding of the steel will only occur at the support section and not at midspan because the structural system of the half slab strip is not symmetrical. The concrete slab strip will fail due to the crushing in the compression zone at the side support. The GNL model leads to a slightly less ductile response of the slab strip.

Analytical results and comparison with numerical results

The GL peak load, the GNL peak load, the second-order reduction effect and the ductility are overestimated by the analytical model. Yet, the responses of both models show several similarities, among others: the second-order effect increases with increasing deflections, the GNL peak load is significantly lower than the GL one, the GNL model leads to a less ductile response.

Comparison between UDL and point load

The shape of the analytical curves for the slab strip loaded by a UDL is equal to the analytical curves for the slab strip loaded by a point load at midspan (see Figure B.6). This makes it easier to compare the numerical models.

The analytical model shows more similarities with the numerical model of the point load than of the UDL considering the maximum capacity and ductility. This is because the UDL leads to a non-symmetrical system of the half slab strip. The shear force is not constant anymore: it has a significant value at the support and is zero at midspan. In addition, the bending moment at the support is higher than the bending moment at midspan.
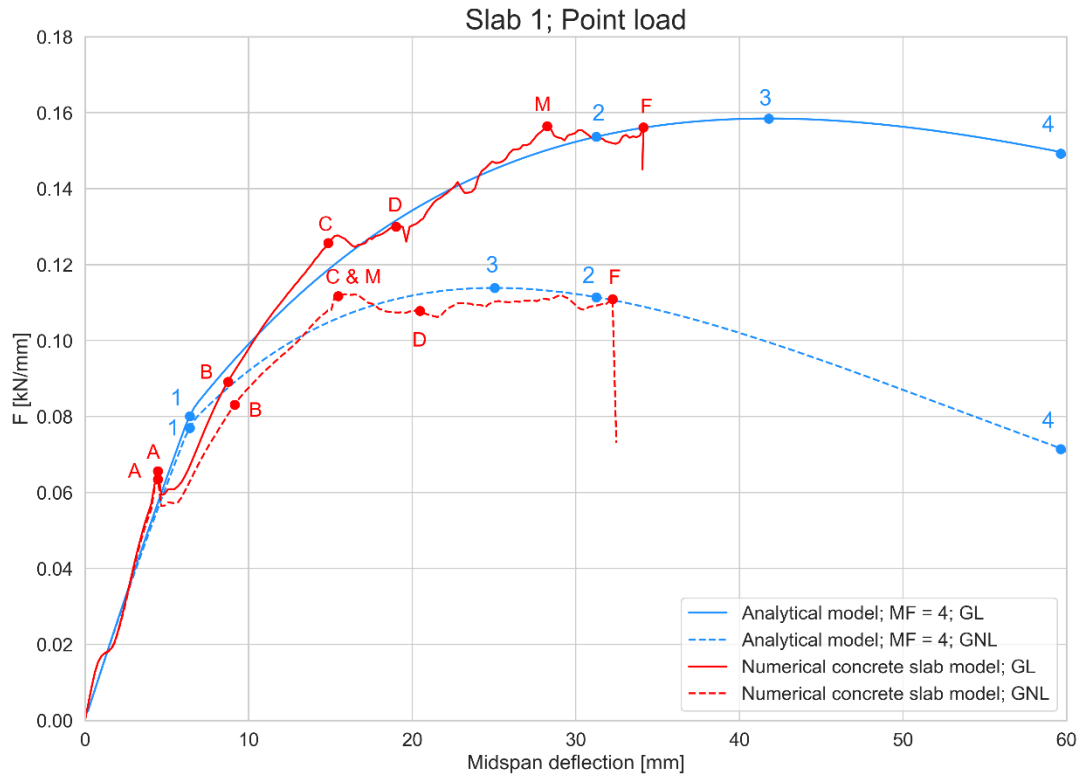
Figure B.6: Load-deflection diagram of Slab 1 loaded with a point load.

Other differences are:

- For the UDL, the compressive stresses in the compression zone at the side support are much higher than the compressive stresses in the compression zone at midspan. For the point load, these compressive stresses are equal. The resultant compressive arch for the point load model can be considered straight. In contrast, the resultant compressive arch for the UDL is curved because the structural system is not symmetric. This can be seen in Figure B.7, in which the contour plots of the principal compressive stress are presented for the indicative points of the GNL model. The height in the slab in the plots is increased with scale factor 2.

- The crack pattern for the UDL model is completely different at the support and midspan: the marginal principal tensile strains (beginning of flexural cracks) spread over a large distance at midspan, while the major flexural cracks at the support are concentrated in a small region. In addition, the principal compressive strains are considerably higher in the compressive zone at the support than at midspan. On the other hand, the principal tensile and compressive strain contour plots for the point load model are symmetrical.

It can be concluded that the developed analytical model is less suitable to estimate the ultimate load and the ductility if a UDL is applied than if a point load at midspan is applied.
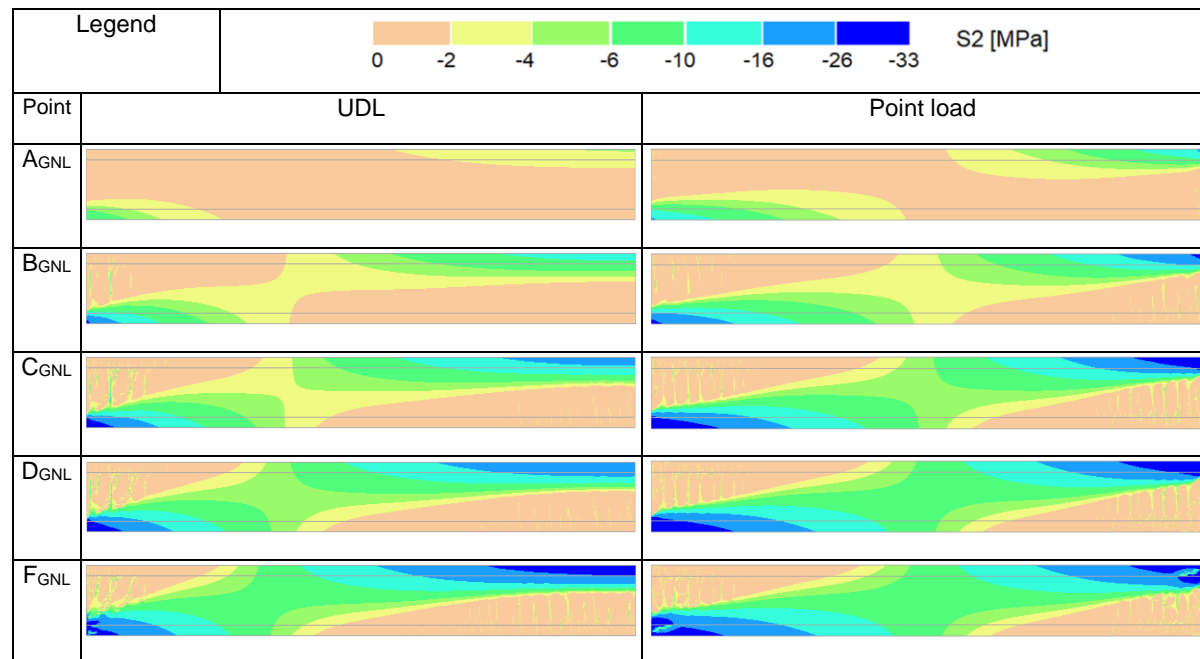
Figure B.7: Compressive arch development for different types of loading on Slab 1.

(a)

(b)
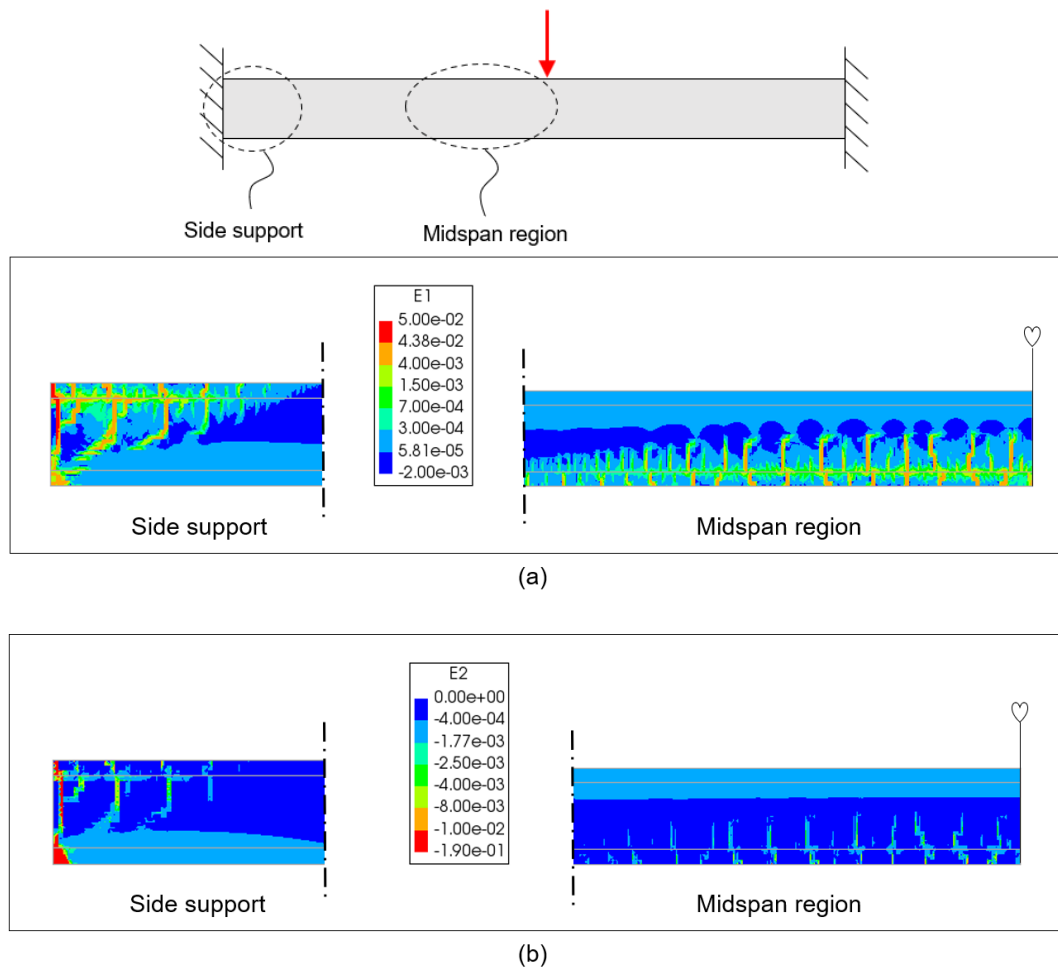
Figure B.8: Principal tensile strain (a) and principal compressive strains (b) plots of Slab 1 loaded with a UDL.

B.4. Principal compressive strains in the longitudinal direction

Principal compressive strain in the longitudinal direction of Slab 1

The compressive strain distribution in the longitudinal direction according to the analytical model and the numerical concrete slab model are compared for Slab 1. The principal compressive strain in the longitudinal direction of three concrete fibres (see Figure B.9) is plotted for points 0-F in Figure B.10, Figure B.11 and Figure B.12. Points 0-F from Figure 5.18 and Table 5.3 have been used.
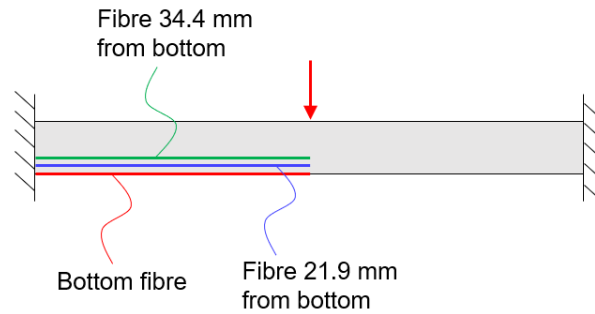
Figure B.9: Three longitudinal concrete fibres in Slab 1.

Bottom fibre
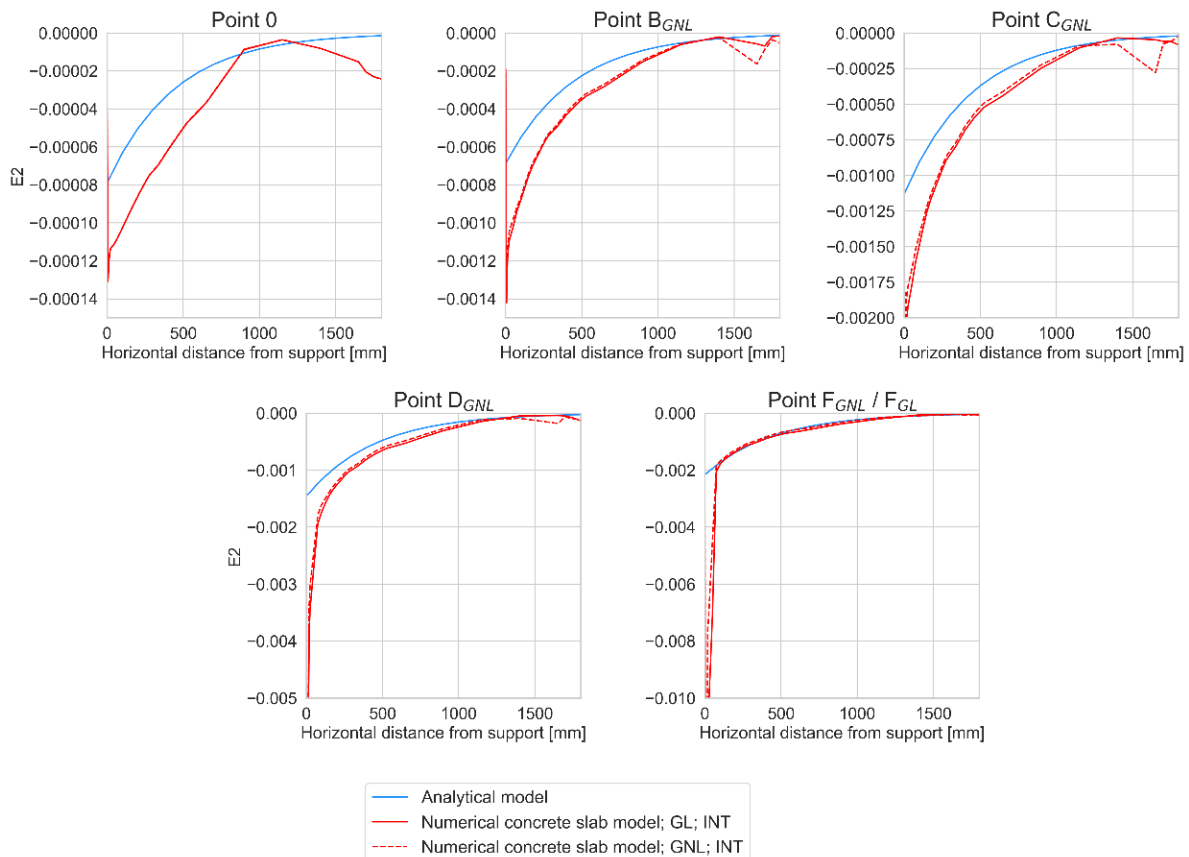
Figure B.10: Principal compressive strains along the bottom fibre of Slab 1.

Fibre at 21.9 mm from bottom
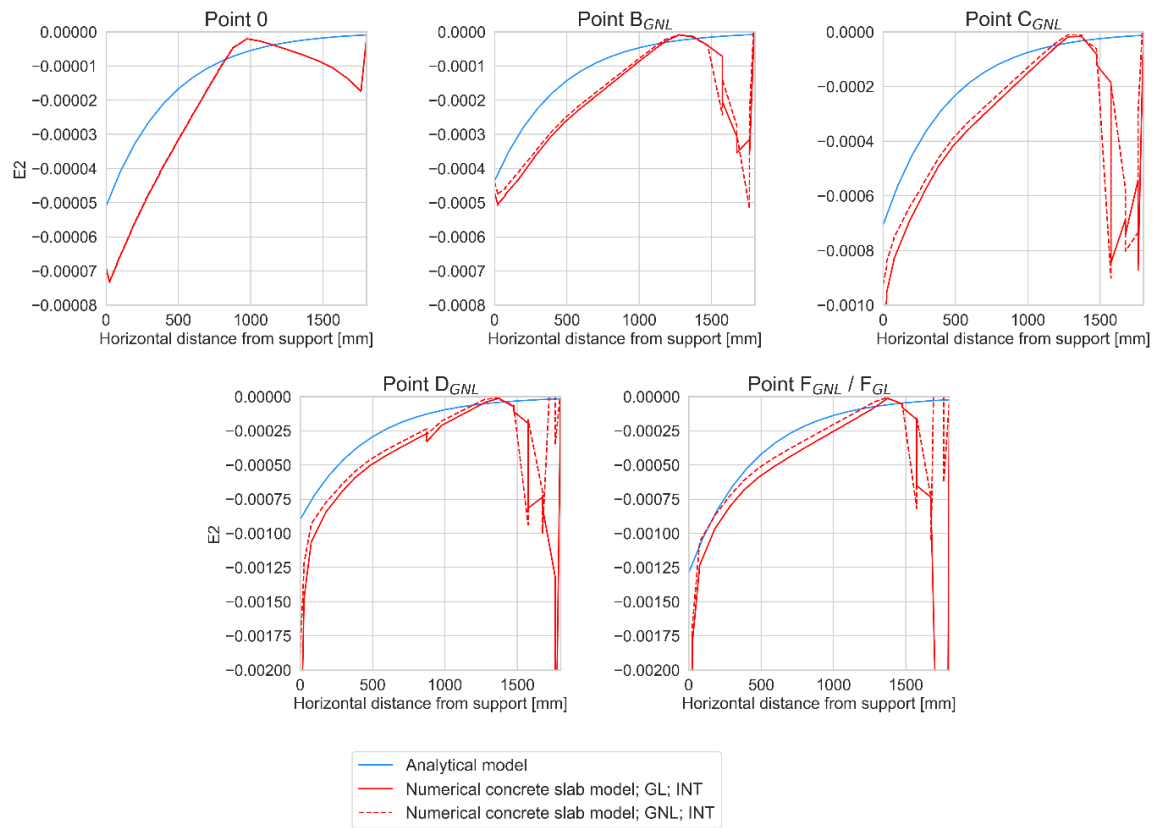
Figure B.11: Principal compressive strains along the fibre 21.9 from the bottom of Slab 1.

Fibre at 34.4 mm from bottom
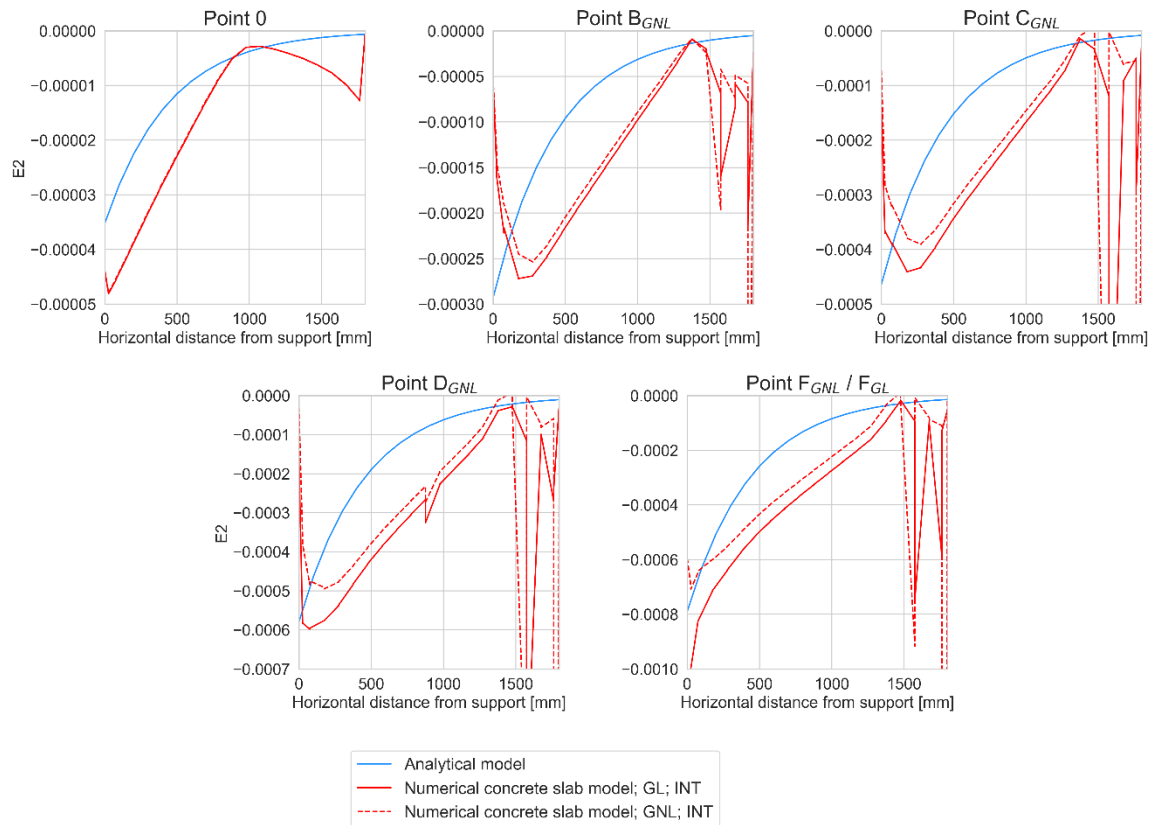
Figure B.12: Principal compressive strains along the fibre 34.4 from the bottom of Slab 1.

From the results in Figure B.10, it can be seen that the assumption for the exponential strain distribution for MF=4 is not in agreement with the numerical results. It should be noted that lower multiplication factors will only cause the analytical and numerical results to differ even more. The maximum compressive strain in the bottom concrete fibre is much larger for the numerical model than for the analytical model. The relative difference between the principal compressive strain at the support according to the analytical and numerical model appears to be increasing with increasing deflection. Also, the compressive strain between the support and midspan is underestimated in the vast majority of cases by the analytical model; the analytical curve is closer to zero than the numerical curve. Yet, there is also some similarity: both the analytical and numerical curves seem to be exponential functions that show similar trends. The trend is that the principal compressive strain is maximal at the support and exponentially decreases to about zero at midspan.

Further to the neutral axis of the slab, the compressive strain curve appears to be changing from an exponential to a more linear distribution (see Figure B.11 and Figure B.12). The multiplication factor decreases with decreasing distance from the neutral axis of the slab. This linear distribution agrees with the theory of Euler-Bernoulli as well as with the linear bending moment distribution of the half concrete slab. It can be concluded that the strain distribution, and therefore the multiplication factor, depends on the location on the vertical height axis of the slab.

B.5. Contour plots

This section contains contour plots of the principal tensile strains, the principal compressive strains and the principal compressive stresses for both Slab 1 and Slab 2. In addition, the in-plane principal stresses or stress trajectories are plotted for several indicative points in the load-deflection diagram.

Slab 1
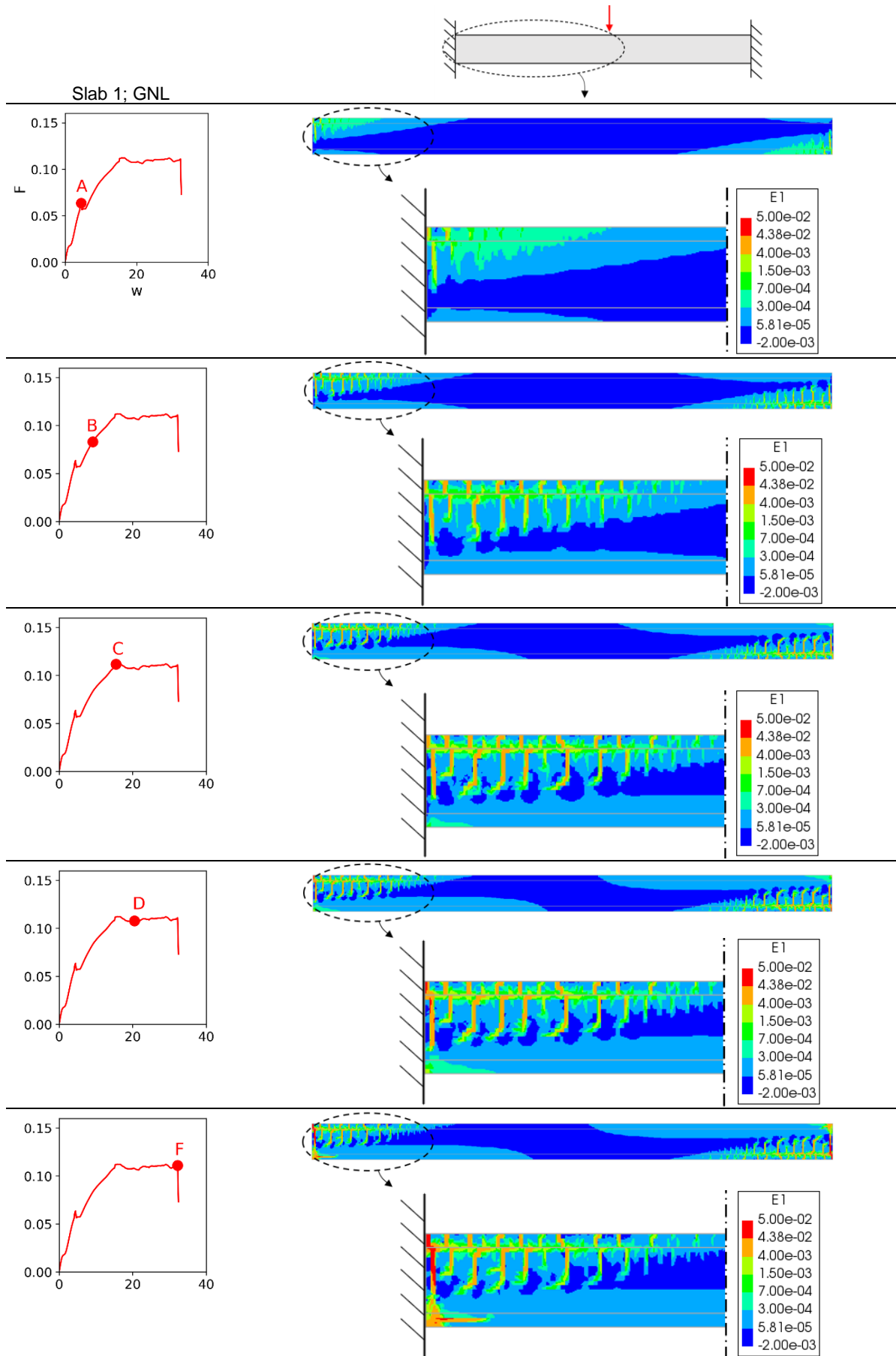
Figure B.13: Principal tensile strains for the GNL analysis of Slab 1.
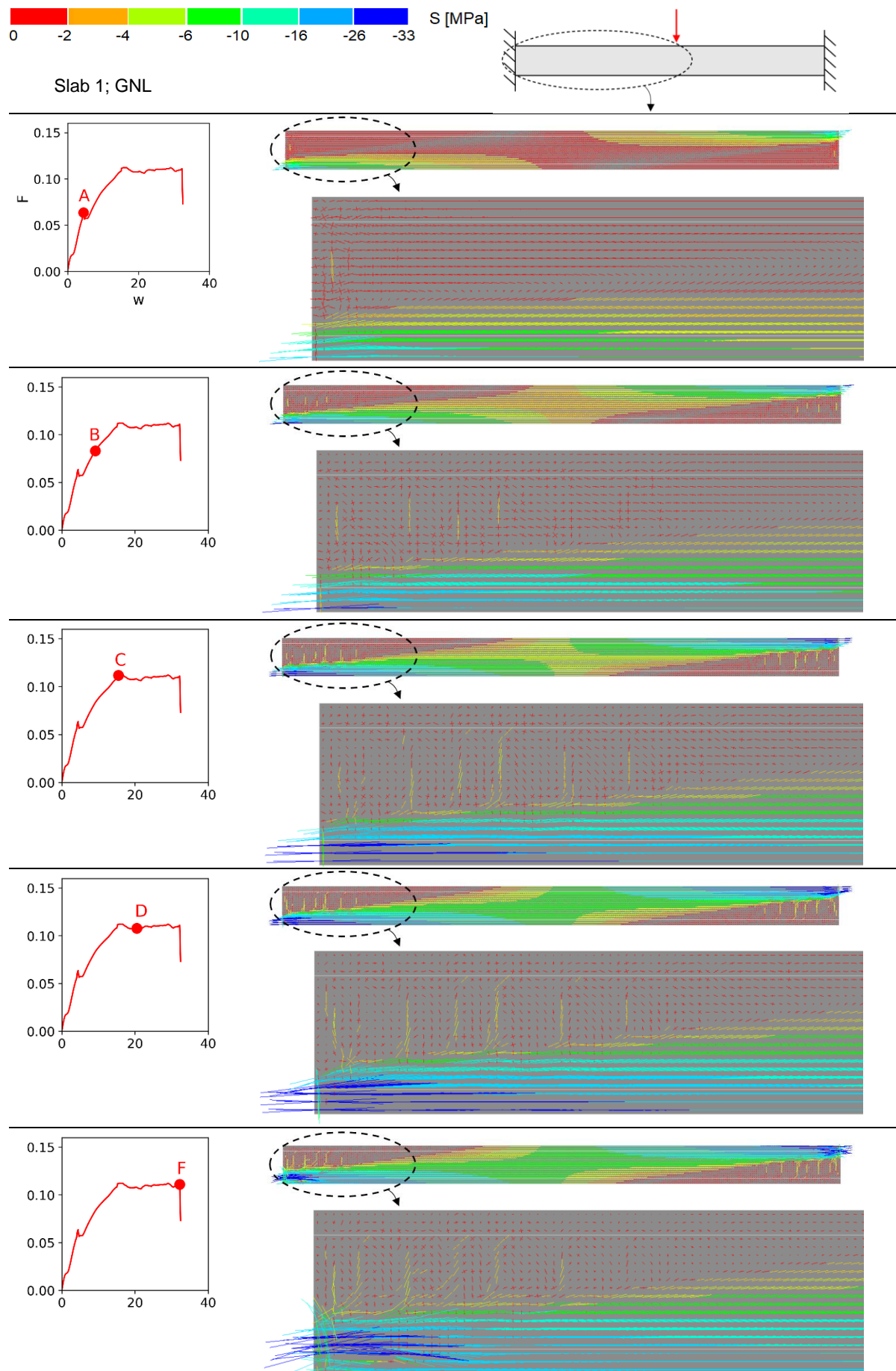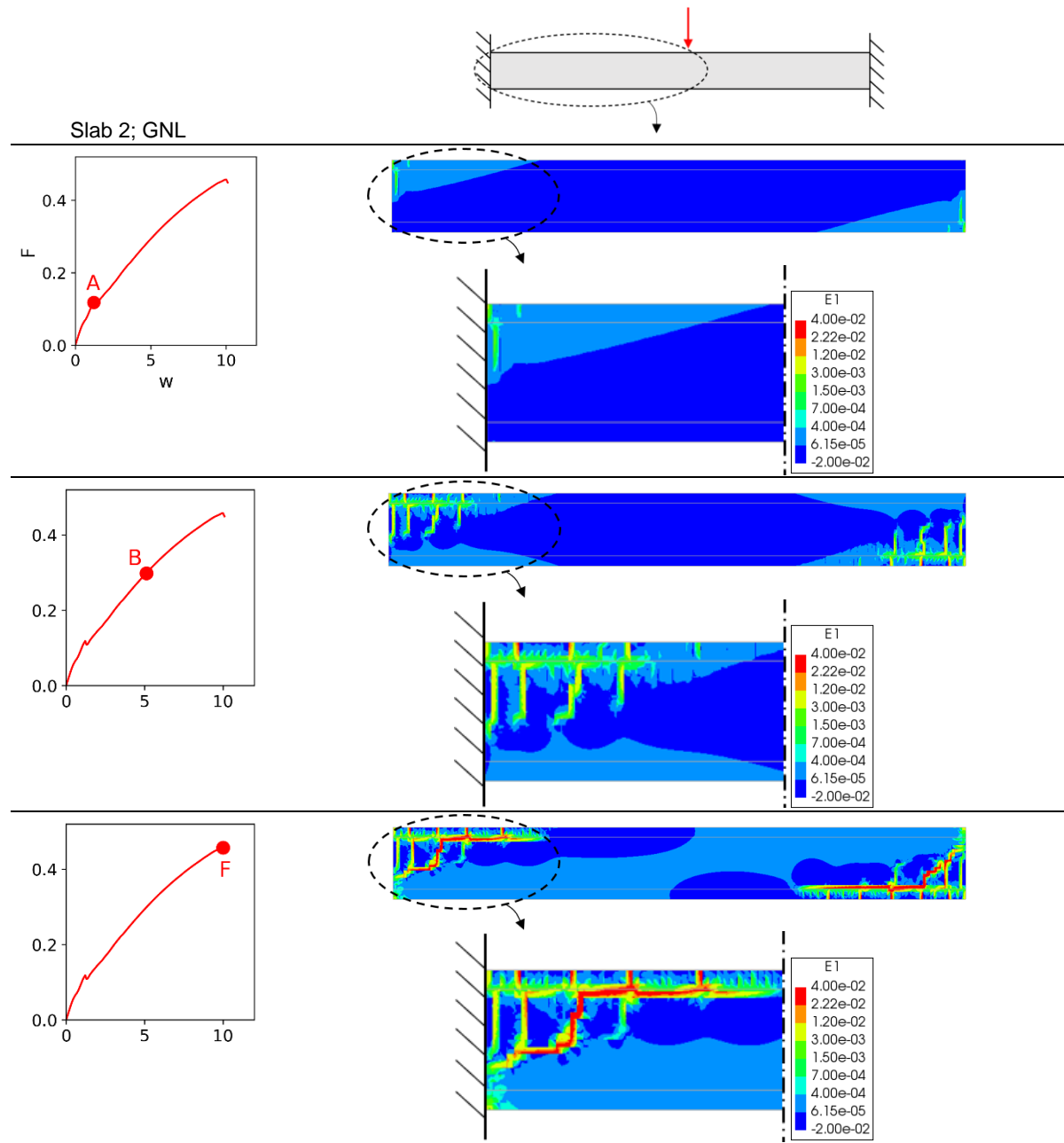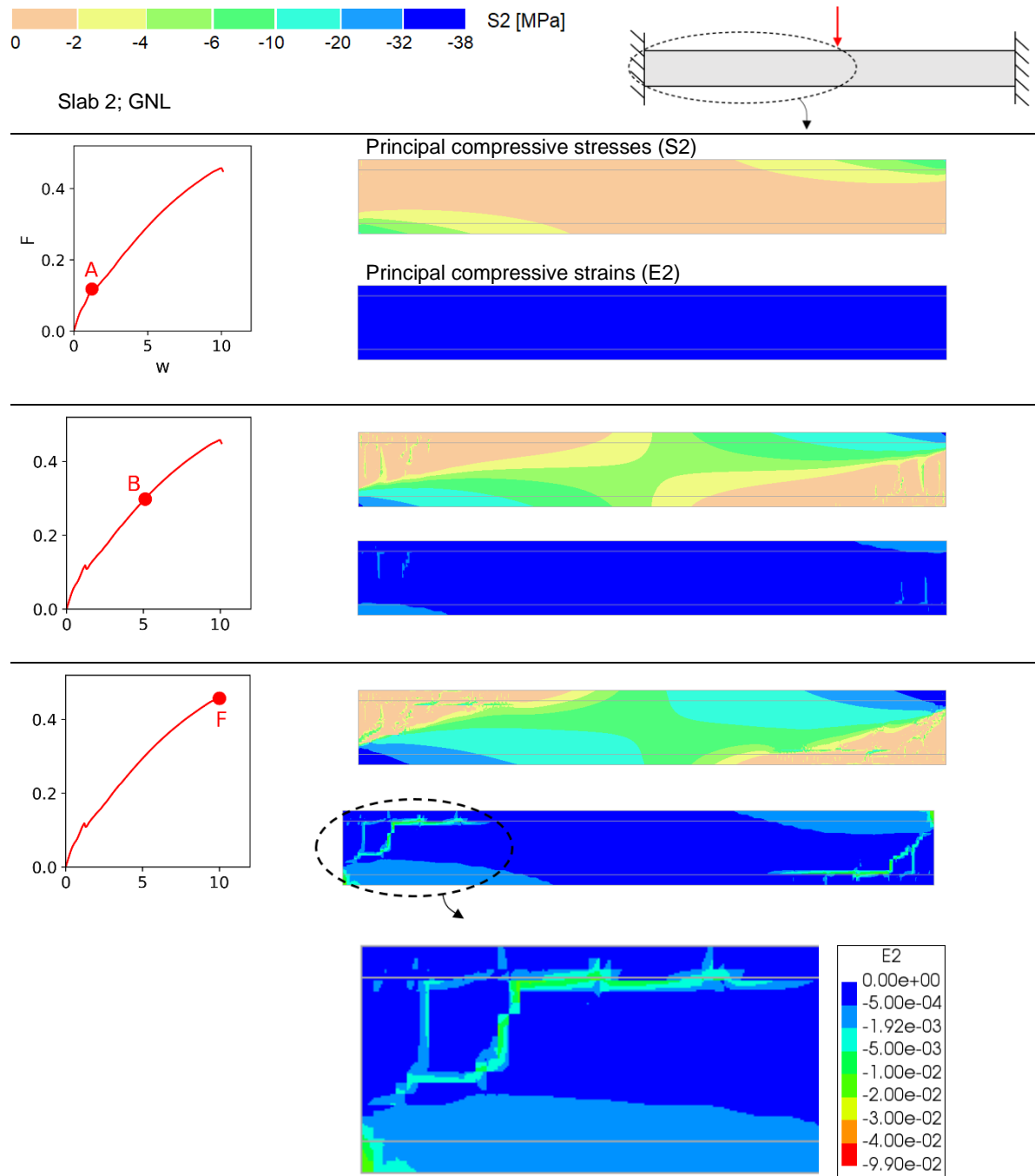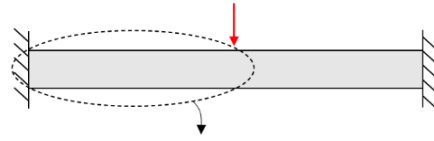
Figure B.14: In-plane principal stresses for the GNL analysis of Slab 1.

Figure B.15: Principal compressive strains and stresses for the GNL analysis of Slab 1.
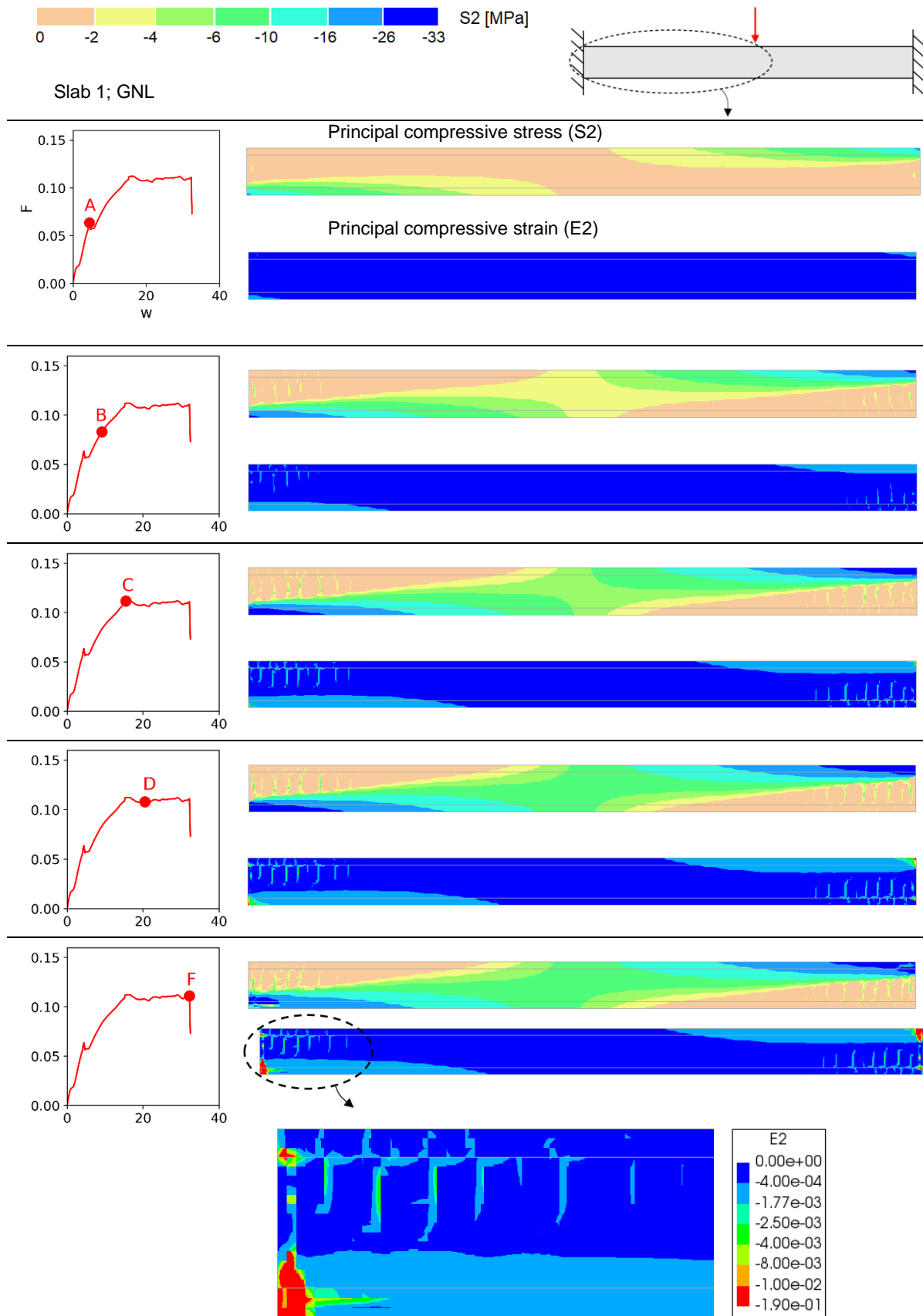
Slab 2

Slab 2 without shear reinforcement

Figure B.16: Principal tensile strains for the GNL analysis of Slab 2.
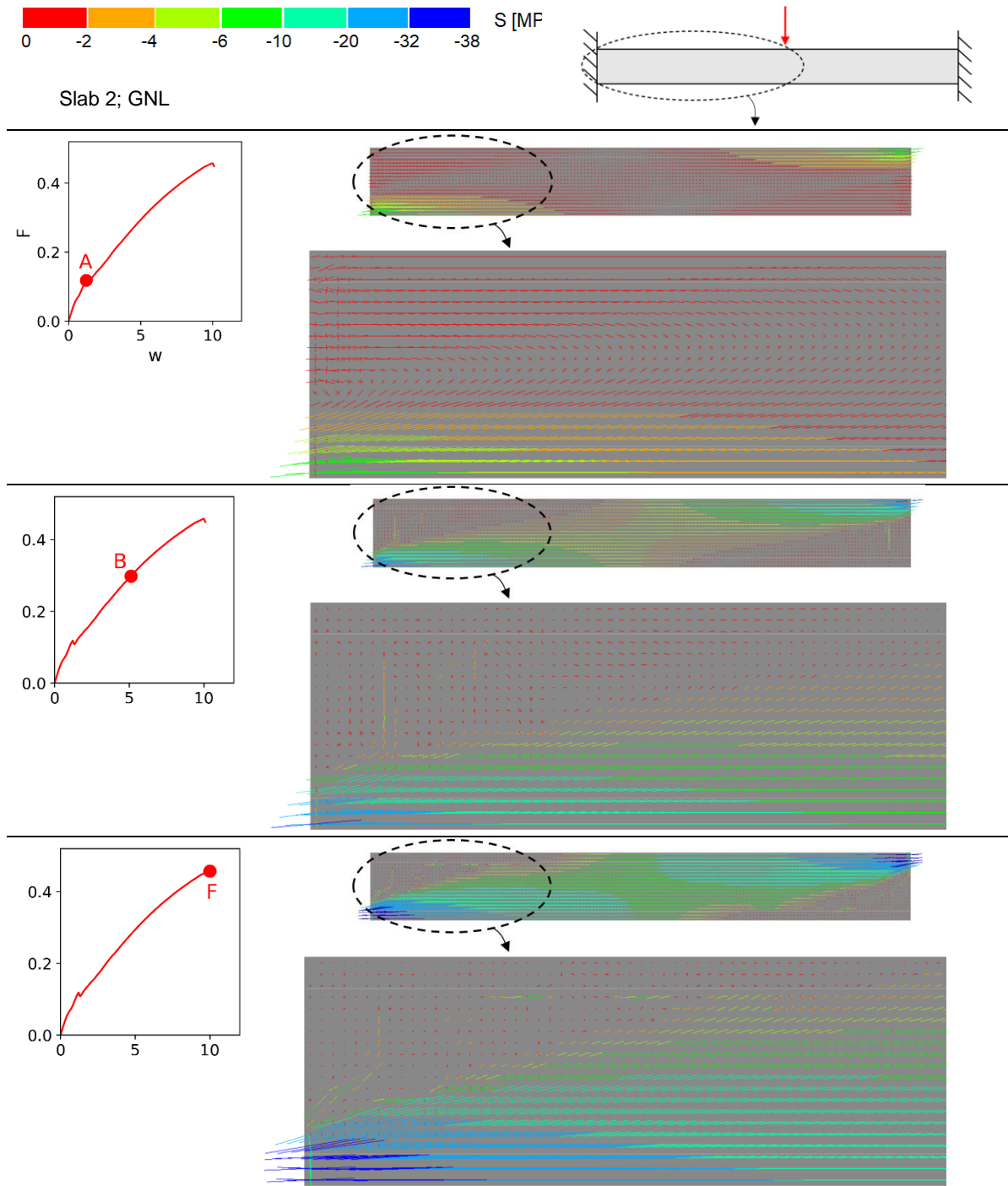
Figure B.17: In-plane principal stresses for the GNL analysis of Slab 2.

Figure B.18: Principal compressive strains and stresses for the GNL analysis of Slab 2.

Slab 2 with shear reinforcement

Slab 2 with shear reinforcement; GNL
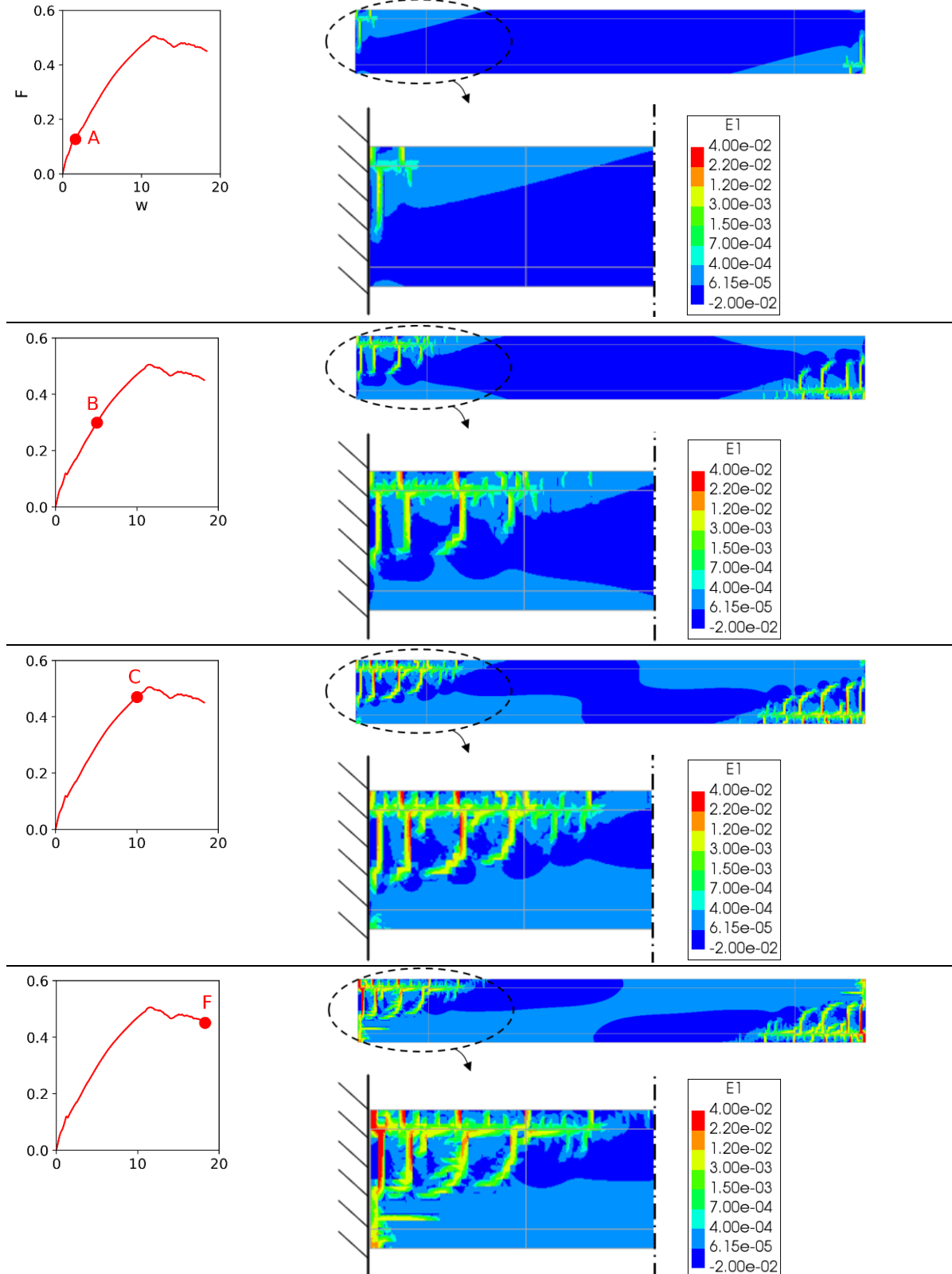
Figure B.19: Principal tensile strains for the GNL analysis of Slab 2 with shear reinforcement.
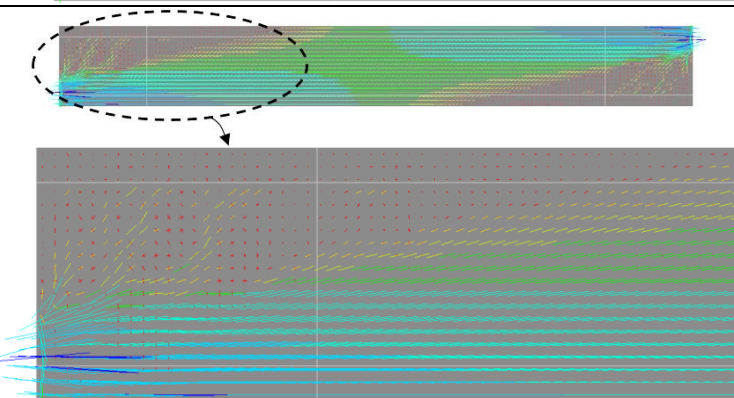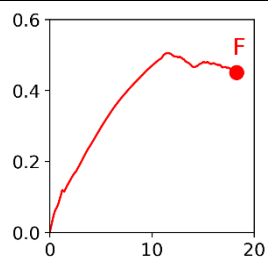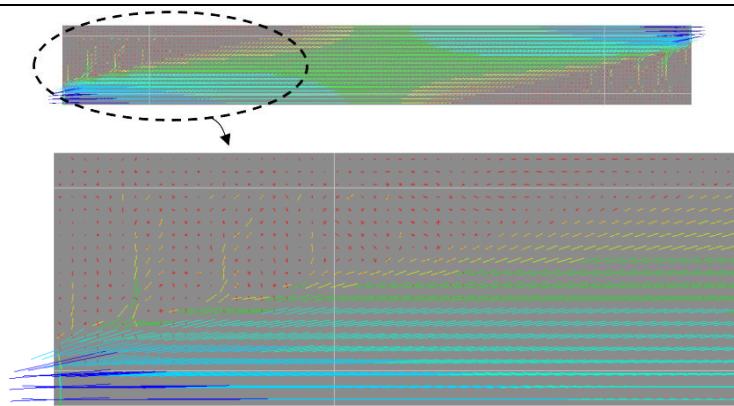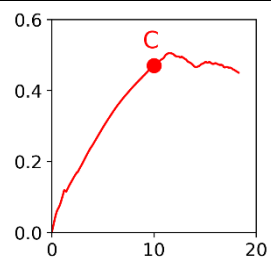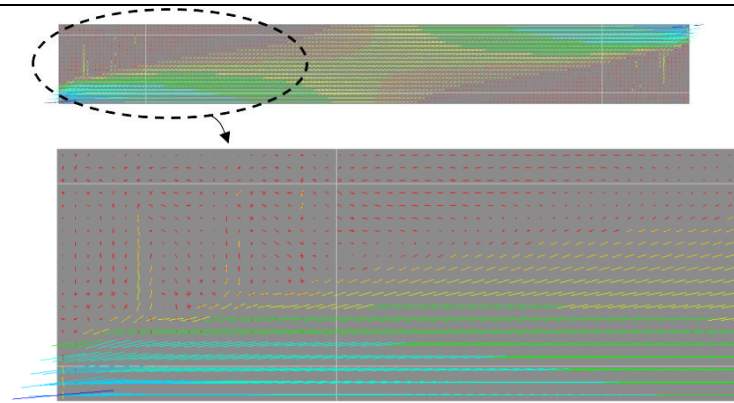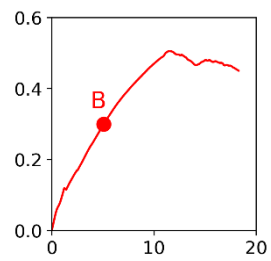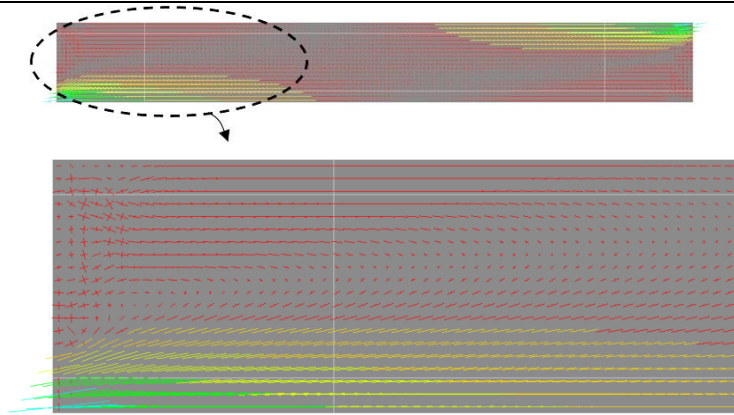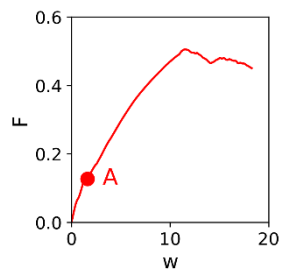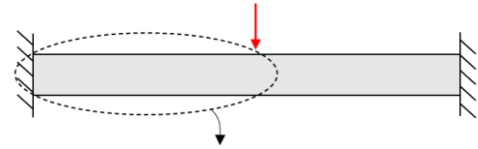
Figure B.20: In-plane principal stresses for the GNL analysis of Slab 2 with shear reinforcement.
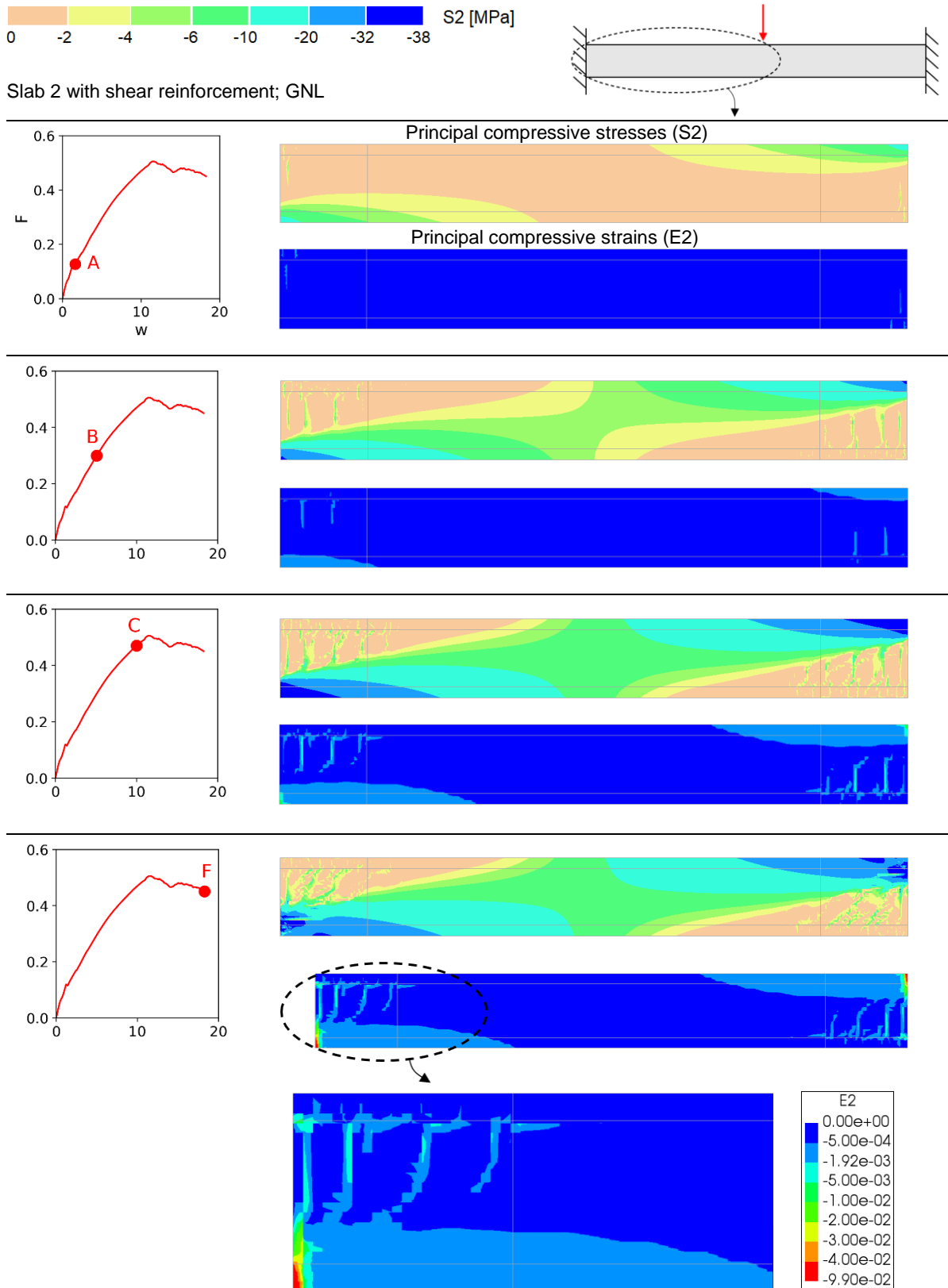
Figure B.21: Principal compressive strains and stresses for the GNL analysis of Slab 2 with shear reinforcement.

Slab 2 including non-convergence

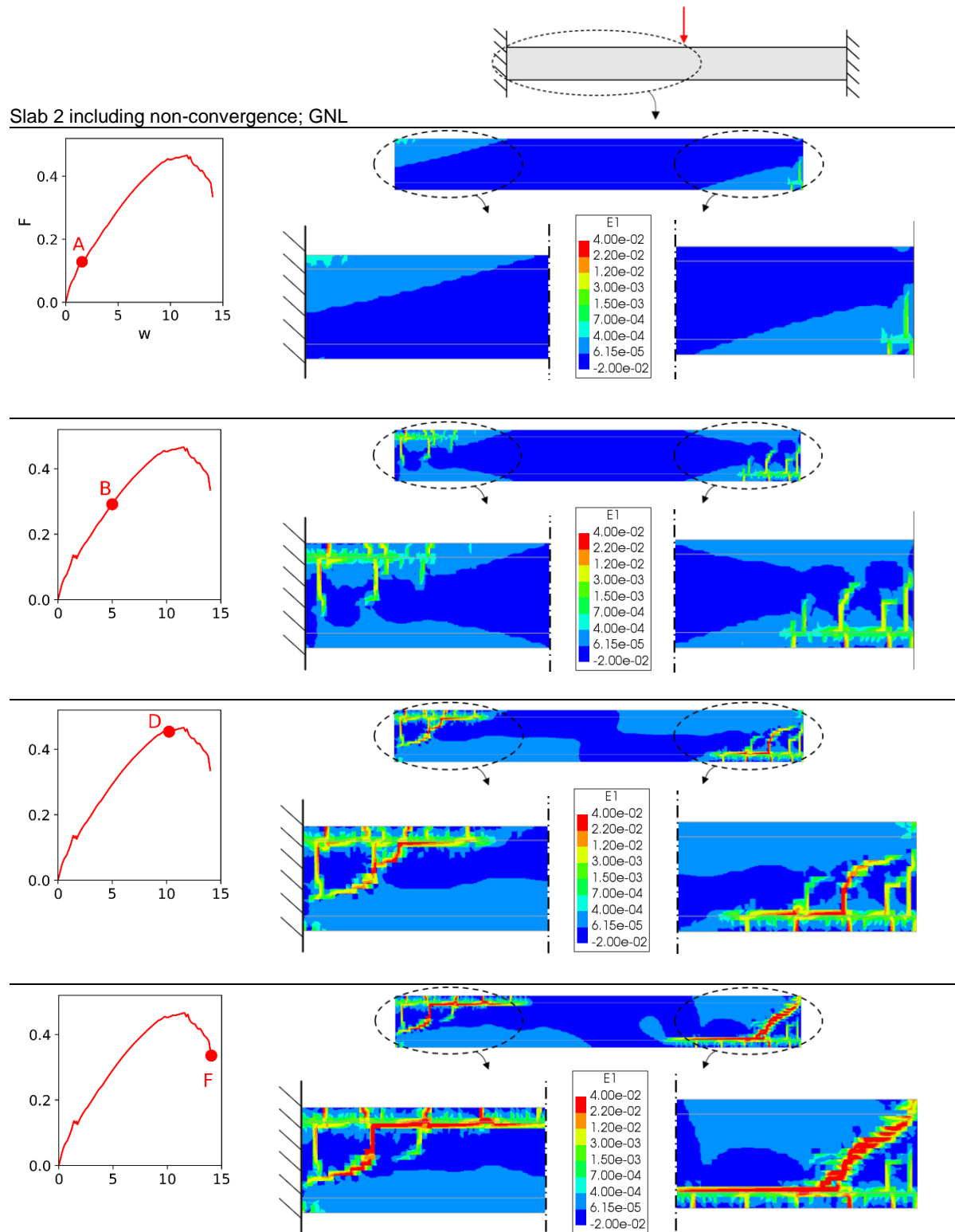Slab 2 including non-convergence; GNL

Figure B.22: Principal tensile strains for the GNL analysis of Slab 2 including non-convergence.
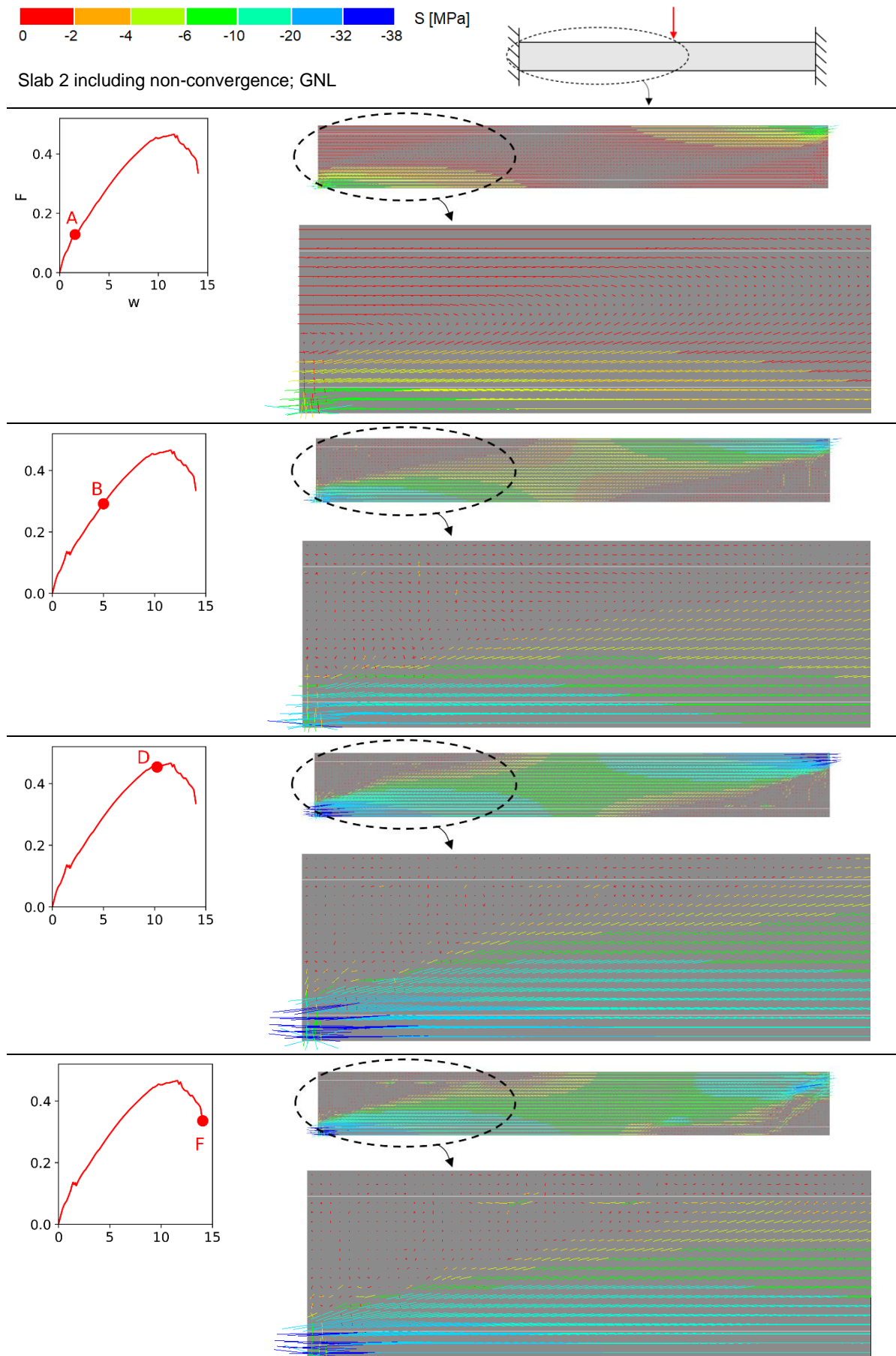
Figure B.23: In-plane principal stresses for the GNL analysis of Slab 2 including non-convergence.
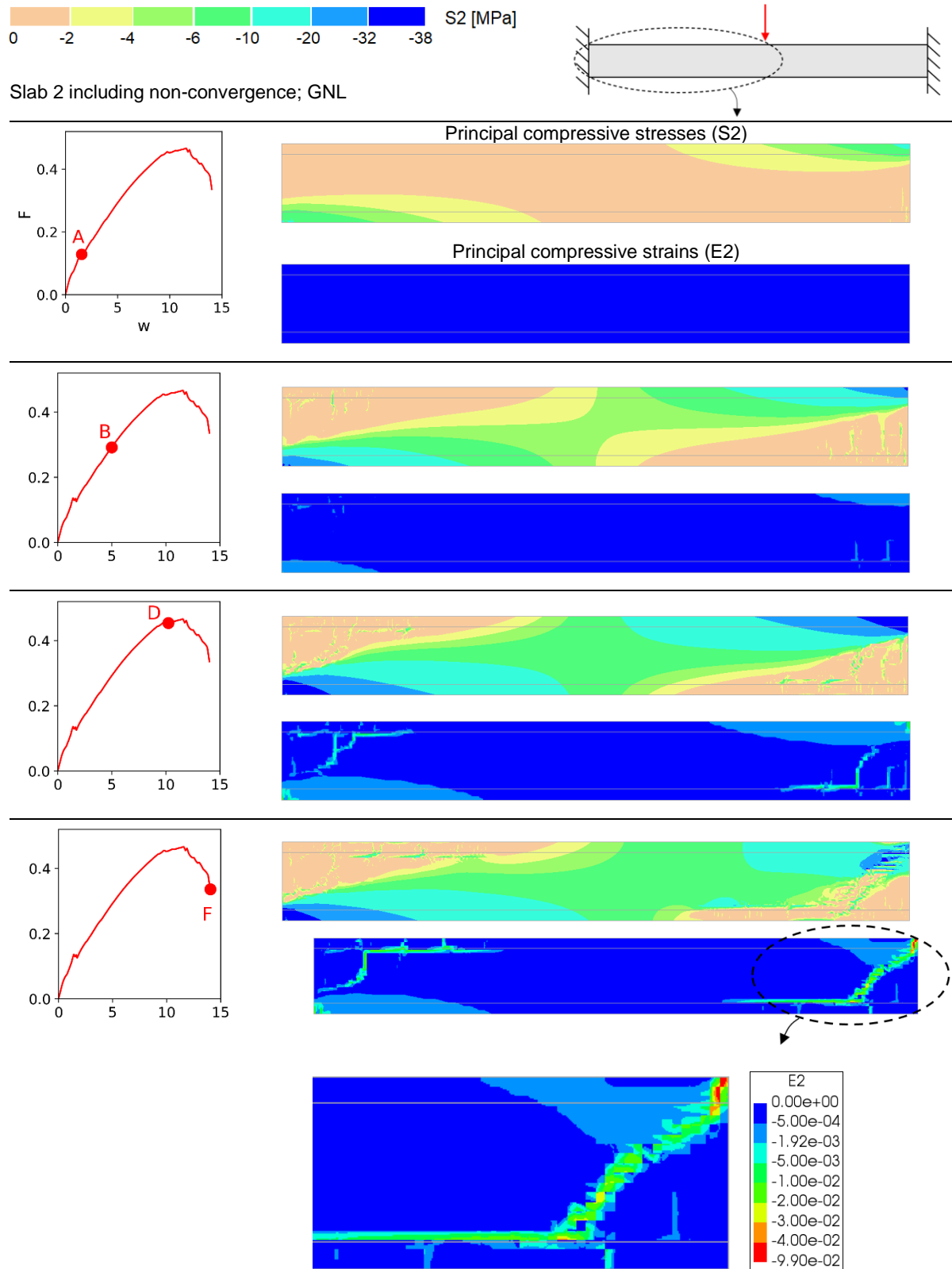
Figure B.24: Principal compressive strains and stresses for the GNL analysis of Slab 2 including non-convergence.

B.6. Strain and stress plots

Principal compressive strains and stresses for Slab 2 with shear reinforcement

Table B.1: Points used for strain and stress plots of Slab 2 with shear reinforcement.
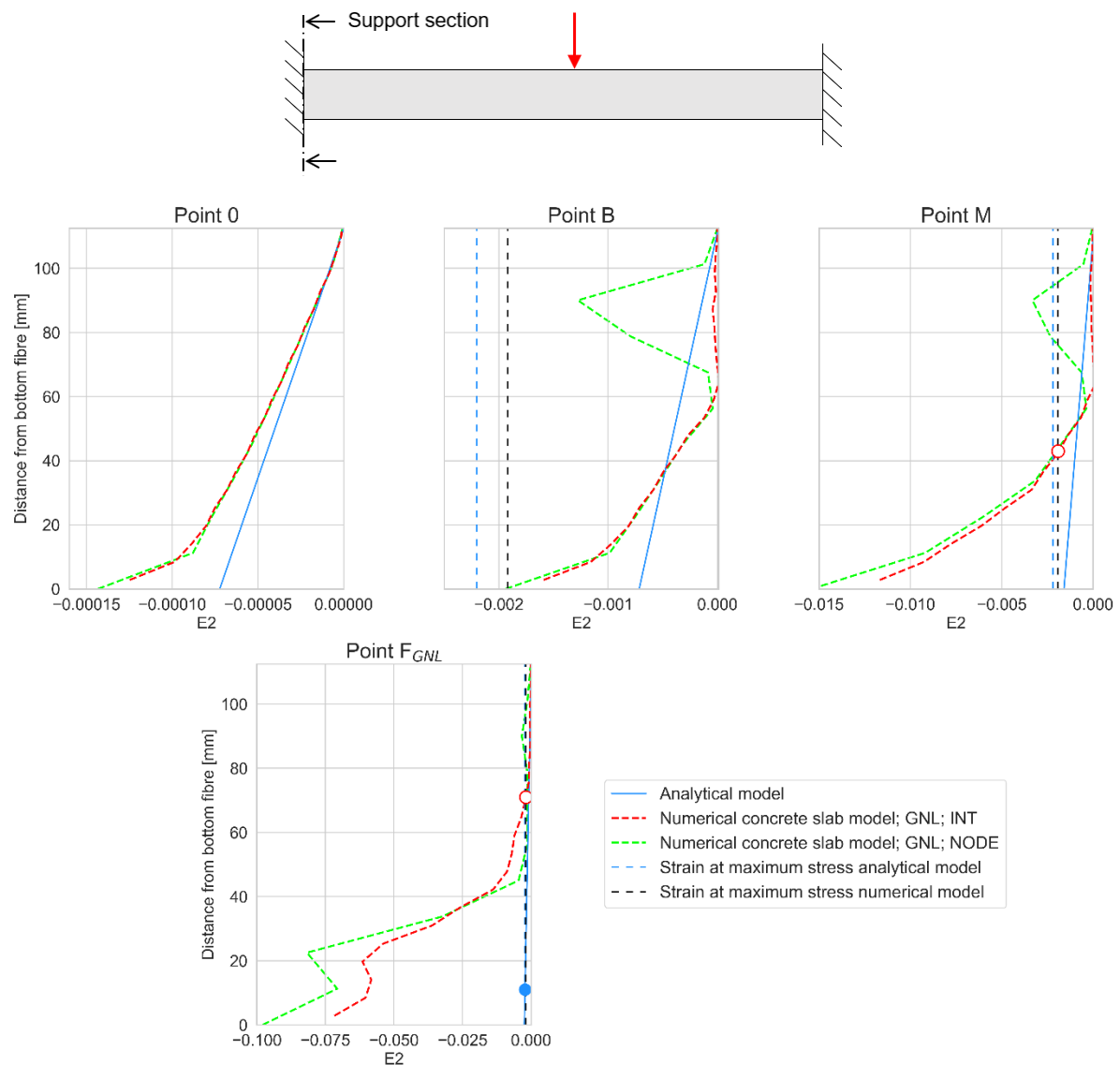
Figure B.25: Principal compressive strains at the support section of Slab 2 with shear reinforcement.
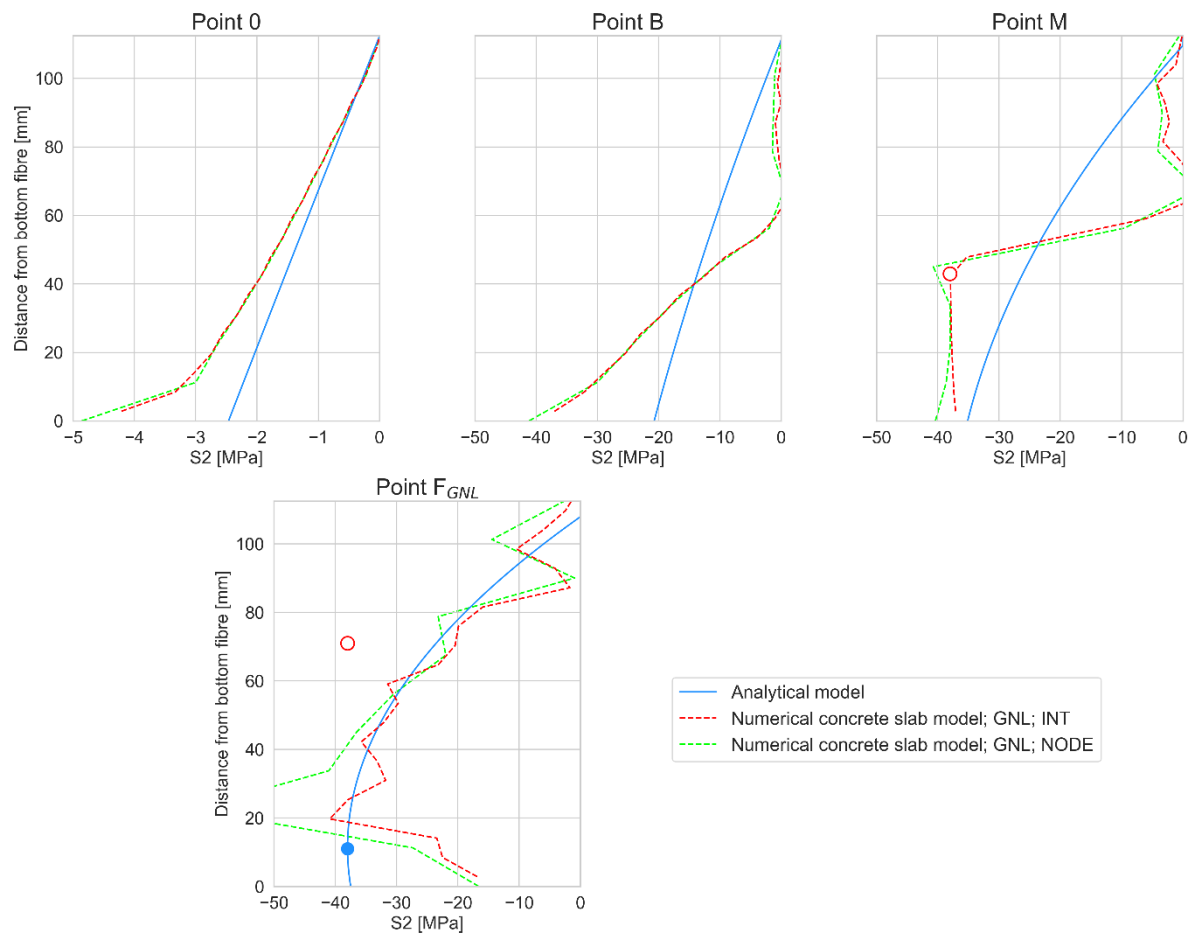
Figure B.26: Principal compressive stresses at the support section of Slab 2 with shear reinforcement.

Principal compressive strains and stresses for Slab 2 including non-convergence
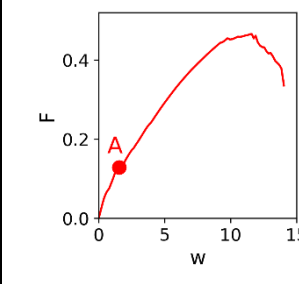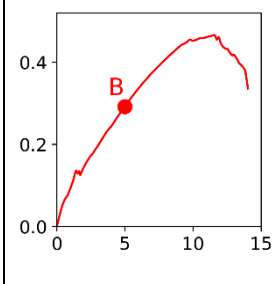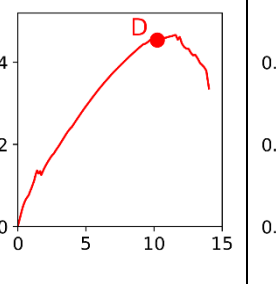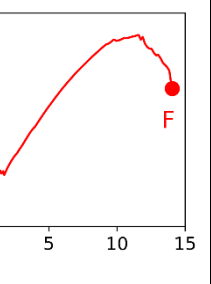
Table B.2: Points used for strain and stress plots of Slab 2 including non-convergence.
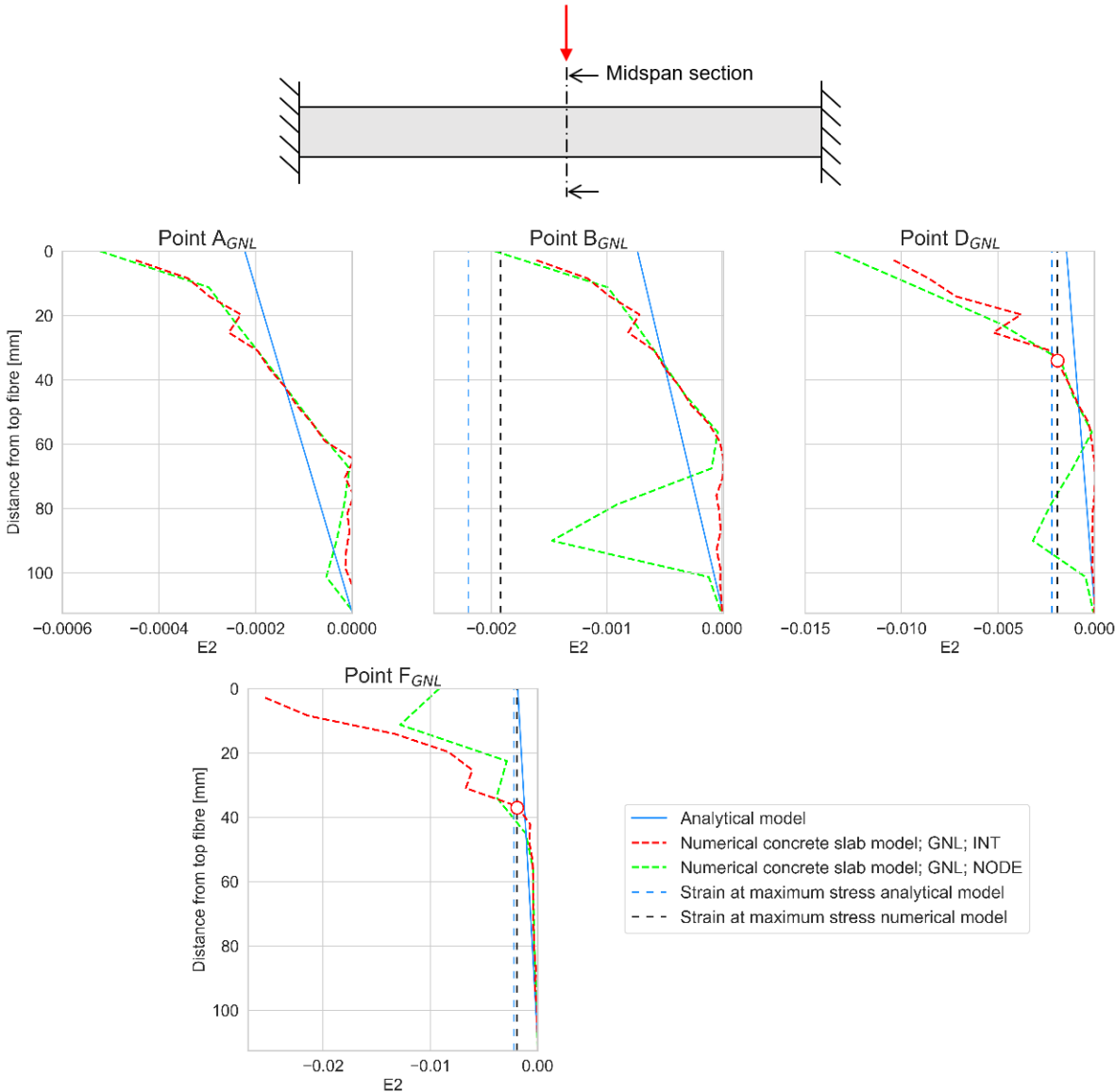
Figure B.27: Principal compressive strains at the midspan section of Slab 2 including non-convergence.
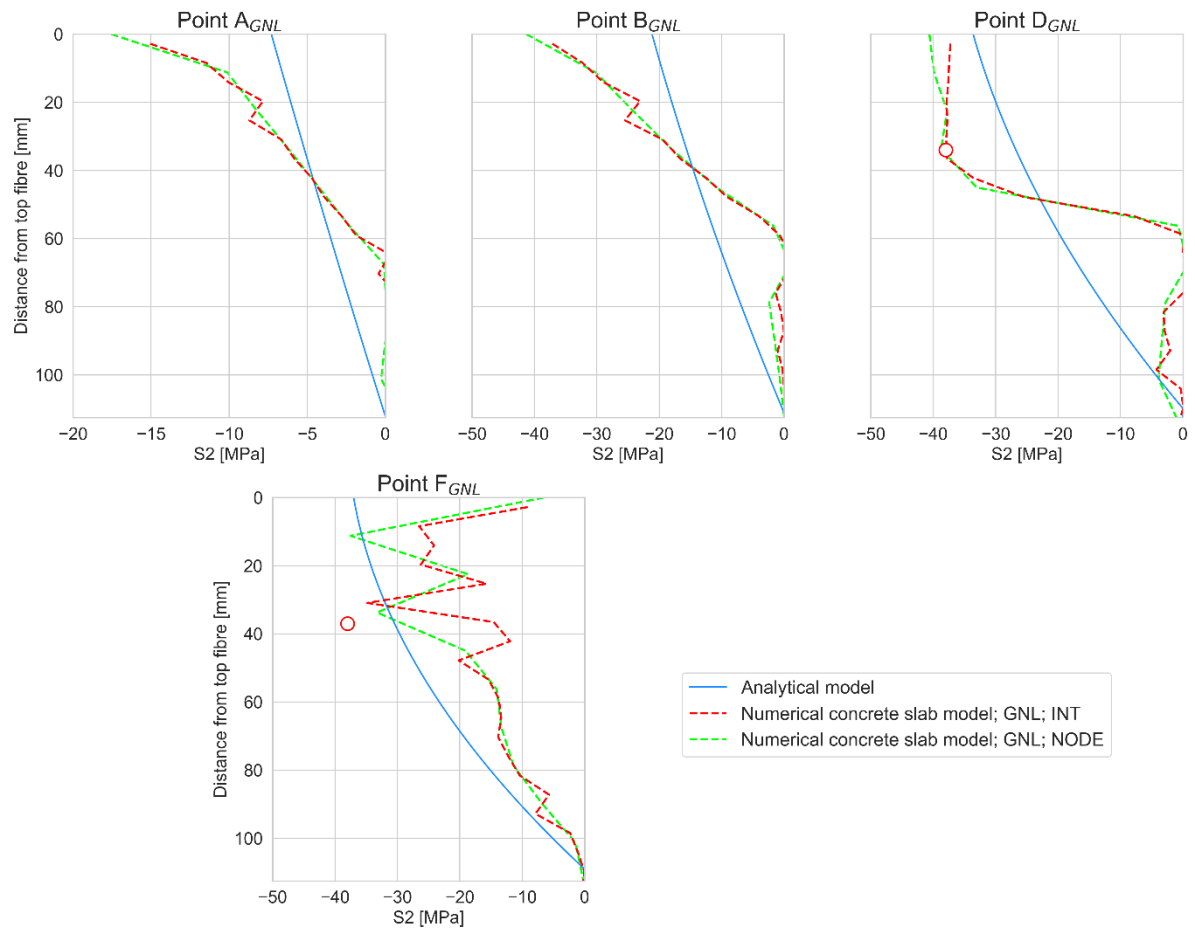
Figure B.28: Principal compressive stresses at the midspan section of Slab 2 including non-convergence

C
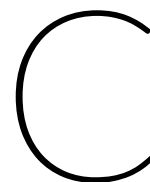
Appendix – Calculation procedure degree of axial restraint

Figure C.1 gives the iterative calculation procedure to obtain the load-deflection behaviour and the ultimate capacity of partly restrained slab strips given a certain value for the degree of axial restraint. Figure C.2 gives the corresponding Python script. Note that the names used for the quantities in both figures do not fully correspond.
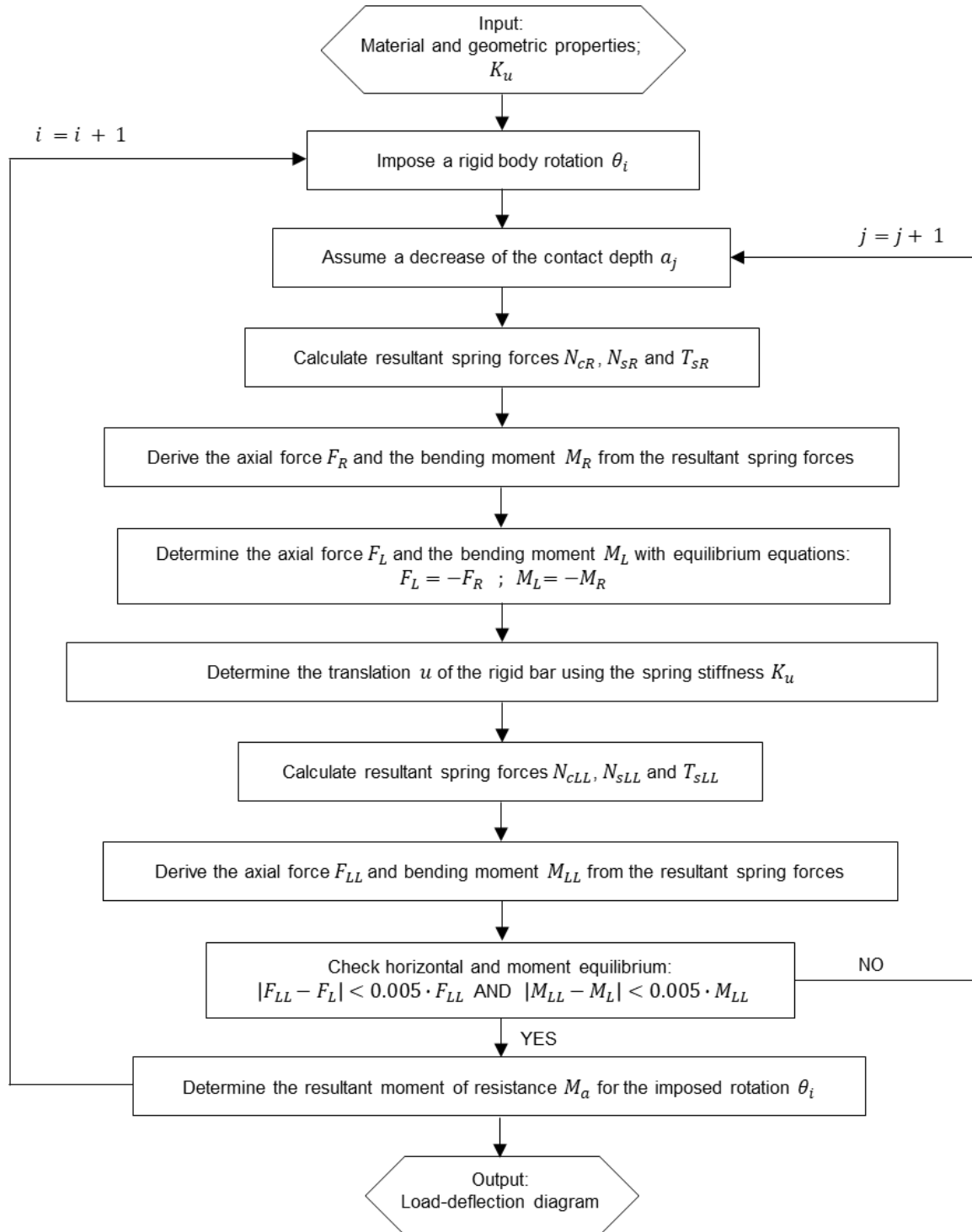
Figure C.1: Iterative calculation procedure for the load-deflection behaviour of the partly restrained concrete slab strip.

```python
fig1, ax1 = plt.subplots(figsize=(6,7))

n_spots = 100
n_steps = 40
u2 = np.zeros(n_spots)
u4 = np.zeros(n_spots)
u3 = np.zeros(n_spots)
k2 = np.zeros(n_spots)
k3 = np.zeros(n_spots)
k4 = np.zeros(n_spots)
s = np.zeros(n_spots)
s2 = np.zeros(n_spots)
s4 = np.zeros(n_spots)
counter = 0

d = 62.5
L = 1800
cc= 15
Es = 200000
diameter_y = 8
cover = cc + diameter_y/2
b = 200
spacing_y = 120
rho_y = 0.25*np.pi*diameter_y**2 *b/spacing_y/(2*d*b)
rho = rho_y
rho_ = rho
A_eq = rho * 2*d
A_eq2 = rho_ * 2*d
slenderness = L*2/(2*d)

theta = np.linspace(0.0001,0.09,n_steps)
M_MNL = np.zeros(len(theta))
M_GNL = np.zeros(len(theta))
w = np.zeros(len(theta))
a = np.zeros(len(theta))
w2 = np.zeros(len(theta))
eps_maxx = np.zeros(len(theta))
perc = np.zeros(len(theta))
Nc = np.zeros(len(theta))
Nc2 = np.zeros(len(theta))
Nc4 = np.zeros(len(theta))
N_steel = np.zeros(len(theta))
N_steel2 = np.zeros(len(theta))
M_total_MNL = np.zeros(len(theta))
M_total_GNL = np.zeros(len(theta))
sigma_steel = np.zeros(len(theta))
sigma_steel2 = np.zeros(len(theta))
epsilon_steel = np.zeros(len(theta))
epsilon_steel2 = np.zeros(len(theta))
u = np.zeros(len(theta))
u1 = np.zeros(len(theta))
u_steel_compression = np.zeros(len(theta))
u_steel_tension = np.zeros(len(theta))
u_steel_compression_new = np.zeros(len(theta))
u_steel_tension_new = np.zeros(len(theta))
sigma_steel_compression = np.zeros(len(theta))
sigma_steel_tension = np.zeros(len(theta))
sigma_steel_compression_new = np.zeros(len(theta))
sigma_steel_tension_new = np.zeros(len(theta))
N_steel_compression = np.zeros(len(theta))
N_steel_tension = np.zeros(len(theta))
N_steel_compression_new = np.zeros(len(theta))
N_steel_tension_new = np.zeros(len(theta))

fcm = 33
Ecm = 31000
e_c1 = 0.0021
e_cu1 = 0.0035
u_c1 = 0.25 * e_c1 * L
u_cu1 = 0.25 * e_cu1 * L
k = 1.05 * Ecm/(0.25*L) * abs(u_c1) / fcm
k1 = 600
fy = 500
Es = 200000
us = fy/Es*d
```

```python
cc1 = []
cc4 = []
nsc1 = []
nsc4 = []
nst1 = []
nst4 = []
nc1 = []
nc4 = []
aaa = []
uuu = []
ttt = []
ttt2 = []
yyy = []

for i in range(n_steps):
    w[i] = 2*L*(1-np.cos(theta[i]))/np.sin(theta[i])
    aa = np.arange(-60,100,0.01)
    u2_max = np.zeros(len(aa))
    u4_max = np.zeros(len(aa))
    for m in range(len(aa)):

        x_part = np.sin(theta[i])*(d+aa[m])
        x1 = L
        x2 = L*np.cos(theta[i]) + x_part
        y1 = - ((d+aa[m]) * (1-np.cos(theta[i])) + (x1-x_part) * np.tan(theta[i]))
        b = y1 + np.tan(theta[i]) * x1
        y2 = -np.tan(theta[i]) * x2 + b
        b2 = y2-(1/np.tan(theta[i]))*x2
        y3 = (1/np.tan(theta[i]))*x1 + b2

        if x2 <= x1:
            counter+=1

            u_steel_compression_new = (x1-x2) + np.sin(theta[i])*cover
            if u_steel_compression_new < us:
                ks_c = Es/L
            if u_steel_compression_new >= us:
                ks_c = fy/u_steel_compression_new
            sigma_steel_compression_new = u_steel_compression_new * ks_c
            N_steel_compression_new = sigma_steel_compression_new * A_eq2

            u_steel_tension_new = (x1-x2) + np.sin(theta[i])*(2*d-cover)
            if u_steel_tension_new < us:
                ks_t = Es/L
            if u_steel_tension_new >= us:
                ks_t = fy/u_steel_tension_new
            sigma_steel_tension_new = u_steel_tension_new * ks_t
            N_steel_tension_new = sigma_steel_tension_new * A_eq

            N_res_2 = -N_steel_compression_new - N_steel_tension_new
            M_res_2 = N_steel_tension_new * (d-(np.cos(theta[i])*cover)) - N_steel_compression_new
                    * (d-(np.cos(theta[i])*cover))

        if x2 > x1:

            com = np.sqrt(abs(y2-y3)**2 + abs(x2-x1)**2)

            if cover > com:
                u_steel_compression_new = np.sin(theta[i])*(cover-com)
                if u_steel_compression_new < us:
                    ks_c = Es/L
                if u_steel_compression_new >= us:
                    ks_c = fy/u_steel_compression_new
                sigma_steel_compression_new = u_steel_compression_new * ks_c
                N_steel_compression_new = sigma_steel_compression_new * A_eq2

            if com >= cover:
                u_steel_compression_new = np.tan(theta[i])*(com-cover)
                if u_steel_compression_new < us:
                    ks_c = Es/L
                if u_steel_compression_new >= us:
                    ks_c = fy/u_steel_compression_new
                sigma_steel_compression_new = u_steel_compression_new * ks_c
                N_steel_compression_new = sigma_steel_compression_new * A_eq

            u_steel_tension_new = (np.sin(theta[i])*(2*d-com-cover))
            if u_steel_tension_new < us:
                ks_t = Es/L
            if u_steel_tension_new >= us:
                ks_t = fy/u_steel_tension_new
            sigma_steel_tension_new = u_steel_tension_new * ks_t
            N_steel_tension_new = sigma_steel_tension_new * A_eq
```

```python
            u4_max[m] = (np.tan(theta[i]))*com
            y4 = np.linspace(0,com,n_spots)
            for j in range(n_spots):
                u4[j] = -u4_max[m]/com * y4[j] + u4_max[m]
                if u4[j] == 0:
                    k4[j] = 0
                if u4[j] != 0:
                    k4[j] = (fcm * ((k*(u4[j]/u_c1)-(u4[j]/u_c1)**2)/(1+(k-2)*(u4[j]/u_c1)))) / u4[j]

                if u4[j] > u_cu1:
                    s4[j] = 0
                if u4[j] > 0 and u4[j] < u_cu1:
                    s4[j] = u4[j]*k4[j]
                if u4[j] < 0:
                    s4[j] = 0

            Nc4[i] = np.trapz(s4,y4,axis=-1)
            centroid4 = 1/Nc4[i] * np.trapz(s4*y4,y4,axis=-1)

            if cover > com:
                N_res_2 = Nc4[i] - N_steel_compression_new - N_steel_tension_new
                M_res_2 = Nc4[i] * (d-centroid4) - N_steel_compression_new * (d-(np.cos(theta[i])*cover))
                        + N_steel_tension_new * (d-(np.cos(theta[i])*cover))

            if com >= cover:
                N_res_2 = Nc4[i] + N_steel_compression_new - N_steel_tension_new
                M_res_2 = Nc4[i] * (d-centroid4) + N_steel_compression_new * (d-cover) + N_steel_tension_new
                        * (d-(np.cos(theta[i]) * cover))

        u1[i] = N_res_2 / k1

        u2_max[m] = (np.tan(theta[i])*(d-aa[m]))-u1[i]/np.cos(theta[i])
        y = np.linspace(0,d-aa[m]-(u1[i]/np.cos(theta[i]))/np.tan(theta[i]),n_spots)
        for j in range(n_spots):
            u2[j] = -u2_max[m]/(d-aa[m]-(u1[i]/np.cos(theta[i]))/np.tan(theta[i])) * y[j] + u2_max[m]
            if u2[j] == 0:
                k2[j] = 0
            if u2[j] != 0:
                k2[j] = (fcm * ((k*(u2[j]/u_c1)-(u2[j]/u_c1)**2)/(1+(k-2)*(u2[j]/u_c1)))) / u2[j]

            if u2[j] > u_cu1:
                s[j] = 0
            if u2[j] > 0 and u2[j] < u_cu1:
                s[j] = u2[j]*k2[j]
            if u2[j] < 0:
                s[j] = 0

    Nc[i] = np.trapz(s,y,axis=-1)
    centroid1 = 1/Nc[i] * np.trapz(s*y,y,axis=-1)

    u_steel_compression = (np.tan(theta[i])*(d-aa[m]-cover))-u1[i]/np.cos(theta[i])
    if u_steel_compression < us and u_steel_compression > -us:
        ks_c = Es/L
    if u_steel_compression >= us:
        ks_c = fy/u_steel_compression
    if u_steel_compression < -us:
        ks_c = -fy/u_steel_compression

    sigma_steel_compression = u_steel_compression * ks_c
    N_steel_compression = sigma_steel_compression * A_eq2

    u_steel_tension = (np.sin(theta[i])*(d+aa[m]-cover))+u1[i]
    if u_steel_tension < us:
        ks_t = Es/L
    if u_steel_tension >= us:
        ks_t = fy/u_steel_tension
    sigma_steel_tension = u_steel_tension * ks_t
    N_steel_tension = sigma_steel_tension * A_eq

    N_res = Nc[i] + N_steel_compression - N_steel_tension
    M_res = Nc[i] * (d-centroid1) + N_steel_compression * (d-cover) + N_steel_tension
            * (d-(np.cos(theta[i])*cover))

    if abs(N_res-N_res_2) < abs(0.003*N_res) and abs(M_res-M_res_2) < abs(0.003*M_res):

        centroid1 = 1/Nc[i] * np.trapz(s*y,y,axis=-1)
        centroid4 = 1/Nc4[i] * np.trapz(s4*y4,y4,axis=-1)
        cc1.append(centroid1)
        cc4.append(centroid4)

        if x2 <= x1:
            nc4.append(0)
            nsc4.append(-N_steel_compression_new)
```

```python
            if x2 > x1:
                nc4.append(Nc4[i])
                if cover > com:
                    nsc4.append(-N_steel_compression_new)
                if com >= cover:
                    nsc4.append(N_steel_compression_new)

            if u2_max[m] > 0:
                nc1.append(Nc[i])
            if u2_max[m] <= 0:
                nc1.append(0)

            nsc1.append(N_steel_compression)
            nst1.append(N_steel_tension)
            nst4.append(N_steel_tension_new)

            break

M_total_MNL = np.zeros(len(cc1))
M_total_GNL = np.zeros(len(cc1))
w_new = np.zeros(len(cc1))

for i in range(len(cc1)):
    w_new[i] = w[aaa[i][1]]
    arm_cc1_MNL = d-cc1[i]
    arm_cc4_MNL = d-cc4[i]
    arm_cc1_GNL = d-cc1[i]-w_new[i]/2
    arm_cc4_GNL = d-cc4[i]-w_new[i]/2

    arm_s_MNL = d-cover
    arm_sc1_GNL = d-cover-w_new[i]/2
    arm_sc4_GNL = d-cover-w_new[i]/2

    arm_st1_GNL = d-cover+w_new[i]/2
    arm_st4_GNL = d-cover+w_new[i]/2

    M_total_MNL[i] = nc1[i]*arm_cc1_MNL + nc4[i]*arm_cc4_MNL + nsc1[i]*arm_s_MNL + nsc4[i]*arm_s_MNL
                     + nst1[i]*arm_s_MNL + nst4[i]*arm_s_MNL
    M_total_GNL[i] = nc1[i]*arm_cc1_GNL + nc4[i]*arm_cc4_GNL + nsc1[i]*arm_sc1_GNL + nsc4[i]*arm_sc4_GNL
                     + nst1[i]*arm_st1_GNL + nst4[i]*arm_st4_GNL

ax1.plot(w_new,4*M_total_GNL/(2*L*1000),color='dodgerblue',linestyle='--',label='GNL')
ax1.plot(w_new,4*M_total_MNL/(2*L*1000),color='dodgerblue',label='GL')
ax1.set_xlabel('w [mm]',fontsize=13)
ax1.set_ylabel('F [kN/mm]',fontsize=13)
ax1.set_ylim([0,0.16])
ax1.set_xlim([0,100])
ax1.tick_params(axis='x', labelsize=13)
ax1.tick_params(axis='y', labelsize=13)

print(np.max(M_total_MNL))
print(np.max(M_total_GNL))
```

Figure C.2: Python script to vary the degree of axial restraint of Slab 1.